NASA Contractor Report 182096

SHOCK TUNNEL STUDIES OF SCRAMJET PHENOMENA

SUPPLEMENT 5

**R. Casey, R. J. Stalker, C. P. Brescianini,
R. G. Morgan, P. A. Jacobs, M. Wendt, N. R. Ward,
N. Akman, G. A. Allen, K. Skinner, S. L. Tuttle,
J. M. Simmons, G. Kelly, R. M. Krek, A. Neely, and A. Paull**

**UNIVERSITY OF QUEENSLAND
St. Lucia, Queensland
AUSTRALIA**

**Grant NAGW-674
October 1990**

National Aeronautics and
Space Administration

Langley Research Center
Hampton, Virginia 23665-5225

REPORT ON SHOCK TUNNEL STUDIES OF SCRAMJET PHENOMENA

NASA GRANT NAGW 674 - Supplement 5, 1989

As in previous reports, this consists of a series of reports on specific project areas, with a brief general introduction commenting on each report. The introduction is structured by project areas, with the title of the relevant report stated under the project area heading. The reports themselves follow in the order of the project area headings.

The commentary begins with a brief review of the program of work planned for 1989.

Planned Program for 1989

Hypersonic Combustion: Continue studies with a central injection configuration, involving pitot and heat transfer surveys of the combustion wake, and the effects of pressure, Mach number and duct cross section.

Experiments on hypersonic combustion with orifice injection from the walls were also requested.

Continue development of a heated hydrogen experimental rig.

Explore the effects of promoting mixing of a film cooling layer, in order to encourage combustion, and continue the development of skin friction gauges.

Continue development of scaling studies experiments.

Drag Measurement: Use a drag balance to measure drag on a cone, as a prelude to measurement of thrust.

Expansion Tube Studies: Continue theoretical studies of expansion tube operation, seeking understanding of the operating limits imposed by flow disturbances, and continue studies of methods for predicting test section flow conditions.

SCRAMJET STUDIES

Investigation of a Supersonic Combustion Layer — R.T. Casey and R.J. Stalker

This work is a fundamental study of the wake formed by mixing of an hydrogen stream, issuing from the trailing edge of an injection strut, with the surrounding highly supersonic air stream. A first attempt at measuring pitot profiles in the wake was made in 1988 but proved unsuccessful because unsatisfactory test flows were produced by the experimental apparatus. This problem has now been overcome, and measurements of pitot pressure and stagnation point heat transfer on small probes have been made in a flow at M = 4.2, and a stagnation enthalpy of 9.4 MJ/kg.

Measurement of static pressure distributions on the wall of the duct indicated that combustion was taking place, but this did not significantly affect the pitot pressure profiles. With an injection slot width of 1.6 mm, measurements taken up to 154 mm downstream of injection indicated that the centreline pitot pressure changed very slowly with distance, indicating slow mixing rates. No significant effects of combustion on the pitot pressure were observed, even when a silane-hydrogen mixture was used as fuel. Preliminary stagnation point heat transfer measurements are somewhat equivocal at this stage, indicating that this may perhaps, be an effective means of detecting combustion.

Wall Injected Scramjet Experiments — C.P. Brescianini

Previous experiments had shown that, when hydrogen was injected in a film cooling mode along one wall of a combustion duct, very effective surface thermal protection was observed, but no significant downstream combustion occurred until equivalence ratios rose to almost 2. Numerical analysis indicated that this was because mixing between the hydrogen fuel and the air was suppressed by the presence of the wall.

These experiments were aimed at promoting combustion by using ramp type mixing protrusions, mounted on the surface downstream of injection. Although a number of different test conditions and mixer configurations were studied, no significant combustion effect was observed.

Supersonic Combustion with Transverse, Circular, Wall Jets

R.G. Morgan and R. Casey

A series of experiments was performed in a constant area duct with fuel injected through orifices in the wall of the duct. The centreline of the orifices was inclined at 30° with respect to the stream direction, and the injection orifices and duct cross sectional dimensions were chosen to maintain a 2:1 aspect ratio for the part of the duct cross section fuelled by each orifice. The experiments were conducted at duct inlet flow Mach numbers of 4.2 and 5.5 approximately.

It was found that substantial static pressure rises occurred in the duct when fuel was injected, indicating that mixing and combustion was taking place. The duct dimensions and operating conditions that supported combustion were found to be the same as those for a central injection strut. This suggests that, providing a configuration is chosen which promotes adequate mixing, the presence of combustion may not be sensitive to the injection configuration.

Dissociated Test Gas Effects on Scramjet Combustors

R.G. Morgan

Free stream freezing of oxygen constitutes a major disadvantage of reflected shock tunnels when operating at moderately high stagnation enthalpies. This is particularly important for combustion experiments, because the energy invested in oxygen dissociation represents a very substantial effective increase in the calorific value of the fuel. Some indication of the seriousness of this effect, in practical terms, may be gained from experiments on the same model to be conducted at G.A.S.L., using the "Hypulse" expansion tube, and at The University of Queensland, using T4.

However, as a prelude to these experiments, the effect of oxygen depletion of the test gas is explored. The aim is to compensate for the increased effective calorific value associated with oxygen freezing by reducing the amount of oxygen in the test gas. In this investigation, one dimensional computations of premixed reacting flows are used to examine the effects of oxygen adjustment, as determined by a heat balance approach. The calculations suggest that simulation of the flow in a combustor is possible in the presence of free stream freezing by suitably adjusting the initial oxygen concentration in the test gas.

Use of Silane as a Fuel Additive for Hypersonic Thrust Production

R.G. Morgan

The difficulties experienced in producing hypersonic combustion (reported in previous grant reports) are thought to be associated with the low pressures associated with hypersonic flow in the shock tunnel. One method of coping with this is to raise the tunnel operating pressures, and the effects of doing this are noted in later parts of this report. Another approach is to add silane to the hydrogen fuel, and this is discussed in this section.

It was found that silane allowed combustion at much lower pressures than with hydrogen alone, and may offer a means of extending combustion studies to the Mach numbers of 7 or 8 associated with very high velocity propulsion.

The experiments were conducted under test conditions such that the nozzle stagnation pressure decayed by 15% during the test period, and the effect of pressure decay on the thrust measurements in the nozzle is discussed. A control volume approach is used, and it is argued that decay in test conditions has negligible influence on thrust increment measurements i.e. fuel-on minus fuel-off valves. A different approach is to use the Hypersonic Equivalence Principle in interpreting results in a decaying pressure state - this yields the same result.

Pressure-Length Correlations in Supersonic Combustion

P.A. Jacobs and R.J. Stalker

This is the first test in what is intended to be a study of scaling effects in scramjet combustors. This is to be an investigation involving three models, of differing scales, and the present results were obtained in the largest of the three models. The results of this test show that the combustor duct is long enough to produce a significant combustion pressure rise (approximately 35%) at static pressures of approximately 30 kPa. This is low enough to permit much higher pressures with smaller models. indicating that the range of pressures available can be expected to be sufficient to allow a meaningful study to be undertaken.

Hot Hydrogen Injection Technique for Shock Tunnels

M. Wendt

A safe, pulsed method of heating hydrogen for heated fuel injection studies is required. A small gun tunnel is being constructed for this purpose. It will be mounted in the dump tank of the shock tunnel and the hot, high pressure sample of hydrogen which is created by the compression process will be fed directly to the fuel injector assembly in the scramjet.

Heat Release - Wave Interaction Phenomena in Hypersonic Flows

N.R. Ward

The management of the wave interactions caused by combustion in a hypersonic duct is expected to be a long term problem in high velocity scramjet propulsion. As a fundamental study of this effect, it is planned to perform experiments with simple duct flows with dissociated nitrogen test gas. The dissociated nitrogen is produced by the shock tunnel nozzle flow and, in recombining, exhibits heat release characteristics which are not unlike a burning hydrogen/air mixture. Observation of the waves produced by the recombination process, using differential interferometry, is to be used to investigate thrust losses caused by wave mismatching.

A Study of the Wave Drag in Hypersonic Scramjets

Nesrin Akman

Previous analytical investigations, using small perturbations theory, have shown that the effects of wave drag in a two dimensional combustion duct can be demonstrated by converting a Busemann Biplane to a Busemann Scramjet through the agency of heat addition. This study carries this approach into the region where the wave interactions are not linear, by simulating the flow numerically.

Progress to date has indicated that matching the duct to the wave patterns involves balancing a number of effects if it is to be done accurately. However with the approximate matching which has been achieved so far, the variation of drag with Mach number for a non-linear Busemann Biplane has been studied, and is seen to exhibit maxima and minima which are qualitatively the same as in linearized theory.

Parametric Study of Thrust Production in the Two Dimensional Scramjet

G.A. Allen Jr.

The process of thrust production in the expansion nozzle of a scramjet involves interaction between the Mach number distribution in the combustion wake produced by the combustion chamber processes, and the expansion waves generated by the walls of the thrust nozzle.

This process is investigated here using the method of characteristics in a numerical simulation. A simple two dimensional configuration is considered, and the effects of varying parameters such as thrust surface angle and combustion wake Mach number distribution are considered.

The Design of a Mass Spectrometer for use in Hypersonic Impulse Facilities

K. Skinner

In order to measure species concentrations in combustion flows, a mass spectrometer is being developed. This is to use "time-of-flight" mass discrimination, and is expected to allow a number of scans of the mass spectrum at a point in the flow during each tunnel test.

Shock Tunnel Drag Measurement — **S.L. Tuttle and J.M. Simmons**

The initial work by Sanderson and Simmons is being extended to drag measurement on a slender cone, with a 5° semi-vertex angle. This involves a cone approximately 400 mm long, and leads to much greater problems with signal to noise ratio than the initial work. Some preliminary results are presented, indicating that accuracies achieved in the earlier work have not yet been achieved with this more difficult model.

Development of a Skin Friction Gauge for use in an Impulse Facility — **Gabrielle Kelly**

This work is proceeding, mainly by meeting a series of difficulties and evolving methods of overcoming them. At this stage, measurements which appear to be skin friction signals are being obtained, and further refinement is expected to produce a working gauge.

SHOCK TUNNEL STUDIES

Hypervelocity Flow in Axisymmetric Nozzles — **P.A. Jacobs and R.J. Stalker**

In developing a set of meaningful scaling experiments, it has been found necessary to design and manufacture shock tunnel nozzles for a range of Mach numbers and sizes. This has provided an opportunity to compare the quality of test flow produced by these nozzles.

The Mach number range of the nozzles was from 4.0 to 10. The M = 4 nozzle produced a nearly uniform and parallel flow, according to design requirements. However, the M = 10 nozzle was found to be much more susceptible to boundary layer effects. In fact, when operating at enthalpies approaching 30 MJ/kg, with a nozzle stagnation pressure of only 20 MPa (both conditions which tend to produce thick nozzle boundary layers) it was found that steady flow could not be established during the test time. Whilst this situation could be rectified for this nozzle by raising the nozzle stagnation pressure, it suggests that it may be difficult to operate axisymmetric nozzles at significantly higher Mach numbers.

Shock Tunnel Development (Supplementary Project) — **R.J. Stalker and R.G. Morgan**

Raising operating test section pressure levels can be done by raising the main diaphragm burst pressure and the driven gas volumetric compression ratio in a range of combinations. The trade off involved in these combinations is discussed.

Hypersonic combustion of hydrogen and ethane is demonstrated. This is made possible by the increased operating pressure levels.

Real Gas Effects in Hypervelocity Flows over an Inclined Cone — **R.M. Krek**

This study has three purposes. It is complementary to the study of drag forces, in that it reveals aspects of pressure measurement which need to be understood if pressure drag is to be calculated accurately. It is a study of the type of flow which is likely to characterize the forebody of a scramjet vehicle at high Mach number. It also constitutes a reasonably careful set of measurements, aimed at validating a 3-D c.f.d. code which, hopefully, may eventually be applied to scramjet flows.

EXPANSION TUBE STUDIES

Investigation of Flow Characteristics in TQ Expansion Tube — A. Neely

This project is aimed at predicting the test section flows generated by an expansion tube. From the point of view of scramjet testing, the presence of dissociated oxygen is particularly important, and a ready means of estimating the conditions under which this occurs is needed. The work reported here is a record of an attempt to generate a theory which will readily predict test section compositions when dissociation fractions are low. It is being conducted in parallel with an experimental program, involving both air and argon (because of its theoretical simplicity) as test gas.

Disturbances in the Driver Gas of a Shock Tube — A. Paull and R.J. Stalker

This is a continuation of a study aimed at understanding the source of the disturbances on the pitot pressure which limit the range of operating conditions of expansion tubes.

It was previously postulated that, over a substantial range of potential operating conditions, these disturbances were associated with inclusions of driver gas in the test gas. In order to test this hypothesis, a differential laser interferometer was used to observe variations in the integral of test gas density across the tube as the flow passed a given station. The variations observed were much smaller than those expected, casting considerable doubt on the "bubbles" theory.

Therefore a new approach was taken. This involved the recognition that the pitot pressure disturbances observed in expansion tube operation may have originated in the shock driver (possibly from disturbances generated at diaphragm rupture), before being transmitted into the shock tube test gas sample prior to its processing in the acceleration tube expansion.

The acoustic disturbance modes which are compatible with the boundary conditions applying the shock tube are analysed, and attention is focused on longitudinal waves, and a first order lateral wave. The structure of the flow in the shock tube driver gas is analysed and it is argued that, under these conditions, the observed pitot pressure fluctuations are evidence of the dominance of the lateral wave. This is consistent with the failure to observe strong disturbances in the laser interferometer experiments.

This work will continue, with a view to studying the way in which the lateral waves penetrate the driver gas-test gas interface, and traverse the acceleration tube expansion, into the test region.

INVESTIGATION OF A SUPERSONIC COMBUSTION LAYER

by

R. T. Casey and R. J. Stalker

In 1989 a set of experiments were conducted in the T4 free piston shock tunnel which sought to investigate the development and mixing of a combustion region in a scramjet duct. The ambient Mach number and enthalpy were 4 and 9.4 MJ/kg respectively. A table of the other flow conditions is given in table 1.Hydrogen was injected into the flow from a 2-D slot type injector parallel to the free stream flow but at a slower velocity. The nominal equivalence ratio for the experiments was 1. A pitot rake and a heat transfer rake were used to measure the pitot pressure and heat transfer rate respectively. The rake was moved to various downstream positions in order to monitor the development of the pitot pressure and heat transfer within the mixing region at various downstream positions. Wall static pressure measurements were also taken. A schematic diagram of the experimental set up is given in figure 2.1.

For each downstream position the rake was moved to, a set of three shots were fired. For the first hydrogen was injected into an ambient airflow,(termed fuel on). For the second shot, hydrogen was injected into an ambient nitrogen flow (termed fuel into nitrogen) and for the third shot, no fuel was injected into an ambient airflow (termed fuel off). Comparison of the wall static pressure measurements for the fuel on and the fuel into nitrogen shots showed an increase in wall static pressure for the fuel on case thus confirming the presence of combustion. Comparison of the pitot pressure and heat transfer measurements between the fuel on and fuel into nitrogen shots served as a useful means of separating mixing effects and combustion enhanced mixing effects.

Figures 2 and 3 each show the pitot pressure measurements taken for the fuel on, fuel off and fuel into nitrogen shots for the case of the rake being 31 mm and 81mm downstream from the exit plane of the injector respectively. Several observations of these plots are as follows:

1)The decay of centre line pitot pressure to its free stream value is very slow indicating that mixing is very weak,

2)Variations between the fuel on, fuel off and fuel into nitrogen profiles is very small for both the 31mm and the 81mm downstream

cases. This suggests that combustion is having little effect on the mixing of hydrogen and air streams

3)A degree of asymmetry exists in the pitot pressure profile.

Nitrogen was injected into quiescent air of ambient temperature and pressure of 40 kpa. The pitot rake was moved to a position 54mm downstream of the injector exit and pitot pressures were measured for this condition. The pitot rake was then adjusted up half the pitch of the transducer spacing to increase the resolution of the pitot measurements. Again, nitrogen was injected into quiescent air. The results of the two shots is shown in figure 4. From this figure, it can be seen, that the injector does not inject the fluid symmetrically about the centre line. This effect explains the asymmetry of the pitot pressure measurements of figures 2 and 3.

Figure 5 gives a comparison of two pitot pressure profiles. The first was taken from a shot where hydrogen was injected into the Mach 4 air stream and the other a 20% silane 80% hydrogen mixture was injected. It was expected that with the addition of silane, the second case would produce improved combustion and this in turn would produce improved mixing. However, little difference can be seen between the hydrogen injection case and the silane/hydrogen injection case.

The signals recorded from the heat transfer transducers were digitally integrated. The value obtained from the fuel on shots and fuel into nitrogen shots were normalized against the value obtained from the fuel off shot. Since the fuel is injected at a cold temperature (approximately 150 K) then this normalized value of heat transfer is expected to be less than unity when close to the fuel jet. When this normalized heat transfer value is higher for the fuel on case than for the fuel off case, then it can be taken that the heat release of combustion accounts for this rise. Six of the ten heat transfer gauges used suffered constant malfunctions after each shot and so no data was collected from these. Consequently heat transfer data from this set of experiments is sparse. Table 2 gives heat transfer data for the case of the pitot rake being 154mm downstream of the injector exit plane. The distances quoted at the top of the table are distances from the centre line of the duct. From this table , it can be seen that -19mm away from the centre line the normalized heat transfer value for the fuel into nitrogen case is higher than for the fuel into air case. This is thought to be a boundary

layer effect.

It is intended for this year to conduct further experiments in this area. The mach number will be varied, up to Mach 5, and the resolution for each pitot profile will be increased.

CONDITIONS	FREESTREAM	HYDROGEN
Stagnation Enthalpy	9.4 Mj/kg	
Stagnation Pressure	13 Mpa	
Density	0.063 kg/m^3	0.081 kg/m^3
Velocity	3531 m/s	2400 m/s
Mach Number	4.2	
Static Pressure	36 kPa	36 kPa
Temperature	1933 K	124 K

Table 1 Experimental conditions

DISTANCE FROM CENTRE LINE	-19 mm	-8 mm	-2.5 mm	14 mm
NORMALIZED HEAT TRANSFER $H_2 \rightarrow N_2$	1.202	0.873	0.476	0.979
NORMALIZED HEAT TRANSFER $H_2 \rightarrow$ AIR	1.035	1.125	0.425	1.420

Table 2 Heat transfer values measured 154 mm downstream from the injector exit

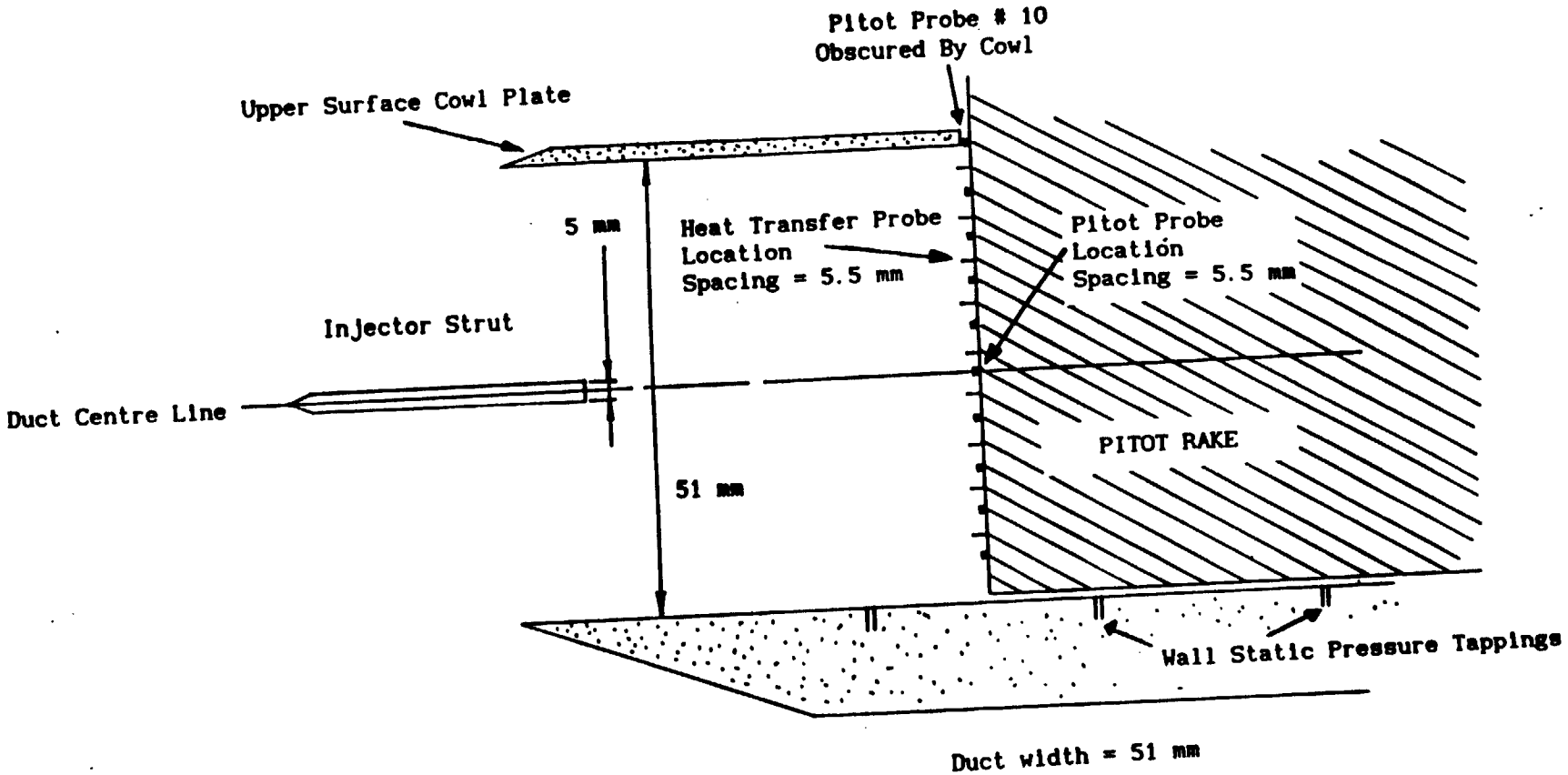

Figure 1 Schematic diagram of experimental set up. Not to scale

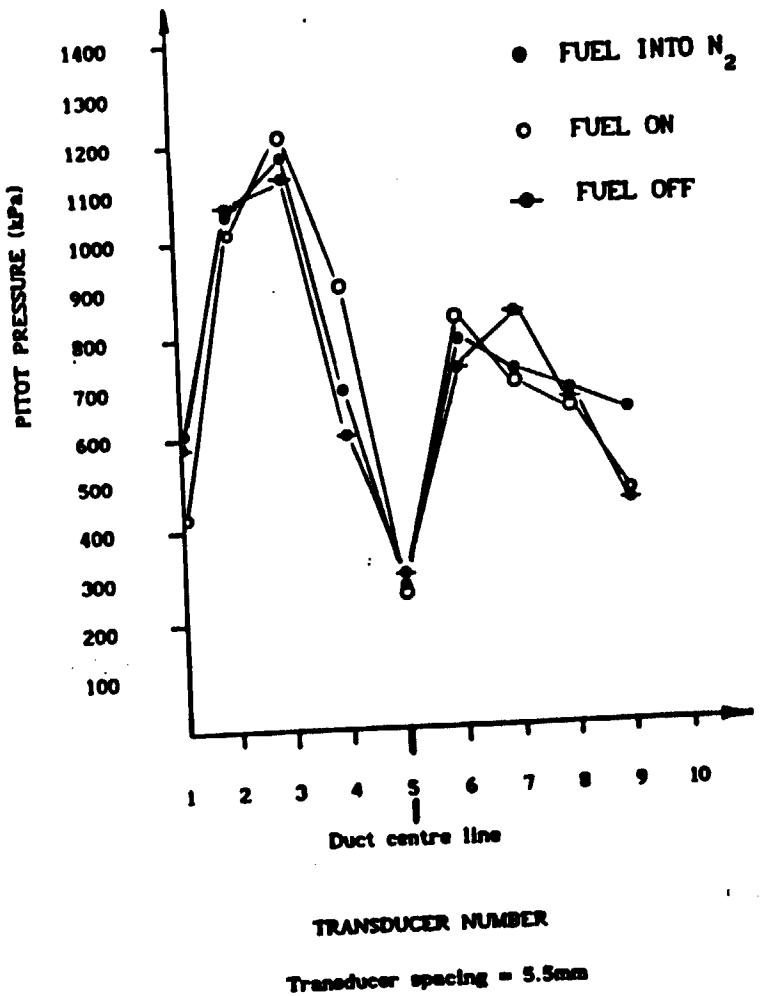

Figure 2 Pitot pressure profiles measured 31 mm downstream from the injector exit

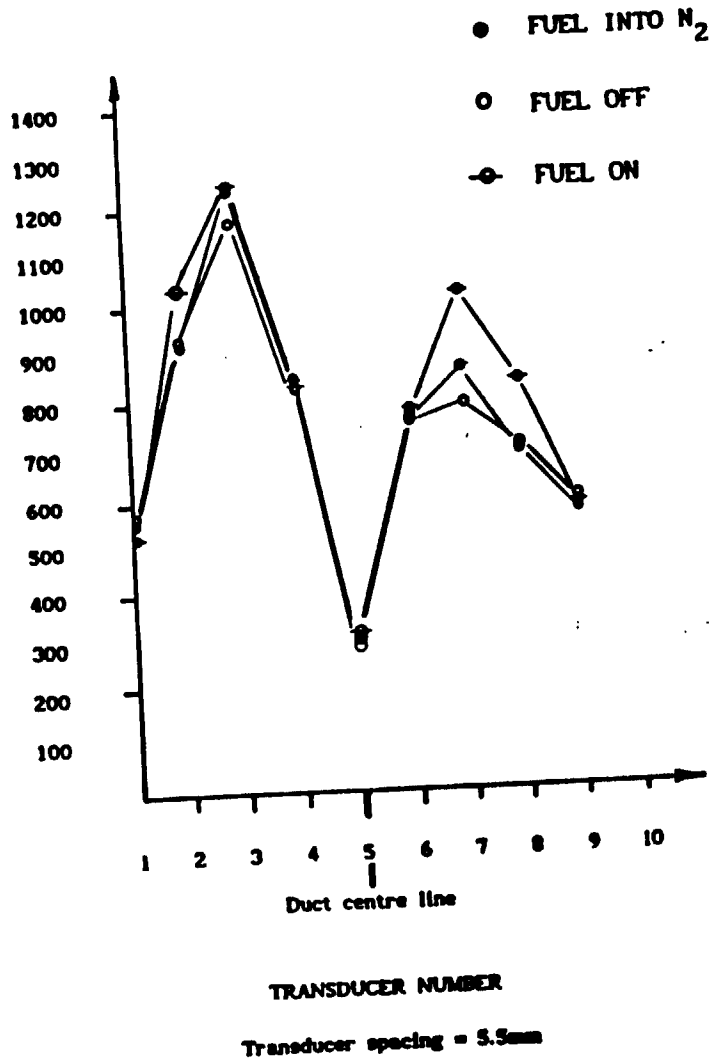

Figure 3 Pitot pressure profiles measured 81 mm downstream from the injector exit

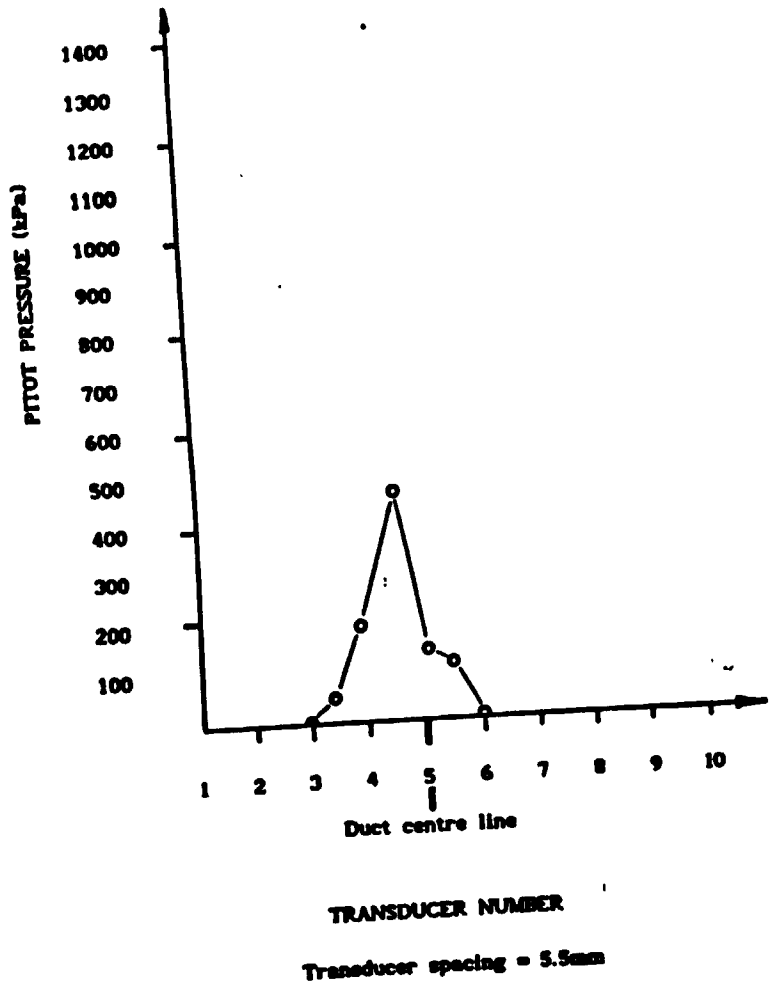

Figure 4 Pitot pressure measured 154 mm downstream from the injector exit for N_2 injected into 40 kPa quiescent air

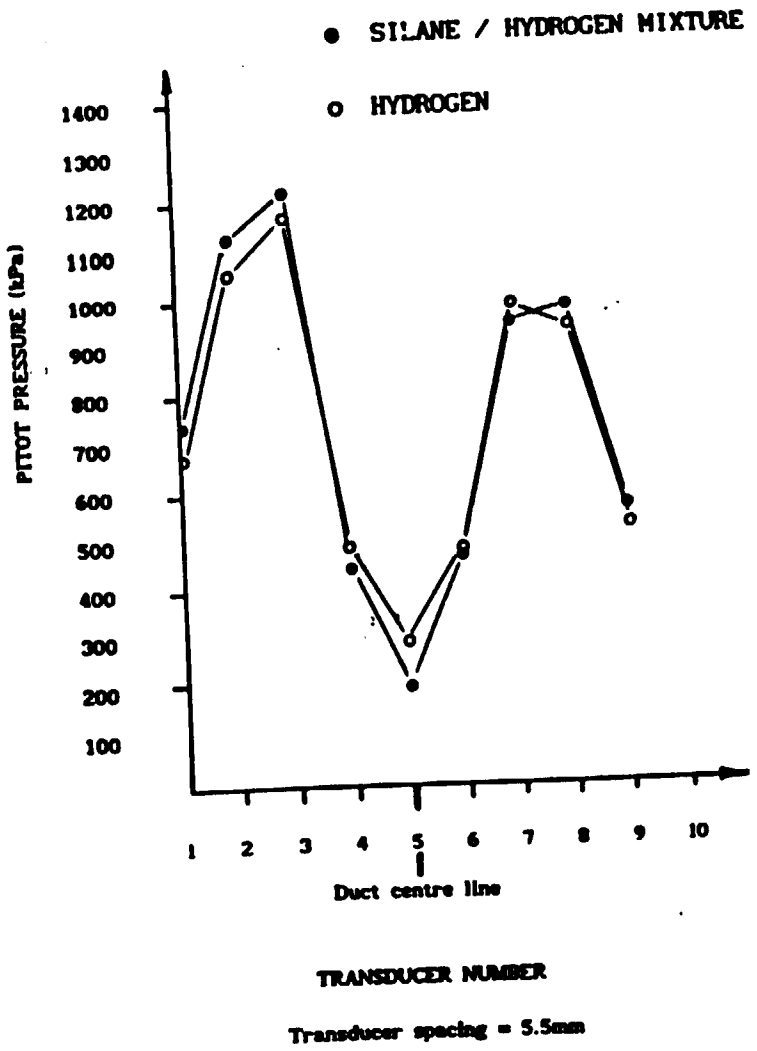

Figure 5 Pitot pressure profiles measured 154 mm downstream from the injector exit

WALL INJECTED SCRAMJET EXPERIMENTS

C. P. Brescianini

A series of two-dimensional wall injected scramjet experiments, performed in the T3 shock tunnel, have been reported previously by Morgan et. al.[1,2] Subsequent numerical simulation of some of these experiments, by Brescianini and Morgan[3], have indicated that combustion was being limited mainly by the fuel/air mixing rates. As a continuation of this earlier work a series of experiments were devised to be performed in the newer T4 shock tunnel at the University of Queensland. The aim of the experiments was to reproduce shock tunnel conditions similar to those experienced in T3, and also to see if fuel/ air mixing could be enhanced by the addition of "mixers" to the wall of the model.

The experiments were based around the same wall injected scramjet model used in the previous T3 experiments. The scramjet was configured as a constant area duct, with a tangental wall injector, for all of the experiments. Three nominal stagnation enthalpy conditions, namely 8.8, 6.6 and 3.8 MJ/kg, were chosen to match as closely as possible the stagnation enthalpy conditions used previously in T3. These three nominal enthalpies were taken from a table of standard T4 shock tunnel operating conditions. The actual experimental stagnation enthalpy was a function of the stagnation pressure at the chosen test time. 2 mm steel diaphragms were chosen for the compression tube/ shock tube junction to keep overall pressures relatively low. This was desired so that less strain was placed upon the compression tube driver.

The only shock tunnel nozzle available during the experiments was the nominally Mach 5 nozzle. To make a more direct comparison with the previous T3 experiments, which were performed at Mach 3.5, it was necessary to pass the flow through oblique shocks, created by 10° wedges, located upstream of the inlet to the scramjet model (See Fig. 1). The Mach number at the inlet to the model was estimated to be approximately 3.8, although the actual value was stagnation enthalpy dependant.

The experimental results to date consist of approximately 28 shock tunnel runs in T4, using hydrogen, helium, silane and ethane, injected over a range of injection pressures. The experiments were supplemented by a further 27 shots using the 4 hump or single hump mixers shown in

Fig. 2. The 4 hump mixer is only of a simple, preliminary design, with the intention of enhancing the fuel/air mixing rate. The mixer has a disadvantage in that the flow created by the mixer no longer remains two-dimensional, making numerical analysis of the results more difficult. Shock waves off the front of the humps will also produce pressure rises which may increase combustion, even if the mixing is not improved. The single hump mixer was devised in an effort to distinguish between these two effects (i.e. pressure and mixing) as no significant mixing enhancement was expected with the single hump. The flow with the single hump mixer remains two-dimensional allowing easier analysis of data.

Experimental data consists mainly of static pressure measurements along the top and lower walls of the model, and a few heat transfer measurements. The experimental data is currently being analyzed, however, an example of the preliminary results can be seen in figure 3. The figure shows static pressure along the lower surface of the model (i.e. the surface containing the wall injector), normalized by the shock tube stagnation pressure, at an "absolute" time of 5 ms, or approximately 1.5 ms after incident shock reflection in the shock tube. The free stream test gas consists of air at a nominal stagnation enthalpy of 8.8 MJ/kg. The figure compares a run when hydrogen fuel was injected (RUN 709 , $P_{0,H2}$= 200 kPa) with a similar run when no fuel was injected (RUN 712 , $P_{0,H2}$= 0 kPa). There is a noticeable, but small, difference between the fuel on and fuel off pressure traces for this low injection pressure case. Also shown on the figure is the result when the 4 hump mixer is added to the lower wall, downstream of the injector (RUN 759 , $P_{0,H2}$= 200 kPa). Unlike the result without the mixer, a significant pressure rise can be observed at the downstream end of the duct. This data will have to be looked at in the context of other experimental (and numerical) results before a definite conclusion can be drawn as to whether this is a genuine improved mixing effect, or whether it is due to shock waves (or both). Unfortunately the single hump mixer was not tried at a similar hydrogen injection pressure in order to make a comparison with the above results.

Experimental work on the wall injected scramjet configuration will continue into 1990. During the year it is hoped that a new mixer design will be tested, along with some perpendicular injection experiments. The T4 shock tunnel is now also equipped with a Mach 4 nozzle, which will do away with the need for the wedges placed in front of the inlet to the model.

REFERENCES

1. Morgan, R.G., Paull, A., Morris, N., and Stalker, R.J., "Scramjet Sidewall Burning - Preliminary Shock Tunnel Results", University of Queensland, Dept. of Mechanical Engineering Research Report No. 12/85, NASA Contract NAGW-674, 1985.

2. Morgan, R.G., Paull, A., Morris, N., and Stalker, R.J., "Further Shock Tunnel Studies of Scramjet Phenomena", University of Queensland, Dept. of Mechanical Engineering Research Report No. 10/86, NASA Contract NAGW-674, 1986.

3. Brescianini, C.P. and Morgan, R.G., "Numerical Modeling of Sidewall Injected Scramjet", contribution to Shock Tunnel Studies of Scramjet Phenomena, NASP CR-1023, NASA CR-181721, 1988.

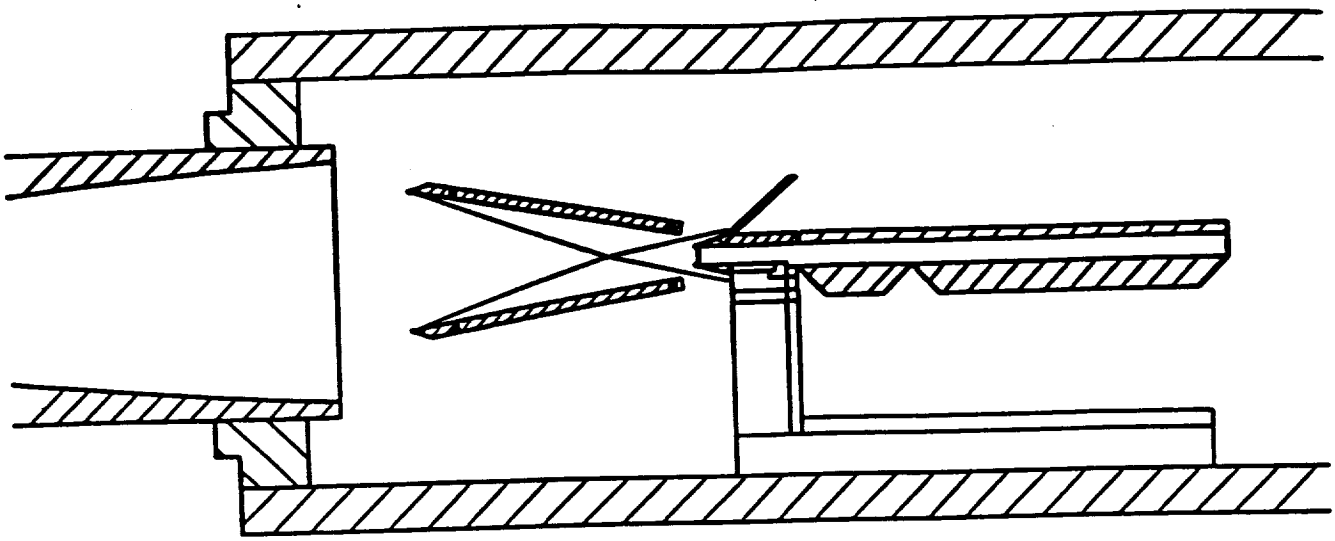

Figure 1 Scramjet Model in Shock Tunnel Test Section

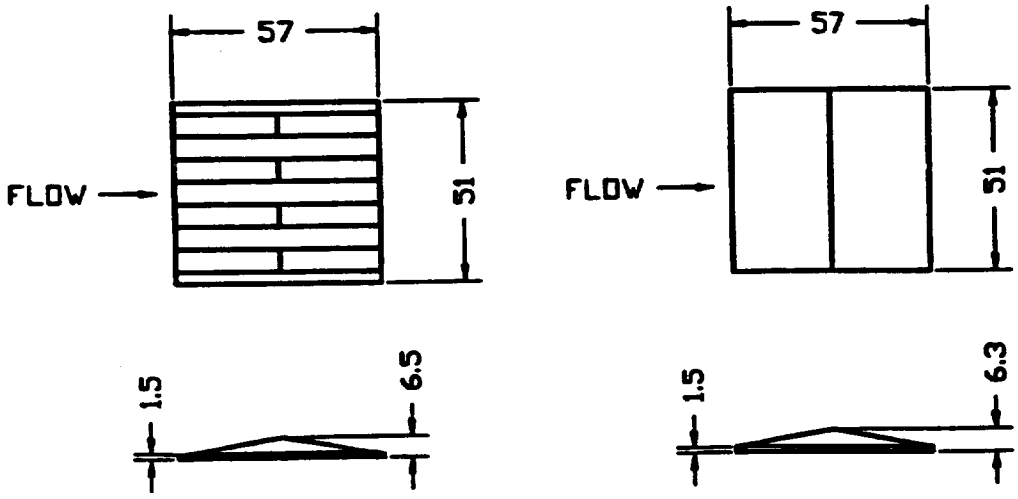

Figure 2(a) Four Hump Mixer Figure 2(b) Single Hump Mixer

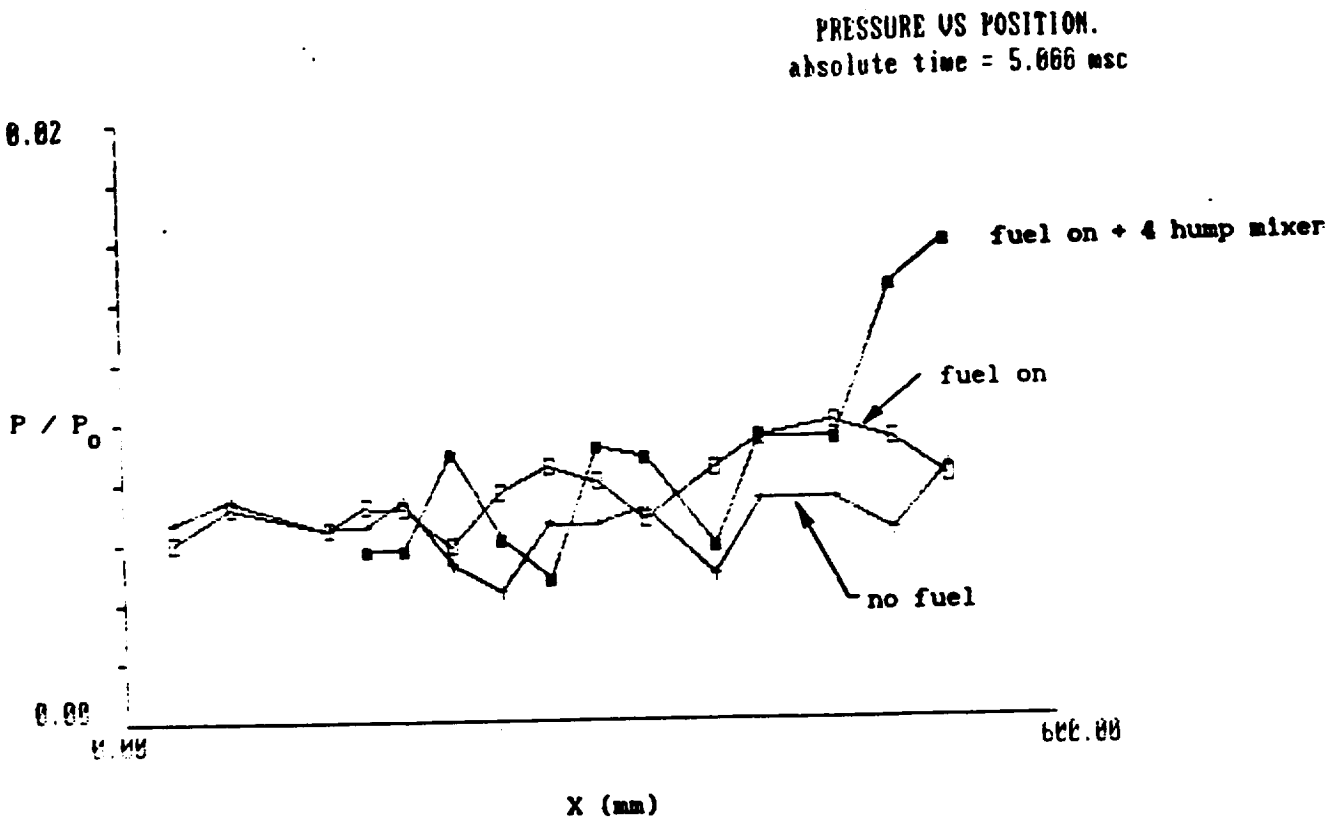

Figure 3 Normalized Static Pressure on Lower Surface of Scramjet Model

SUPERSONIC COMBUSTION WITH TRANSVERSE, CIRCULAR WALL JETS

R.G. Morgan, R. Casey (Mechanical Engineering Department)

The University of Queensland

ABSTRACT

A series of experiments are reported using inclined circular wall jets in rectangular scramjet combustion chambers configured as constant area ducts. A Free Piston shock tunnel was used to create inlet flow Mach numbers between 4.2 and 5.5, at enthalpies corresponding to flight speeds of between 3.5 and 5.3 km/s Measurements of duct static pressure levels indicated that significant mixing and combustion was achieved. Using hydrogen as a fuel, it was found that multi-point injection from two sides of the duct gave a larger, and more rapid pressure rise.

In hypersonic flow it was found that combustion only occurred for the duct dimensions and operating conditions that support combustion with central injection from a 2 dimensional strut.

1.0 INTRODUCTION

To achieve efficient combustion in an air breathing combustor, mixing must take place on a scale varying from the molecular, to a characteristic duct dimension. In a two dimensional flow situation the mixing layer must propagate from the injection point to the duct walls, or to a plane of symmetry if multi layer injection is used, Figure 1.

In this instance, the primary requirement is to allow adequate axial length in the combustion chamber for the mixing layer to speed across the duct. Because of the 2 dimensional nature of the flow, the transverse length scale is decoupled and, except for the edge effects, the inlet aspect ratio is not a consideration.

However, in a flight configuration it may be necessary to depart from 2 dimensional flows. Central, parallel injection has been shown to be effective in supersonic flow, (reference 1), but there are likely to be structural problems with struts spanning the flow in real flight. Two dimensional injection has been used from a wall, with both parallel an transverse components, (reference 2), but the results were not very promising. In particular, as the combustion chamber mach number increases, the rate of spread of a two dimensional mixing layer is known to decrease, (reference 3).

Mixing may in principle be enhanced by using 3 dimensional configurations which allow the fuel jet to penetrate into the free stream flow. For instance, a circular jet as shown in Figure 2 may have sufficient momentum normal to the flow direction to carry fuel right across the duct.

However, the fact that injection is now from discrete stations, rather than as a continuous sheet means that the jet has an extra dimension to spread in, and that the mixing will be a more complicated process.

For purposes of analysis it is convenient to treat the combustion chamber as a number of cells, each centered on a circular jet. Apart from differing boundary conditions, i.e. walls as opposed to planes of symmetry, the cells are considered

to be identical with respect to the major features of the flow.

Intuitively, it would seem that the overall length scale of the cells, and the aspect ratio would be important parameters for this sort of injection. The length scale determines the total cross flow distance over which the fuel has to be transported, and the aspect ratio gives a measure of the relative required in the two transverse dimensions propagation. Work performed at the NASA Langley Research Center, (reference 4), has indicated that a width to height ratio of 2:1 may be optimal for achieving good mixing throughout the cell. This shape is consistant with the assumption that the primary mechanism for large scale mixing is the formation of circular vortices on both sides of the fuel jet.

The experiments reported in this paper were designed to test the effectiveness of the injection concept in both supersonic and hypersonic flows.

2.0 APPARATUS

The facility used for the tests reported here was the Free Piston shock tunnel, T4 at the University of Queensland, (reference 5). The model used was a constant area duct, Figure 3 configured for single or two point injection from one, or both sides of the duct. The duct could be configured with an intake cross section with nominal dimensions 25 mm high by 50 mm wide, or 50 mm square.

From Figure 4 it can be seen that 3 basic configurations are available which preserve the 2:1 aspect ratio.

Comparisons between configurations A and B, Figure 4 involve a change of length scale, and boundary conditions, as 2 walls are replaced by a plane of symmetry. Comparisons between configurations A and C involve only a change in boundary conditions, as one wall is replaced by a plane of symmetry.

Using the same apparatus it is evidently possible to produce for comparison other intake aspect ratios, Figure 5. Not all available configurations were tested. Injection was through sonic throats, inclined at 30° to the flow direction and flush with the wall surface, Figure 6. The fuel was supplied from a Ludweig tube

reservoir, (reference 6), with equivalence ratio being controlled by the reservoir pressure. When comparing single and multipoint injection, i.e. configurations A and B Figure 4, the total throat area was maintained constant. This was done so that the primary jet parameters of dynamic pressure ratio, mach number and temperature would be conserved at a given equivalence ratio.

In calculating the fuel jet flow properties, it was assumed that the injectant expands isentropicaly from the throat conditions to the free stream static pressure level.

3.0 RESULTS

In table 1 a manifest of the runs performed in this series of tests is presented. The characteristic dimension chosen to categorize the cell sizes is the diagonal. Note that this refers not to the external duct geometry but to the size of the similar interval units which the injection pattern creates Figure 4. In table 2 a summary of the test conditions is given.

The first test was primarily to determine if combustion would occur at all, and configuration A, Figure 4 was used. The results are displayed for an enthalpy of 6 mj/kg in Figure 7, as a plot of static pressure against distance down the duct. The static pressure levels are normalized by the shock tube stagnation pressure to compensate for minor variations between runs. An indication of combustion was given by comparing the relative pressure rises produced by injecting fuel into air, and fuel into a flow of nitrogen at the same conditions.

At this stage, a problem of interpreting the results of 3D flow data becomes apparent. In 2D flow a single static pressure monitoring point is adequate to fully define the wall static pressure at any axial location.

To do the same thing in a flow where the pressure may vary in any of 3 dimensions requires a 2 dimensional array of pressure transducers for all surfaces of interest. Such instrumentation was beyond the scope of the present series of experiments, and the pressure monitoring points were mainly located on the center line. This introduces the possibility that the pressure at the point chosen for

the measurement might be significantly different than the average wall static pressure at the axial location. This data should therefore be interpreted with care, especially when trying to compare the efficiency of different injection configurations which produce different cross flow pressure profiles.

Some indication of the order of the transverse pressure changes which apply is given by the 2 transducers mounted 335 mm from the intake. One of them is on the centerline, and the other is offset. A difference in pressure was sometimes measured by these transducers, as seen for instance in the injection into nitrogen data in Figure 7. Transverse pressure gradients in supersonic flow create a wave pattern, the overall effect of which is to reduce the pressure difference. The data was obtained in a duct with a length to height ratio of 30, and a length to width ratio of 15. This would allow for multiple reflection of waves within the duct, so that a local perturbation to the transverse pressure profile would not be maintained throughout the length of the duct. In Figure 7 it is seen that the increased pressure measured when injecting fuel into air, as opposed to nitrogen, is sustained over a substantial length of the duct. This is taken as evidence of a genuine combustion effect, rather than an accident of transducer location in a complicated flow field.

Another indication that transverse pressure gradients, in either direction, are not unduely distorting the measurements is given in Figure 8. Pressure measurements were taken on the top and bottom surfaces simultaneously, and are represented by the symbols + and x, without lines. The axial development of pressure with distance is seen to be sensibly the same on both sides of the duct.

Using the same configuration, the tests were repeated at two different stagnation enthalpies. The results, presented in Figure 9, show no significant temperature dependency. This is surprising, as the static temperature levels were varied between 1200 and 3075k, over which range a significant change in combustion heat release would be expected. The injection conditions for the 3 different enthalpies are included in table 1A, and are seen to be similar in jet mach number and dynamic pressure ratio.

The model was then re-configured as shown in Figure 4B, in order to investigate

the effects of varying the length scale of the mixing cells, but maintaining the 2:1 aspect ratio. In Figure 8 a comparison is shown at an enthalpy of 6 mj/kg and an equivalence ratio of approximately 1 of the effect of the cell size. It is seen that a significantly increased pressure rise occurred with smaller cells. This is an intuitively sensible result, as the large scale eddies have to decay over a smaller range before molecular mixing is complete.

Fuel was again injected into nitrogen test gas to confirm that the pressure rise was combustion induced. In Figure 10, the fuel into nitrogen profiles for both configurations are shown. It is seen that without reactions, the presence for 4 inert jets does not significantly after the duct static pressure levels.

This configuration was also tested at 13.9 mj/kg, Figure 11 and it was again seen to give larger pressure rise than the single jets. However, once again it was noted that the pressure profiles were not strongly temperature sensitive, (Figure 12). Combustion of a given fraction of the fuel would be expected to generate a larger pressure rise in the low enthalpy, cold test gas. The fact that this effect was not observed suggests that either more fuel was burned in the high enthalpy flow, or that for some reason the heat release was enhanced.

The dissociated test gas at the higher enthalpies provides a possible mechanism for extra heat release due to the heat of formation of oxygen molecules. When combustion is from atomic rather than molecular oxygen the effective heat of combustion is increased. However, this would be in contradiction to previous results in a supersonic constant area duct using two dimensional injection, where the pressure rise was lower at the higher enthalpies.

The model was then reconfigured as a 50x50 mm^2 duct with injection from single holes on the top and bottom surfaces, as shown in Figure 4C. The aspect ratio of 2:1 was preserved, the purpose of the tests was to investigate the effects of changing the boundary condition from a wall to an axis of symmetry. Unfortunately, the model was assembled with nozzles of a smaller area than was used for the 25x50 mm^2 duct tests in Table 1A. This meant that it was not possible to use the same jet conditions to match equivalence ratios for the 2 tests. It was chosen to keep the same injection parameters and to reduce the

equilvalence ratio to nominally 0.5. The results of the two configurations are therefore not directly comparable, but useful data was nevertheless obtained.

The runs performed in this configuration are tabulated in Table 1C. The results are summarized in Figure 13, plotted in the form of pressure difference between injection into air and injection into nitrogen. The smaller duct, with each injection cell enclosed by four walls was seen to give a lower pressure rise downstream in the duct than the larger two cell configuration. However, the difference in the pressure rises is roughly in proportion to the equivalence ratios, and it is tentatively concluded that the changing boundary condition did not leave a major impact on the flow.

The model was then reconfigured with a single jet as shown in Figure 5C, giving a square aspect ratio in a 50x50 mm^2 duct. The runs for this geometry were done with the mach 4 nozzle as tabulated in Table 1D. The equivalence ratio was set at 0.5, and the total nozzle area was unchanged so that a direct comparison with the results of Table 1C could be made.

The results of these tests are shown in Figure 16, in the form of the pressure differentials between injecting fuel into air and into nitrogen test gases. The shape of the surface pressure profiles is evidently different in the two cases, but the overall pressure levels were similar. On the basis of this single comparison, it would be premature to make any conclusions as to the relative efficiencies of the two aspects ratios.

The next series of tests were performed using the hypersonic M5 contoured nozzle to evaluate the circular jets in a hypersonic flow field. The model was configured as in Figure 4B, which had been found the most effective for the supersonic flow. The runs performed in this mode are listed in Table 1E.

The results of these tests are shown in Figure 14. A substantial pressure rise was measured when injecting fuel into air, indicating that circular wall jets may be an effective injection technique in a hypersonic duct. This is similar to the results reported in reference 7, where with central injection it was concluded that the compressive effects of the wall boundary layers were required

to initiate combustion.

When the duct was subsequently enlarged to a 50x50 mm^2 section combustion could no longer be sustained. The dashed line in Figure 14 indicates the theoretical fuel off pressure level in the absence of boundary layers, and the duct pressure is seen to be much higher than this.

The circular jet model was therefore set up as a 50x50 mm^2 duct to see if the same effect reported in reference 7 would be observed. The configuration of Figure 4C was used, and the runs are listed in Table 1F.

The results are shown in Figure 15, and it is seen that no combustion was evident.

4.0 CONCLUSIONS

The results show that 13 wall injection through inclined circular jets can be effective in supersonic and hypersonic combustion chambers. Most of the tests were performed with mixing cells having a width to height aspect ratio of 2:1. Duct static pressure levels rose higher, and more rapidly when the transverse length scale of the mixing cells was reduced.

Preliminary tests indicated that the mixing cell dimensions are the primary parameters governing mixing and combustion, when the injection conditions were maintained constant. Replacing wall boundary conditions with planes of symmetry did not appear to have a major influence on performance in supersonic flow although this test was not rigorous, as injection parameters were changed at the same time. This result, if confirmed, is significant in that combustion chambers could be designed with multiple internal cells, centered on wall jets, based on the results of scale testing of a single cell. A single comparison where the mixing cell aspect ratio was changed to 1:1 did not show a significant difference.

In hypersonic flow the wall jets were found to produce combustion where it had previously been observed with central injection. The range of conditions where

combustion was sustainable in hypersonic flow was not extended by the use of the wall jets.

The axial pressure profiles were found to be largely independent of duct static temperature, and this is not understood at present.

REFERENCES:

1. R.G. Morgan, R.J. Stalker, "Pressures Scaling Effects in a Scramjet Combustion Chamber", 8th Int. Symp. on Air Breathing Engines, Cincinnati, Ohio, June 15-19, 1987

2. R.G. Morgan, A. Paull, N.A. Morris, R.J. Stalker, "Hydrogen Scramjet with Side Wall Injection", I.E. Aust Multidisciplinary Transactions, Vol. GE 11 No. 1, April 1987, pp. 45-51

3. R.M. Thomas, J.A. Shetz, F.S. Billig, "Gaseos Injection in High Speed Flow", 9th Int. Symp. on Air Breathing Engines Athens, Greece, 3-8 September 1989

4. Dr. G. Anderson, NASA Langley Research Center Private Communication 1988

5. R.J. Stalker, R.G. Morgan, "The University of Queensland Free Piston Shock Tunnel T4, Initial Operation and Preliminary Calibration", 4th National Space Engineering Symposium Adelaide, 12-14 July, 1988

6. R.G. Morgan, R.J. Stalker, "Fast Acting Hydrogen Valve", Journal of Physics E Sci. Inst. Vol. 16, 1983 pp.205-207

7. R.G. Morgan, R.J. Stalker, "Hypersonic Combustion of Hydrogen in a Shock Tunnel", 9th Int. Symp. on Air Breathing Engines, Athens, Greece, 3-8 September, 1989.

NOTATION

H_s	Stagnation Enthalpy
P	Duct Static Pressure
P_{sts}	Stagnation Pressure Measured in Shock Tube
U	Velocity of Free Stream
M	Mach Number
Mc	Convective Mach Number Based on Axial Velocity Component
X	Distance from Intake
Uj	Velocity of Injectant after Isentropic Expansion to Free Stream Pressure
ρ	Free Stream Density
ρj	Density of Injectant after Expansion

TABLE 1. RUN MANIFEST

A. 50x25 mm^2 Duct, Single Injector Diameter 7mm, Configuration Fig. 4A, Mach 4 Nozzle

Run Number	Hs(mj/kg)	ϕ	$Uj_{(m/s)}$	Mj	$\rho_j U_j^2/\rho u^2$	Mc
1380	6.1	0	2150	2.38	0.29	0.782
1381	6.1	1	2150	2.38	0.29	0.782
1382	6.1(N2)	-	2150	2.38	0.29	0.782
1385	6.1	0.8	20% Si_4H_4/H_2 mixture			
1383	9.1	1	2072	2.2	0.32	0.97
1384	13.9	1	1990	2.04	0.31	1.25

B. 50x25 mm^2 Duct, 4 Injectors Diameter 3.45 mm, Configuration Fig. 4B, Mach 4 Nozzle

Run Number	Hs(mj/kg)	ϕ	$Uj_{(m/s)}$	Mj	$\rho_j U_j^2/\rho u^2$	Mc
1386	6.1	1	2150	2.38	0.29	0.782
1388	6.1(N2)	-	2150	2.38	0.29	0.782
1389	13.9	-	1960	1.98	0.301	1.25
1391	13.9(N2)	-	1960	1.98	0.301	1.25
1392	13.9	0				
1383	9.1	1	2072	2.2	0.32	0.97
1384	13.9	1	1990	2.04	0.31	1.25

C. 50x50 mm^2 Duct, 2 Injectors Diameter 5 mm, Configuration Fig. 4C, Mach 4 Nozzle

Run Number	Hs(mj/kg)	ϕ	$Uj_{(m/s)}$	Mj	$\rho_j U_j^2/\rho u^2$	Mc
1399	6.1	0.5	2210	2.53	0.33	0.76
1400	6.1(N2)	-	2130	2.33	0.315	0.79
1401	6.1	0				

D. 50x50 mm^2 Duct, 1 Injector Diameter 7 mm, Configuration Fig. 5C, Mach 4 Nozzle

Run Number	Hs(mj/kg)	ϕ	$Uj_{(m/s)}$	Mj	$\rho_j U_j^2/\rho u^2$	Mc
1403	6.1	0.5	2170	2.43	0.32	0.77
1400	6.1(N2)	-	2170	2.43	0.32	0.77
1401	6.1	0				

D. 50x50 mm² Duct, 1 Injector Diameter 7 mm, Configuration Fig. 5C, Mach 4 Nozzle

Run Number	Hs(mj/kg)	ϕ	$Uj_{(m/s)}$	Mj	$\rho_j U_j^2/\rho u^2$	Mc
1403	6.1	0.5	2170	2.43	0.32	0.77
1400	6.1(N2)	-	2170	2.43	0.32	0.77
1401	6.1	0				

E. 50x25 mm² Duct, 4 Injectors Diameter 3.45 mm, Configuration Fig. 4B, Mach 5 Nozzle

Run Number	Hs(mj/kg)	ϕ	$Uj_{(m/s)}$	Mj	$\rho_j U_j^2/\rho u^2$	Mc
1394	8.4	1	2290	2.74	0.265	1.14
1395	8.4(N2)	-	2290	2.74	0.265	1.14
1396	8.4	0				

F. 50x50 mm² Duct, 2 Injectors Diameter 5 mm, Configuration Fig. 4C, Mach 5 Nozzle

Run Number	Hs(mj/kg)	ϕ	$Uj_{(m/s)}$	Mj	$\rho_j U_j^2/\rho u^2$	Mc
1397	8.4	0.5	2290	2.74	0.265	1.14
1398	8.4(N2)	-	2290	2.74	0.265	1.14
1396	8.4	0				

TABLE 2 TEST CONDITIONS

A. Nominal Mach 4 Nozzle

Flight Speed Km/s	$Hs_{(mj/kg)}$	P(kpa)	T(k)	$U_{(m/s)}$	$\rho(kg/m^3)$	M	ρu Kg/s/m²
3.5	6.1	71	1200	3110	0.2	4.5	622
4.3	9.1	97	2025	3520	0.165	4.2	580
5.3	13.9	109	3075	4120	0.1168	4.35	481

B. Nominal Mach 5 Nozzle

Flight Speed Km/s	$Hs_{(mj/kg)}$	P(kpa)	T(k)	$U_{(m/s)}$	$\rho(kg/m^3)$	M	ρu Kg/s/m²
4.1	8.4	20.5	1160	3700	.0609	5.54	225

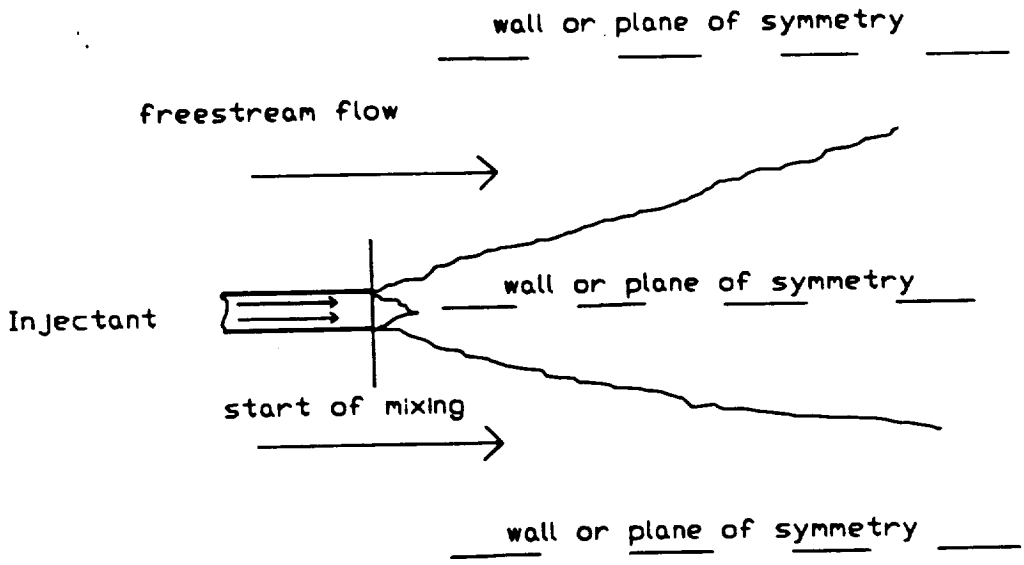

Fig 1, Two dimensional mixing layer.

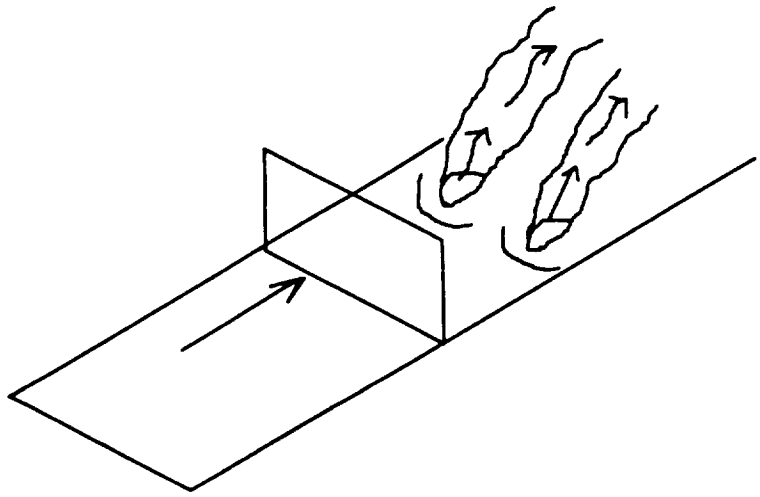

Fig 2 Transverse circular wall jets

Shock tunnel nozzle

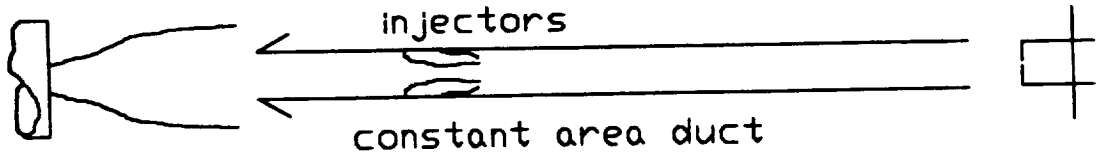

Fig 3 Constant area duct configuration.

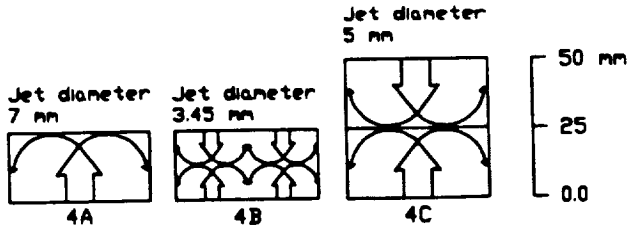

Fig 4 configurations conserving 2:1 aspect ratio

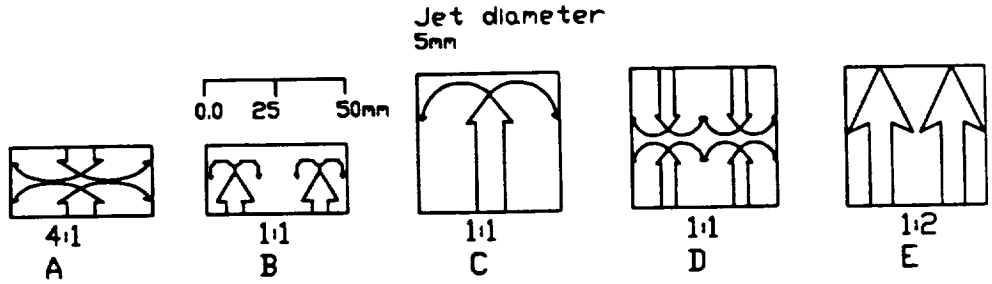

Fig 5 Alternative aspect ratios with sc ramjet geometry.

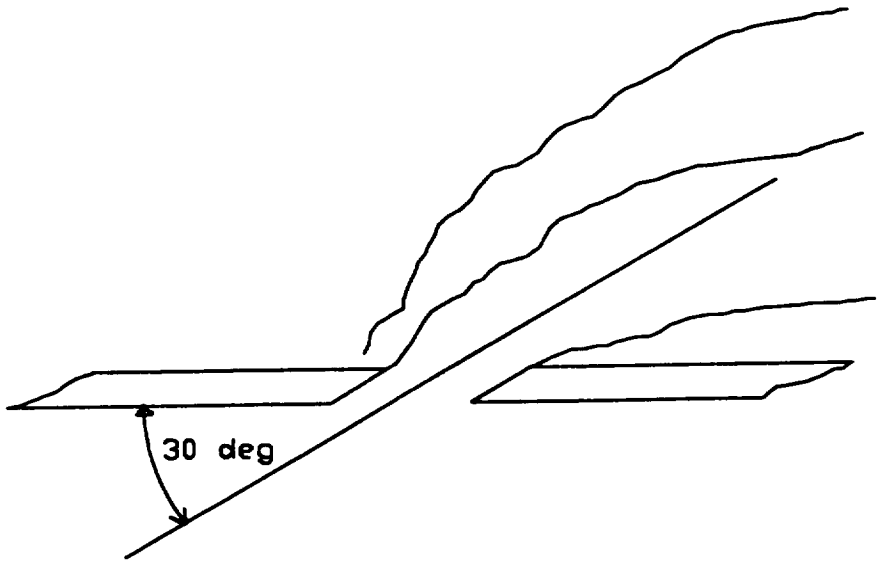

Fig 6 injector schemtatic.

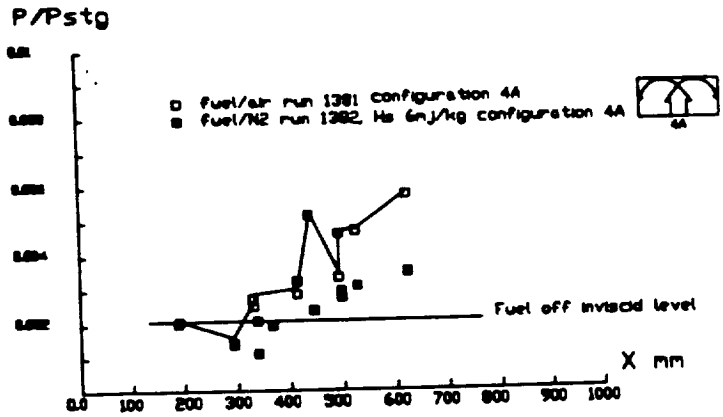

Fig 7 P/X 25*50mm duct, single injector supersonic flow @M4, Hs 6mj/kg

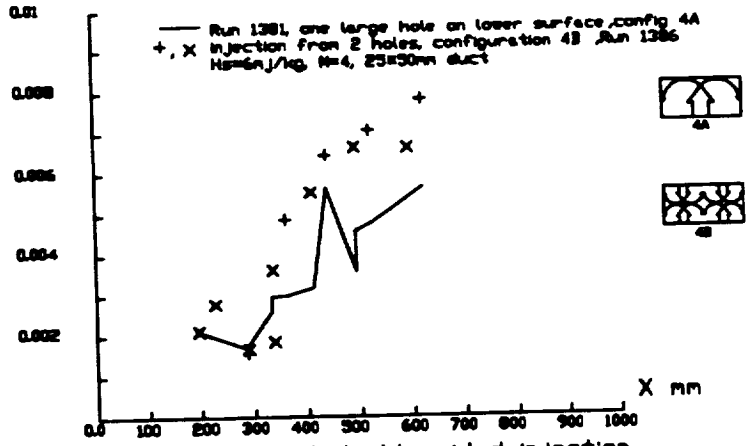

Fig 8 P/X single and double sided injection 25*50 mm duct, supersonic flow @ M4

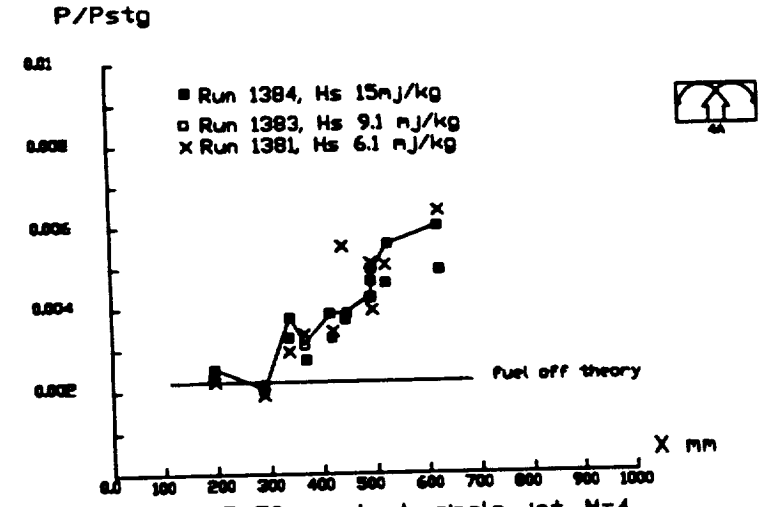

Fig 9,P/X 25*50 mm duct, single jet, M=4 effect of stagnation enthalpy

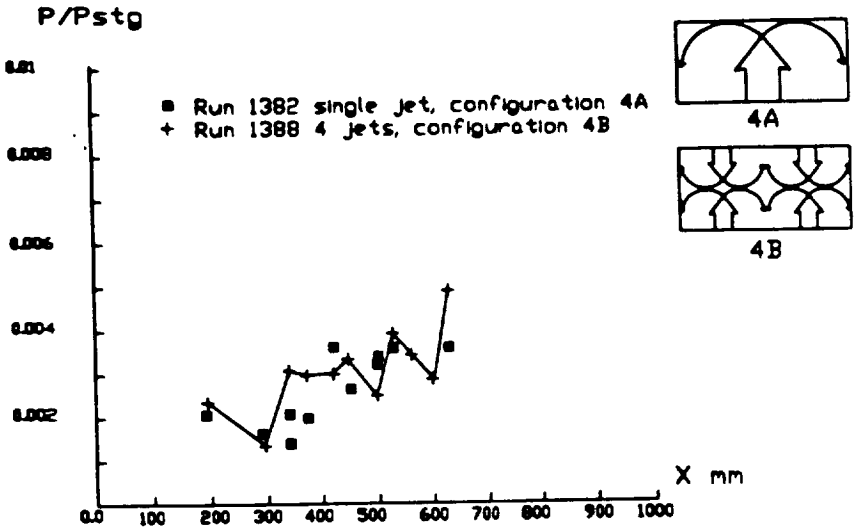

Fir 10, Hydrogen injection into nitrogen, 25*50 mm duct.
Effect of injector configuration.

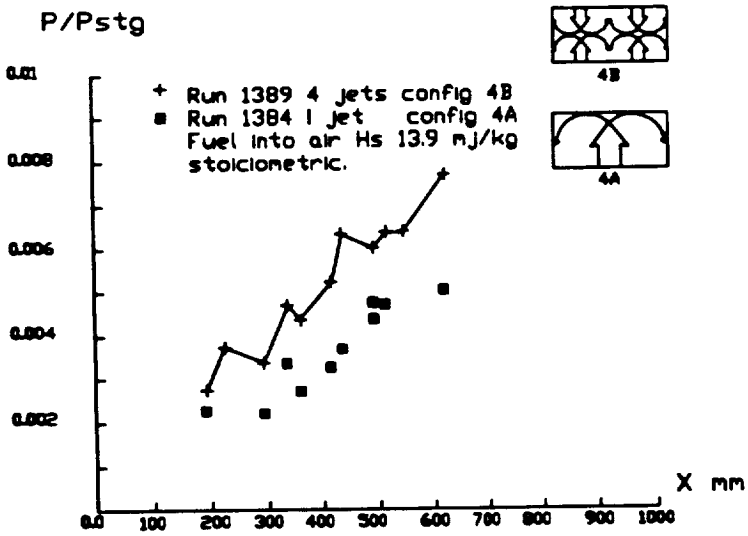

Fig 11 Effect of internal length scale, 25*50mm duct.

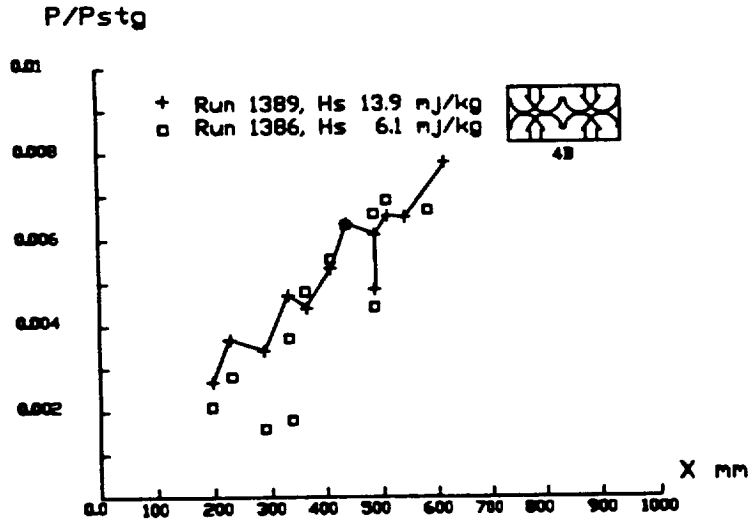

Fig 12 Effect of enthalpy change, 25*50mm duct.
Fuel into air 4 point injection.

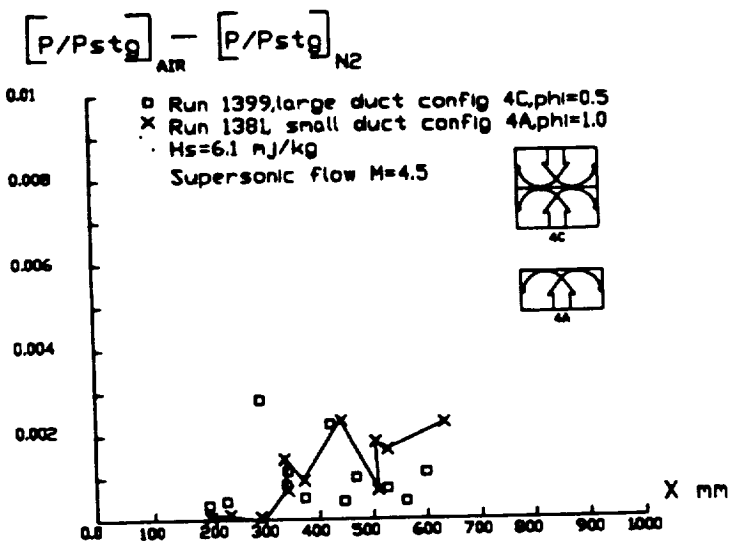

Fig 13. Pressure differentials, injection into air minus injection into nitrogen.

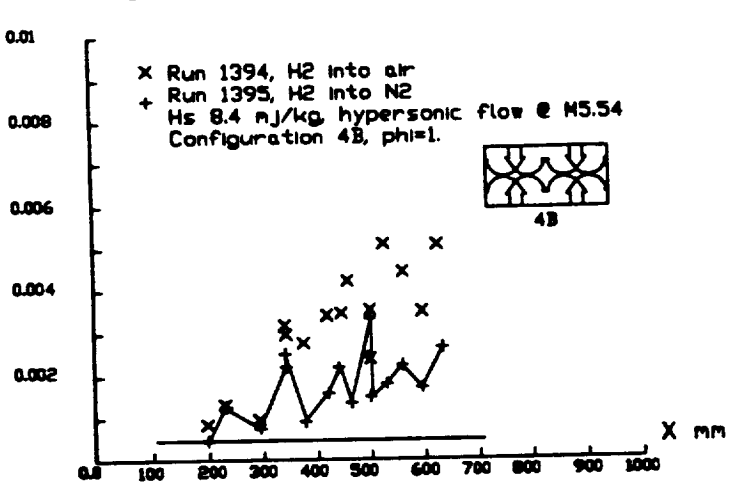

Fig 14, Hypersonic flow, 25*50 mm duct, 4 point injection, nitrogen/air comparison.

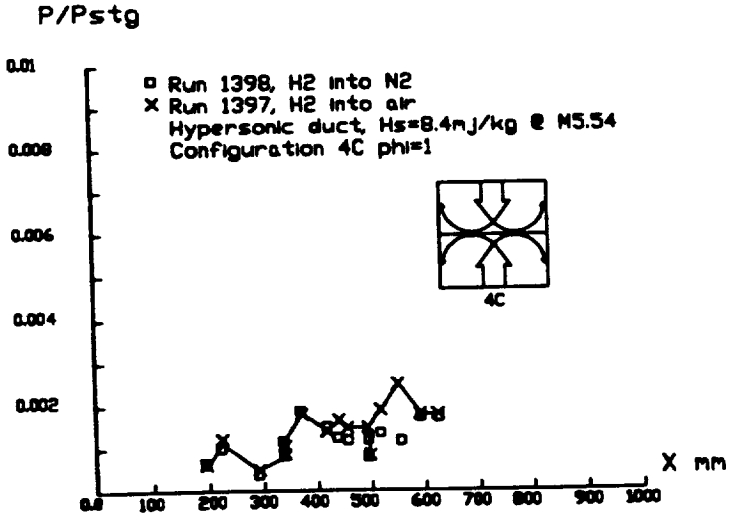

Fig 15, Hypersonic duct 50*50 mm, 2 point injection comparison of injection into air and nitrogen.

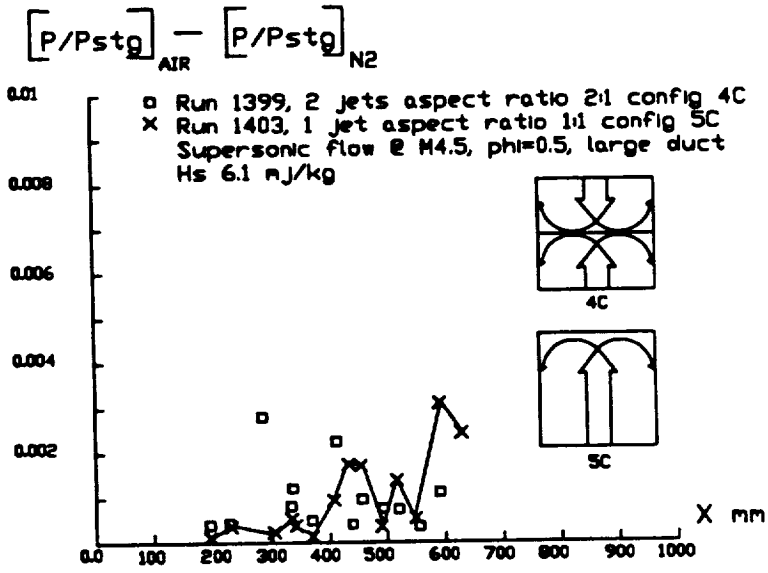

Fig 16, Effects of internal aspect ratio on pressure differential, large duct 50*50mm.

"DISSOCIATED TEST GAS, EFFECTS ON SCRAMJET COMBUSTORS"

R.G. Morgan, Mechanical Engineering, The University of Queensland

ABSTRACT

The problem of the dissociated test gas produced by reflected shock tunnels is addressed as it relates to heat release in supersonic combustors. When hydrogen burns with dissociated oxygen atoms, the heat of formation of the oxygen adds to the normal enthalpy of combustion. It is proposed that this effect be compensated for by reducing the oxygen concentration of the test gas. A procedure for doing this is presented based on a simple heat balance approach. One dimensional computations of premixed reacting flow are used to support the calculations. It is suggested that direct simulation of the flow in a combustor is achieved if the oxygen adjustment is made.

NOTATION

α	mass fraction of total oxygen in the form of O atoms
α_N	" " " " " " " " NO molecules
ϕ	equivalence ratio
ϕ^*=	ϕ for ϕ < 1, = 1 for ϕ > 1
h_c	heat of combustion of H2 from O2 (90 Mj/kg H2)
h_f	heat of formation of O atoms from O2 (15.7 Mj/kg)
h_n	heat of formation of NO Molecules from N2 + O2 (2.93 Mj/kg)
h_m	heat release per of combustion products
O2	mass fraction O2
O	mass fraction O
N2	mass fraction N2
NO	mass fraction NO
X	mass fraction total O content
X_a	mass fraction total content in "ideal" air
P	static pressure
u	velocity
p	density
T	temperature
M	Mach No.
H_s	stagnation enthalpy

INTRODUCTION

Wind tunnel facilities have traditionally had a dual role as a tool for the investigation of Aerodynamics phenomena. Firstly they may be used to study fundamental physical processes, using models which may not necessarily relate directly to flight configurations. Secondly, they may be used for the testing of models where the results may be used directly, with appropriate scaling laws, to indicate the performance of flight hardware. Since the advent of high speed computers wind tunnels have increasingly been used for the validification of computer codes rather than for direct simulation. This application may be said to combine the two roles mentioned above, with the code being validated using contrived models, but subsequently being applied to real flight configurations.

In recent times some doubt has been expressed as to the value and usefulness of the direct simulation role of high speed wind tunnels. This particularly relates to hypersonic combustion where the dissociated test gas produced by ground facilities leads to changes in chemical kinetics and an increase in the effective enthalpy of combustion. It is the contention of this paper that these problems can be adequately addressed, and that direct simulation is still necessary given the current status of numerical and analytical understanding.

The test flow in a reflected shock tunnel is created by means of a steady expansion from the stagnation region in the shock tube. The gas in the stagnation region is approximately in a condition of equilibrium composition due to the high density levels and the low velocity. At the stagnation enthalpies corresponding to high flight speeds, the stagnation temperatures are such that significant dissociation occurs to the nitrogen and oxygen molecules. As the flow starts to travel down the expansion nozzle, the temperature drops and the equilibrium composition shifts towards a reduced dissociated content. However, due to the high particle velocities and lower density in the nozzle, reaction rates may in some circumstances be inadequate to maintain equilibrium composition. The test gas at the nozzle exit will therefore have a frozen content of dissociated radicals created in the stagnation region. The higher the stagnation enthalpy, the higher will be the concentration of dissociated gas.

The presence of the dissociated components may effect the flow in several ways. Some of the stagnation enthalpy will be stored as the atomic heat of formation, and will not be converted directly to thermal or kinetic energy. It is important, when comparing the results of shock tunnel tests with real flight, or with other tunnels which do not produce dissociated air, to match the total enthalpy including thermal, chemical and kinetic components. If the flow is subsequently processed by a strong shock, then the increased pressure and density levels lead to rapid reaction rates and the establishment of near equilibrium conditions, with the recovery of the heat of formation.

When the flow is subsequently expanded around the body, it will be insensitive to the gas condition upstream of the shock. In these circumstances very little difference will be observed between shock tunnel tests and tests on an ideal wind tunnel producing undissociated test gas.

For the purposes of aerodynamic testing, Mach number independence applies for flows behind a strong shock, and matching of the total enthalpy has been shown to give good simulation of flight conditions. However for shock tunnel testing of scramjets the situation is slightly different. The flow is never processed by a strong shock, and non equilibrium gas composition persists throughout the duct.

The presence of free stream oxygen atoms may have a significant effect on combustion and it has to be examined closely. There are three main mechanisms by which the free stream oxygen atoms may be seen to enhance combustion, and influence comparisons made between shock tunnel experiments and real flight.

(i) Combustion heat release. When combustion is from the atomic oxygen form, the heat of formation is added to the combustion heat release. This increases the net energy release from approximately 90 Mj to 215 Mj per kg of hydrogen burned. This is clearly a substantial increase, and relatively small oxygen dissociation fractions may be significant.

(ii) Ignition delay times. Forming of oxygen radicals is a necessary step in the combustion of hydrogen, and the pre dissociated shock tunnel flow may be expected to react faster than ordinary air.

(iii) Mixing Effects. In some circumstances a scramjet may be considered to be a pure diffusion flame, where reaction rates are so fast that heat release is mixing controlled. Oxygen molecules have different diffusion rates than the atoms, and the local chemical composition will effect the rate of heat release. Furthermore, the macroscopic development of the fuel air mixing layer is dependent on the local flow properties such as Reynolds number, this may also be influenced by the dissociated oxygen content.

For a given static pressure, dissociated oxygen increases the partial pressure of the oxygen components, effectively enhancing mixing and combustion.

In this report only the first mechanism will be addressed, that of predicting, and allowing for, the enhanced heat release due to the chemical enthalpy of the dissociated oxygen. The shock tunnel oxygen composition is adjusted in such a way that the net heat release ofcombustion is conserved, when compared to tests in undissociated air. In this way it is possible to produce pressure profiles which decouple the effects of differing levels of free stream dissociation, and allow a direct comparison between shock tunnel experiments and tests using undissociated air.

However, the heat release per unit mass of fuel is still higher, despite the reduced free stream oxygen content, and this should be taken into consideration when comparing specific impulse measurements.

ANALYSIS

The comparison of wind tunnel tests with flight conditions generally involves scaling of a number of flow parameters. When dealing with high energy shock tunnels, an additional uncertainty arises due to the difference in gas composition. The scope of this paper is to address the difference between a wind tunnel using dissociated oxygen and nitrogen, and an idealised wind tunnel using air with normal atmospheric composition. The more generalised problem of comparing an idealised wind tunnel and free flight is well understood, and is not considered here.

Analysis of the reacting nozzle flow using a non-equilibrium chemical kinetics code, Ref. 1 indicates there are 4 significant species present as far as hydrogen combustion is concerned, namely N2, O2, NO, O.

Combustion to water from the 3 oxygen bearing constituents proceeds with heat release as indicated below

(i) $H_2 + \frac{1}{2} O_2 = H_2O + 120.6$ Mj/kg H2
(ii) $H_2 + O = H_2O + 246$ Mj/kg H2
(iii) $H_2 + NO = H_2O + \frac{1}{2} N_2 + 164.6$ Mj/kg H2

Note These equations are not intended to represent reaction schemes, but are used to calculate energy release between end products.

Combustion of undissociated air involves only reaction from oxygen molecules, and may be seen to give significantly less heat release than the two other main combustion paths. The approach of this paper is to apply a correction to the free stream oxygen concentration in order to match the heat release. In other words the shock tunnel tests would be performed with a reduced oxygen concentration intended to reproduce the results of combustion in atmospheric air with the same flow properties.

The primary measured experimental parameter in scramjet testing is duct static pressure level, and corrections made to the oxygen levels would be calculated to produce identical pressure/distance profiles in the two test facilities. To match this exactly a numerical simulation is required which fully evaluates the changes in combustion species

composition produced by changing the free stream oxygen level. However, the approach of this paper is to do a first order correction based on the heat release of the three reaction mechanisms identified above. Numerical simulation is then performed to assess the validity of this approach. A series of experiments is envisaged for 1990 to evaluate the concept. The analysis of this preliminary paper is based on 1D premixed fuel/air flow.

The heat release of 120.6 mj/kg for reaction (i), combustion from oxygen molecules, is based on combustion to water alone. The equilibrium composition of a hydrogen flame contains dissociated radicals, and the full heat release is not achieved. A heat release of 90 mj/kg H2 is more representative of that developed in a real combustion chamber, and this value is used here.

For a kilogram of test gas the number of moles of each species will be as follows:

$$\left.\begin{array}{l} \dfrac{X\alpha}{16} \quad \text{of atomic oxygen} \\ \dfrac{X\alpha_n}{16} \quad \text{of NO} \\ \dfrac{X}{32}\,(1-\alpha-\alpha_n) \quad \text{of molecular oxygen} \\ \left\{1 - X\left[1 + \alpha_n\dfrac{14}{16}\right]\right\}\dfrac{1}{28} \quad \text{of molecular nitrogen} \end{array}\right\}$$

This will require $\left\{\dfrac{X\alpha}{26} + \dfrac{X(1-\alpha-\alpha_n)}{16} + \dfrac{X\alpha_n}{16}\right\}\phi$ moles of molecular hydrogen to establish the equivalence ratio ϕ.

The idealised reaction scheme for the 4 component air mixture is therefore as given below:

$$\frac{X\alpha}{16}\,[O] + \frac{X\alpha_n}{16}\,[NO] + \frac{X}{32}\,(1-\alpha-\alpha_n)\,[O2] + \left\{1-X\left(1+\alpha_n\ \ \frac{14}{16}\right)\right\}\frac{1}{28}\,[N2]$$

$$+\left\{\frac{X\alpha}{26} + \frac{X(1-\alpha-\alpha_n)}{16} + \frac{X\alpha_n}{16}\right\}\phi\,[H2]$$

$$= \left\{\frac{X\alpha}{16} + \frac{X\alpha_n}{16} + \frac{X}{16}\,(1-\alpha-\alpha_n)\right\}\phi^{\bullet}[H2O] + \frac{X\alpha_n}{32}\,\phi^{\bullet}[N2] + \left\{1-X\left(1+\frac{\alpha_n\ 14}{16}\right)\right\}\frac{1}{28}\,[N2]$$

↑ ↑ ↑ ↑ ↑

from O (add h_f) — from NO (add h_n) — from O2 (h_c) — from NO — original free H2

$$+\frac{X}{32}\,(1-\alpha-\alpha_n)(1-\phi^{\bullet})[O2] + \frac{X\alpha_n}{16}(1-\phi^{\bullet})[NO] + \frac{X\alpha}{16}(1-\phi^{\bullet})[O] + \frac{X}{16}(\phi-\phi^{\bullet})\,[H2]$$

↑ ↑ ↑ ↑

residual O2 — residual NO — residual O — residual N2

$$+ \text{ heat release } \left\{\frac{X}{16}\,2\,h_c + X\alpha\,h_f + X\alpha_n\,h_n\,\frac{30}{16}\right\}\phi^{\bullet} \qquad (4)$$

↑ ↑ ↑

heat release from $H2, O2 \rightarrow H2O$ — heat release converting $O \rightarrow O2$ — heat release converting $NO \rightarrow N2, O2$

where [ ] denotes a mol of a species.

The function $\phi^{\bullet}$ is used to allow for equivalence ratios other than 1 where there is either unburned fuel of oxidant.

$$\text{For} \qquad \begin{matrix} \phi < 1\ ,\ \phi^{\bullet} = \phi \\ \phi > 1\ ,\ \phi^{\bullet} = 1 \end{matrix}$$

The coefficients on the RHS of Eq. (4) may evidently be simplified slightly, but they are presented here in full in order to clearly illustrate the origin of the end products. For equivalence ratios of

less than 1 it is assumed that the O, O2 and NO are consumed in equal proportions.

Lowering the oxygen mass fraction reduces the heat release, as may be seen from inspection of Eq. 4. However, the question arises as to the flow parameter against which the heat release should be conserved when comparing different test facilities. With respect to the fuel content, energy release is a function only of α and α_n, and cannot be matched by changing the total oxygen mass fraction. Comparisons of measured specific impulse therefore will still have to be adjusted to correct. For the effective change in fuel calorific value even if oxygen depleted test gas is used.

Ideally the heat added due to combustion at a given equivalence ratio should release the same amount of heat when normalised by the stagnation enthalpy. When comparing results at a given stagnation enthalpy, this is equivalent to matching heat release per unit mass of air flow. However, reducing the oxygen content changes the composition of the combustion products, and therefore conserving heat release on a unit mass basis will lead to different pressure rises in the two cases.

For the purposes of this study it was chosen to conserve heat release per unit mol of combustion product. To a first order this should lead to the same pressure rise, and should create the same wave pattern and flow field for the 2 cases. This is considered to be of fundamental importance for scramjet ducts, which can only be analysed correctly in the light of a full wave capturing treatment, Ref. 8.

The heat release per mol of combustion products is given by

$$h_m = \frac{\phi^* h_c \left(1 + \frac{8\alpha h_f}{h_c} + 15\,\alpha_n \frac{h_n}{h_c}\right)}{\frac{1}{2}\left(2\phi - \phi^* - \alpha\phi^* - \frac{4}{28} + \alpha\right) + \frac{8}{28X}} \qquad (5)$$

From this the modified oxygen mass fraction for the shock tube test gas may be computed to be:

$$X = \frac{32}{28\left\{B\left(A + \frac{32}{28\,X_a}\right) - A - \alpha(1-\phi^*)\right\}} \qquad (6)$$

Where $A = 2\phi - \phi^* - 4/28$ and $B = 1 + \frac{8\alpha h_f}{h_c} + \frac{15\alpha_n h_n}{h_c}$

Note that this mass fraction includes the total oxygen content in all its forms. It is sensitive to O and NO concentrations, which are

functions of flow enthalpy, and also equivalence ratio. The test gas mixture must therefore be specifically targeted to precise test conditions, which will require careful planning for any experimental program.

It is not possible to conserve all the flow parameters when comparing the 'real' and 'ideal' facilities. For instance, the molecular weights of the two test gases will be different, and therefore if flow velocity and temperature are matched then the Mach number will have to be different.

The approach of this paper is to identify certain 'primary flow parameters' which it is thought important to conserve, and small discrepancies will be required in the other parameters in order to achieve this.

The primary flow parameters are as listed below.

(1) Total Enthalpy This is an important parameter as it relates directly to flight speed. Furthermore, it may be calculated with reasonable accuracy from shock speed and pressure measurements. Energy stored in heats of formation for shock tunnel flow means that the balance between kinetic, thermal and chemical storage must change.

(2) Pitot Pressure. This relates directly to the free stream for scramjet flight path evaluation and high altitude performance. Can easily be measured or calculated in most situations.

(3) Static Temperature. This is not normally conserved in hypersonic aerodynamic testing. Mach number independence applies behind strong shocks, and the free stream temperature is allowed to rise so that the total enthalpy can be achieved at a lower Mach number. However, when the combustion chamber alone is modelled, the flow Mach number can be matched quite closely and real static temperature levels can be used. Temperature is so important in combustion processes that it is preferred to conserve temperature at the expense of static pressure.

The total enthalpy restriction means that once a static temperature and gas composition have been selected, then the velocity is prescribed. The pitot pressure restriction then determines the density, and hence the static pressure level. Static temperature and pressure can both be matched, but only at the expense of pitot pressure.

When analysing premixed combustion processes which are meant to represent the combustion of fuel and air jets which were initially separated, it would seem appropriate to calculate an equivalent premixed flow conserving energy, momentum and mass fluxes. However, it has been found in the past, that better agreement with experiment is obtained by using the flow properties of the air, rather than the mixture in the 1D analysis. This may be because in a reacting/mixing process combustion is expected to start in a region with a local equivalence ratio of ~ 0.2, and the flow properties here would be

closer to the free stream values.

In this analysis the flow properties were calculated using the air fluxes only, and the hydrogen was added as a diluent at the calculated temperature and pressure. At this stage it is not important, as the comparison is between analytical and numerical procedures, but it will have to be looked at more closely when experimental comparisons are made.

The effect of the changes in oxygen level were assessed using a 1D chemical kinetics code, Ref. 3, and a 28 reaction hydrogen combustion scheme outlined in table 4. The flow was constrained to follow a constant area duct configuration. The computations were allowed to progress until steady pressure levels indicated that equilibrium composition was being approached.

Results

Representative shock tunnel test conditions were chosen at two enthalpies for the evaluation, having total dissociated oxygen mass fractions (including O and NO) of 0.35 and 0.63. The flow properties and gas composition are presented in table 1 and were calculated according to the procedure outlined in Ref. 2. These are established operating conditions using air, and were obtained using a contoured nozzle with an area ratio of 109.

When modified conditions were postulated with reduced oxygen content the values of α and α_n were assumed to remain constant for ease of computation. To use this analysis in conjunction with experiments the flow conditions would have to be recalculated using experimental data from the new test gas.

At the 2 enthalpies the analysis was performed for equivalence ratios of 0.5, 1 and 2 both for the shock tube and for ideal gas flows.

The modified flow conditions were calculated as described in the previous section, and are displayed in tables 2 and 3. Hydrogen was then added to the air flow to give the target equivalence ratio, maintaining free stream pressure, temperature and velocity.
The predicted pressure-distance profiles are shown in Figs. 1 to 3 for the 13 mj/kg condition. The results show that the shock tunnel with reduced oxygen concentration gives very good agreement with the ideal tunnel, except for the $\phi = 0.5$ case.

Inspection of the species concentration axial profiles indicated that the oxygen atoms were being preferentially consumed in favour of the molecules for equivalence ratios of less than 1. The oxygen adjustment had been calculated assuming that the O, O2 and NO would be consumed in equal proportions when the hydrogen content was not enough for full combustion. This leads to underestimation of the heat release and overestimation of the number of mols of combustion products. The latter arises because although the same amount of water is produced, more mols of O are required to produce it than would be needed for combustion from the O2 molecules. The net result is overprediction of the

The heat release was then recomputed assuming the O and NO burn, preferentially to the O2 molecules. The results of this analysis is shown as the diagonal crosses in Fig. 1, and is in reasonably good agreement with the ideal flow predictions.

The results for the 18.6 mj/kg enthalpy case are presented in Fig. 4-6. For the ϕ = 0.5 case, Fig. 4, the oxygen content was calculated assuming combustion was only from the monatomic O form because the α value was bigger than 0.5. The results are shown to give reasonable agreement with the ideal case, but it is not as close as for the lower enthalpy.

One reason for this is possibly the lower pressure levels required in the ideal flow in order to conserve the ρu^2 product. The temperature levels at this enthalpy are very high, ~ 3000 K after combustion, and heat release will be reduced due to dissociation of combustion products. Equilibrium composition is highly sensitive to static pressure level, and to check this the ideal gas computations were repeated with the pressure levels matched to the corresponding shock tunnel cases. The results of this are shown as the diagonal crosses in Figs. 4-6, and they do show a reduction in the discrepancy between modified shock tunnel and ideal flow profiles. This correction is achieved at the sacrifice of the ρu^2 parameter by about 15%.

At an equivalence ratio of 1, Fig. 5, there is significant disagreement between the 2 flows, as shown by the open and closed squares. Stoichiometric mixtures produce the hottest combustion temperatures, and are the most subject to dissociation. The effects of dissociation have been included in the analytical treatment by using a reduced value for the heat of combustion from molecular oxygen, h_c. For most of the cases considered this has proven to give a good first order estimate of the eventual heat release. It would appear, however, that at the hottest case considered ϕ = 1, H_s = 18.6 mj/kg, the assumption is beginning to break down. The effective value of h_c is being reduced, and with the heats of formation remaining constant the effect of the dissociated oxygen content becomes more significant. Intuitively, and by inspection of Eq. 6, it can be seen that the oxygen levels must be reduced even further at the conditions of highest heat release in order to match the ideal flow. At this point, the analysis has passed beyond the scope of a simple heat balance calculation and a trial and error approach must be made, using the 1D reaction code, to find the level of free stream oxygen concentration which produces the required result. The calculated gas composition would be used when experiments were required for that condition.

PROPOSALS FOR FUTURE WORK

This paper justifies the use of a heat balance approach for tailoring the oxygen concentration of the test gas to match the combustion heat release achieved in different test facilities. Premixed one dimensional flow is assumed, and preliminary experiments should preferably approximate this condition as closely as possible.

Shock induced ignition rigs, as used in Refs. 4 and 5 come close to achieving this. The fuel is injected into a hypersonic flow at a low pressure where it can mix, but cannot burn. Ignition is subsequently

initiated by the passage of an oblique shock through the partially premixed layer. Experiments using the same apparatus, and adjusting the oxygen level should give some indication as to the validity of the concept.

As mentioned in the introduction, the heat release parameter is only one way in which the oxygen composition influences combustion. A more complete 2 dimensional approach is required to fully analyse the mixing and combustion processes. It is intended that this will be done firstly by means of an existing code, Ref. 6. This will be followed by a series of experiments to see if the macroscopic features of the supersonic flow are unduly influenced by the changes. That is, it is important that the same basic flow pattern is being produced in both cases.

Conclusive proof of the validity of the technique can only come through comparison of the same experiment in different facilities. The expansion tube at GASL, Ref. 7, and the reflected shock tunnel T4 of The University of Queensland, Ref. 2 provide the potential for doing this. The expansion tube can produce the same enthalpy as the shock tunnel, but with a lower level of free stream dissociation. Parallel experiments are planned for the 2 facilities in 1990 to confirm that the same pressure/distance profiles can be produced in both cases.

CONCLUSIONS

Based on a 1 dimensional analysis it is shown that the effects of free stream dissociation in shock tunnels can be accounted for in scramjet combustors. A simple heat balance approach gives adequate correction for most of the conditions considered. At the highest enthalpy examined, and at an equivalence ratio of 1, the heat balance approach was found to be inadequate, and a numerical analysis would be needed to match pressure profiles. Pressure rise downstream in the duct was used as the criteria to evaluate the effectiveness of the corrections, which consist of making adjustments to the oxygen content of the test gas. The effect of changing oxygen concentration on ignition and reaction delays, mixing and other flow properties was not considered.

REFERENCES

1. J.A. Lordi, R.E. Mates and J.R. Moselle, "Computer program for the numerical solution of non-equilibrium expansion of reacting gas mixtures", NASA rep. NASA CR-472. 1966.

2. R.J. Stalker, R.G. Morgan, "The University of Queensland free piston shock tunnel T4, initial operation and preliminary calibration", 4th National Space Engineering Symposium, Adelaide 12-14 July, 1988.

3. D.A. Bittker, V.J. Scullin, "General chemical kinetics computer program for static and flow reactions with application to combustion and shock tube kinetics", NASA TN D-6586.

4. R.G. Morgan, C. Brescianini, A. Paull, N.A. Morris and R.J. Stalker, "Shock induced ignition in a model scramjet". IEAust 3rd National Space Engineering Symposium, Canberra, June 1987.

5. J.L. Cambier, H. Adelman, G. Menees, "Numerical simulations of oblique detonations in supersonic combustion chambers". 8th ISABE, Ohio, 1987.

6. C. Brencianini and R.G. Morgan, "Numerical modelling of side wall injected scramjet" Extract from NASA CR 181721, Sept 1988.

7. R.J. Bakos, J. Tamagno, O. Rizkalla, M.V. Pulsonetti, and J.I. Erdos, "Mach 17 scramjet combustor data", Paper No. 32, 8th National Aerospaceplane Technology Symposium, March 1990.

8. R.J. Stalker, R.G. Morgan and M.P. Netterfield, "Wave pProcesses in scramjet thrust generation", Combustion and Flame 71:63-77, 1988.

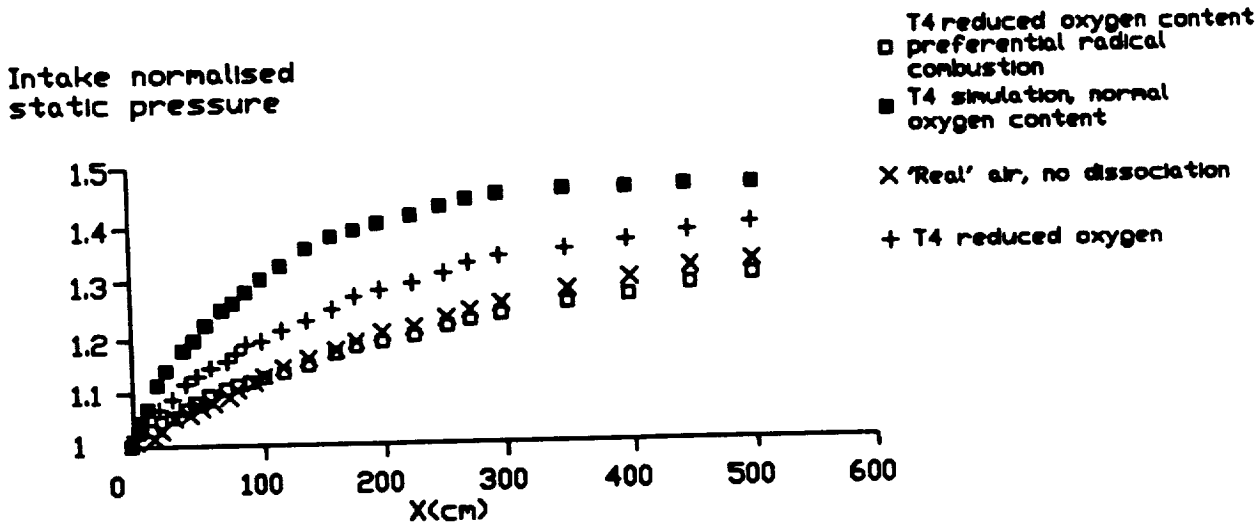

Fig 1 Hs=12.98 MJ/kg, phi=0.5, p/x.

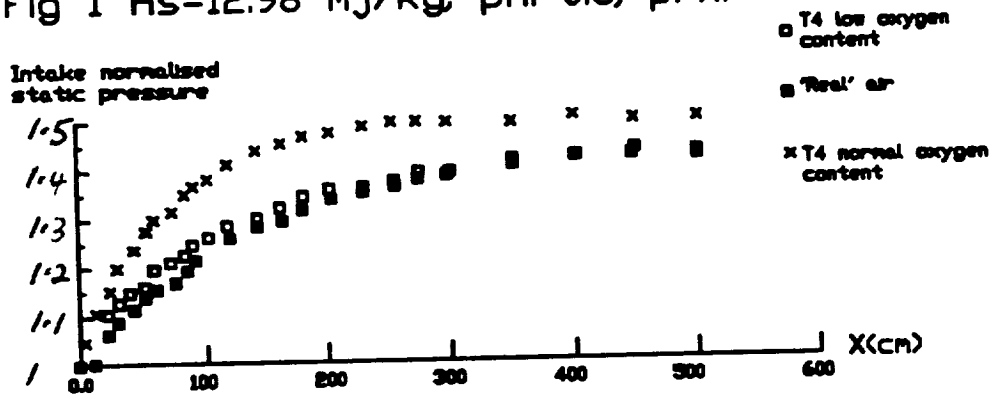

Fig 2, Hs=12.98 MJ/kg, phi=1, p/x.

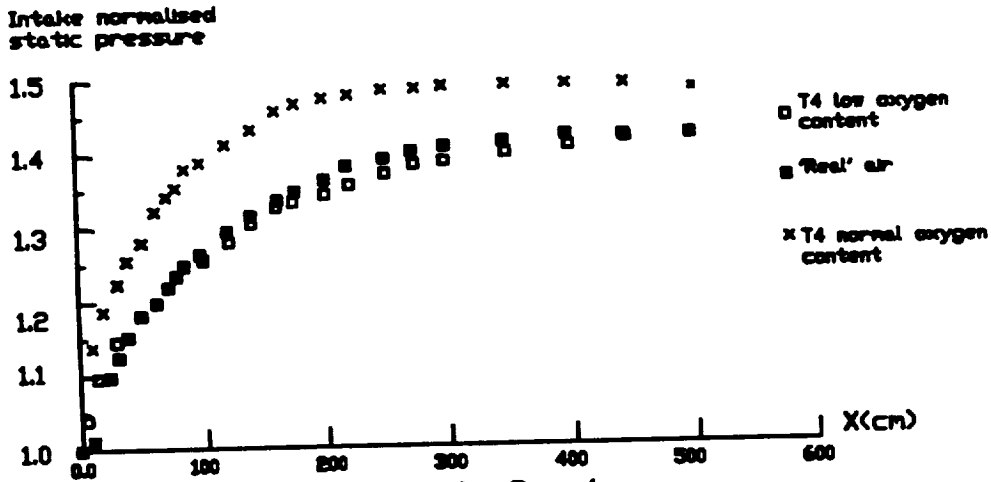

Fig 3, Hs=12.98MJ/kg,phi=2, p/x.

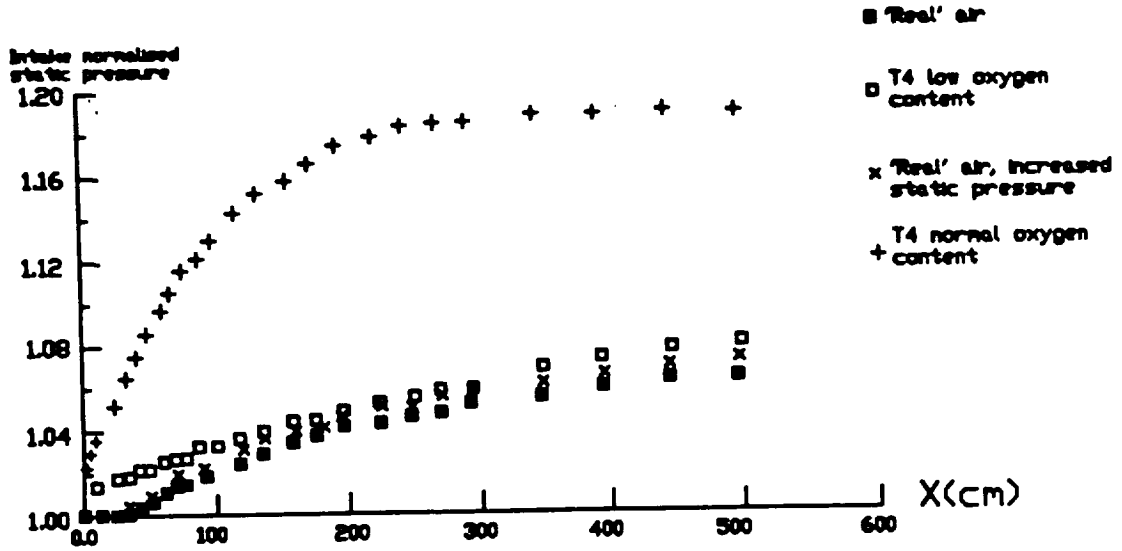

Fig 4 Hs=18.04 MJ/kg, phi=0.5, p/x.

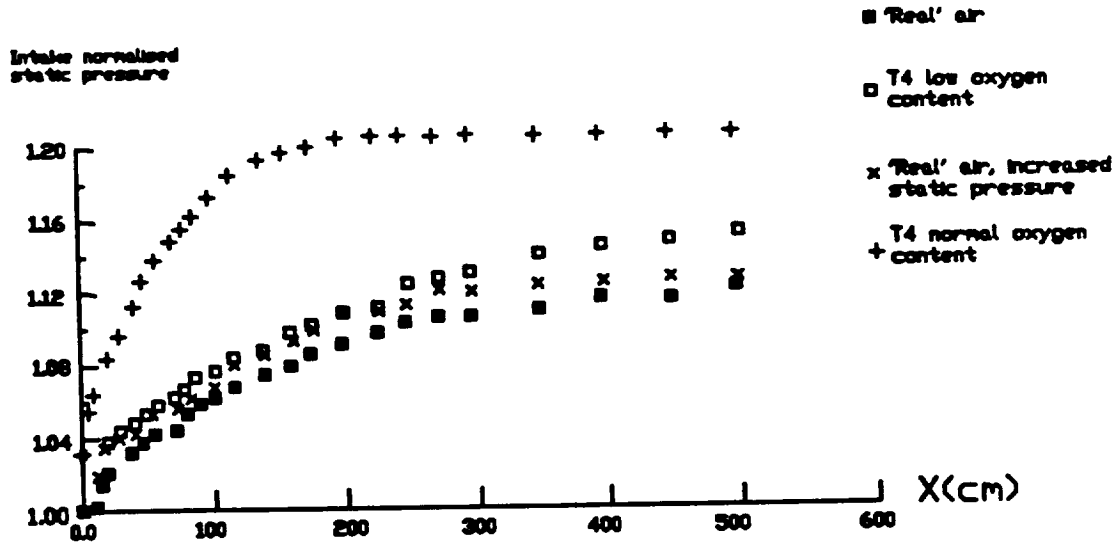

Fig 5, Hs=18.04 MJ/kg, phi=1, p/x.

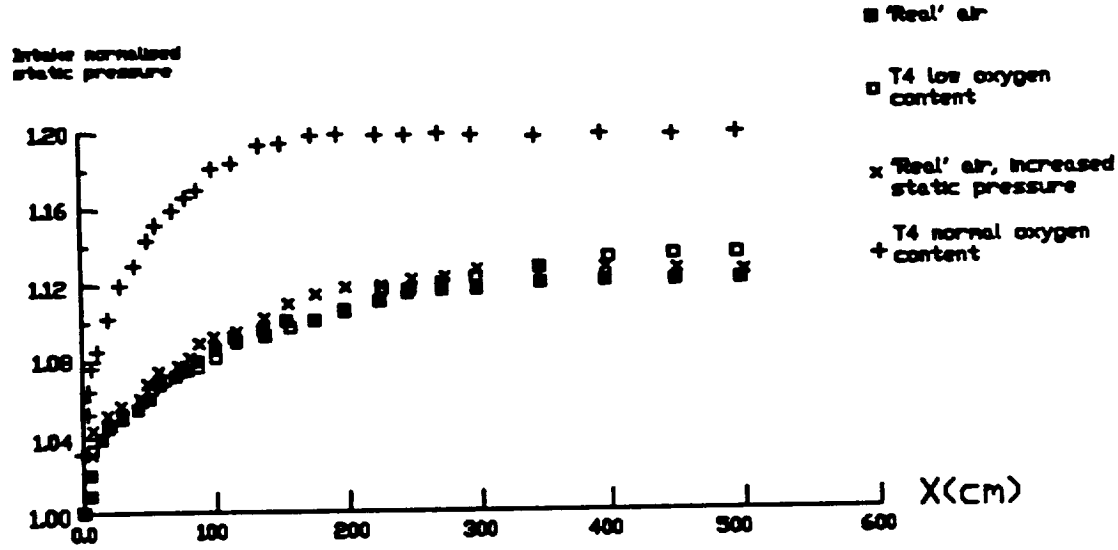

Fig 6, Hs=18.04MJ/kg, phi=2 p/x

TABLE 1 Representative Shock Tunnel Test Conditions for Air.

Flow Parameters	Flight Speed 5.1 Km/s	Flight Speed 6.1 Km/s
H_s (mj/kg)	13	18.6
T (K)	1874	2520
ρu^2(Kpa)	823	847
p (Kpa)	23.2	24.3
ρ (Kg/m^3)	0.0412	0.03026
u (m/s)	4467	5237
M	5.25	5.18
Gas Composition (mass fractions)		
α	0.203	0.532
α_N	0.145	0.0988
$\alpha + \alpha_N$	0.348	0.63
O2	0.145	0.08192
O	0.0451	0.1183
N2	0.7493	0.758
NO	0.0603	0.412

TABLE 2 Flow Conditions Before Mixing.

PRIMARY FLOW PARAMETERS: H_s = 13 MJ/Kg; $\rho\bar{s}$ = 823 Kpa, T = 1874 K

		SHOCK TUNNEL FLOW			IDEAL FLOW
		Unmodified Air	Reduced Oxygen	Preferential 'O' burn	
ϕ = 0.5	x	0.2223	0.1636	0.128	0.2223
	O_2	0.145	0.1067	0.0835	0.2223
	O	0.0451	0.0332	0.026	0
	N_2	0.7493	0.8157	0.8558	0.7777
	NO	0.0603	0.0444	0.0347	0
	P (Kpa)	23.2	22.7	22.3	20.5
	u (m/s)	4467	4514	4548	4662
	ρ (Kg/m^3)	0.0412	0.04041	0.03982	0.03789
	M	5.25	5.26	5.3	5.55
ϕ = 1	x	0.2223	0.1573		0.2223
	O_2	0.145	0.1027		0.2223
	O	0.0451	0.0319		0
	N_2	0.7493	0.8227		0.7777
	NO	0.0603	0.0427		0
	P (Kpa)	23.2	22.6		20.5
	u (m/s)	4467	4519		4662
	ρ (Kg/m^3)	0.0412	0.04032		0.03789
	M	5.25	5.26		5.55
ϕ = 2	x	0.2223	0.1434		0.2223
	O_2	0.145	0.0935		0.2223
	O	0.0451	0.02909		0
	N_2	0.7493	0.8385		0.7777
	NO	0.0603	0.0389		0
	P (Kpa)	23.2	22.6		20.5
	u (m/s)	4467	4519		4662
	ρ (Kg/m^3)	0.0412	0.04032		0.03789
	M	5.25	5.26		5.55

TABLE 3 Flow Conditions Before Mixing

PRIMARY FLOW PARAMETERS: H_o = 18.6 KJ/Kg; ρu^2 = 847 Kpa, T = 2520 K

		SHOCK TUNNEL FLOW			IDEAL FLOW
		Unmodified Air	Reduced Oxygen	Preferential 'O' burn	
ϕ = 0.5	x	0.2223	0.1238	0.0911	0.2223
	O_2	0.08192	0.0456	0.03358	0.2223
	O	0.1183	0.0659	0.0485	0
	N_2	0.758	0.8655	0.901	0.7777
	NO	0.0412	0.02296	0.0169	0
	P (Kpa)	24.3	23.6	22.9	20.4
	u (m/s)	5237	5284	5339	5489
	ρ (Kg/m^3)	0.03026	0.03032	0.0297	0.0281
	M	5.18	5.22	5.31	5.66
ϕ = 1	x	0.2223	0.1155		0.2223
	O_2	0.08192	0.0426		0.2223
	O	0.1183	0.06151		0
	N_2	0.758	0.8745		0.7777
	NO	0.0412	0.0214		0
	P (Kpa)	24.3	23.5		20.4
	u (m/s)	5237	5298		5489
	ρ (Kg/m^3)	0.03026	0.03016		0.02819
	M	5.18	5.24		5.66
ϕ = 2	x	0.2223	0.0996		0.2223
	O_2	0.08192	0.03672		0.2223
	O	0.1183	0.053		0
	N_2	0.758	0.8918		0.7777
	NO	0.0412	0.0185		0
	P (Kpa)	24.3	23.1		20.4
	u (m/s)	5237	5324		5489
	ρ (Kg/m^3)	0.03026	0.02987		0.02819
	M	5.18	5.28		5.66

```
FAIR     DAT      A1  F 132          6 BLKS 89/07/27 LINE     111 OF     16
 ===>                                                                  BROWS
END          TABLE 4
Real air,static pressure level increased,Xa=.2222 18.04 mj/kg phi=2.0
  M        1 O2       1 O        1 O          7.2E18  -1.      11790E
  M        1 H2       1 H        1 H          5.5E18  -1.      10329E
  M        1 H2O      1 H        1 OH         5.2E21  -1.5     11800C
  M        1 O2       1 HO2        M          2.3E15   0.0      -800.
  M        1 NO2      1 NO       1 O          1.1E16   0.0     64995.
1 H        1 NO       1 HNO        M          5.4E15   0.0      -596.
  OH       1 NO       1 HNO2       M          8.0E15   0.0     -1987.
  O        1 H        1 OH         M          7.1E18  -1.0      0.
1 H2       1 OH       1 H2O      1 H          2.0E13   0.0      5166.
  O2       1 H        1 OH       1 O          2.2E14   0.0     16800
  H2       1 O        1 OH       1 H          7.5E13   0.0     11099
1 H        1 HO2      1 H2       1 O2         2.4E13   0.0      695.
1 H        1 HO2      1 OH       1 OH         2.4E14   0.0      1887.
1 H2O      1 O        1 H        1 HO2        5.8E11   0.5     57000
1 O        1 HO2      1 OH       1 O2         5.0E13   0.0      1000.
1 OH       1 HO2      1 O2       1 H2O        3.0E13   0.0      0.
1 H2       1 HO2      1 H2O      1 OH         2.0E13   0.0     25000
1 O        1 N2       1 NO       1 N          5.0E13   0.0     75380
1 H        1 NO       1 OH       1 N          1.7E14   0.0     48681
1 O        1 NO       1 O2       1 N          1.5E09   1.0     38746

 FAIR     DAT      A1  F 132          6 BLKS 89/07/27 LINE     133 OF      1
 ===>                                                                  BROW
1 NO2      1 H        1 NO       1 OH         3.5E14   0.0      1470.
1 NO2      1 O        1 NO       1 O2         1.0E13   0.0      600.
1 NO2      1 H2       1 HNO2     1 H          2.4E13   0.0      2900.
1 HO2      1 NO       1 NO2      1 OH         3.0E12   0.5      2400
1 HNO      1 H        1 H2       1 NO         4.8E12   0.0      0.
1 HNO      1 OH       1 H2O      1 NO         3.6E13   0.0      0.
1 NO       1 HO2      1 HNO      1 O2         7.2E11   0.5     10928
1 HNO      1 O        1 NO       1 OH         5.0E11   0.5      0.

AR
DISTANCE  AREA       CGS        CGS
 &PROB HMIN=1.0E-20,EMAX=.001,HMAX=.01,
 CONC=.FALSE.,PAPS=.TRUE.,COMBUS=.FALSE.,ALLM1=.FALSE.,
 ITPSZ=2,IPROD=1,CX0=2.5,END=500,NPRIN=29,
 TPRINT=0,1.0,2.0,3.0,4.0,5.0,10,20,30,40,50,60,70,80,90,100,
 120,140,160,180,200,225,250,275,300,350,400,450,500,
 &END
  M        1 O2       1 O        1 O        H2O      2       O2
  M        1 O2       1 O        1 O        O       10
  M        1 H2       1 H        1 H        H2O      8       H2
  M        1 H2       1 H        1 H        H        5
  M        1 H2O      1 H        1 OH       H2O      6

 FAIR     DAT      A1, F 132          6 BLKS 89/07/27 LINE     155 OF
 ===>                                                                  BRC
1 H        1 O2       1 HO2        M        H2O     13       H2
1 H        1 NO       1 HNO        M        H2O      3

 &START
 MOLEF=.FALSE.,MMHG=.FALSE.,
 X=0.0,V=548900,P=0.228,T=2520.,AREA=2.5,TIME=0.0,
 N2=.736755,O2=.210596,O=0.0,H2=0.052649,NO=0.0,
 AR=.0,
 &END

FINIS
  * * * END OF FILE * * *
```

TABLE 2 Flow Conditions Before Mixing.

PRIMARY FLOW PARAMETERS: H_o = 13 MJ/Kg; $\rho\bar{a}$ = 823 Kpa, T = 1874 K

		SHOCK TUNNEL FLOW			IDEAL FLOW
		Unmodified Air	Reduced Oxygen	Preferential 'O' burn	
ϕ = 0.5	x	0.2223	0.1636	0.128	0.2223
	O_2	0.145	0.1067	0.0835	0.2223
	O	0.0451	0.0332	0.026	0
	N_2	0.7493	0.8157	0.8558	0.7777
	NO	0.0603	0.0444	0.0347	0
	P (Kpa)	23.2	22.7	22.3	20.5
	u (m/s)	4467	4514	4548	4662
	ρ (Kg/m^3)	0.0412	0.04041	0.03982	0.03789
	M	5.25	5.26	5.3	5.55
ϕ = 1	x	0.2223	0.1573		0.2223
	O_2	0.145	0.1027		0.2223
	O	0.0451	0.0319		0
	N_2	0.7493	0.8227		0.7777
	NO	0.0603	0.0427		0
	P (Kpa)	23.2	22.6		20.5
	u (m/s)	4467	4519		4662
	ρ (Kg/m^3)	0.0412	0.04032		0.03789
	M	5.25	5.26		5.55
ϕ = 2	x	0.2223	0.1434		0.2223
	O_2	0.145	0.0935		0.2223
	O	0.0451	0.02909		0
	N_2	0.7493	0.8385		0.7777
	NO	0.0603	0.0389		0
	P (Kpa)	23.2	22.6		20.5
	u (m/s)	4467	4519		4662
	ρ (Kg/m^3)	0.0412	0.04032		0.03789
	M	5.25	5.26		5.55

TABLE 3 Flow Conditions Before Mixing

PRIMARY FLOW PARAMETERS: H_s = 18.6 KJ/Kg; ρu^2 = 847 Kpa, T = 2520 K

		SHOCK TUNNEL FLOW			IDEAL FLOW
		Unmodified Air	Reduced Oxygen	Preferential 'O' burn	
ϕ = 0.5	x	0.2223	0.1238	0.0911	0.2223
	O_2	0.08192	0.0456	0.03358	0.2223
	O	0.1183	0.0659	0.0485	0
	N_2	0.758	0.8655	0.901	0.7777
	NO	0.0412	0.02296	0.0169	0
	P (Kpa)	24.3	23.6	22.9	20.4
	u (m/s)	5237	5284	5339	5489
	ρ (Kg/m^3)	0.03026	0.03032	0.0297	0.0281
	M	5.18	5.22	5.31	5.66
ϕ = 1	x	0.2223	0.1155		0.2223
	O_2	0.08192	0.0426		0.2223
	O	0.1183	0.06151		0
	N_2	0.758	0.8745		0.7777
	NO	0.0412	0.0214		0
	P (Kpa)	24.3	23.5		20.4
	u (m/s)	5237	5298		5489
	ρ (Kg/m^3)	0.03026	0.03016		0.02819
	M	5.18	5.24		5.66
ϕ = 2	x	0.2223	0.0996		0.2223
	O_2	0.08192	0.03672		0.2223
	O	0.1183	0.053		0
	N_2	0.758	0.8918		0.7777
	NO	0.0412	0.0185		0
	P (Kpa)	24.3	23.1		20.4
	u (m/s)	5237	5324		5489
	ρ (Kg/m^3)	0.03026	0.02987		0.02819
	M	5.18	5.28		5.66

THE USE OF SILANE AS A FUEL ADDITIVE FOR HYPERSONIC THRUST PRODUCTION

R.G. Morgan, Department of Mechanical Engineering,

The University of Queensland

ABSTRACT.

Scramjet propulsive ducts operate by converting some of the flight free stream kinetic energy to heat in order to initiate combustion. As the flight speed increases, the available kinetic energy which can be used for heating also increases. However, the required temperature range for efficient combustion does not change much with flight speed. Temperatures are limited at the lower end by ignition and reaction characteristics, and at the upper end by combustion product dissociation. It is realistic to expect combustion chamber intake temperatures to be within the range of 800 to 1800 K throughout the whole flight envelope. This means that at the higher flight Mach numbers, the combustion chamber Mach number must be in the hypersonic regime in order to avoid overheating the flow. The static pressure levels associated with the hypersonic flow will be low, and this will adversely effect combustion and heat release characteristics. This paper reports on the use of silane as an additive to enhance combustion in shock tunnel tests of a hypersonic scramjet. Silane, which is spontaneously combustible at room temperature, was mixed with hydrogen at 20% by volume. The mixture has been used before in a constant area duct configuration, and for this work a 2 dimensional nozzle was added to produce thrust.

The silane was found to produce vigorous combustion, and significant thrust, but when specific impulse was calculated, on a per unit mass flow rate basis, it did not perform better than pure hydrogen over the same enthalpy range but at a higher static pressure. This is attributed to the high molecular weight of the silane molecules, and the associated high mass flow rate of fuel required to burn the oxygen. At the static pressure levels for which the tests were performed, pure hydrogen did not burn at all within the confines of the duct. In conclusion, the silane was useful for performing hypersonic combustion studies under test conditions where hydrogen combustion was not possible. Additionally, the tests indicate that combustion can be enhanced, but that the specific impulse will not exceed that of hydrogen in regions where the hydrogen itself can be made to burn well.

1. INTRODUCTION.

Experiments in hypersonic combustion of hydrogen have been performed in The University of Queensland shock tunnel, T4[1]. Whilst the results indicate that some mixing and combustion does occur,[2], the performance when a thrust nozzle is attached does not approach that achieved in a supersonic duct in the shock tunnel T3,[3], at the Australian National University. The reason for this is not fully understood at present.

The hypersonic flow is created at the expense of free stream static pressure, and pressure scaling tests in a supersonic duct in T3[4] have shown combustion to be very pressure sensitive.

The supersonic duct typically operates at static pressure levels ~ 150 kpa, but when the pressure level is reduced below 50 kpa combustion is inhibited. The hypersonic duct has an intake pressure level of ~ 20 kpa, and if a direct comparison with the supersonic tests applies, it might be expected to be adversely effected by the low pressures.

There is some evidence to suggest that low static pressure levels are the primary cause of the poor combustion. When the scramjet was configured as a 51 x 25 mm section constant area duct, boundary layer growth on the internal walls caused significant pressure rise, [2] and Fig. 1. When hydrogen was injected at this condition it burned fairly readily, Fig. 2. However, the boundary layer compressive effects would have reduced the free stream Mach number to ~ 4.5, and it could not truly be called hypersonic combustion.

When the duct section was increased to 50 x 51 mm the compressive effect of the boundary lawyer was reduced, the Fuel Off pressure levels were lower and the flame was extinguished, Fig. 3. When the pressure levels in the square duct were subsequently increased by means of a compression wedge, Fig. 4, combustion effects were again evident in the duct. Fig. 5.

Both the compression wedge, and compression waves off the developing boundary layer, increase the static temperature as well as static pressure levels. However the static temperature levels may be held constant by adjusting the stagnation enthalpy. This leaves only Mach number and static pressure level as the parameters which are different between conditions where combustion does, and does not occur.

The pressure may influence combustion through it's effect on density, in two ways. Firstly, reaction rates will be enhanced, to a degree depending on the order of the reaction mechanisms involved, due to increased collision rates. In a flame where mixing is expected to occur rapidly, this will be the major heat release controlling factor at a given free stream static temperature.

Secondly, the increased Reynolds number may increase the rate of entrainment between the fuel and air layers, which, if reaction rates are fast will increase the overall rate of heat release. The T3 supersonic duct tests were performed in the free stream unit Reynolds number range of 1 to 2 10^7 m^{-1}, whilst the T4 hypersonic runs were in

the range 0.5 to 1 $*10^7$ m^{-1}. This in itself may be enough to explain the increased combustion in the supersonic flow. This effect could be partially checked by raising the pressure levels of the T4 tunnel, and this will be done when the facility is capable of doing so. However, any change would be coupled with increased reaction rates and may be hard to interpret.

The hypersonic conditions where combustion occurs have, as well as higher static pressure levels, lower Mach numbers than for test cases where no combustion is observed. The effect of Mach number on the rate of development of a mixing layer is not fully understood,[5], however it may be a significant factor.

The purpose of these experiments was to partially decouple the effects of chemical kinetics by the use of a combustion enhancing additive in the fuel. Silane at 20% by volume was mixed with hydrogen and injected at equivalence ratios of up to 1, based on the consumption of all fuel and oxygen components. The resulting pressure traces indicated substantial combustion and heat release. However, this cannot be solely attributed to increased reaction rates, as the silane mixture has a molecular weight of 8, and has to be injected at 2.5 times the mass flow rate of hydrogen for the same equivalence ratio. This leads to a slower jet, with a large momentum deficit which may enhance the mixing.

When a nozzle was added to the combustion chamber, significant thrust was measured for the fuel on condition. The thrust levels when normalised against reservoir stagnation pressure were constant over the

usable test time of the shock tunnel, indicating that steady flow and combustion had been achieved by the use of the silane additive. This enabled thrust and specific impulse measurements to be made in a hypersonic flow where current T4 pressure limitations preclude combustion of hydrogen.

2. EXPERIMENTS.

The initial experiments were performed in a constant area duct configuration to confirm that significant combustion could be achieved, and to determine at what axial location the thrust nozzle should start. A sample set of Fuel On and Fuel off pressure profiles are shown in Fig. 6 for a nominal stagnation enthalpy of 6.8 Mj/kg.

In the light of these results the scramjet was re-configured for thrust production as shown in Fig. 7. The thrust surface diverged at an angle of 15^{0} from the incoming flow, and started at a distance of 225 mm downstream of injection. Injection was from a two dimensional central injector with a throat of 1.6 mm height. The injector spanned the full width of the duct. Fuel mass flow rate was controlled by adjusting the stagnation pressure of the fuel reservoir, which was maintained at room temperature. Changes in equivalence ratio therefore were coupled to changes in fuel Mach number, velocity and temperature, which had an unknown effect on the rate of fuel air mixing.

The thrust surface on the duct was instrumented with quartz transient pressure transducers, and thrust was calculated assuming 2-dimensional flow with linear interpolation between data points.

3. RESULTS.

Shock tunnels are inherently unsteady facilities, and care must be taken when trying to draw conclusions based on steady combustion assumptions from transient data. The first step when analysing shock tunnel data must be to confirm that steady flow has been established. As the stagnation pressure decays during the test time of the tunnel, steady Mach number will only be maintained if the pressure ratio across the nozzle attached to the shock tube is constant.

In Fig. 8 the static pressure/time history is shown for a typical fuel on shot for a transducer on the thrust surface. It should be noted that for the duration of the steady flow period, although the stagnation pressure changes by ± 15%, the normalized static pressure level stays sensibly constant. Similarly, the integrated thrust when normalised in the same manner is nearly constant, indicating that the macroscopic flow field is steady.

If therefore the nozzle exit conditions are calculated on the assumption of a steady expansion from the stagnation region, then the scramjet tests are conducted in an intake flow field with the following approximate variation in properties from the nominal conditions:

Flow duration	1 ms
Stagnation pressure variation	± 15%
Stagnation enthalpy variation	± 4%
Static pressure variation	± 15%
Static temperature variation	± 4%
Mach number	constant
Velocity variation	± 2%
Density variation	± 10%
Momentum flux variation	± 15%
Equivalence ratio variation	± 13%
Reynolds number variation	± 10%

[These quantities estimated at a stagnation enthalpy at 12.5 MJ/kg from run 874].

To assess the significance of this unsteadiness on thrust production, it is necessary to estimate the decay of momentum within the control volume during the test period. The total momentum stored within the control volume is 0.135 $kg.ms^{-1}$ for the 12.5 MJ/kg case, and the decay rate during the 1 ms of test time therefore represents a force of ~ 35 N.

It can be seen from the thrust balance illustrated schematically in Fig. 11 for a 2-dimensional duct of unit width that this momentum decay will detract directly from the measured thrust on the thrust surface. Moreover, this value of 35 N is a significant fraction of the fuel on steady thrust levels of ~ 50 N.

However, when comparing Fuel On and Fuel Off thrust levels it is estimated that the difference between the two due to unsteady momentum effects reduces to a second order error. This is because, due to the lack of upstream influence in supersonic flow, the intake time history of pressure and momentum flux is the same for both Fuel On and Fuel Off cases. The new thrust and specific impulse calculated by subtracting Fuel Off from Fuel On values will therefore be primarily due to the presence of the fuel jet as governed by steady flow and steady combustion effects.

Also, the internal momentum decay can be considered to detract directly from the thrust as indicated in Fig. 11 only when comparing steady and

unsteady flows with the same incoming and outgoing momentum flux and pressure integrals. In practice with the onset of unsteady flow the momentum decay term will be partially met by changes to the incoming and outgoing integrals. Take for example the case of a constant area duct in unsteady flow. No thrust is produced, and a rise in downstream pressure balances the momentum decay. The more the nozzle departs from a constant area duct, the more sensitive the thrust production will be to unsteady effects.

In Fig. 9 scatter bars are shown illustrating how the normalised pressure/distance profiles change over the nominal test period. The steadiness of the profiles indicates that the macroscopic features of the flow, such as wave propagation and thrust production are constant. In Fig. 10 the normalised integrated thrust/time profiles are shown for Fuel On and Fuel Off conditions. The constant levels of the two traces adds credibility to the assumption that the unsteady thrust decrement is the same for Fuel On and Fuel Off runs.

In Figs. 12-17 the pressure profiles are shown for 20% silane injection in the enthalpy range 4.46 to 17.1 Mj/kg. For all of the conditions tested except 4.46 Mj/kg strong combustion affects were observed in terms of increased pressure on the thrust surface. At the lower enthalpy the static temperature was ~ 500 K which appears to be too low for silane combustion at this pressure level.

In Fig. 18 the effects of injecting helium into a flow at 6.81 Mj/kg are shown. It is seen to produce negligible pressure rise over the Fuel Off

case. This suggests that the pressure rises observed when injecting the silane mixture are due to combustion rather than the intrusive presence of an inert jet. The molecular weight of helium was 4, compared with 8 for the silane mixture, but when coupled with the evidence of the low enthalpy, no pressure rise test, Fig. 12, it seems certain that the silane mixture was burning at the high enthalpies.

The measured net thrust with silane injection was high, but when the specific impulse was computed, Fig. 19, it did not compare favourably with the hydrogen results from [2], shown in Fig. 20. This is attributed to the high molecular weight and mass flow requirements of the heavy silane molecules. However, the pressure level of these tests was lower than for [2], and hydrogen would not burn at all under these conditions.

4. CONCLUSIONS.

The use of silane additive at 20% induced vigorous combustion at conditions where hydrogen was not able to burn. This tends to suggest that kinetics, rather than mixing are limiting heat release in the hypersonic duct. However, this contradicts to some extent the findings of [6] whose numerical study suggests that mixing will be the limiting factor. A possible reason for enhanced mixing with silane might be the lower velocity, high density fuel jet required for stoichiometric combustion.

Alternatively, rapid vogorous combustion might induce turbulence which enables the fuel to mix over a wide spread region of the duct.

An estimate of the extent of the mixing layer may be made by inspection of the fuel on pressure traces, such as Fig. 9 and Figs. 13-17. As discussed in Ref. (9), thrust is transmitted to the thrust surface by two separate mechanisms. These mechanisms are (1) direct propagation of waves from the combustion zone to the walls, and (2) the interaction of the corner expansion fan with the Mach number gradients in the flow. Waves from mechanism 1 are evident upstream of the thrust surface, whilst the onset of mechanism 2 is clearly shown from the pressure rise downstream of the corner. By following waves back upstream from the start of the thrust surface pressure rise, it is possible to locate where the leading edge of the expansion fan first starts producing compression waves. This identifies the point where perturbations first occur in the free stream Mach number profile, which may be taken to represent the limits of the combustion zone.

The results of these calculations are shown in Fig. 21. The Mach number before the expansion fan is estimated by assuming that the freestream flow upstream of the corner is compressed isentropically from the nominal intake conditions to the locally measured static pressure. The compression waves are assumed to propagate at the local Mach angle. Run 874, equivalence ratio of 1 at a stagnation enthalpy of 12.5 Mj/kg was used for the calculations. The first compression waves are noticed incident on the thrust surface at a distance of approximately 70 mm from the corner.

The results of this treatment indicate that the combustion zone extends

to within approximately 3.5 mm of the wall. Given that the wall boundary layer at the wetted length of ~ 400 mm will be of the order of 2 mm, this implies that the mixing layer has effectively propagated across the whole duct. If this result can later be confirmed by optical techniques, and by a more detailed wave analysis of the pressure profiles, then the prospects for hypersonic combustion are good.

Silane with vigorous combustion produces comparable performance to hydrogen with partial combustion, as indicated by small pressure rises associated with injection. This suggests that complete combustion of hydrogen, whether induced by increased pressure levels or though mixing enhancement techniques, can potentially perform very well in a hypersonic duct. Alternatively, the use of a lower concentration of silane, as tested by [7] might be used to improve specific impulse.

Scramjet performance in a hypersonic duct does not yet compare with that of combustion in a supersonic duct at higher pressure levels. However, it is hoped that increased pressure simulation capability will be able to improve hypersonic performance.

5. REFERENCES.

1. R.J. Stalker, R.G. Morgan. "The University of Queensland Free Piston Shock Tunnel, T4, Initial Operation and Preliminary Calibration". Paper presented to the 4th National Space Engineering Symposium, Adelaide. 12-14 July 1988.

2. R.G. Morgan. "Hypersonic Combustion of Hydrogen in a Shock Tunnel". Extract from (8).

3. R.J. Stalker, R.G. Morgan. "Scramjet testing in impulse facilities". ISABE-87-7010. Invited lecture 8th International Symposium on Air Breathing Engines. June 14-19 1987, Cincinnati, Ohio.

4. R.G. Morgan, R.J. Stalker. "Pressure Scaling Effects in a Scramjet Combustion Chamber". ISABE paper 87-7080 presented to 8th International Symposium on Air Breathing Engines". June 14-19 1987 Cincinnati, Ohio.

5. R. Casey. "Hypersonic Injection". Extract from "Shock Tunnel Studies of Scramjet Phenomena". Progress report for 1988 on NASA grant NAGW 674, supplement 4, 1988.

6. C. Brescianni. "Computer Simulation of a Hypersonic Combustion Experiment". Extract from "Shock Tunnel Studies of Scramjet Phenomena". Progress report 1988 on NASA grant NAGW 674, supplement 4, 1988.

7. N.A. Morris, R.G. Morgan, A. Paull, R.J. Stalker. "Silane as an ignition aid in scramjets". Presented to 22nd AIAA Thermophysics Conference, Honolulu, 1987.

8. R.G. Morgan, A. Paull, R.J. Stalker, P. Jacobs, N.A. Morris, I.A. Stringer, C. Brescianini. "Shock Tunnel Studies of Scramjet Phenomena". Progress report 1987 on NASA grant NAGW 674, supplement 3 1987.

9. R.J. Stalker, R.G. Morgan, and M.P. Netterfield. "Wave Processes in Scramjet Thrust Generation". Combustion and Flame 71:63-77 (1988).

TABLE 1 RUN MANIFEST IN 15° THRUST MODE

Stagnation Enthalpy (H_s) Mj/kg	Run No.	Injection Pressure kPa	Equivalence Ratio
4.46	875	325 S_iH_4 mix	0.99
4.46	883	Fuel Off	0
6.81	882	0	0
6.81	871	0	0
6.81	876	202 S_iH_4 mix	0.66
6.81	870	393 S_iH_4 mix	1.28
6.81	884	380 H_e	—
8.5	880	0	0
8.5	879	217 S_iH_4 mix	0.82
8.5	873	373 S_iH_4 mix	1.41
8.5	885	473 H_e	—
10	868	0	0
10	877	209 S_iH_4 mix	0.88
10	867	410 S_iH_4 mix	1.73
10	886	382 H_e	—
12.5	881	0	0
12.5	874	373 S_iH_4 mix	1.77
12.5	887	366 H_e	—
17.1	889	0	0
17.1	888	350 S_iH_4 mix	2.1
17.1	891	399 H_e	—

(Injector calibration 6.6 10^{-5} Kg s^{-1} kg^{-1}

TABLE 2 - NOMINAL TEST CONDITIONS

H_s Mj/kg	Static Temp. K	Static pressure kPa	density Kg/m^3	Mach No.	Velocity m/s	Intake Oxygen mass flow
4.46	529	7.54	0.0493	6.09	2820	.0695
6.81	888	9.72	0.0379	5.73	3430	.065
8.5	1120	9.8	0.0303	5.5	3700	.056
10	1350	10.1	0.025	5.43	4000	.05
12.5	1570	10	0.0205	5.43	4350	.0446
17.1	1980	8.98	0.014	5.44	5000	.035

LIST OF FIGURES

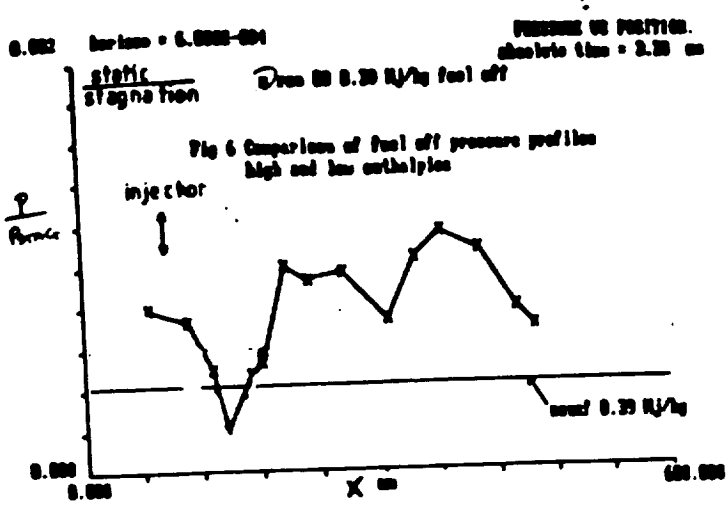

Fig 6 Comparisons of fuel off pressure profiles high and low enthalpies

Fig1 fuel off pressure
constant area duct

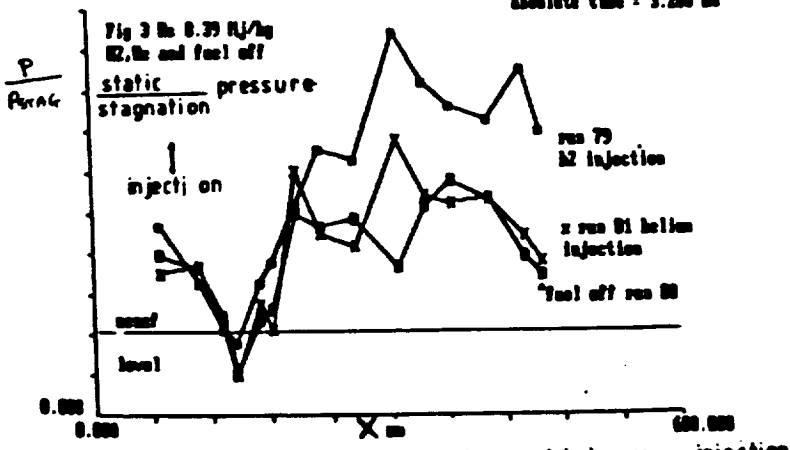

Fig2 Constant area duct, helium and hydrogen injection
stagnation enthalpy 8.39 Mj/kg

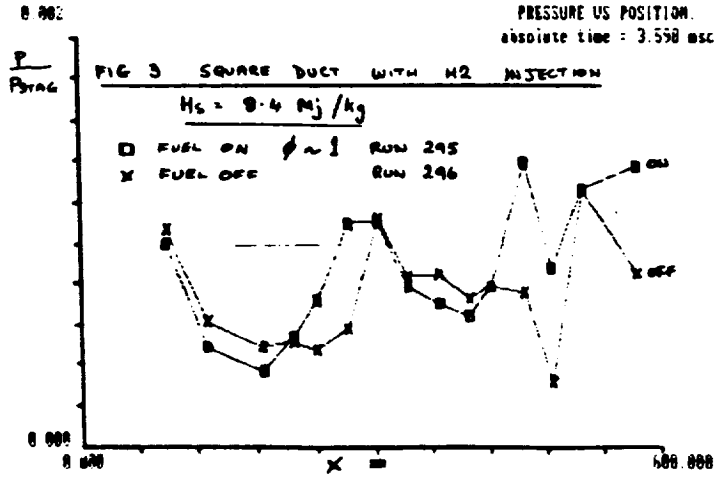

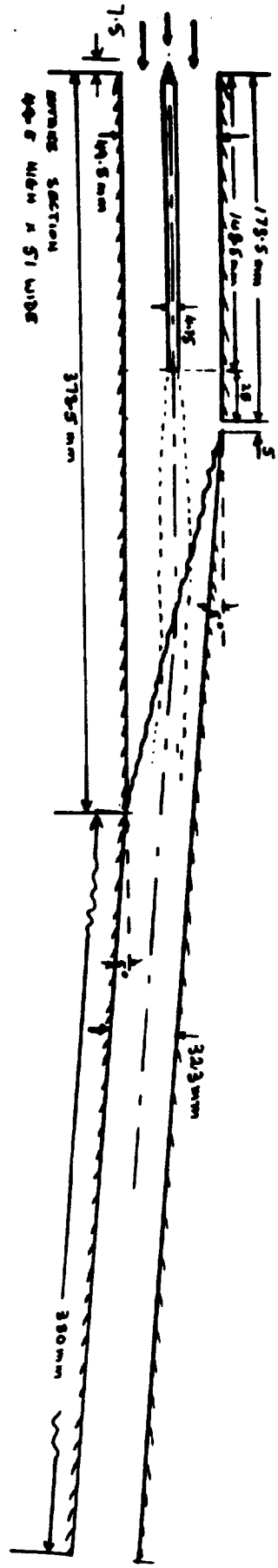

Fig 4 SCHEMATIC OF SQUARE DUCT WITH SHOCK INDUCED IGNITION WEDGE

ORIGINAL PAGE IS
OF POOR QUALITY

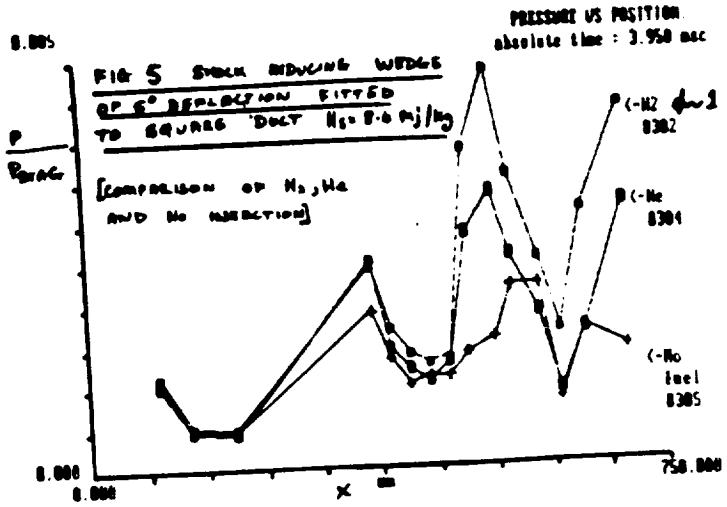

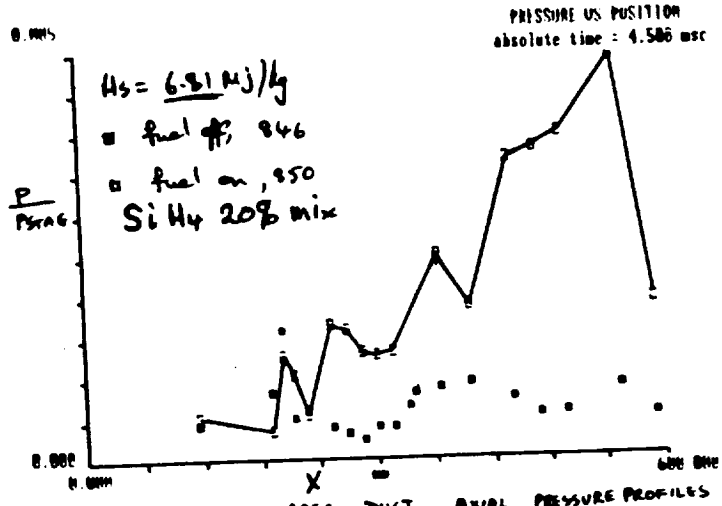

FIG 6. CONSTANT AREA DUCT AXIAL PRESSURE PROFILES

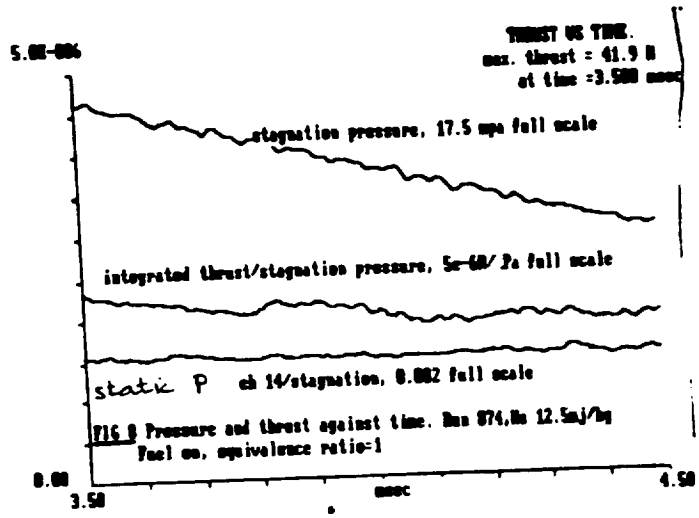

FIG 8 Pressure and thrust against time. Hss 874,Hs 12.5mj/kg
Fuel on, equivalence ratio=1

FIG 7 SCHEMATIC OF SCRAMJET IN 2D THRUST PRODUCING CONFIGURATION

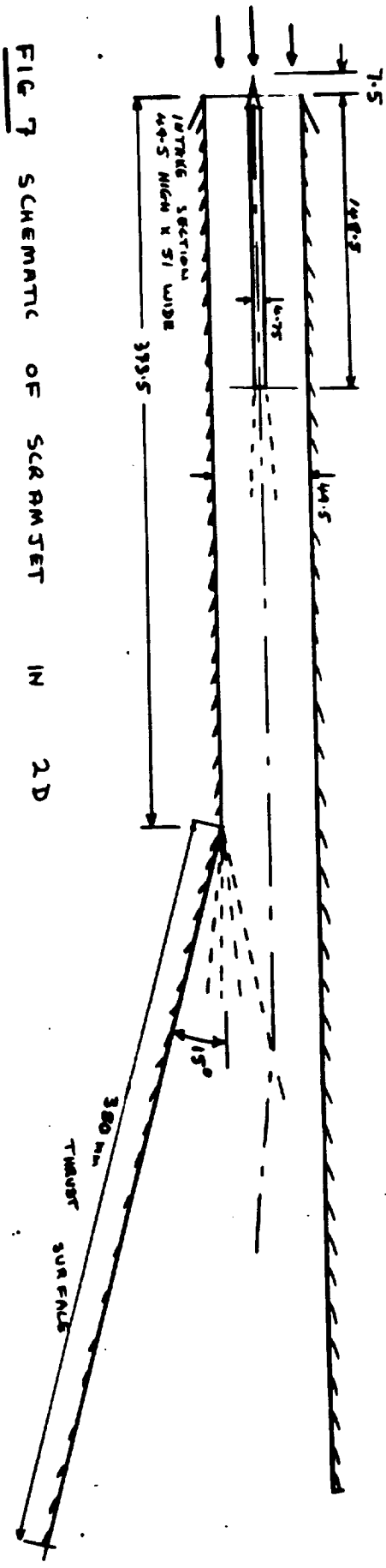

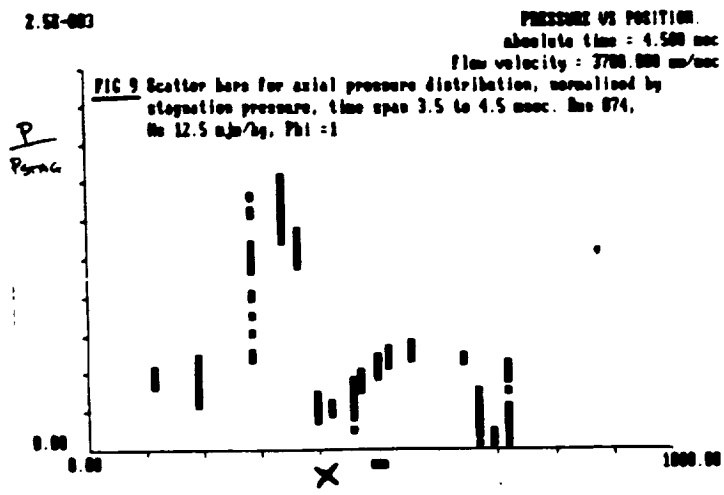

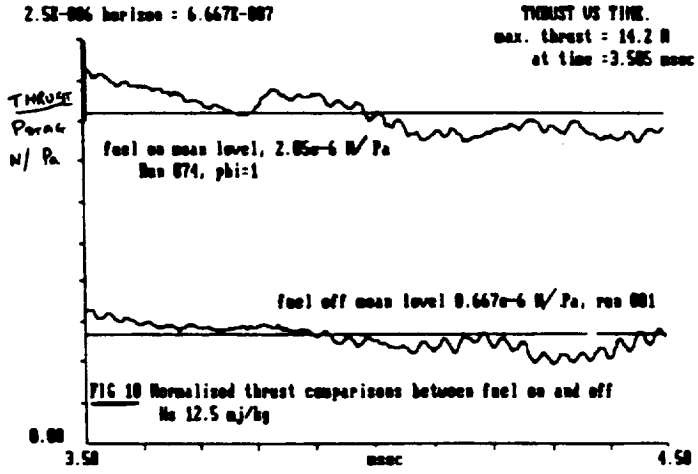

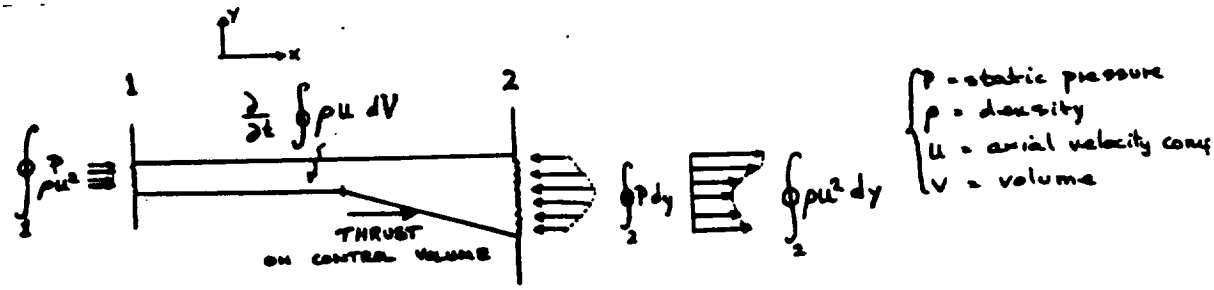

CONSERVATION OF AXIAL MOMENTUM

$$\Rightarrow \quad \text{THRUST} = \int_2 (p + \rho u^2)\,dy - \int_1 (p + \rho u^2)\,dy + \frac{\partial}{\partial t}\int \rho u\, dV$$

FIG 11 THRUST BALANCE FOR UNIT WIDTH OF 2D NOZZLE

ORIGINAL PAGE IS
OF POOR QUALITY

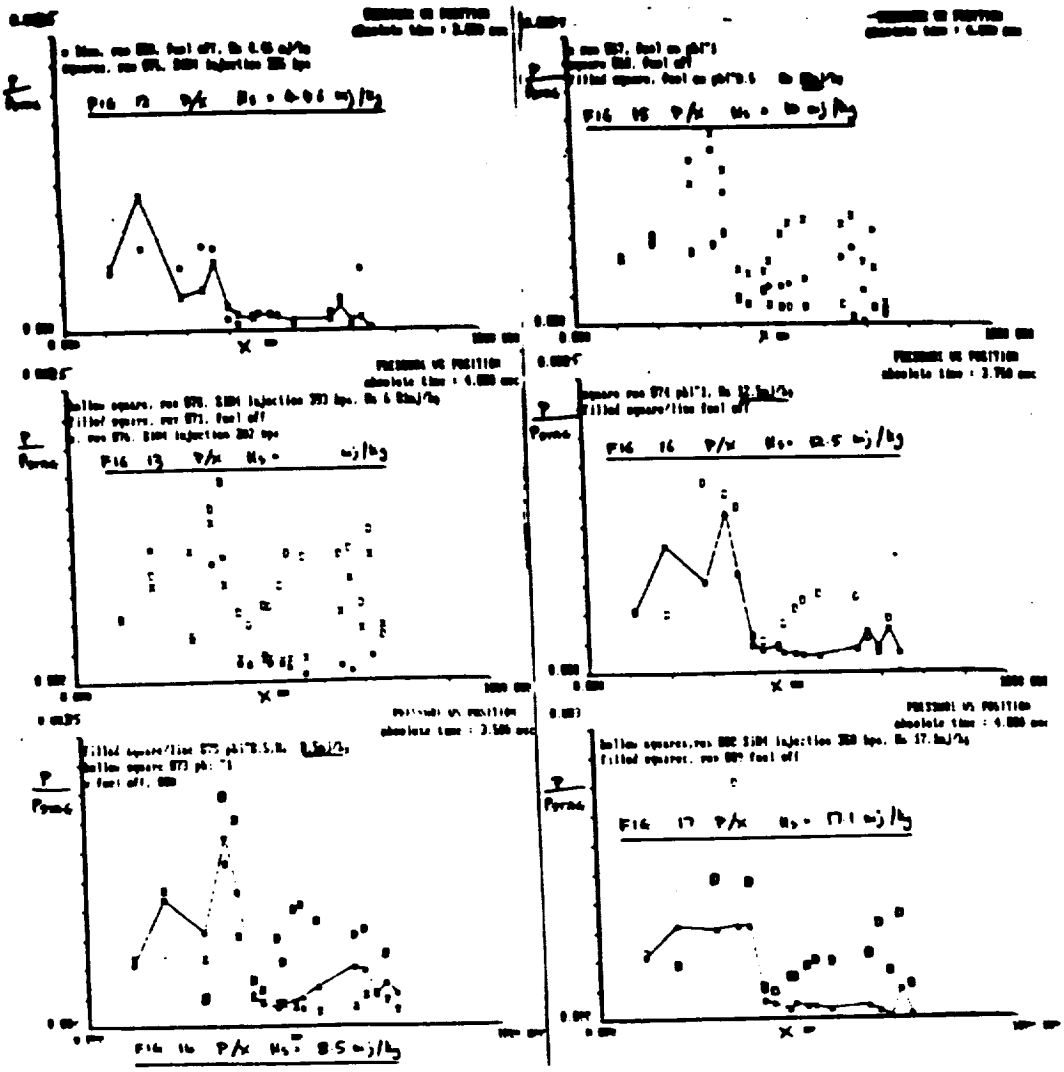

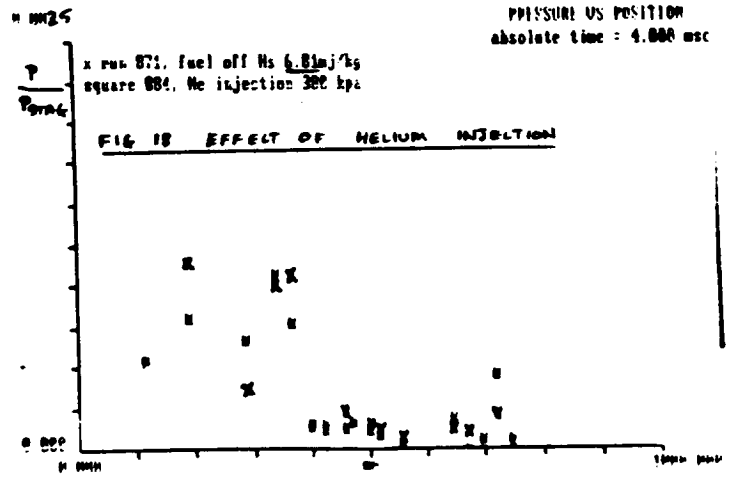

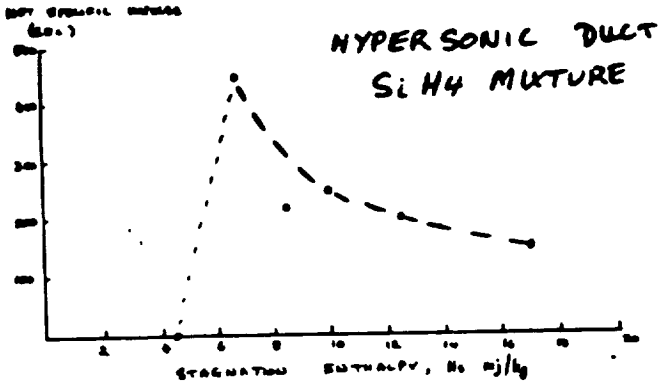

FIG 19 SPECIFIC IMPULSE / STAGNATION ENTHALPY FOR 20% $Si H_4$ MIXTURE

I/Hs, super/hypersonic

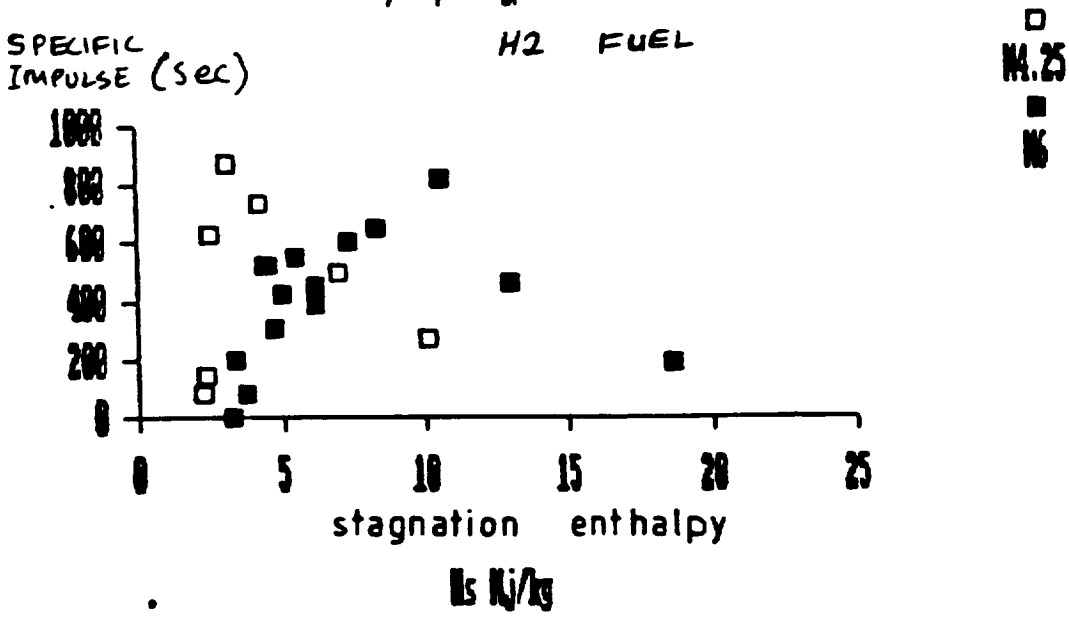

Fig 20 Super / hyper sonic combustion

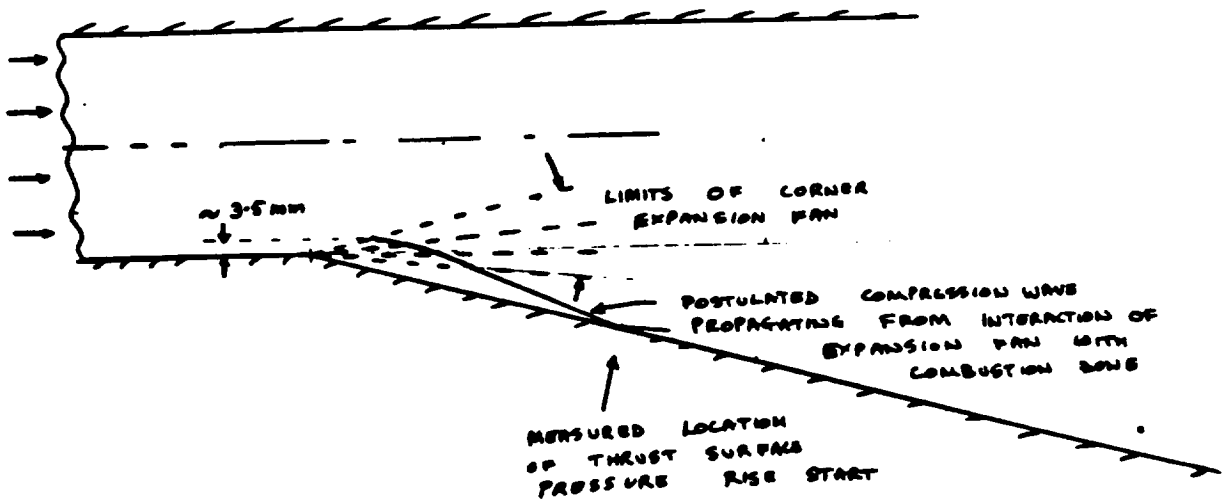

FIG 21 COMPRESSION WAVE TRACKING

ORIGINAL PAGE IS OF POOR QUALITY

PRESSURE-LENGTH CORRELATIONS IN SUPERSONIC COMBUSTION

P.A. JACOBS & R.J. STALKER

An experiment[1] has been proposed for study of the pressure sensitivity of supersonic hydrogen combustion in a constant-area combustor. The specific aim of the experiment was to investigate the theoretical pressure-length correlations[2] by conducting trials in three geometrically similar models. The pressure in the models was to vary over an order of magnitude but the pressure by model - length product was to be held constant.

Here we report that the largest of the three models (and in some ways the most difficult model) has been constructed and the initial flow measurements have been made. The correlation $P^{1.7}\,\ell$ = const and the length of the combustor (1.2m) determined the smallest pressure below which we would not get combustion in the largest of the three models. The duct pressure in these runs was ~ 29 kPa.

The overall flow configuration is shown in figure 1. The shock tunnel is fitted with a nozzle that expands the gas to approximately M = 8 (design area ratio = 670). The test gas is recompressed to $M \approx 3.4$ through a pair of wedges (and their associated shocks) and is then allowed to enter the model. The first 113 mm of the duct expands the gas flow to $M \approx 4.4$ and at the end of this expansion the hydrogen fuel is injected from the rear of a centrally located strut. The hydrogen is injected parallel with the air flow and forms a wake-like mixing region downstream of the injector. The estimated flow conditions at

the injector exit plane are given in table 1.

The wall pressure, as a function of distance downstream of the injector, is shown in figure 3 for hydrogen injection into air, hydrogen injection into nitrogen and air flow without hydrogen injection. From the general trend of increasing pressure when hydrogen is injected into the air flow and constant pressure otherwise, it appears that the hydrogen does burn at these conditions. ($H_s \approx 9.1$ MJ/kg, $P_{duct} \approx 29$ kPa $\phi = 0.76$). Hence we have something interesting to measure.

The next step is to try to match the CFD codes to these pressure data and then use the codes to compute burning lengths and ignition lengths.

REFERENCES

1. R.G.Morgan et al 1987: "Shock tunnel studies of scramjet phenomena", NASA Grant NAGW 674, Supplement 3.

2. P.W. Huber, C.J.Schexnayder & C.R. McClinton 1979: "Criteria for self-ignition of supersonic hydrogen-air mixtures", NASA Technical Paper 1457.

TABLE 1: Nominal conditions in large scramjet.

Shock tube tube data taken from shot 1410.

diaphragm thickness = 5mm

fill pressure = 150 kPa

fill temperature = 300K

Shock speed = 3.145 km/sec

steady reservoir pressure $\approx$ 60 MPa = P_s

ESTC (conditions after expanding reservoir to 60 MPa)

stagnation enthalpy $H_s \approx 9.13$ MJ/kg

temperature $T_s \approx 5747$ K

NENZF calculation of conditions at the end of the M=8 nozzle. (stop expansion when $P_{pilot}/P_s \approx 0.004$, assume $P_{pilot} \approx 0.92\ \rho u^2$)

effective length of nozzle = 9.89 cm

$M = 7.12$ $\gamma = 1.36$ $u = 3962\ ms^{-1}$

$P = 0.01660\ kg/m^3$ $P_{static} = 3.795$ kPa $T_{static} = 790$ K

flow through shocks (15^0 wedges) and then an isentropic expansion through the initial part of the duct (area ratio = 2.653) to the exit plane of the injector.

$M_{duct} \approx 4.37$

$P_{static} \approx 28.8$ kPa

$T_{static} \approx 1802$ K

disassociation fraction (assuming the composition remains frozen through shocks)

$$\alpha_O = \frac{[O] + [NO]}{[O] + [NO] = 2[O_2]} = 0.207$$

Table 1 (continued): Nominal conditions in large scramjet.

Mass flow of air

after shocks ρ = 0.1571 kg/m^3 , u = 3420 ms^{-1}

intake size = 0.014 m x 0.100 m

$\dot{m}_{air}$ = 0.7522 kg/sec

$\dot{m}_{O2}$ = 0.232 $\dot{M}_{air}$ = 0.1745 kg/sec

Mass flow of hydrogen

H_2 manifold pressure $\propto$ 250 kPa (shot 1420)

Injector calibration constant = 6.60e-5 kg/sec /kPa

$\dot{m}H_2$ = 0.0165 kg/sec

Equivalence Ratio $\phi = \frac{\dot{m}_{H_2}}{\dot{m}_{O_2}} \frac{16}{2} = 0.756$

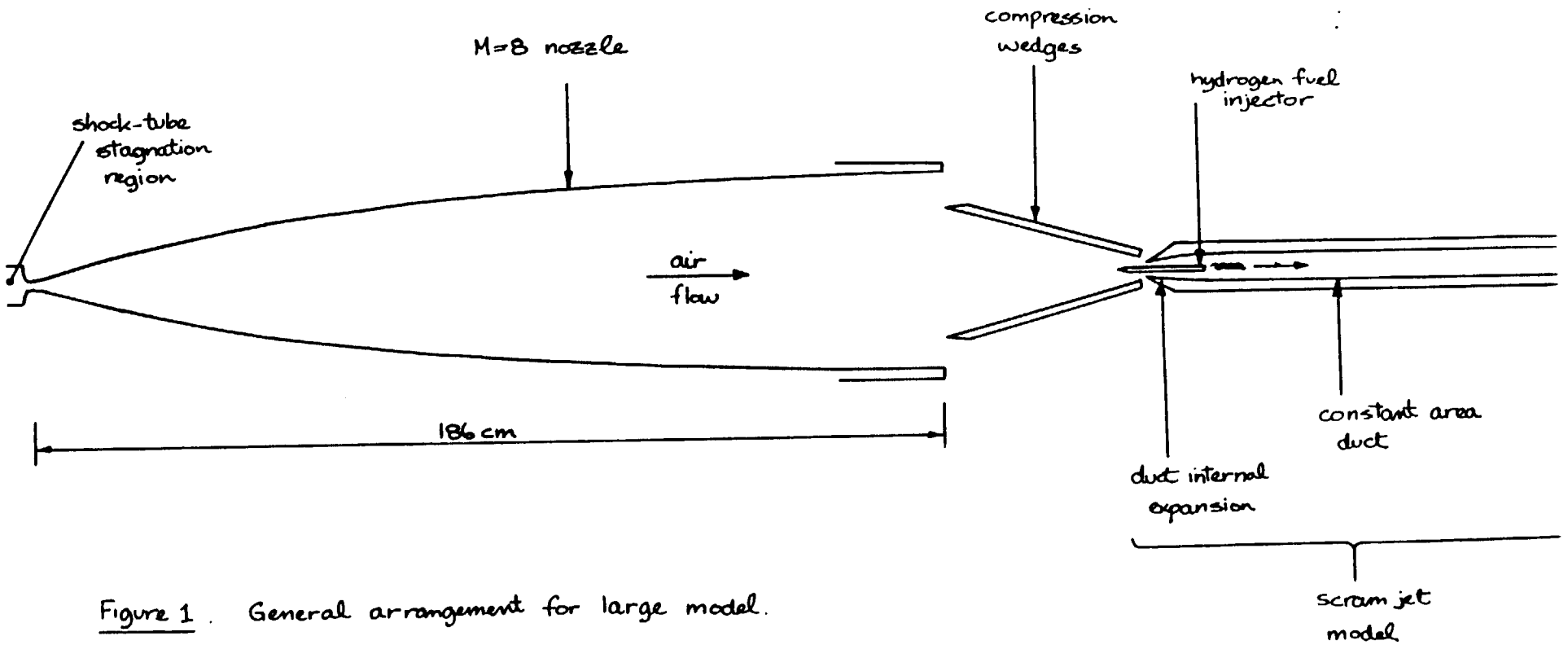

Figure 1. General arrangement for large model.

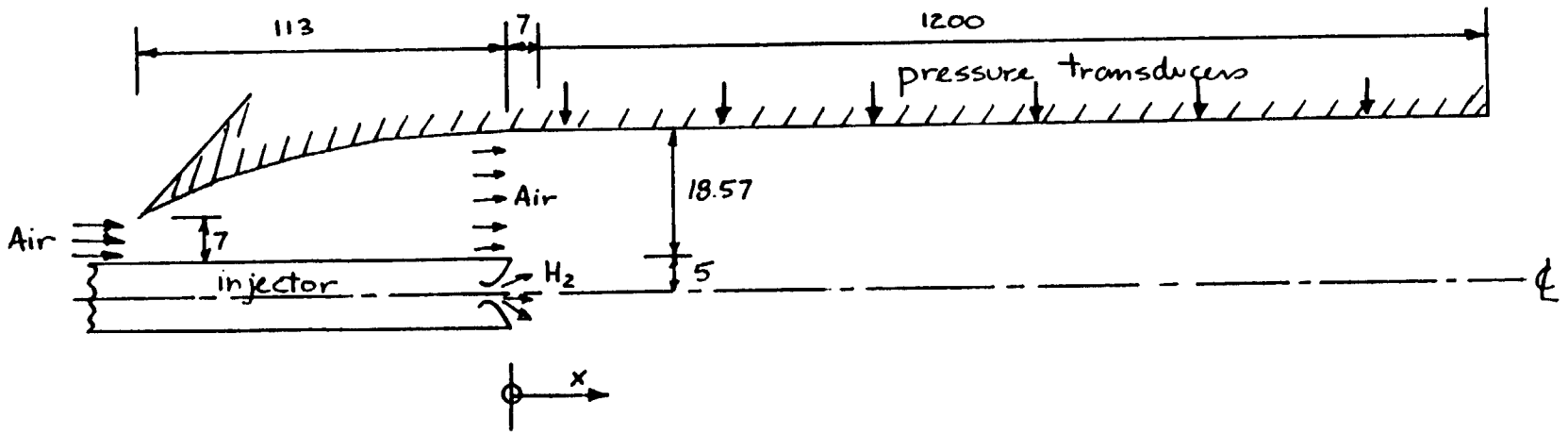

Figure 2: Combustor flow configuration

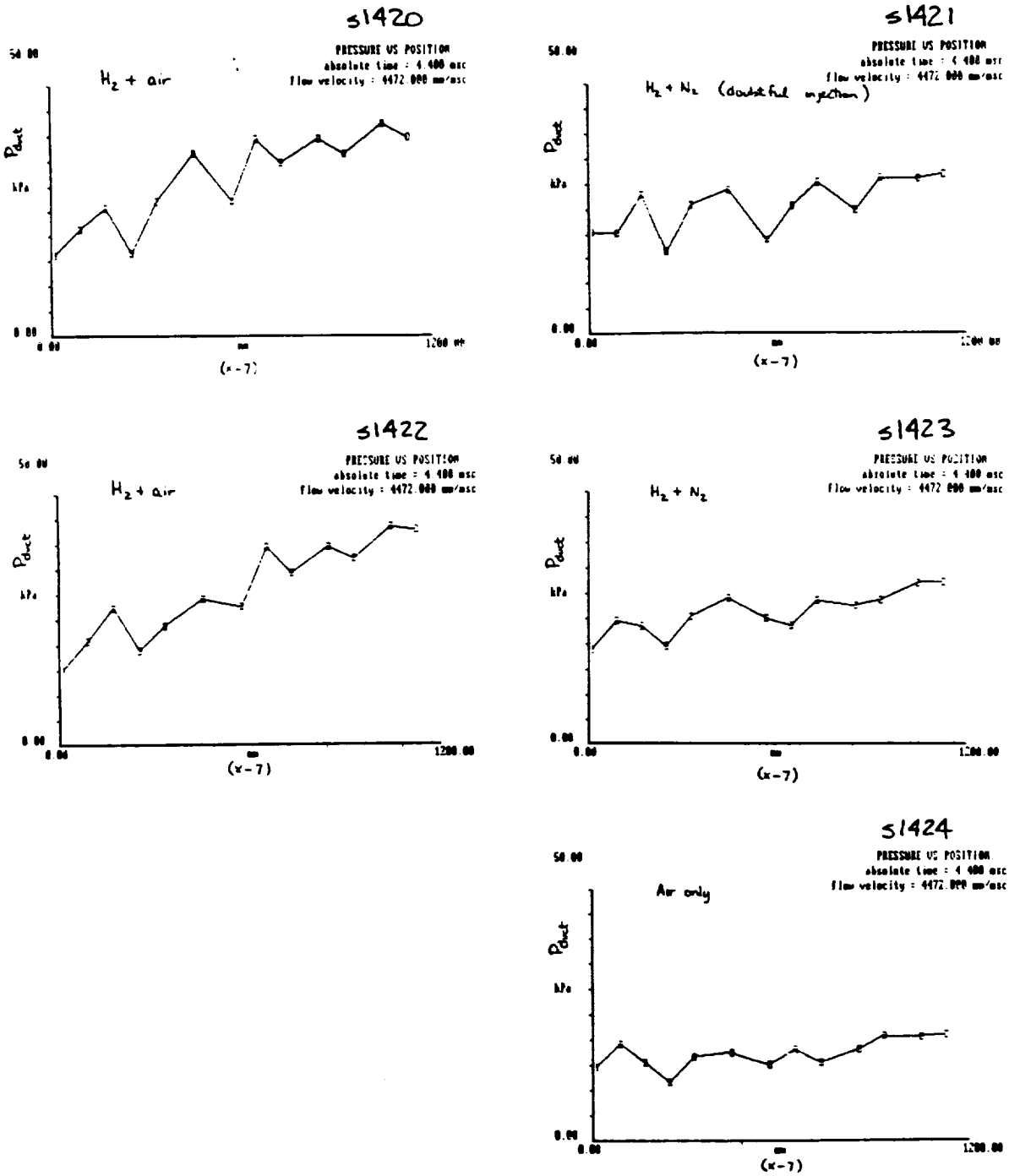

Figure 3: Wall pressures for the large scramjet trials (Dec 1989). Shot numbers and test gases as shown on each frame. The data points represent averages over a 0.1 msec interval.

HOT HYDROGEN INJECTION TECHNIQUE FOR SHOCK TUNNELS

by Michael Wendt

The effect of fuel temperature on combustion in a supersonically and hypersonically combusting ramjet is currently being studied in the T4 shock tunnel. It is intended to not only study the temperature effect, but the corresponding density distribution and velocity distribution effects as well.

A device is currently being manufactured to produce hot hydrogen for injection into the ramjet model. Many difficulties were encountered in its development, including:

i) The ramjet model instrumentation calibration was very temperature sensitive and hence heat sources had to be kept well away from the test area.

ii) To minimize losses only a short length of piping was allowable between the heat source and injector nozzle.

iii) Many standard components had difficulty withstanding the required stagnation temperature (1200 K) at the injection pressure.

iv) Only a small amount of fuel was to be used to minimize the build up of unburnt hydrogen inside the Dump Tank. This corresponded to a maximum supply time of 20 - 40 milliseconds.

After evaluating a number of solutions it was decided to use a Gun Tunnel. The gas is heated by a combination of free piston compression and entropy rise through shock waves. It has the advantages of:

i) The hydrogen is only hot for a very short duration (< 30 msecs) and hence the temperature of the vessel walls is only raised slightly.

ii) The danger of having hot fuel in a vessel for an extended period of time is reduced.

ii) No heat is transferred to the ramjet model.

iii) Dry hydrogen is produced.

The layout of the gun tunnel is shown in the diagram over leaf. It consists of two tubes separated by a bursting diaphragm. The high pressure reservoir contains nitrogen and provides the driving pressure for the piston. The compression tube initially contains hydrogen at low pressure. A light nylon piston initially sits in the compression tube just in front of the primary diaphragm. The diaphragm is mechanically burst allowing the high pressure nitrogen to expand and drive the piston down the compression tube. The light piston is fast enough to cause shock waves ahead of it in the hydrogen gas giving an entropy increase (the entropy rise is small, however, due to the high speed of sound in H_2). The pressure in front of the piston increases causing the piston to decelerate near the high pressure end. The pressure increase also bursts the secondary diaphragm. The piston fluctuation dampens rapidly as pressure on both sides of the piston approach equality. Steady injection occurs with a near constant pressure on the rear of the piston.

The tunnel design has the following notable features:

i) The tunnel is positioned within the Dump Tank of T4 to increase the safety in event of explosion and to minimize the length of tubing between the hot hydrogen reservoir and ramjet model injector.

ii) The entire assembly is free to reciprocate linearly to allow the dynamics of the device to lower the stress induced in its structure.

iii) Bursting diaphragms are used to provide simple, low maintenance, reliable flow control capable of containing the high temperatures and pressures.

Construction of the tunnel is due to be completed in early 1990 with the first ramjet experiments due in the middle of the year.

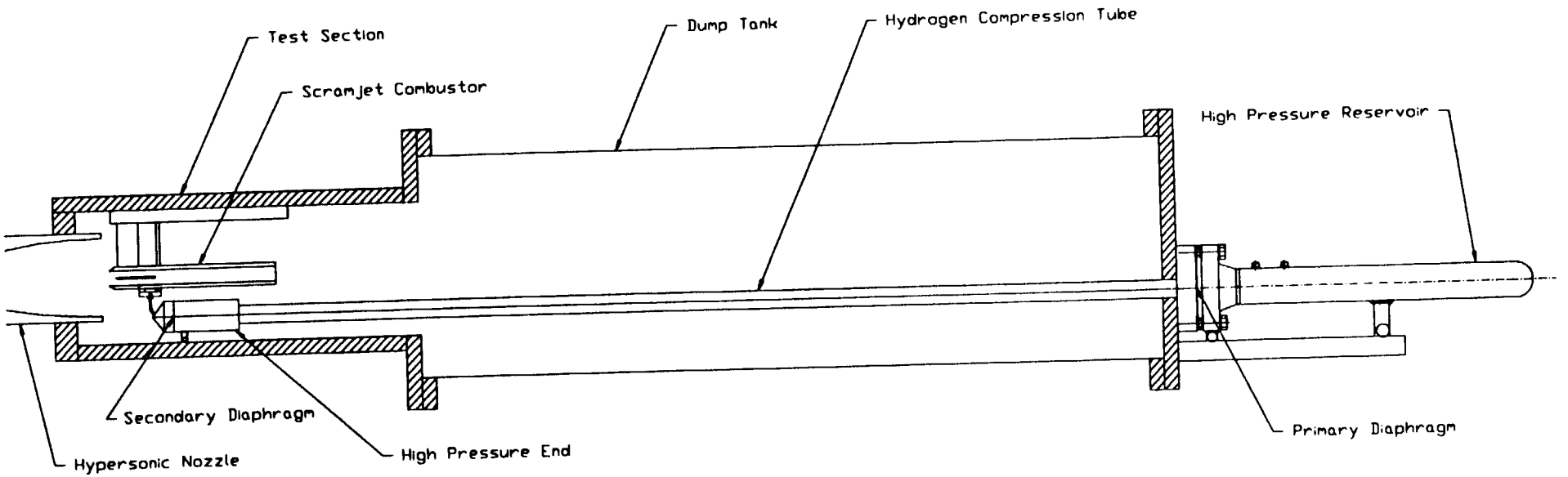

Hydrogen Gun Tunnel Layout

HEAT RELEASE - WAVE INTERACTION PHENOMENA IN HYPERSONIC FLOWS

AN OPTICAL STUDY

Annual Report, February 1990
by N.R.Ward

INTRODUCTION

The study of combustion waves in a scramjet duct is made very difficult due to the imperfect nature of the injection and mixing of fuel into the flow and the inherent disturbance to the flow which this causes to produce the desired heat release. This can be avoided by bringing about this heat release in another way. The flow produced by a free piston shock tunnel using a nitrogen test gas is highly dissociated but basically 'frozen' in this state due to it having been expanded to a temperature too low for a significant rate of recombination. When, however, it has its temperature and pressure raised passing through the system of shocks at the entry to the scramjet duct recombination progresses rapidly to bring the flow to its equilibrium level of dissociation. This recombination results in heat release, simulating quite closely the heat release during combustion. Thus by studying the waves generated in this way in a scramjet model in nitrogen flow in the T4 shock tunnel it is hoped that much can be learned about 'ideal' combustion and the combustion waves it generates.

It was decided to study these waves using optical techniques in order to keep disturbance of the flow to a minimum and collect as much information at each shot of the shock tunnel as possible. The optical system decided upon was the Differential or Schlieren Interferometer.

Since the analysis of these flows was to be done using optical methods development of a short exposure shutter and

associated triggering system was, in 1988, carried out. Combined with a polaroid camera this was used to take photographs of test flow over models. Some of the information gathered was then used to check experimental T4 test conditions against those computationally predicted, showing good agreement. A computer program was then developed to predict post-shock recombination profiles for different experimental conditions, allowing for detailed design of test conditions and model shapes for future tests in the T4 shock tunnel.

REPORT

In preparation for experiments in the T4 shock tunnel it was neccessary to design and build a model of an open-sided scramjet duct in which generated 'combustion' waves could be studied freely using optical methods. It was decided to begin with a simple model consisting of a pair of wedges as an intake followed by a pair of plates as a duct, with simply an open path to exit. Predicted intake shock wave angles were calculated to allow mapping of these shocks and consequent design of the model components such that these shocks are allowed to escape the duct through gaps in the walls rather than having them reflect and propagate the length of the duct, thus confusing the wave pattern. The resultant model design is shown in Figure 1. This model was then built.

The most critical task to be completed before the actual experiments with the T4 shock tunnel could begin was to be the design, assembly and alignment of the optical system. The extent of the difficulties would, however, exceed all expectations.

A CCD camera system capable of capturing images with exposure times of as low as 100 μs, which had been developed

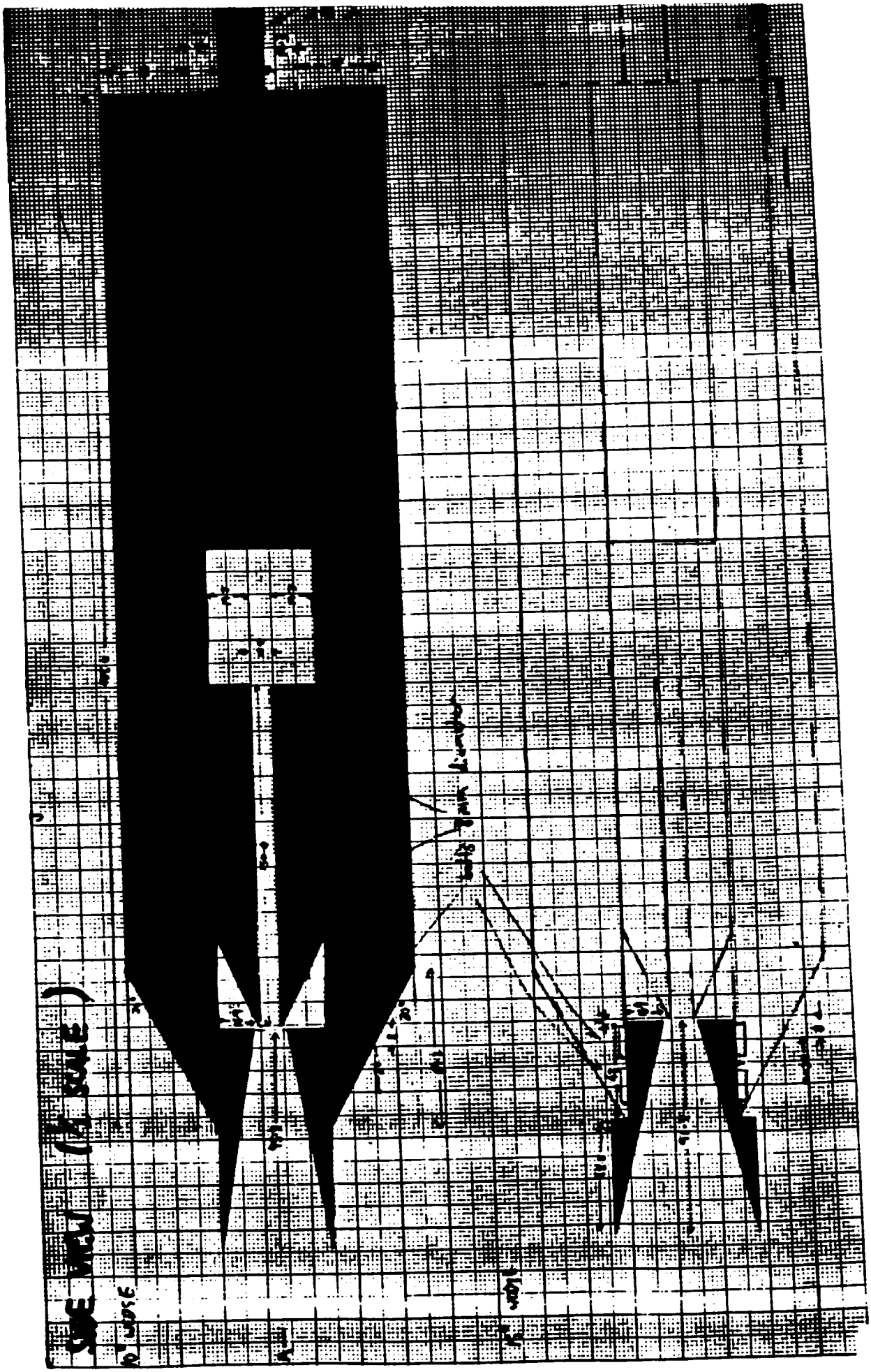

in this department, was used with only a few teething problems. Details of this system can be found in reference (5).

A Laser Electronics ruby laser system with He-Ne alignment laser was installed on the roof of an enclosed optics box mounted on rails on the test section 'dance floor' of T4. See Figure 2 for sketch diagram of the optics box. The laser output beam was lead down into the optics box using an optic fibre. It was decided that due to the short test time in T4 the image recorded by the optics should be as close as possible to instantaneous, thus it was decided to install an electronic Q-switch to bring the ruby laser pulse time down from about 1 ms to less than 50 μs.

Unfortunately the Pockells Cell component of the Q-switch proved, after much searching, to be faulty, and was sent away for replacement. Subsequently it was decided to leave the laser without a Q-switch until after the first set of T4 experiments.

FIGURE 2. SKETCH OF OPTICS BOX FROM THE SIDE

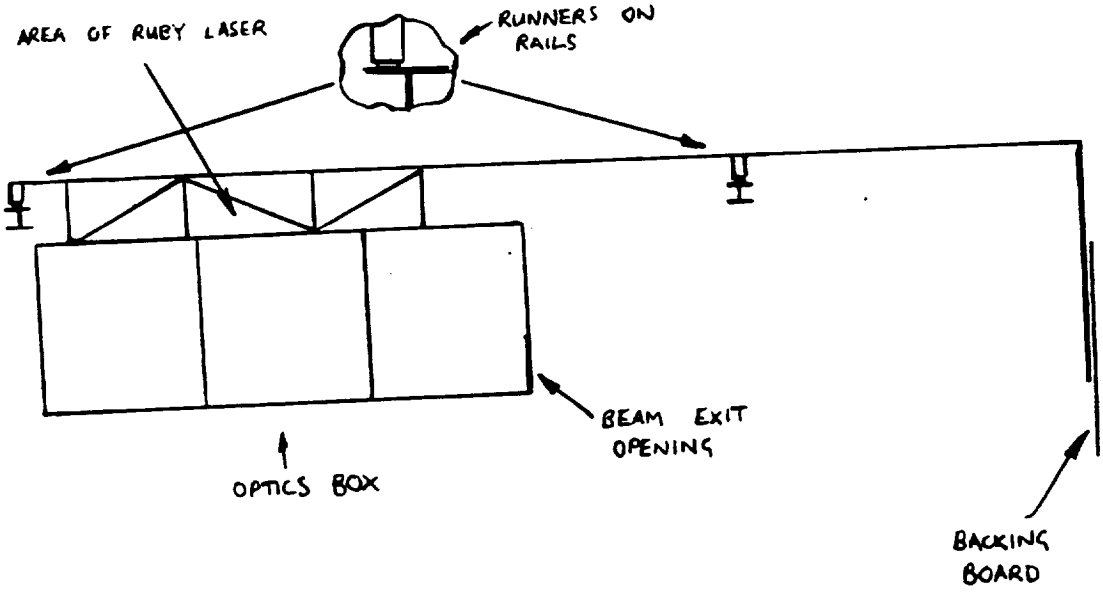

The next task was to design and build mounts for the optical components of the actual optical system. Once the components were mounted it was time to develop a procedure for aligning them so as to give a proper interference pattern and a sharp image of an object in the test section, and hence a good differential interferogram. The design that had been settled upon was that of a double pass differential interferometer, which made the alignment more difficult. The layout for this optical system is shown in Figure 3.

It was found that most of the alignment was easiest carried out using an extra He-Ne laser in place of the output end of the fibre optic inside the optics box, as this gave a bright and non-diverging colimated beam which was easy to trace through the system. Also, in the course of alignment a number of the optical components were found to be of insufficiently high quality or of inappropriate specifications to be able to obtain an image. These were replaced in due course and eventually a systematic procedure for aligning the system was developed. This can be summarised as follows:

(i) Centre alignment laser to give a well directed and horizontal beam.

(ii) Work through the system of mirrors (with other components removed) adjusting each to pass the beam on to the centre of the next.

(iii) Use a screen with a hole for the outgoing beam in it to adjust the final mirror so that the returning beam follows the same path as the outgoing beam.

(iv) Position each lens in turn in the beam centred so as to not alter the path of the outgoing beam.

(v) Adjust lens positions in direction of beam so that the focus of the beam before the concave mirror coincides for the incoming and outgoing beams. Readjust the final mirror if neccessary so that incoming and outgoing beams still coincide.

FIGURE 3. OPTICAL SYSTEM : DIFFERENTIAL INTERFEROMETER.

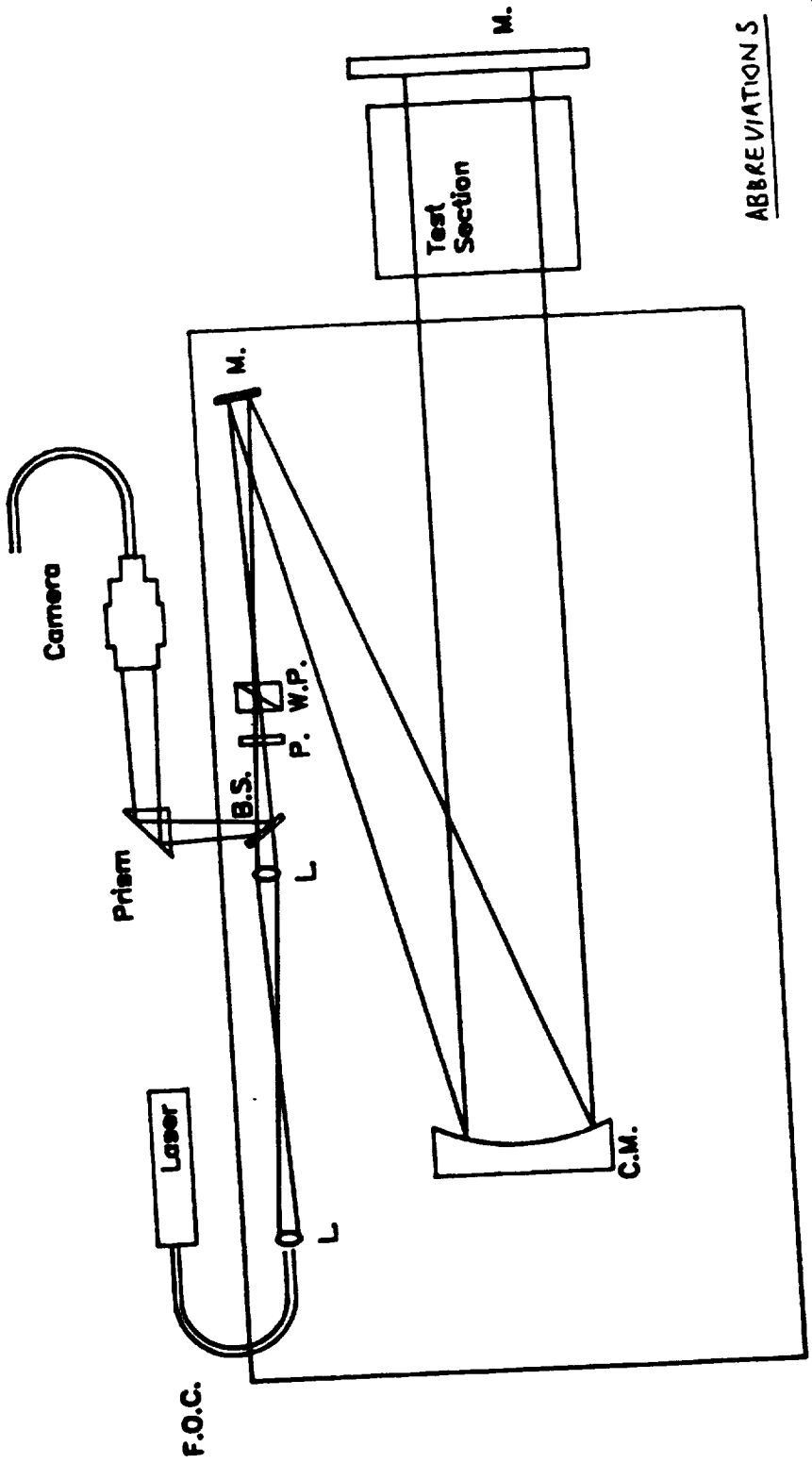

ABBREVIATIONS

L.	LENS
M.	PLANE MIRROR
C.M.	CONCAVE MIRROR
B.S.	BEAM SPLITTER
P.	POLAROID
W.P.	WOLLASTON PRISM
F.O.C.	FIBRE OPTIC CABLE

(vi) Place polaroid and wollaston prism in the path of the beam near the focus of the concave mirror.

Some adjustment of some components (such as the cubic beamsplitter) has also been found neccessary to eliminate stray reflections which disturb the image. This procedure has been found successful and good interferograms (using the direct He-Ne beam as a source) have been obtained.

Currently final alignment is being carried out with the laser source travelling through the fibre optic. Presently the original multi-mode fibre optic is being replaced with single-mode fibre optic to eliminate severe distortion in the illumination pattern of the light emitted from the fibre.

FUTURE

It is expected that the differential interferometer will be fully operational shortly. Tests to determine how severely the vibrations during the operation of the shock tunnel affect the alignment of the optical system will then be carried out in order to minimise this disturbance.

Experiments with the previously described model in the T4 shock tunnel will follow, using the differential interferometer to obtain information on the simulated combustion waves caused by nitrogen recombination aswell as other wave phenomena in the scramjet duct.

REFERENCES

(1) J.E.A.John 'Gas Dynamics'

(2) Vincenti and Kruger 'Introduction to Physical Gas Dynamics'

(3) R.J.Stalker 'Post Shock Non-Equilibrium Flows in Hypervelocity Aerodynamics' AIAA Conference 1988

(4) Merzkirch 'Flow Visualisation'

(5) B.C.Daniel 'Snapshot Video Camera System' Manual November 1988

A STUDY OF THE WAVE DRAG IN HYPERSONIC SCRAMJETS

Nesrin Akman

The Mechanical Engineering Deptartment

The University of Queensland, St. Lucia, 4067

ABSTRACT

A model two-dimensional flow in a convergent-divergent duct is analysed. It is found that wave drag varies with the Mach number in a "saw tooth" manner with increasing amplitude and period. The drag value reaches its minimum when symmetrical wave distribution can be obtained in linear theory within the system. the maximum drag value coincides with Mach numbers larger than that in which the shock wave emanating at the leading edge of one plane completely misses the other plane. It is also found that the thrust varies linearly when combustion is simulated by adding heat without addition of mass or change in the compressibility factor.

1.0 INTRODUCTION

Wave phenomena and management of waves play an important role in hypersonic scramjets. In order to achieve beneficial interaction

between the waves and the thrust surfaces, it is necessary to understand the drag produced within the system as a result of the wave distribution. This understanding becomes more critical as the flow Mach numbers within the duct take hypersonic values, and inefficient flow management results in increased drag.

To compare the results obtained in this study with that of linearized theory, and validate the numerical method used in the analysis, an inviscid perfect gas with constant ratio of specific heats is initially used in the analysis. Presently, the temperature dependence effects of the specific heat constants, and the viscosity effects are included in the study. The concept of "boundary layer bleeding" to achieve better thrust is examined. Combustion is represented by heat addition at the throat, without the addition of mass or change in the compressibility factor which normally is associated with combustion. The flow is assumed to be two-dimensional.

2. The Busemann Biplane.

A two dimensional convergent-divergent duct, formed by placing two thin, double wedge aerofoils opposite to each other, is called a "Busemann biplane' (Figure 1). The beneficial effect of the Busemann biplane in the reduction of wave drag is well discussed in the

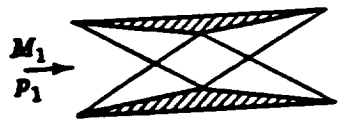

Figure 1. Busemann biplane.

literature and the author's earlier report (1989).

The drag of the busemann biplane according to the two dimensional linear theory as a function of the Mach number is given in Figure 2.

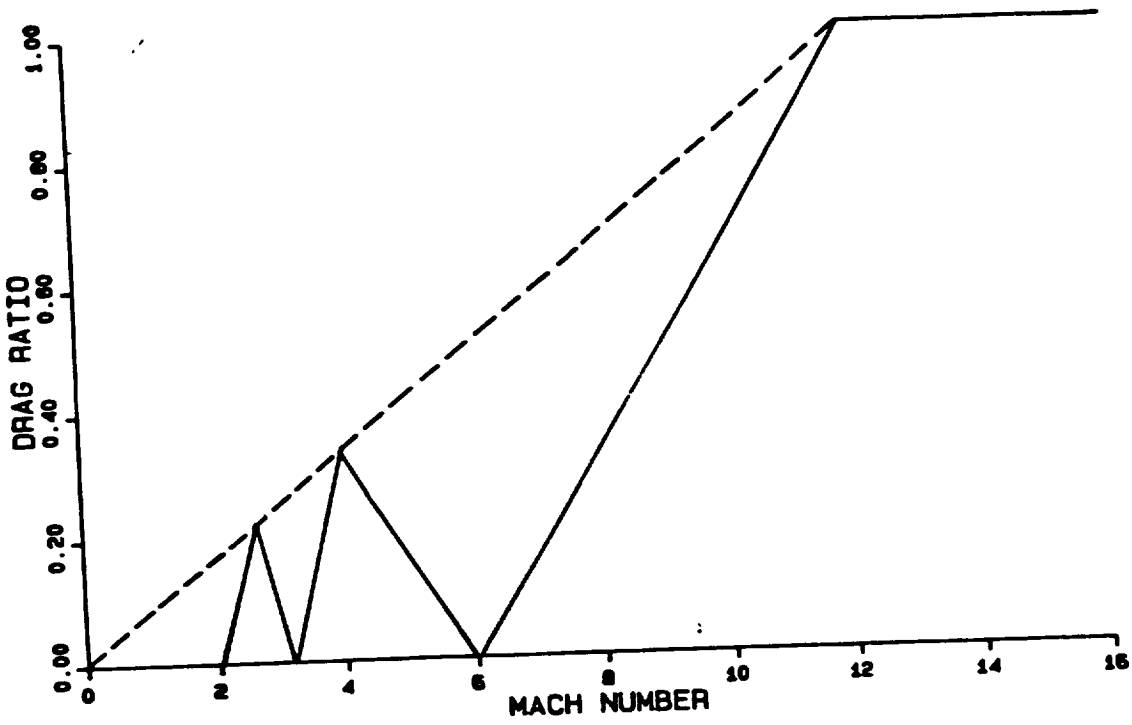

Figure 2. Drag of the Busemann biplane as a function of the Mach Mach number obtained by two dimensional linear theory.

The Busemann biplane is referred to as the "Busemann Scramjet" (Supersonic Combustion Ramjet) when fuel is injected into the system. The combustion of the fuel at supersonic velocities and at low densities is very difficult to achieve. To obtain good mixing, and hence efficient burning of the fuel, is a study in its own and will not be discussed here. However, the allowable temperature within the scramjet should be limited to 2000 K; since, the fuel will not burn at higher temperatures.

In the context of this study, the combustion is represented by heat addition at the throat, without addition of mass or change in the compressibility factor which is normally associated with combustion.

3. The Numerical Code

The code written is based on the two-dimensional unsteady Euler equations and the Godunov's method. The geometry adopted to represent the scramjet is that of the Busemann bi-plane. Due to the symmetry only the upper half of the duct is considered.

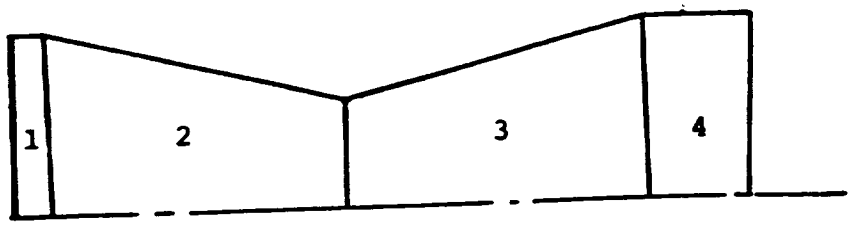

Figure 3. The adopted geometry of the scramjet

The upstream (region 1) and downstream (region 4) regions are added to the Busemann biplane configuration. The regions 2 and 3 are termed the "compression" and "expansion" regions (Figure 3). The angle between the x-axis and the compression (drag) surface is taken to be equal to the angle between the x-axis and the expansion (thrust) surface, corresponding to optimum thrust conditions in linearized theory.

Deflection angles of 1°, 2°, 4°, 6°, 10°, 15° have been studied. In all cases the design condition was taken to be at the upstream Mach number of 6. The results for deflection angle of 2° have been

presented in the earlier report (1989).

4. Results

The results obtained using the numerical code are presented above in Figure 4. These results are in close agreement with the linearized theory in the prediction of the drag within the system (Figure 2). The wave drag varies with the Mach number as predicted from the linear theory.

The code fails to give zero drag at the design Mach number. The non-zero result is more accurate since in the region of interaction between the expansion fan and the surface, the pressure drops isentropically, reducing the amount of thrust which would have been otherwise developed The percentage of the expansion surface which intercepts the expansion fan increases in a non-linear fashion as shown in Figure 5.

Surface contouring may be employed to counteract the effect of the expansion fan on the surface pressures. This procedure $\overset{re}{\wedge}$ stores the pressure values to the value prior to the expansion fan; however, this procedure reduces the projected thrust surface, hence the available thrust (Figure 6).

For six degree deflection angle the ratio of the calculated biplane drag coefficient to the monoplane drag coefficient at the design condition increases from 0.18613 to 0.29896 due to decrease in the projected thrust surface when the surface contouring is employed.

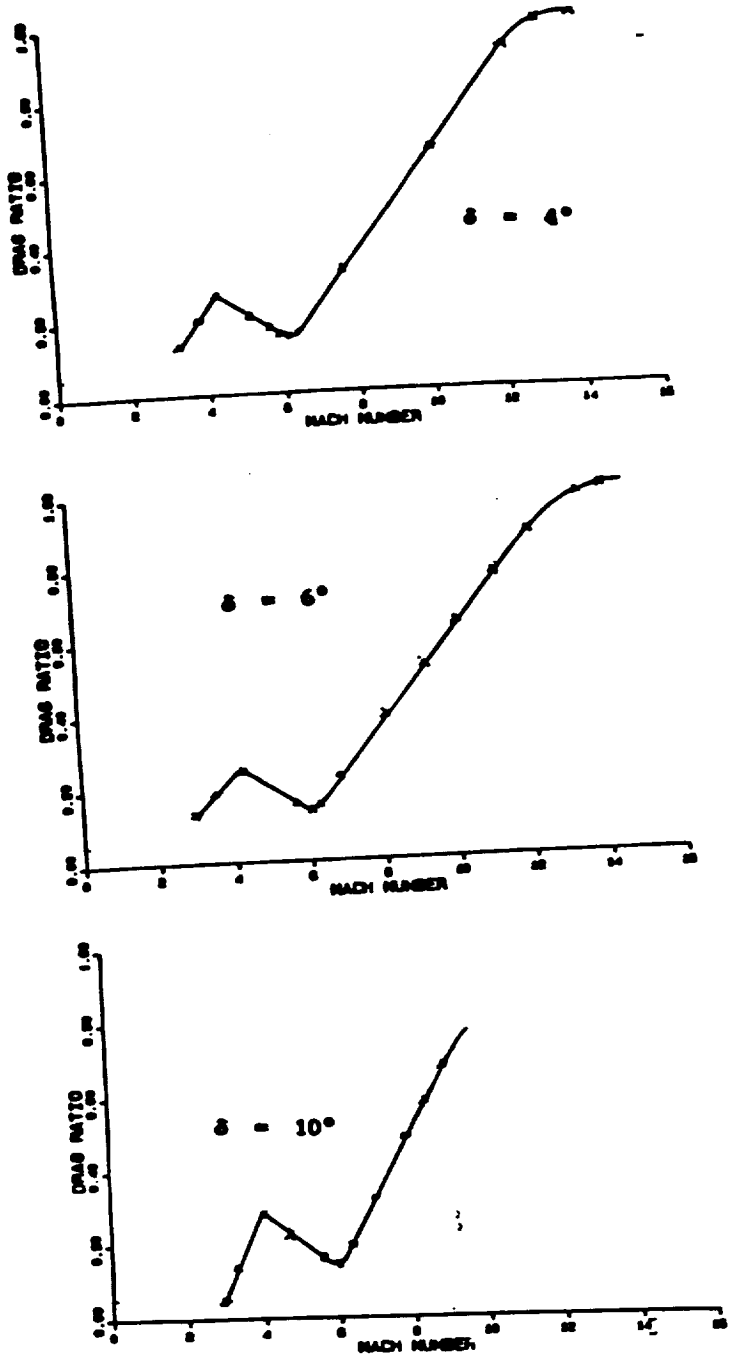

Figure 4. Ratio of the biplane drag coefficient to the monoplane drag coefficient as a function of the Mach number. Design Mach number is 6.

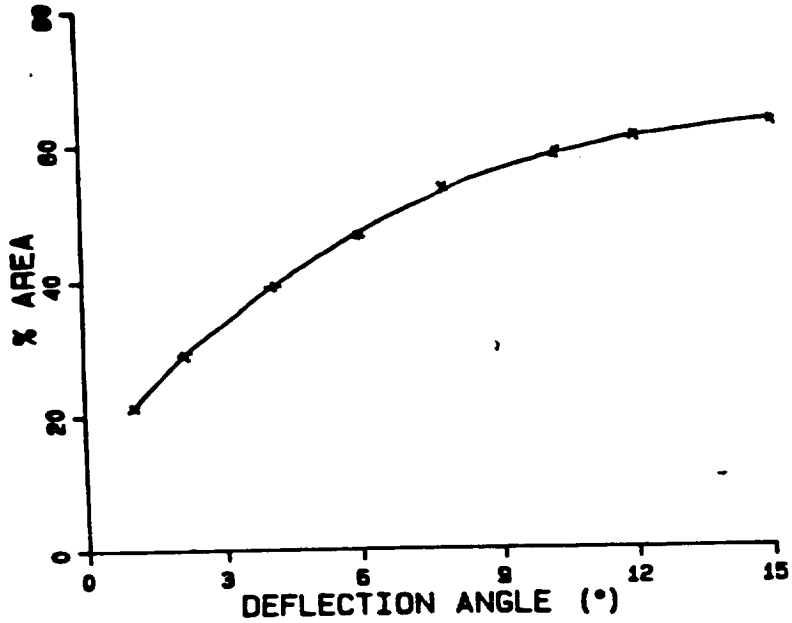

Figure 5 The percentage of the surface which intercepts the expansion fan as a function of the deflection angle.

If the pressures in the affected portion of the surface are restored to the value prior to that where the expansion fan intercepts the surface, without change of the surface geometry, the drag reduces to zero.

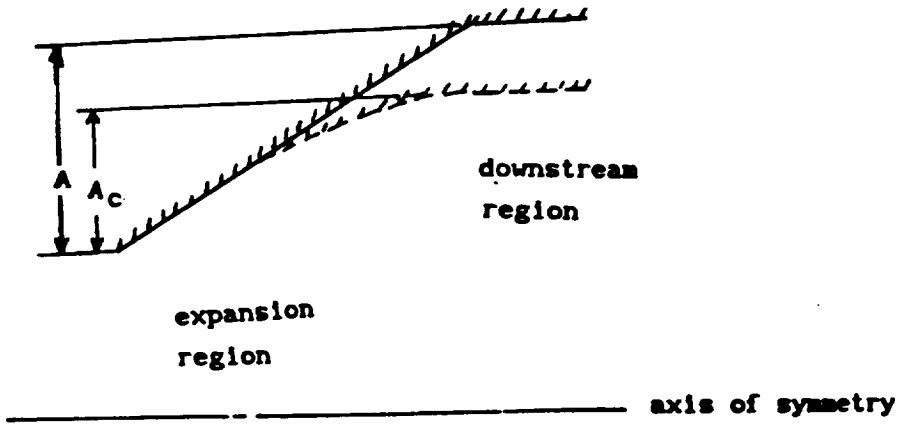

Figure 6. The effect of surface contouring on the projected thrust surface. (A, A=Projected thrust area)

The pressure contours and the pressure distribution along the surface for various deflection angles at the design Mach number 6, are given in Figures 7 and 8.

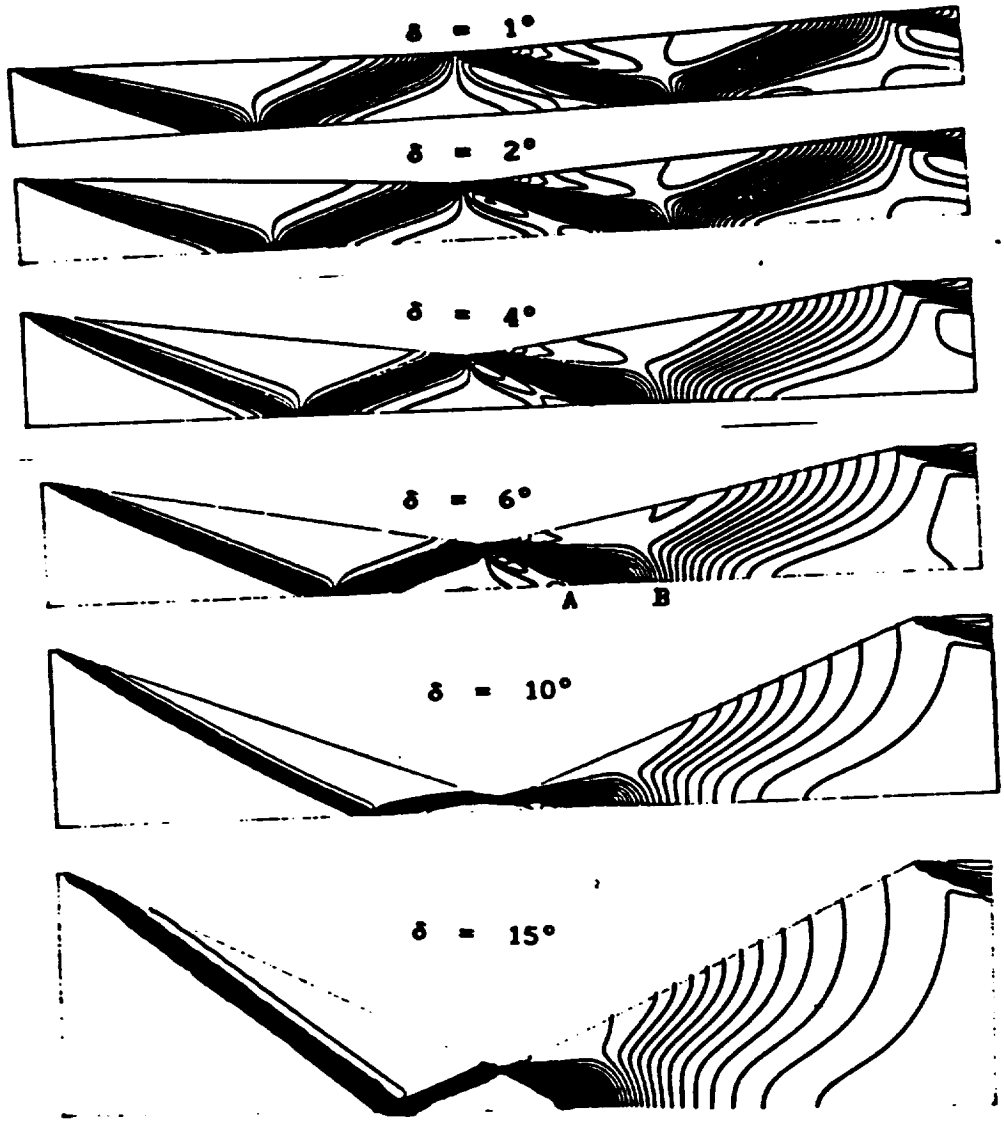

Figure 7. Pressure contours at various deflection angles

All of the reflected expansion fan does not meet the surface as seen in the Figure 7. In other words, part of the expansion fan spills from

the system and interacts further with a shock at the trailing edge of the duct. The expansion fan generated at the shoulder meets the axis of symmetry at AB. The reflected expansion fan therefore starts at point A and interacts with the original expansion fan. The effect of this is seen as the curved contour lines in Figure 7.

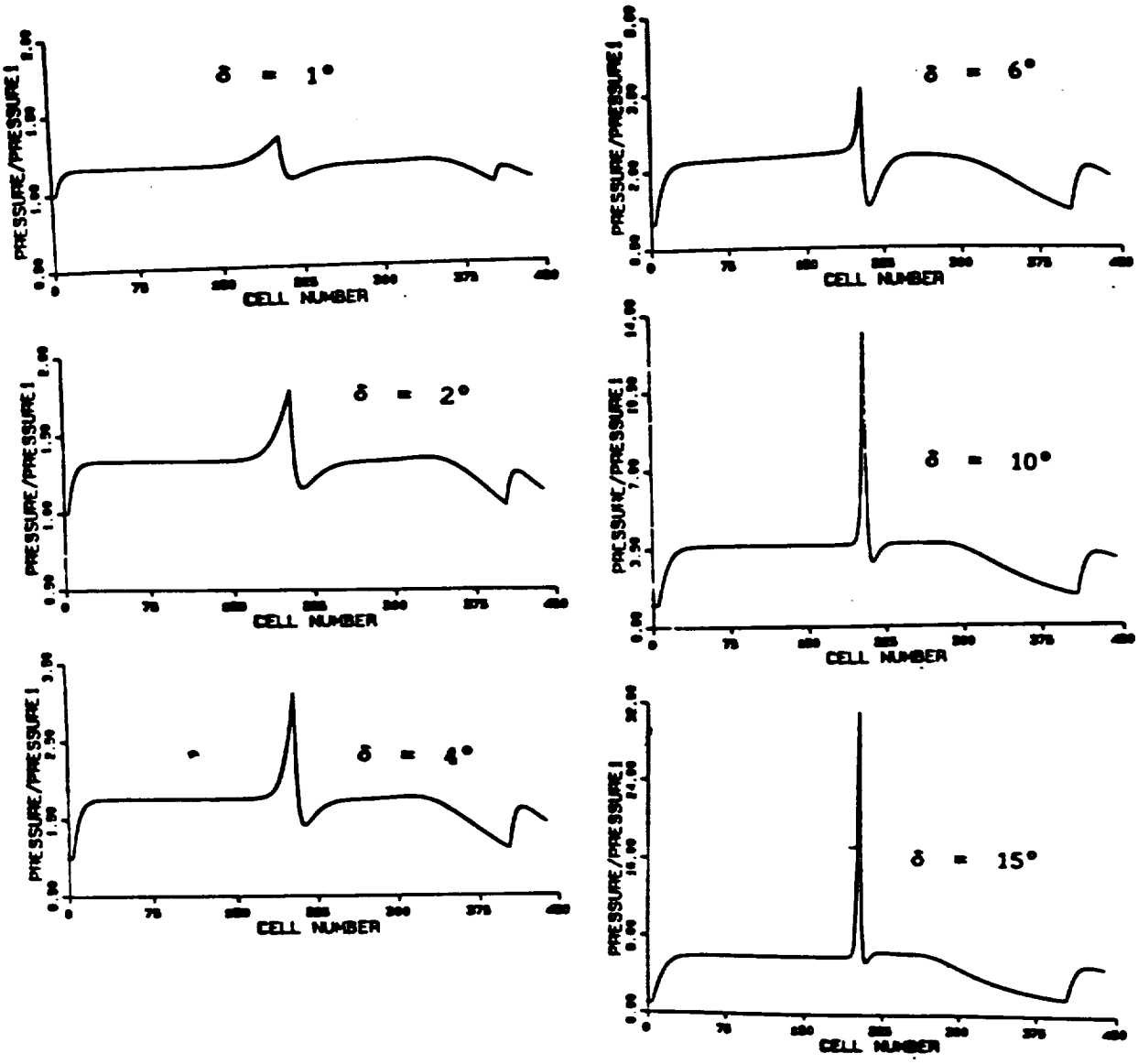

Figure 8. Pressure distribution along the surface for various deflection angles.

A similar problem exists at Mach numbers at which the reflected shock wave interacts with the expansion wave. At these Mach numbers, the reflected shock wave curves and meets the surface earlier than is predicted from the linear theory (Figure 9). This results in increased thrust in the expansion region. Instead of the ratio of the biplane drag to that of monoplane drag increasing to the value of 1.0 along a straight line, a more gradual increase is obtained as shown in Figure 9.

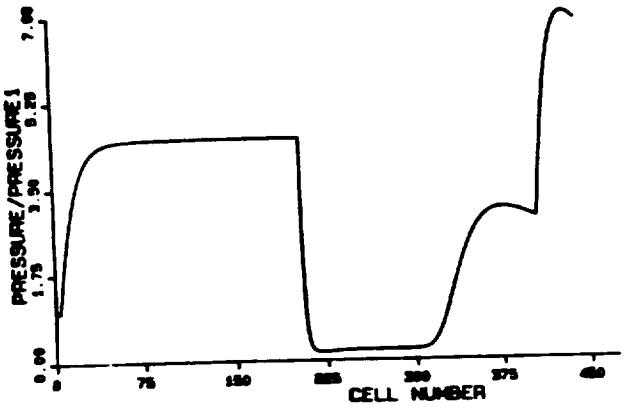

(a) Pressure distribution along the surface.

(b) Pressure contours within the system.

Figure 9. The interaction of the reflected shock wave with the expansion wave from the shoulder.

4.1 Shock Smearing

The smearing of the discontinuities, such as shocks, presents a problem

in numerical methods when high accuracies are required. The calculation of the wave drag and complex geometries usually require such discontinuities to be represented quite precisely. Godunov's first order method tends to be diffusive at weaker shocks in two dimensional flows. However, it does capture the shock well, and the calculated pressure, density and temperatures agree with the values obtained using the oblique shock equations within 2% in the range of deflection angles studied (1° - 15°).

The Busemann scramjet used in this study is a long and very narrow biplane. In order to show pressure contours clearly they are plotted on a geometry which is stretched in the vertical direction by a factor of 2. This tends to spread the shock waves twice as much in this direction hence falsely accentuates the smearing.

The width of the shock waves seen in these pressure contours is not only due to the smearing but also due to the finite dimensions of the cells. Shock waves will pass through several cells on each row as shown in Figure 10.

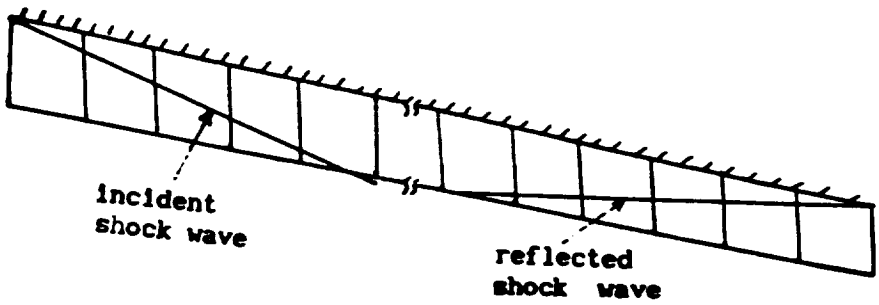

Figure 10: Surface cells which the incident and reflected shock waves pass through at the design condition.

Figure 11 gives the pressure distribution along the axis of symmetry for the various deflection angles at the design condition. The small hump, A, seen in these pressure profiles is the result of this averaging process. The shock wave reflects from the surface just prior to the shoulder causing the small increase, hence the hump in the pressure distribution along the axis of the symmetry. This effect is cancelled with the expansion wave emanating from the shoulder.

At the design Mach number and at Mach numbers less than that of the design value (at which a symmetrical wave is a distribution obtained in linear theory) there is an over-expansion region starting at the shoulder (Figure 8). The flow conditions recover and reach the correct values rapidly. This effect again is due to the finite dimensions of the cells employed to represent the flow and the first order nature of the code, and proved to be very difficult to overcome without post processing of the results.

The advantage of the Godunov's method is its accurate prediction of the fluid properties in complex flows. From the ratio of the predicted pressure to the upstream pressure and upstream Mach number the shock angles can be calculated accurately. This allows the use of post processors to eliminate the numerical diffusion of the discontinuities from the results. However, writing a post processor which deals with the regions where the interaction of waves take place, is difficult due to the complexity of the logic involved.

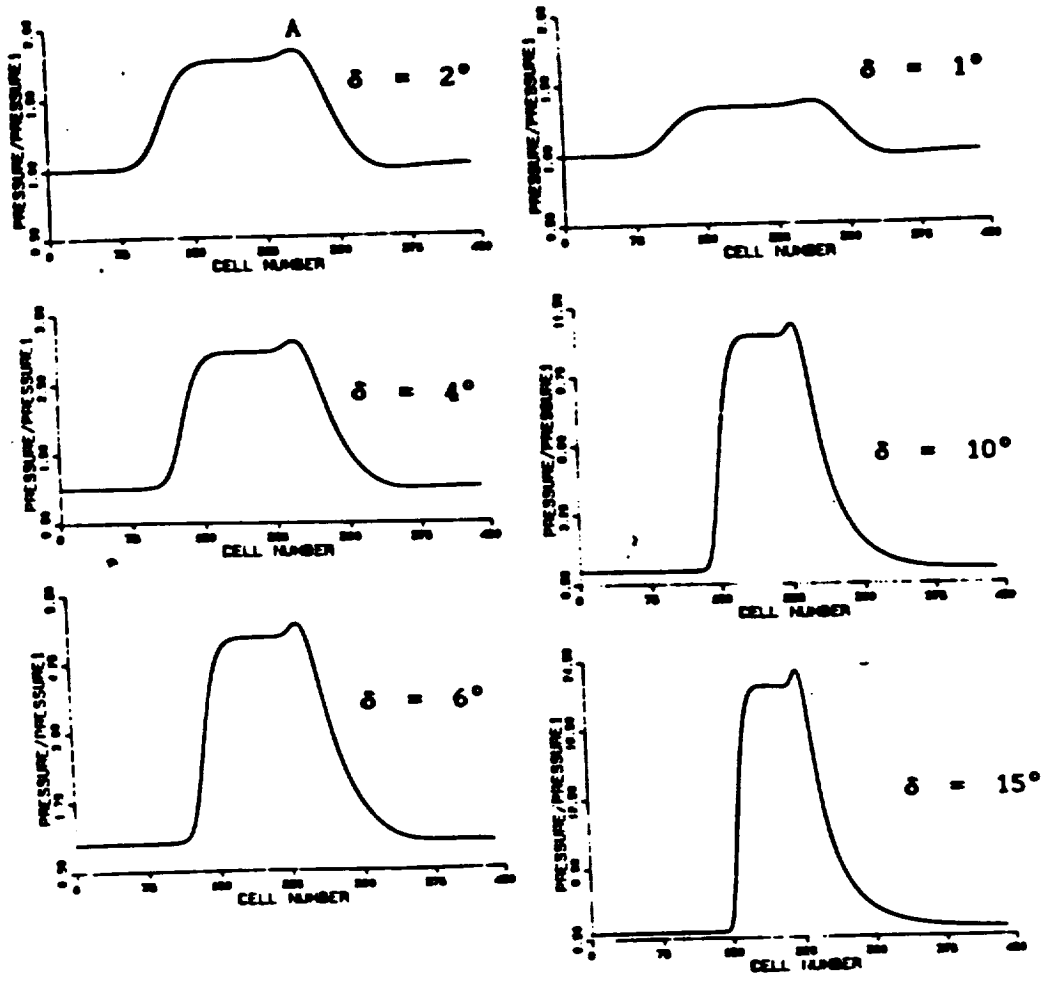

Figure 11: The pressure distribution along the axis of symmetry at the design mach number, 6.

4.2 A Primitive Combustion Model

A primitive attempt has been made to study the fuel combustion in the Busemann scramjet by adding heat at the throat (Figure 12). This is an idealized situation, in which it is assumed that the fuel is added and completely burned in the rectangular combustion chamber located between the combustion and the expansion regions. In this approximation, the increase in mass and the change in the compressibility factor which is normally associated with combustion, are ignored.

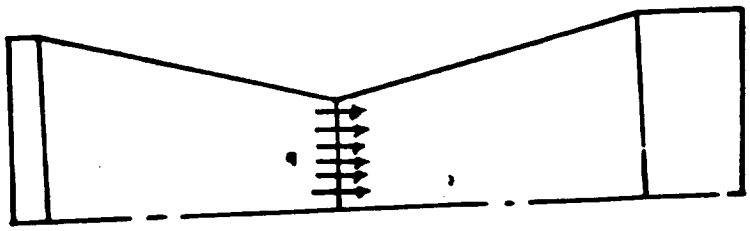

Figure 12. Heat addition at the throat of the Busemann scramjet.

The results obtained by adding heat at the throat are given in Figures 12 and 13. Even at high deflection angles and Mach numbers, thrust varies linearly with the amount of heat added. The experimental work shows that, the fuel at the hypersonic speeds does not burn efficiently. Further study is required to examine various mixing functions and numerically determine the most efficient ones. Once this is achieved, work has to be carried out on how to achieve such mixing in the physical sense.

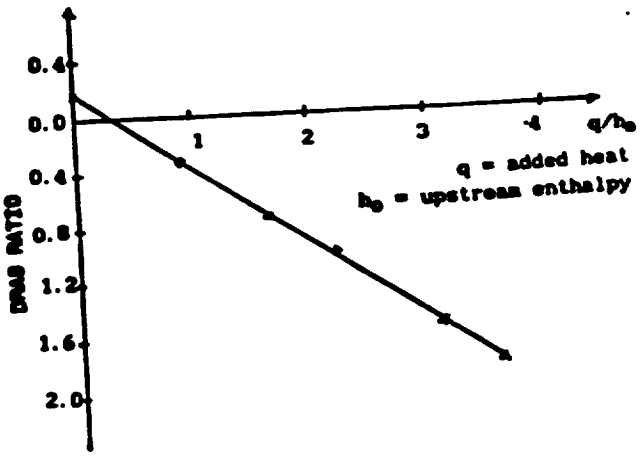

Figure 12. Variation of thrust as a function of added heat at the design Mach number, 6.

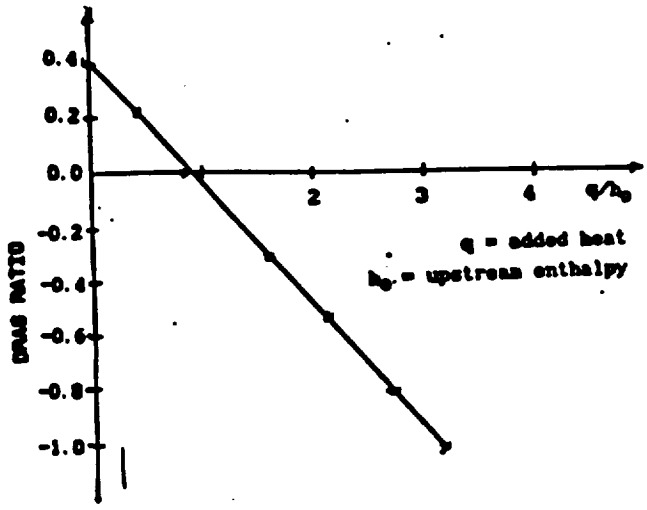

Figure 13: Variation of thrust as a function of added heat at M = 8.

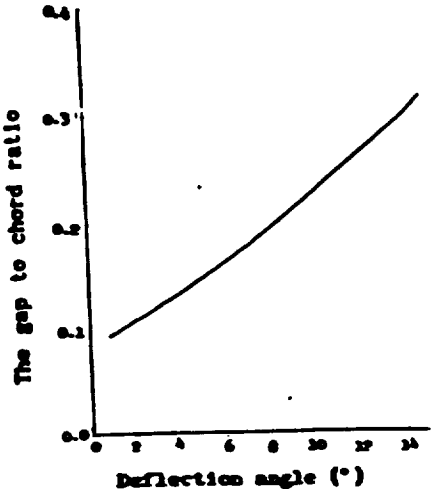

Figure 14: The gap to chord ratio as a function of the deflection angle.

7.0 Conclusion

The results obtained with the code, agree closely with the results

derived from the two-dimensional linear theory. In the linear theory the width of the expansion fan, hence the isentropic pressure drop at the surface, as well as the non-linear effects of expansion and shock wave interactions are ignored. The numerical analysis includes these, therefore the numerical results at the Mach numbers, where the symmetrical wave distributions and monoplane drag obtained in the linear theory, are better representations of the physical solutions. At the other Mach numbers, the results of the code and the linear theory agree within 0.1%.

The non-linear effects increase rapidly at first with the increasing deflection angle. This increase becomes more gradual for the larger values.

For deciding the value of the deflection angle to be used, one has to consider the overall problem. As the deflection angle increases the gap to chord ratio (Figure 14) increases. The scramjet has to be located at the bottom of the spacecraft for aerodynamic considerations. This allows the more dense and high pressure air behind the shock wave originating at the leading edge of the craft to be used as the upstream air entering the scramjet. Hence, the gap to chord ratio should be such that only the air behind the shock can enter the scramjet. The other crucial consideration is that, the temperatures should be limited to 2000° in order to facilitate combustion. For this reason, deflection angles of 4° - 6° are thought to be suitable in this application.

The combustion model used in this study is not an adequate one by any

means. The aim of this study is to determine, if possible, a mixing function which will allow the fuel to mix at the hypersonic speeds. Once this is achieved, physical means of achieving such mixing have to be sought.

It is possible to obtain more accurate results by using a second order method. However, this procedure is expensive in computer memory since it requires four times the memory of the first order method and may become prohibitive if the real gas effects are to be included without the use of supercomputers. Supercomputers seem to be outside the budget of many universities at present. This may force more experienced researches into developing post processors which require better understanding of the physical problem under study, but does not require the use of the larger and more expensive computers.

8.0 REFERENCES

1. Book, D.L., "Finite Difference Techniques for Vectorized Fluid Dynamics Calculations", Springer-Verlag, New York, 1981.
2. Cotella, P., "Efficient Solution Algorithms for the Reimann Problem for Real Gases", J. of Comp. Physics, Vol. 59, 1985.
3. Cox, R.N., and Crabtree, L.H., "Elements of Hypersonic Aerodynamics", Academic Press, New York, 1965.
4. Henshaw, W.D., "A Scheme for the Numerical Solution of Hyperbolic Systems of Conservation Laws", J. of Comp. Physics, Vol. 68, No. 1, 1987.
5. Houghton, E.L., Broch, A.E., "Tables for the Compressible Flow of Dry Air", Edward Arudd Ltd., London, 1961.
6. Hung, C.M., and MacCormack, R.W., "Numerical Solutions of

Supersonic and Hypersonic Laminar Compression Corner Flows", AIAA Journal, Vol. 14, No. 4, 1976.

7. Liepmann, H.W., Roshko, A. "Elements of Gasdynamics", John Wiley & Sons, Inc., New York, 1957.

8. Maurice, H., " Numerical Methods in Fluid Dynamics", 2nd. Rev. Ed., Springer-Verloq, 1984.

9. Merriam, M.L., "Smoothing and the Second Law", Computer Methods in Applied Mechanics and Engineering, Vol. 64, 1987.

10. Power, G.D. and Barber, T.J., " Analysis of Complex Hypersonic Flows with Strong Viscous/Invisvid Interaction", AIAA Journal, Vol. 26, No. 7, 1988.

11. Stalker, R.J., "Thermodynamics and Wave Process in High Mach Number Propulsive Ducts", 27th Aerospace Science Meeting, Jan. 9-12, 1989/Reno, Nevada.

12. Turkel, E., "Progress in Computational Physics", Computational Physics", Computers and Fluids, Vol. II, No. 2, 1983.

13. Van Leer, B., "Towards the Ultimate Conservative Difference Scheme. A Second-order Sequel to Godunov's Methos", J. of Comp. Physics, 32, 1979.

14. Van Wylen, G.J., Senntag, R.E., "Fundamentals of Classical Thermodynamics", 2nd. Ed., John Wiley, New York, 1976.

15. White, F.M., "Viscous Fluid Flow", McGraw Hill, New Work, 1974.

Parametric Study on Thrust Production in the Two Dimensional Scramjet

by

Gary A. Allen, Jr.

1. Introduction

There are many possible scramjet geometries with different thrust production processes. In this paper we will examine one of the simplest geometries which is the two dimensional open duct scramjet. The particular thrust production process which we will study occurs where the burnt and quenched fuel-air mixture has passed over the diverging section of the scramjet. A phenomena of particular interest in this paper is the influence upon thrust by the variation of diverging section angle.

Our theoretical model for the thrust production process was the steady, compressible, two dimensional Euler equations, assuming a perfect gas. The Euler equations were solved through a computer program using a numerically integrated form of the nonhomentropic method of characteristics. The advantages in using this simple theoretical model were in the resultant computer program being small, extremely fast and usable on a low cost personal computer.

2. Theory

The use of characteristics in studying the scramjet is by no means original. Antonio Ferri in his classic paper [1] on axisymmetric scramjets used characteristics with a simple combustion model. In a paper by R.J. Stalker, et al. [2] the thrust production process for a two dimensional scramjet was described using diverging and converging Mach waves based on an approximate theory developed by Weinbaum [3]. Our approach to this problem employs the physical model used by Stalker, et al. with a nonisentropic (or more precisely a *nonhomentropic)* characteristics method as shown in Vincetti and Kruger [4].

The fundamental equations are the steady, two dimensional, compressible Euler equations cast in Cartesian coordinates:

$$\frac{\partial(\rho u)}{\partial x} + \frac{\partial(\rho v)}{\partial y} = 0 \qquad \text{equ(1)}$$

$$\rho\left[u\frac{\partial u}{\partial x} + \frac{\partial u}{\partial y}\right] = -\frac{\partial p}{\partial x} \qquad \text{equ(2)}$$

$$\rho\left[u\frac{\partial v}{\partial x} + \frac{\partial v}{\partial y}\right] = -\frac{\partial p}{\partial y} \qquad \text{equ(3)}$$

Where ρ is density. u is velocity in the x direction. v is velocity in the y direction. p is pressure. The x direction is parallel to the local streamline. The y direction is normal to the local streamline. If we assume the flow is isentropic along the streamline (but not necessarily isentropic normal to the streamline), we may recast equations (1)-(3) into the more simplified form:

$$\frac{\partial\theta}{\partial\eta} = -\frac{[M^2-1]^{\frac{1}{2}}}{\gamma M^2 P}\frac{\partial p}{\partial\eta} \qquad \text{equ(4)}$$

$$\frac{\partial\theta}{\partial\xi} = \frac{[M^2-1]^{\frac{1}{2}}}{\gamma M^2 P}\frac{\partial p}{\partial\xi} \qquad \text{equ(5)}$$

Where θ is the streamline angle with respect to an axis in inertial space. M is the Mach number. γ is the ratio of specific heats. η is the coordinate along the characteristic (Mach wave) which is deflected by an angle μ from the streamline. ξ is the coordinate along the characteristic which is deflected by an angle minus μ from the streamline. Figure 1 depicts the streamline with these different coordinate systems and the two characteristics.

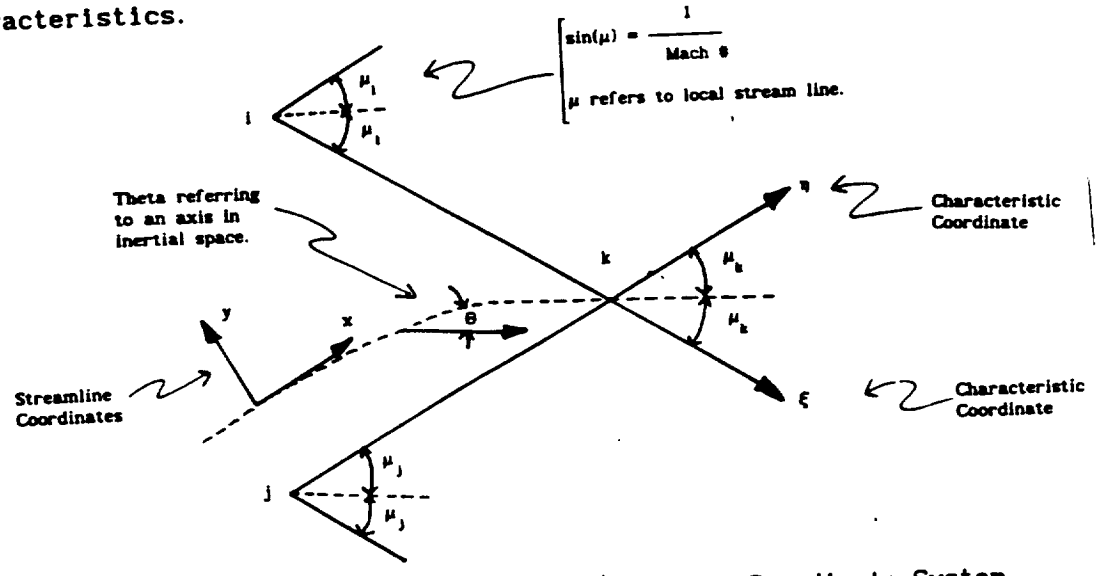

Figure 1. Streamline, Characteristics and Coordinate System

If we were to assume the flow was completely isentropic (a false assumption for the scramjet problem), then we could further simplify equations (4) & (5) into the classical Method of Characteristics solution form:

$$\frac{\partial}{\partial \eta} (\omega - \theta) = 0 \qquad \text{equ(6)}$$

$$\frac{\partial}{\partial \xi} (\omega + \theta) = 0 \qquad \text{equ(7)}$$

Where ω is the Prandtl-Meyer function which is defined as:

$$\omega = \left[\frac{\gamma - 1}{\gamma + 1}\right]^{\frac{1}{2}} \text{ARCTAN}\left[\left[\frac{\gamma + 1}{\gamma - 1} [M^2 - 1]\right]^{\frac{1}{2}}\right] - \text{ARCTAN}[\, [M^2 - 1]^{\frac{1}{2}}\,] \qquad \text{equ(8)}$$

It should be mentioned there is a nonhomentropic formulation which uses the Prandtl-Meyer function as a dependent variable. This form can be found in Liepmann and Roshko [5]. Using the Prandtl-Meyer function for the nonhomentropic case initially seemed advantageous since this formulation is quite compact and accurate for the isentropic regions of the flow. Unfortunately the use of the Prandtl-Meyer function in nonhomentropic flow requires carrying the temperature as a dependent variable in the vorticity terms. This created a host of added and unnecessary problems. Therefore it was concluded the pressure, theta technique shown in equations (4) & (5) was the superior approach.

The classical Method of Characteristics method shown in equation (6) & (7) can be integrated exactly. However the nonhomentropic formulation in equations (4) & (5) needs to be integrated numerically. If a first order finite difference technique is used on equations (4) & (5) then the following is derived:

$$\theta_k - \theta_j = - \frac{[M_j^2 - 1]^{\frac{1}{2}}}{\gamma M_j^2 P_j} [P_k - P_j] \qquad \text{equ(9)}$$

$$\theta_k - \theta_i = \frac{[M_i^2 - 1]^{\frac{1}{2}}}{\gamma M_i^2 P_i} [P_k - P_i] \qquad \text{equ(10)}$$

The solution procedure assumes all conditions are known at points: i and j. The values for P_k and θ_k are found directly from equations (9) & (10). However in order to propagate the solution the Mach number for point k needs

to be calculated as well. This Mach number is found by assuming the flow is isentropic along streamlines. The solution procedure is to extrapolate the path of the streamline backwards to a region in the flow where pressure and Mach number are known. The values for pressure and Mach number are then found by interpolation. This process of stream line path extrapolation following by interpolation is the most computer time intensive activity in the program. Once the Mach number and pressure have been found on the stream line then one can calculate pressure at point k by utilizing the isentropic chain.

The main source of error in using this method comes from the growing uncertainty in the streamline's position with respect to the location of the two corresponding Mach waves. This uncertainty in the streamline's position degrades the accuracy of the interpolation process. This in turn reduces the accuracy of the solution at point k thus propagating the error.

In principle this method can deal with shock waves since the theory allows for changes in entropy along a streamline. However this theory was usable only because the combustion process was assumed to be quenched before it encountered the scramjet's thrust producing expansion fan. Unfortunately it is likely that induced shock waves would cause local reignition of the fuel-air mixture introducing complicated chemical and real gas effects which were not modeled by the theory. Therefore the computer program developed with this theory looks for the coalescence of Mach waves which would indicate the formation of a shock wave. When a shock wave is detected, the program prints out a warning message. Fortunately induced shock waves do not occur until the scramjet is near its operating limit. Therefore induced shock waves were not a serious limitation to this method.

3. Computer Program

The computer program developed in this study was written to be usable on a personal computer or work station employing the MS-DOS or UNIX operating systems. The computer program's source code (written in C) can compile first time without error on a wide variety of computers, i.e. IBM-PC, HP-9000, Perkin-Elmer, Iris, etc. The compiled program is optimized for both speed and minimum memory requirement (25 CPU seconds on an IBM-PC/AT). The basic scramjet geometry described by the computer program is depicted in Figure 2:

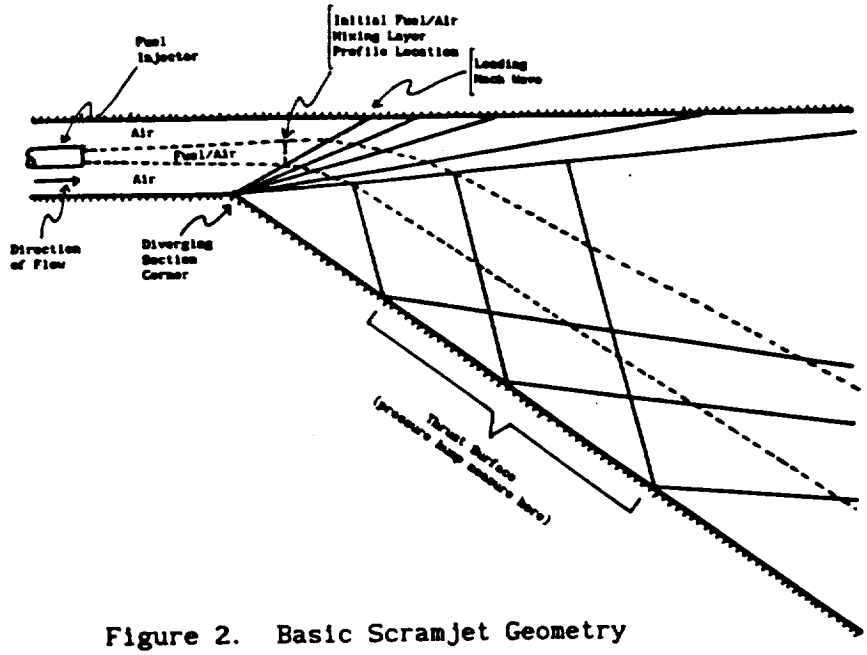

Figure 2. Basic Scramjet Geometry

The computation starts at the leading Mach wave which is the first Mach wave of the expansion fan radiating from the diverging section corner as shown in Figure 2. The fuel/air mixing layer along the leading Mach wave is divided into forty characteristic pairs. The air region above the fuel/air layer region is divided into another forty pairs up to the top of the duct. The scramjet is assumed to be an open duct type, viz. no upper surface.

The expansion fan is divided into five regions where each region is subdivided into seven sectors. Six hundred and forty characteristic pairs are generated for each region. When the next region is calculated, all but the last sector of characteristic pairs from the previous region are thrown away resulting in the computer's data memory requirement being kept below 64 kilobytes. This 64 kilobyte memory restriction is a consequence of using personal computers with the Intel 80x86 microprocessor. There are programing methods for getting around this problem, i.e. dynamic memory allocation with pointer arrays. However these alternative methods increase the program's complexity, and reduce portability.

Once the expansion fan has been calculated, the program then calculates the characteristics down to the surface of the diverging section (thrust surface). The characteristics are each evaluated to determine if they cross prior to encountering the thrust surface. If the characteristics do cross, then it is assumed a shock wave has formed resulting in the computer program generating a warning message. Characteristics reflecting away from the thrust surface are *not* checked to see if they cross since it is not believed that reflected induced shock waves are significant to thrust production.

The characteristics leading to the thrust surface are divided into ten regions each with six hundred and forty characteristic pairs. Calculation of total thrust is found by integrating the local wall pressure over the thrust region using the trapezoidal rule.

The scramjet is assumed to always have central fuel injection. Wall injection is certainly worth investigation. However to theoretically investigate wall injection, one must consider boundary layer effects and wall heat transfer, both of which would greatly complicate the theory and computer program.

The fuel/air mixing layer as it encounters the leading Mach wave is described by Gaussian distributions for the Mach number. The initial velocity vector is assumed to be parallel to the wall. The initial static pressure is assumed to be uniform across the duct. The Gaussian distributions Mach number are matched to the duct air layers on both boundaries of the fuel/air mixing layer. The ratio of specific heats is assumed to be uniform throughout the scramjet. It should be emphasized that these initial conditions are input parameters based on experimental data and are not actually calculated.

The program was tested against a nozzle designing program written by P. Jacobs [6] to establish it's basic validity. The nozzle designing program was developed to solve for homentropic flow with Riemann invariant characteristics. It was found the two programs generated results with very good agreement even though the characteristic mesh resolution and solution procedures were different.

4. Experimental Data

The experimental data used for comparison with this computer program was taken from the R.J. Stalker, et al. paper. The data was generated in the T-3 shock tunnel at the Australian National University, Canberra. Table 1 shows the test conditions for the three experiments used in calibrating the software. This data roughly corresponds to a flight Mach number of about eight.

Table 1. Experimental Test Conditions (from ref. [2])

Flight Mach No.	8	9.5	13
Test Case No.	1	2	3
Stagnation Enthalpy (MJ/kg)[a]	4.3	6.1	8.7
Precombustion Pressure (kPa)[b]	140	180	160
Precombustion Temperature (K)	1300	1900	2500
Precombustion Velocity (km/sec)	2.42	2.85	3.26
Precombustion Mach Number	3.50	3.35	3.40
Ratio of Specific Heats, γ	1.35	1.32	1.32

[a]Experimental error ± 3%, [b]Experimental error ± 5%

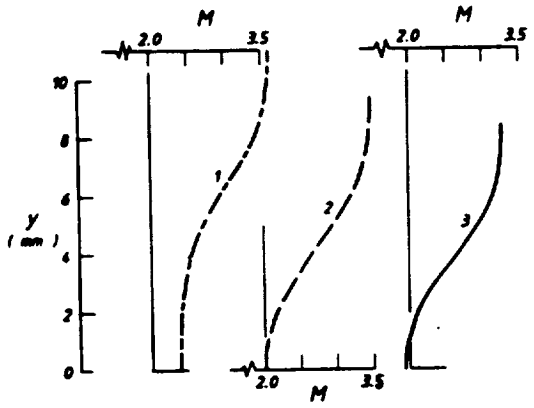

Figure 3. Mach Number Profiles Prior to the Expansion Fan (from ref. [2])

The initial Mach number profiles in the duct are shown in Figure 3. These Mach number profiles are measured normal to the duct's axis of symmetry in the fuel/air mixing layer just prior to where the duct's flow encounters the leading Mach wave (see Figure 2).

Figure 4 shows the pressure on the thrust surface corresponding to the three test conditions. The vertical axis in Figure 4 uses the pressure parameter $\Delta P/P$. This pressure parameter is based on static pressures and is defined as:

$$\frac{\Delta P}{P} = \frac{\text{Pressure(Fuel On)} - \text{Pressure(Fuel Off)}}{\text{Pressure(Precombustion)}} \qquad \text{equ(10)}$$

The precombustion pressure was measured in the duct just prior to the leading Mach wave of the expansion fan. The Fuel On and Fuel Off pressures were measured from a set of pressure taps on the thrust surface. The Fuel On value was the wall pressure measured when combustion had occurred. The Fuel Off value was the wall pressure measured when combustion had not occurred due

to the fuel (hydrogen) not being injected. The horizontal axis in Figure 4 is the radial distance in millimeters downstream from the diverging section corner as shown in Figure 2.

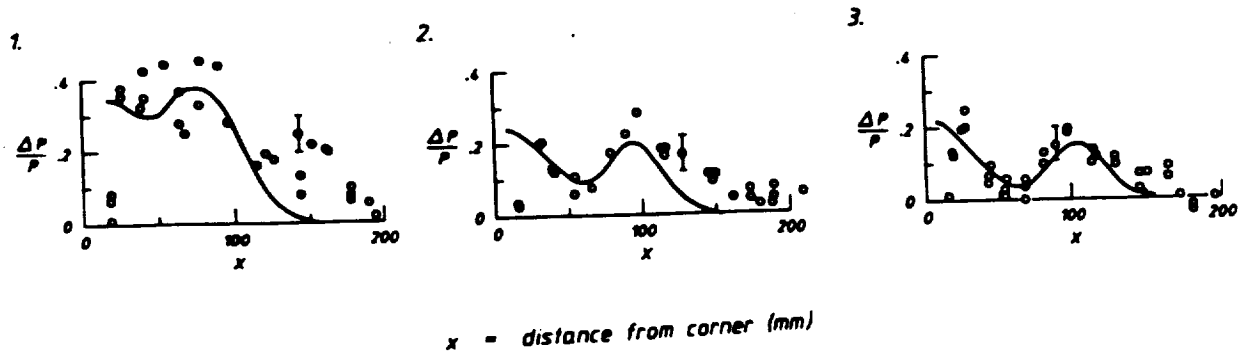

Figure 4. Open Duct Pressure Distributions (from ref.[2])

The pressure profiles shown in Figure 4 are double humped. The right most hump is relevant to the analysis of this paper while the left hump pertains to other combustion processes within the duct.

The actual dimensions of the experimental scramjet were not provided in the original paper. They are now provided in Figure 5.

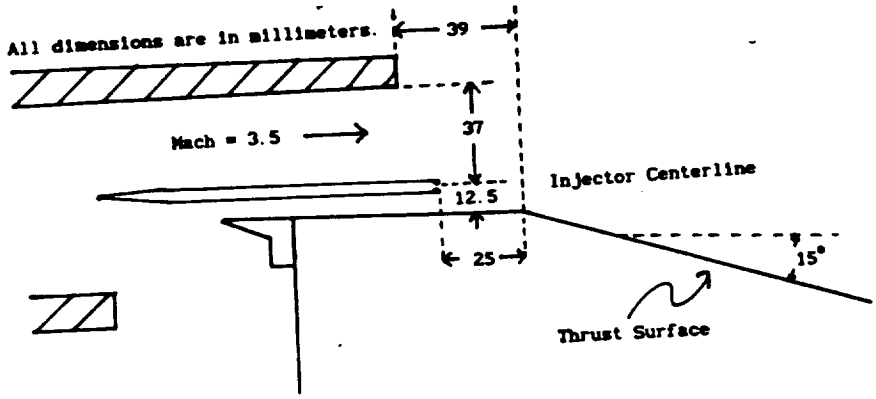

Figure 5. Physical Dimensions of the Experimental Scramjet

5. The Effect of Ramp Angle on Thrust Production

The angle of the T-3 experimental diverging section was fifteen degrees (see Figure 5). A parametric study was performed which involved varying the angle of the diverging section. The results of this studying are depicted in Figures 6.1-6.3 which correspond to the three cases examined experimentally.

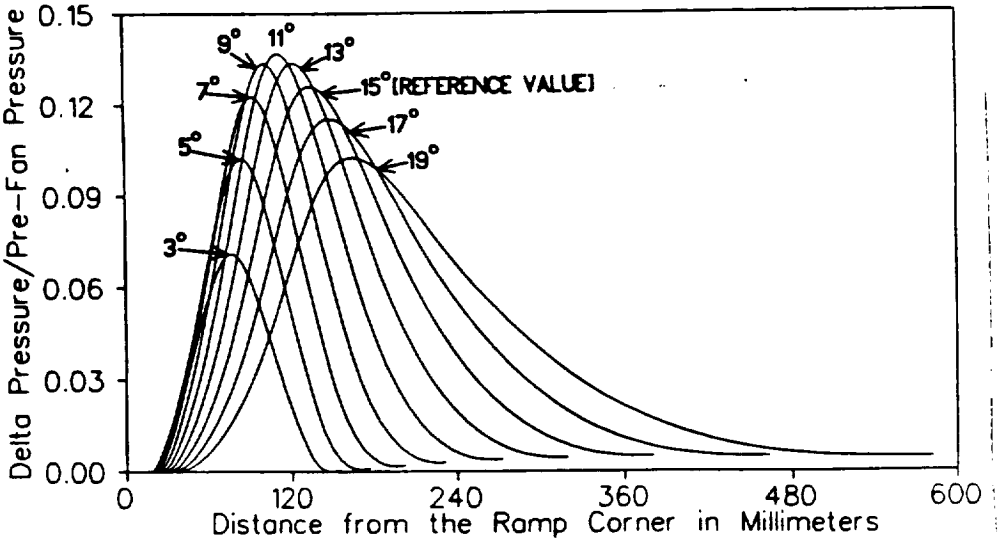

Figure 6.1. Variation of the Diverging Sections Angle for Case 1

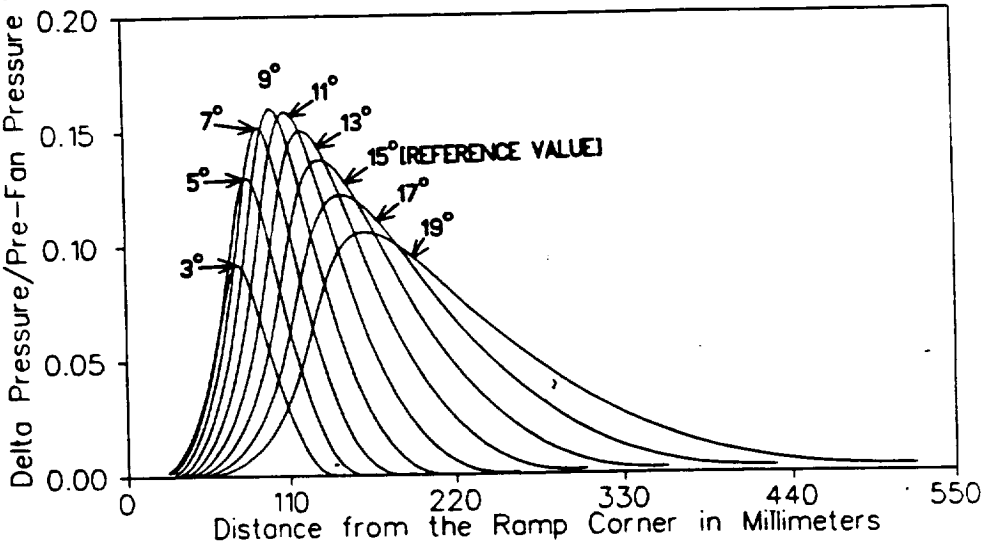

Figure 6.2. Variation of the Diverging Sections Angle for Case 2

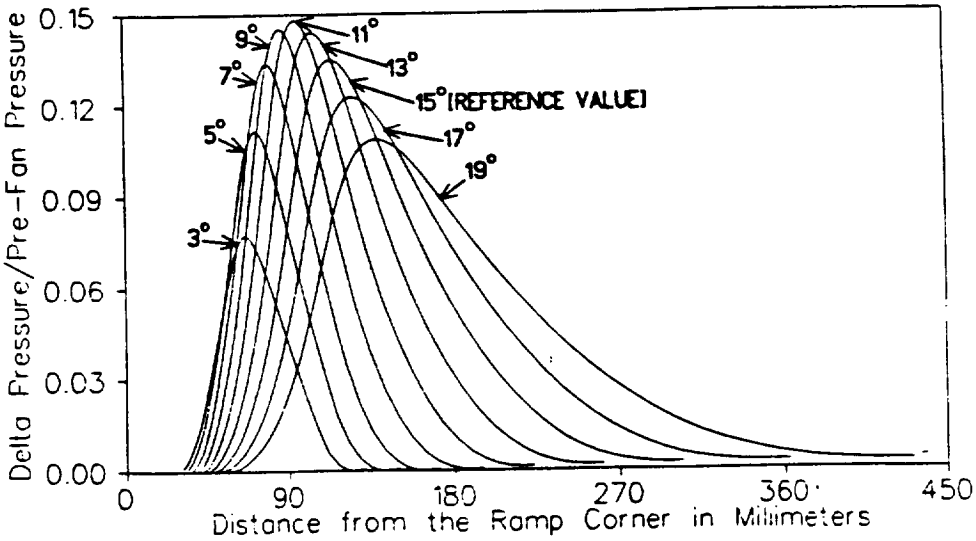

Figure 6.2. Variation of the Diverging Sections Angle for Case 3

The vertical and horizontal axis are the same as used in Figure 4. Each plot shows nine different pressure traces for different diverging section angles starting with an angle of three degrees and going through a range of angles at two degree increments to a final diverging section angle of nineteen degrees. It was observed that the maximum pressure occurred in Figure 6.1 at a ramp angle of 10.9 degrees. In Figure 6.2 the maximum pressure occurred at a ramp angle of 9.7 degrees. In Figure 6.3 the maximum pressure occurred at a ramp angle of 10.6 degrees.

Thrust was calculate by integrating the pressure over the entire length of the trace. Plots showing thrust as a function of diverging section angle for the three test cases are shown in Figure 7.

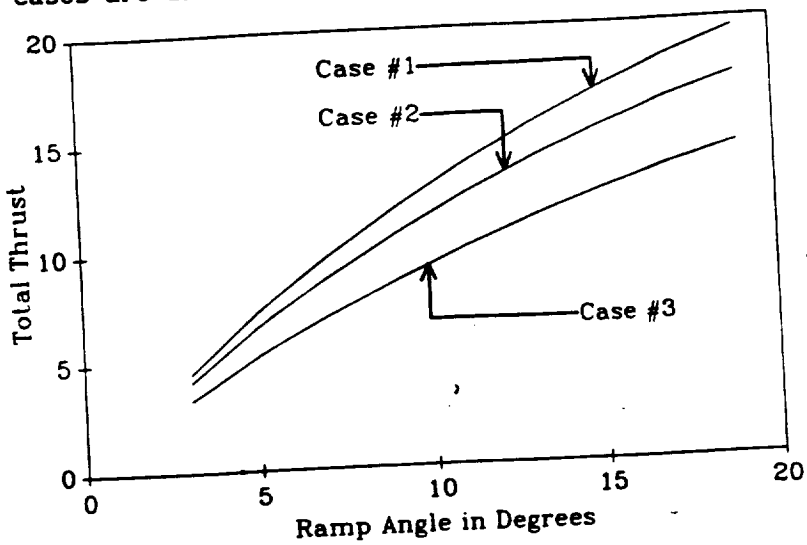

Figure 7. Scramjet Thrust as a Function of Diverging Section Angle

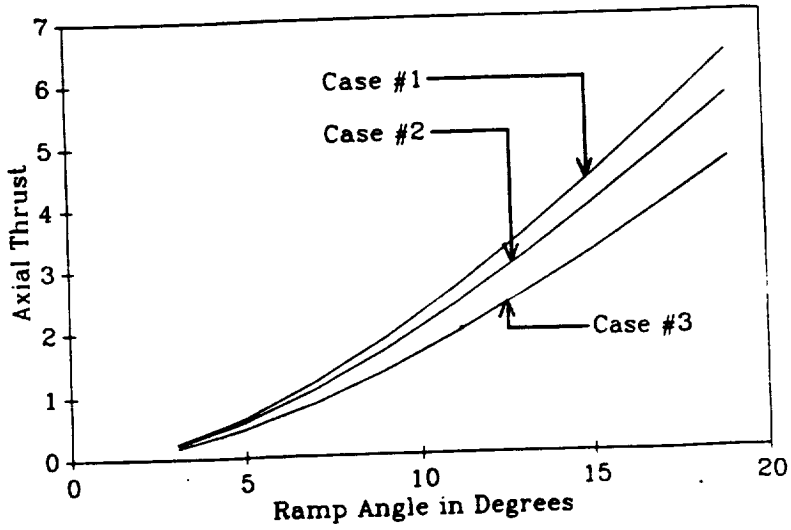

Figure 8. Scramjet Axial Thrust as a Function of Diverging Section Angle

Before this study was performed, it was speculated that the Euler equations might reveal an optimum diverging section angle which yielded maximum thrust. Figure 7 shows the total thrust increased monotonically as diverging section angle increased. Axial thrust is the component of total thrust which would overcome drag in a hypersonic vehicle. Figure 8 shows axial thrust increased as diverging section angle increased. Obviously the Euler equation model for thrust production would breakdown where the diverging section angle increased sufficiently to cause flow separation from the wall. Also our model of a scramjet assumed the thrust surface was infinitely long. Clearly in an actual scramjet the thrust surface must have a finite length. The relevance of thrust surface length was demonstrated in Figures 6.1 - 6.3, where the pressure hump increased in length with an increase in diverging section angle. At some angle the pressure hump would spill off of the thrust surface. Although it was not revealed by our approach with the Euler equations, for a real scramjet there would be an optimal diverging section angle for maximum thrust production.

6. Conclusions

In this paper we have investigated the thrust production process in the two dimensional scramjet using a high speed computer program written for small personal computers. We have shown that for specific diverging section angles the peak pressure on the thrust surface achieves a maximum value. However we have also shown the axial thrust does not have a maximum value for a specific diverging section angle provided the thrust surface is infinitely long. Rather the axial thrust increases monotonically with diverging section angle.

Computer investigations of the scramjet are usually restricted to the province of super computers doing runs on the order of CPU hours. This study has demonstrated that useful information can be obtained from a small and fast computer program using the Method of Characteristics.

References

1. Ferri, A., *Journal of the Royal Aero. Society* 68:575-597 (1964).
2. Stalker, R. J., Morgan, R. G., and Netterfield, M. P., *Combust. Flame* 71: 63-77 (1988).
3. Weinbaum, S., *A.I.A.A. Journal* 4:217-226 (1966).
4. Vincenti, W.G., and Kruger, C.. *Introduction to Physical Gas Dynamics,* John Wiley & Sons, New York, 1965.

5. Liepmann, H. W., and Roshko, A., *Elements of Gasdynamics*, John Wiley & Sons, New York, 1967, p. 295.

6. Jacobs, P.A., *An Interactive Graphics Program for Computer-Assisted Calculation of Isentropic Supersonic Flows*, Report 7/88 Department of Mechanical Engineering, University of Queensland, 1988.

The Design of a Mass Spectrometer for use in Hypersonic Impulse Facilities

K. Skinner

The value of Mass Spectroscopy as an analytical tool to Chemists has long been established. The use of Shock Tunnels to produce high density particle flows (of the order of 0.1 atmospheres) with a stream energy of up to 10eV, although not as widely applied, has also become well established. Little work has been done utilising both techniques simultaneously and what has been done has been mostly concerned with the study of transient chemical species produced in the reflected shock region of the tunnel. Several researchers have expanded the test gas through nozzles and skimmers before sampling the chemistry of the gas. Crane and Stalker[1] were the first to attempt Mass Spectroscopy in a high density hypersonic flow expanded from a reflected shock region through a contoured nozzle, whose purpose was to produce a uniform test flow, rather than to chemically freeze the expanding gas in its stagnation state. Their work, however, was never applied to hypersonic combustion. This work has been to investigate the use of a mass spectrometer to analyse the reacting gases in hypersonic combustion.

While hypersonic combustion is uniquely suited to mass spectroscopic analysis, a rather severe set of constraints exist at present which act to limit and define the design and the performance of such an experiment. A mass spectrometer is uniquely suited analysis of hypersonic combustion because it provides the possibility of sampling free stream flow without causing the chemistry of the sample to be altered. Static combustion mass spectroscopy suffers from the handicap that the sample that is analysed is drawn from a region adjacent to the combustion chamber wall and the presence of the wall influences the chemistry. If the combustion is occuring in a flow at subsonic speeds then the presence of the instrument in the flow will affect the flow upstream of the instrument and hence perturb the chemistry. In supersonic flow it is possible to introduce a hollow conical skimmer which samples the flow at the tip of the cone without affecting the flow upstream. The cone angle on such a skimmer must be kept sufficiently low that the shock wave off the nose must remain attached. The cone angle of the hollow interior of the skimmer must be large enough to prevent those molecules which strike the inside walls of the skimmer from having a large effect on the chemistry of the axial flow. Only in hypersonic flow can these mutual conditions be satisfied.

Due to the nature of hypersonic facilities which are currently

available, the design of a mass spectrometer is limited in several critical aspects:

1. Hypersonic test facilities typically have very short test times.
2. They deliver an impulsive load to test instruments.
3. In all Mass Spectrometers a high vacuum must be maintained throughout the test.
4. For safety reasons combustion experiments must take place within a pressure vessel.

1. Test Time

The very short test time immediately restricts the general type of Mass Spectrometer which may be used productively to a Time-of-Flight instrument. Magnetic Sector or Quadrupole mass filters may be used, but if so, then only one mass may be sampled during each test time. A Time-of-Flight mass spectrometer, however, is capable of mass analysing a complete spectrum in only 100 microseconds from a single pulse of ionised sample gas. Magnetic sector mass filtering or magnetic focussing are also undesirable on the grounds that they require precise mechanical alignment and suffer from vibration problems.

2. Impulsive Test Flow

Regardless of the available volume of the test section of the flow facility, the cross-sectional area of the instrument must be kept to a minimum. This is to avoid the problems of choking and/or upstream influence which may occur when the instrument is moved close to a wall, strut or fuel injector, and to reduce the amount of impulsive force which is applied during a test run. To attain any required internal volume, therefore, the length of the instrument must be adjusted while the cross section is kept to the mimimum required to maintain sufficient expansion of the sample within the instrument.

3.(a) Vacuum - Pump requirements

The vacuum needed within the Mass Spectrometer is determined by the length through which the ions must travel to the ion detector after leaving the ionisation region. The mean free path of particles must be longer than this distance, which we may assume to be of the order of one meter. This means that the vacuum necessary is of the order of 0.001 Pascals. Pumps that are used to produce this order of vacuum are usually complex and sometimes delicate. Whatever type of pump is used, it should be built into the instrument so that the distance between pump and the high vacuum regions is kept to a minimum. Placing the pump at some distance from the instrument,

possibly even outside the test section vessel, limits the effective pumping speed to the diffusion rate along the connecting tube.

3.(b) Vacuum - Skimmer Constraints

As mentioned, a sample of gas from the combustion region may be expanded within a hollow conical skimmer with a small orifice at its tip. The stream tube, passing through this orifice, experiences close to a free jet expansion when the interior walls move away from the molecules faster than their thermal velocity. An important consideration in the design of these skimmers is the detrimental effect that the front orifice is going to have on the vacuum inside the instrument. The final vacuum attainable inside the instrument prior to a test, is determined when the leak rate through the front orifice is equal to the pump throughput. Small orificed hollow skimmers are hard to manufacture in practice, so a better ultimate vacuum may be attained by increasing the number of skimmers and introducing intermediate volumes which are kept at intermediate pressures. Each extra skimmer, however, introduces new possibilities for interference with the sample and the need for another vacuum pump.

3.(c) Vacuum - During Test

During a test, while gas is flowing into the instrument through the skimmer orifices, the vacuum inside the instrument will deteriorate unless the volume behind the skimmmers is large. In a time-of-flight instrument, the important regions requiring a high vacuum are in the ionisation region, the drift region for the ions, and the ion detection region. (See Figure 1.) Since the molecules passing through the skimmer have highest mobility in the direction of the skimmer axis, the vacuum in these important regions are maintained longest if they are situated at an angle (optimally 90 degrees) to the direction of the molecular beam. Another consideration limits the extent to which this can be achieved, however. Ions which are formed from the molecular beam behind the skimmer have an initial velocity component in the direction of the neutral beam. Different masses, however, have different energies which correspond to an equivalent velocity. This means that as the ions are accelerated radially by an electrostatic field, and thus given different radial velocities, their resultant velocity vectors will make different angles to the axis of the skimmers. This fanning out of the ions can be minimised by reducing the angle at which the ions are accelerated and by increasing the accelerating voltage on the ions. A limit is placed on the accelerating voltage, however, as a high ion energy implies a faster ion transit time and hence a faster output spectrum. The speed of the available

data recorder places an upper limit on the value of the ion accelerating voltage.

4. Pressure Vessel

Conducting experiments with combustion of flammable gases requires a design which will not endanger lives and if possible, equipment. The test section must therefore also be a pressure vessel, and the experiment should be completely confined within this vessel. In the normal course of operation of an impulse test facility, this test section will hold any pressure from vacuum up to the maximum rating of the vessel. This means that Pumps must be able to operate within a fluctuating pressure environment and all electrical connections must be insulated against arcing.

Clearly the shape, size, skimmer arrangement, and the vacuum system for the mass spectrometer are strictly limited by the environment of the Impulse Hypersonic facility. Remaining design questions focus on the production, treatment and detection of the ions within the instrument.

When deciding what method of ionisation to use, three things need to be considered: Will all the different species be ionised approximately equally in a predictable way? Will the ioniser interfere with the chemistry of the sample in an unpredictable way? And will the ioniser be cheap, dependable, small and robust? The first two requirements will only be satisfied by a beam style of ioniser, as all other methods require avalanches of electrons, accelerated in an external field. Of the possible beams, (ion, electron, or photon), only electron beams satisfy most of the third requirement. Ion beams are not simple to produce and will pollute the chemistry of the sample. Photo-ionisation occurs at wavelengths of 800 angstroms or less (far ultra-violet) for single photon ionisation, and even so, the ionisation cross-section is two or three orders of magnitude smaller than for an electron beam.

The treatment of the ions after formation consists of passing them through an acceleration region and then focusing them onto an ion detector. The choice of ion detector is not constrained by this application. Constraint is placed on the means of data recording, however. It must be fast enough to maintain reasonable resolution over the period between the arrival of the first and last ions in the spectrum. With a sufficiently fast data recorder multiple spectra may be taken throughout the test time of the flow, each spectra corresponding to a single pulse of ionising electrons.

1. Crane, K.C.A., and Stalker, R.J., "Mass Spectrometric analysis of hypersonic flows", J Phys. D: Appl. Phys., Vol. 10, pp. 679, 1977.

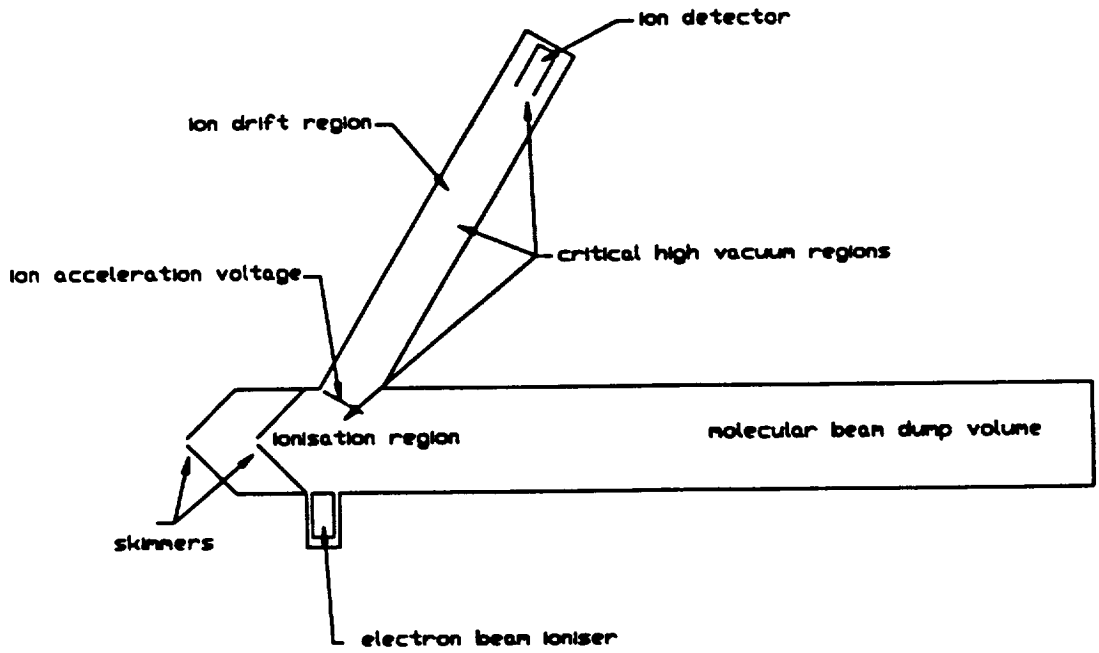

Figure 1. The regions of critical high vacuum

SHOCK TUNNEL DRAG MEASUREMENT

By S.L. Tuttle & J.M. Simmons

SHOCK TUNNEL DRAG MEASUREMENT - S.L. Tuttle & J.M. Simmons

The development of the drag measurement technique initially started by Sanderson and Simmons in 1988 was continued in 1989. The method was to allow a stress wave caused by the impact of the flow on the model to propagate along a sting of sufficient length to enable the measurement of the resulting compressive strain before the return of any reflection. This requires the knowledge of the model's impulse response so that the inverse force problem may be solved by means of deconvolution.

The method was at a stage where the measured and deconvoluted drag would agree with Taylor-Maccoll theory to within 10%. The model geometry was such that skin friction could be entirely neglected (the model was a cone of 15 degree semi-vertex angle).

The new model was a 5 degree semi-vertex angle cone of more than double the length of the previous one. This made the inclusion of skin friction essential, and made the stress waves reflected within the model very apparent.

Probably the single most significant difference was the signal-to-noise ratio. The strains measured were of the order of several microstrain only, the drag being a factor of between 4 and 10 less than for the 15 degree cone. The noise on the signals obtained from the shots with the 5 degree cone was in many cases the same size as the overall signal upon which it was superimposed. The noise in the case of the earlier 15 degree cone was on average only about 6% of the total signal, and could effectively be completely filtered out.

The term 'noise' in the case of the 5 degree cone data refers not only to the random electrical noise, but also to the passage of small 'packets' of reflected stress waves through the overall signal. These were most apparent in the dynamic calibrations where the loading was far more coherent than that occuring in the shock tunnel.

The process of filtering the data was thoroughly explored and it soon became apparent that no filter would remove sufficient noise, whilst leaving the overall signal acceptably unaltered, to enable an

intelligible level of drag to be deduced after deconvolution.

This then necessitated polynomial curve fitting to the experimental data in order to obtain a sufficiently clean signal, as noise is greatly amplified in the deconvolution. This curve fitting approach gives quite close agreement between the measured and predicted drag, although there are short comings with the method, again predominantly due to the excessive amount of noise which makes a very good curve fit difficult.

Two methods are being used to predict the drag, each a variation on Newtonian theory. The first uses the measured pitot pressure, while the second replaces this with ρv^2 calculated from T4 data. Both methods include a skin friction component which is scaled to follow the T4 pitot pressure trace, starting from an initial value calculated using simple boundary layer theory.

At this stage the agreement varies between very good and about 10% difference at worst. Five shots were done covering four different tunnel conditions and examples of these results are attached, with the shock tunnel conditions included for each. For each shot there is data from wire resistance strain gauges and semiconductor strain gauges, both mounted at the same axial sting location.

Another area which needs to be addressed is the curve fit which is again due to the poor signal-to-noise ratio and it is believed that this can be improved.

In conclusion, it can be seen that despite the severe difficulties imposed by the excessive amount of noise on the signals, the drag ,which may consist of a significant amount of skin friction, can be measured to a reasonable degree of accuracy for this stage in the development of this drag measuring technique.

Shot # 1186 : Stagnation enthalpy : 18.67 Mj/kg
Stagnation pressure : 48 MPa
Mach number : 5.18
Static pressure : 24.31 kPa
Static temperature : 2516 K
Density : 0.0303 kg/m^3
Velocity : 5240 m/s

Shot # 1187 : Stagnation enthalpy : 10.60 Mj/kg
Stagnation pressure : 49 MPa
Mach number : 5.40
Static pressure : 22.00 kPa
Static temperature : 1500 K
Density : 0.052 kg/m^3
Velocity : 4050 m/s

Shot # 1189 : Stagnation enthalpy : 6.20 Mj/kg
Stagnation pressure : 50 MPa
Mach number : 5.81
Static pressure : 18.40 kPa
Static temperature : 785 K
Density : 0.0811 kg/m^3
Velocity : 3220 m/s

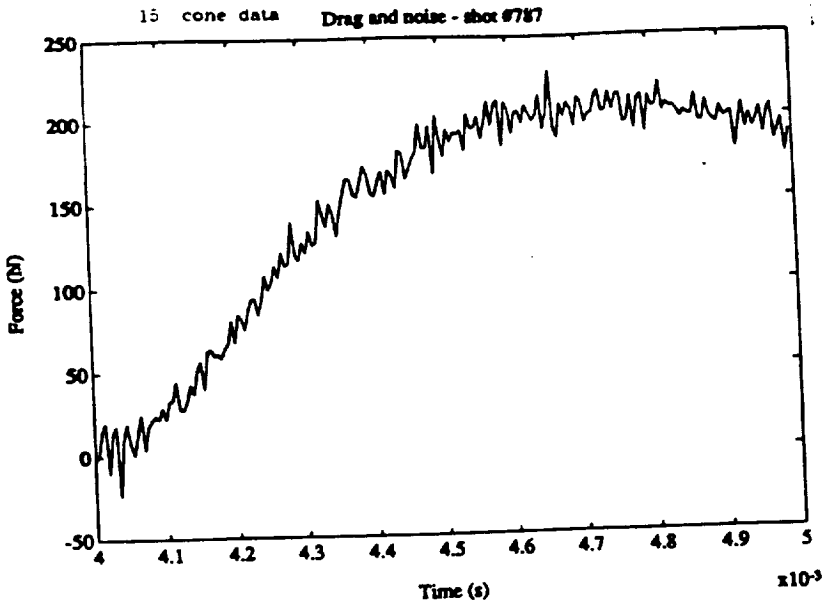
15 cone data
Drag and noise - shot #787
Force (N)
Time (s)
x10⁻³

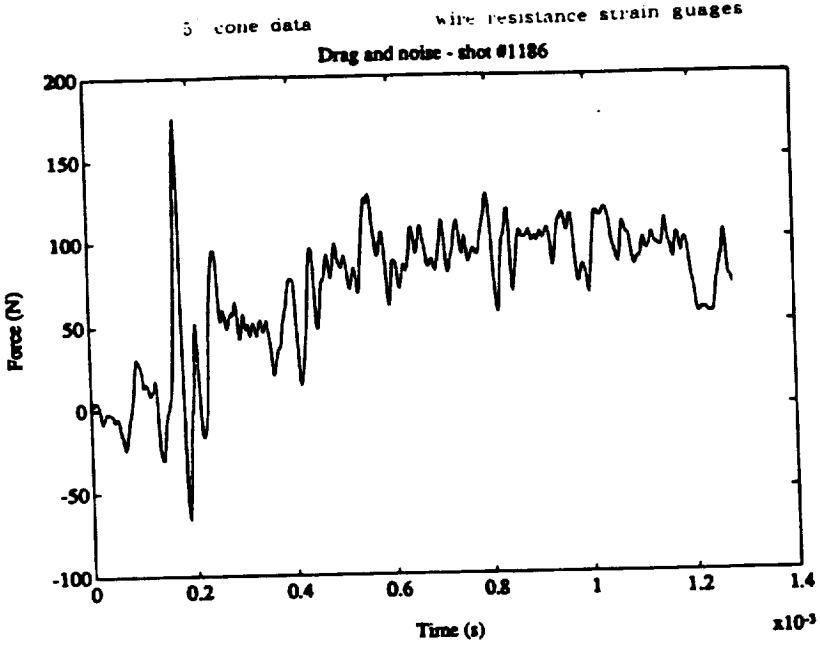
5 cone data
wire resistance strain guages
Drag and noise - shot #1186
Force (N)
Time (s)
x10⁻³

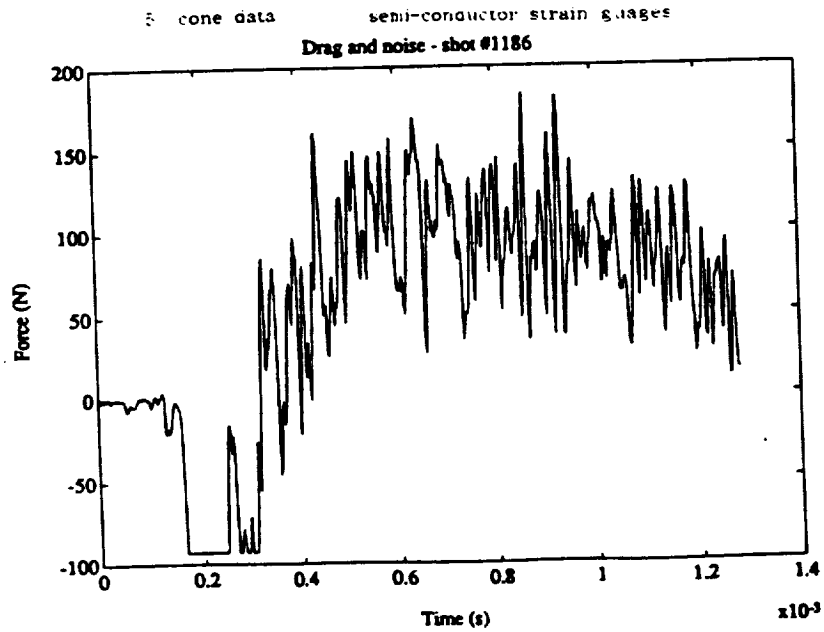
5 cone data
semi-conductor strain guages
Drag and noise - shot #1186
Force (N)
Time (s)
x10⁻³

KEY TO DRAG PLOTS

- - - - ρV^2 Newtonian + skin friction

-.-.-.- pitot Newtonian + skin friction

——— deconvoluted drag

..... curve fit to measured drag

SHOT # 1186 - wire resistance strain guages

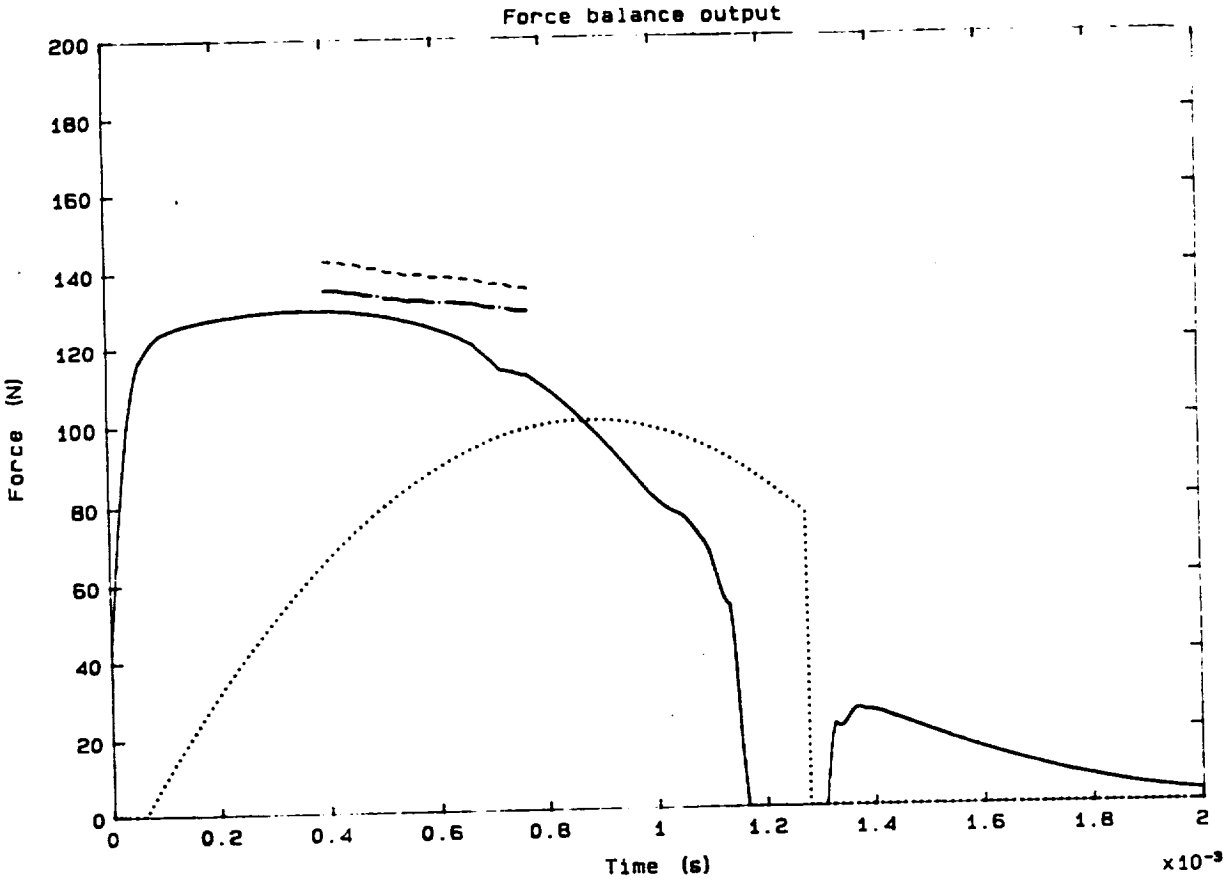

SHOT # 1186 - semi-conductor strain guages

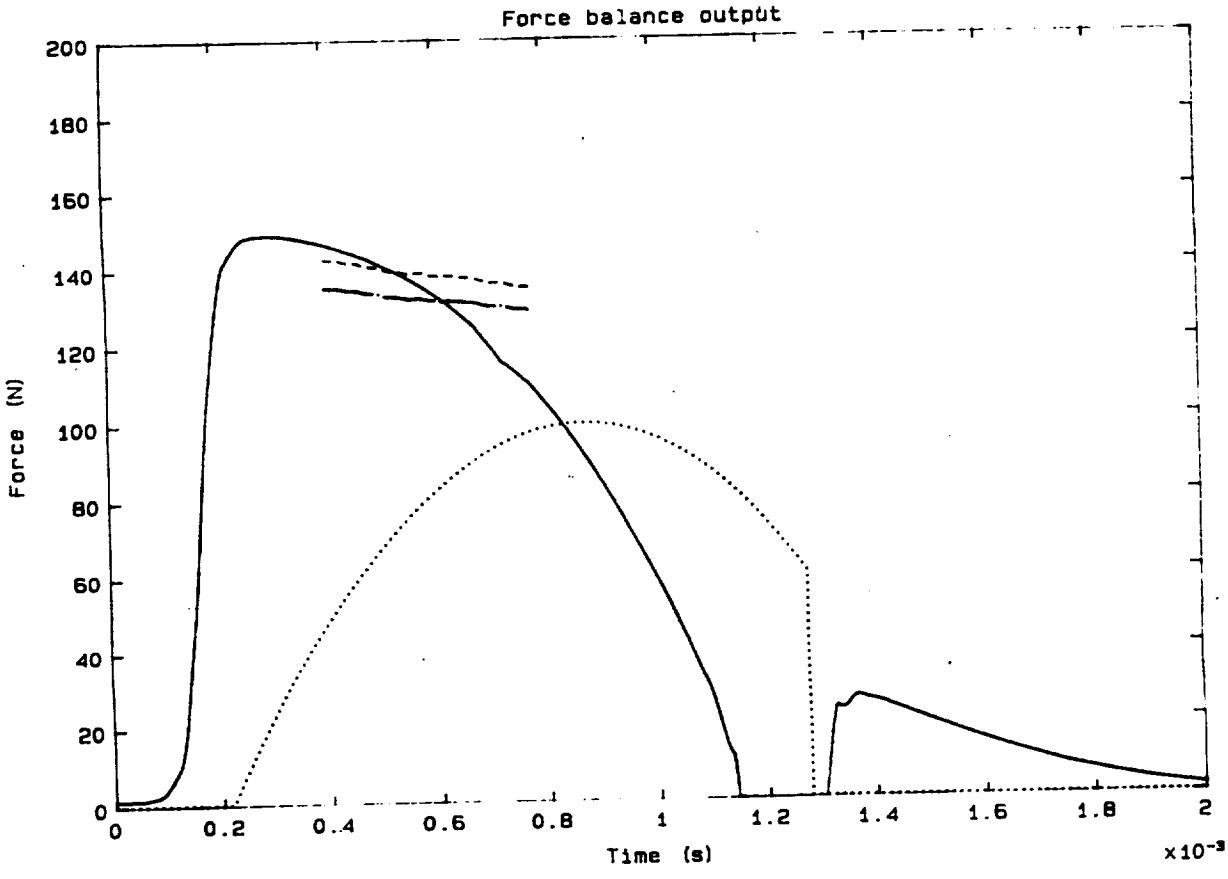

SHOT # 1187 - wire resistance strain guages

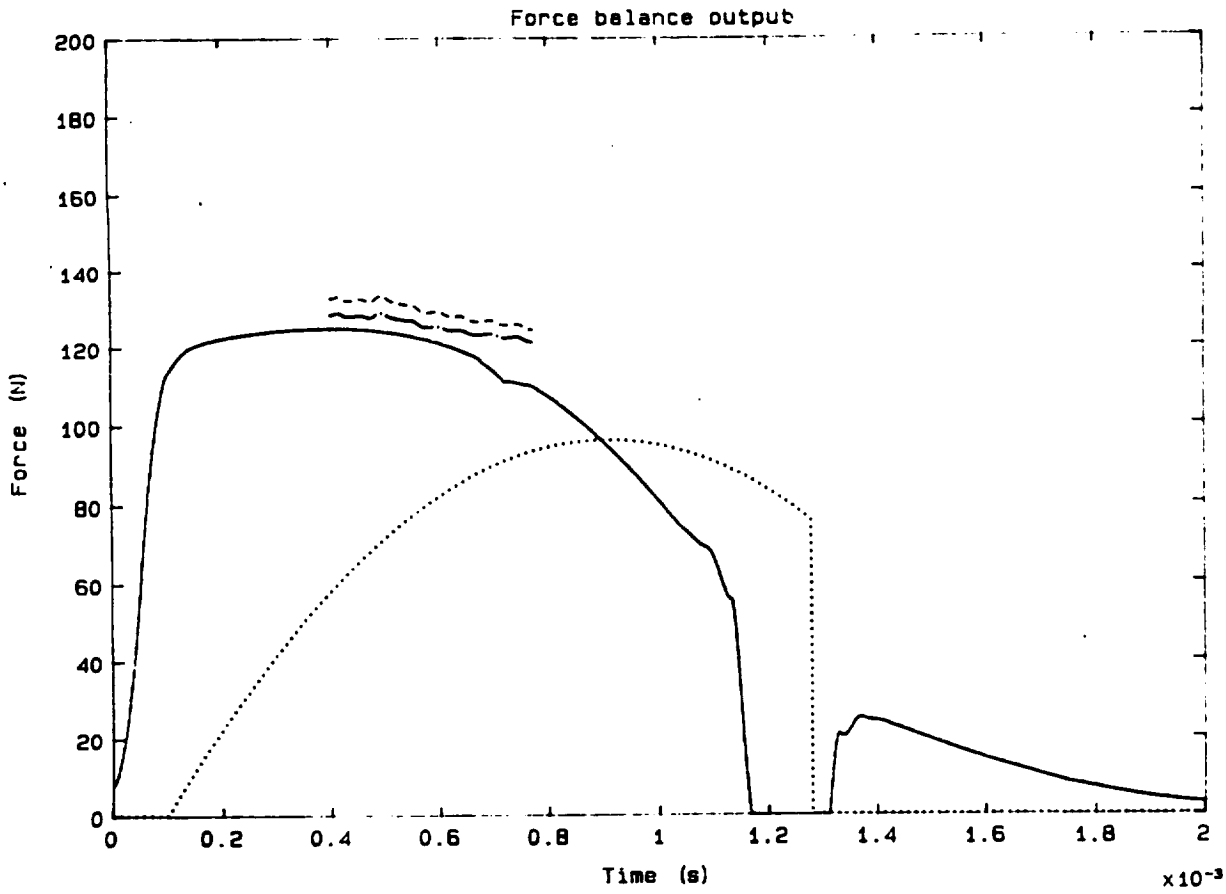

SHOT # 1187 - semi-conductor strain guages

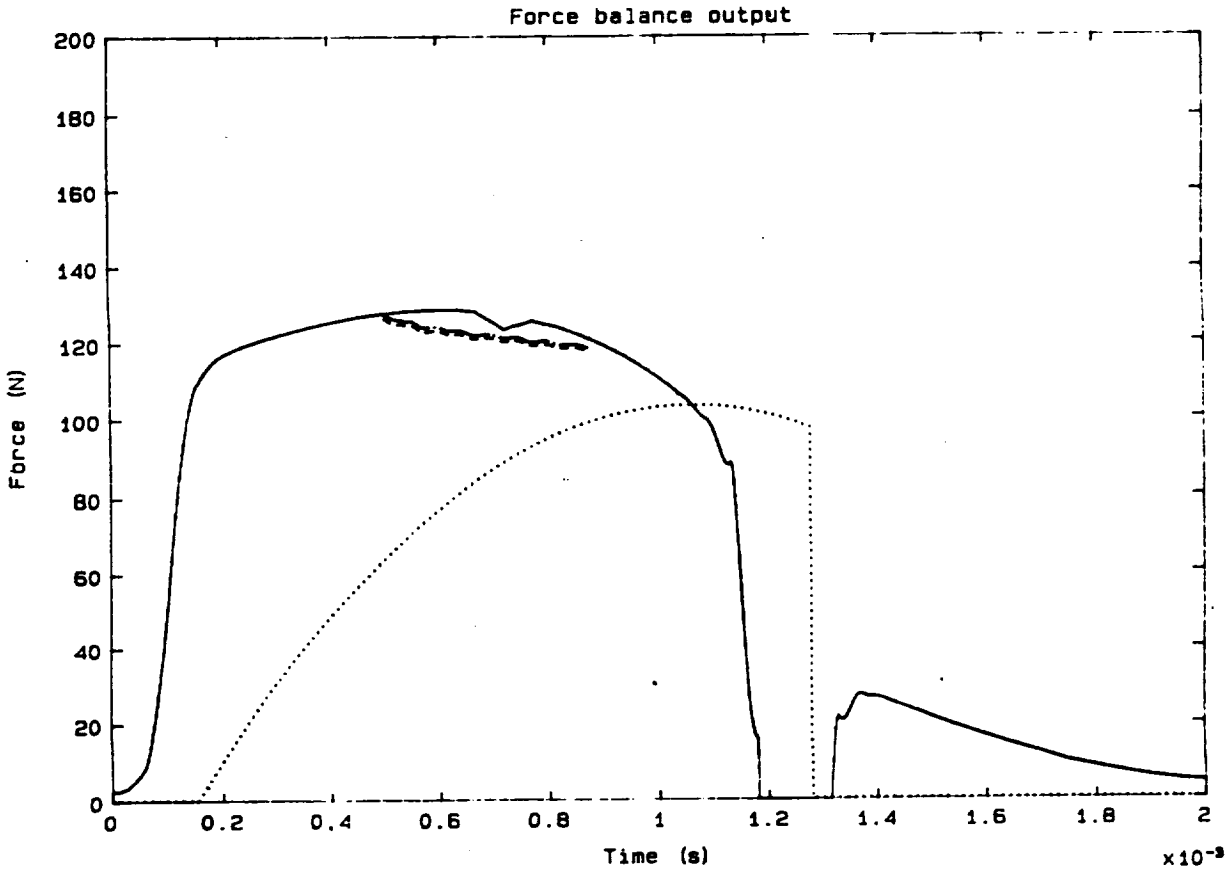

SHOT # 1189 - wire resistance strain guages

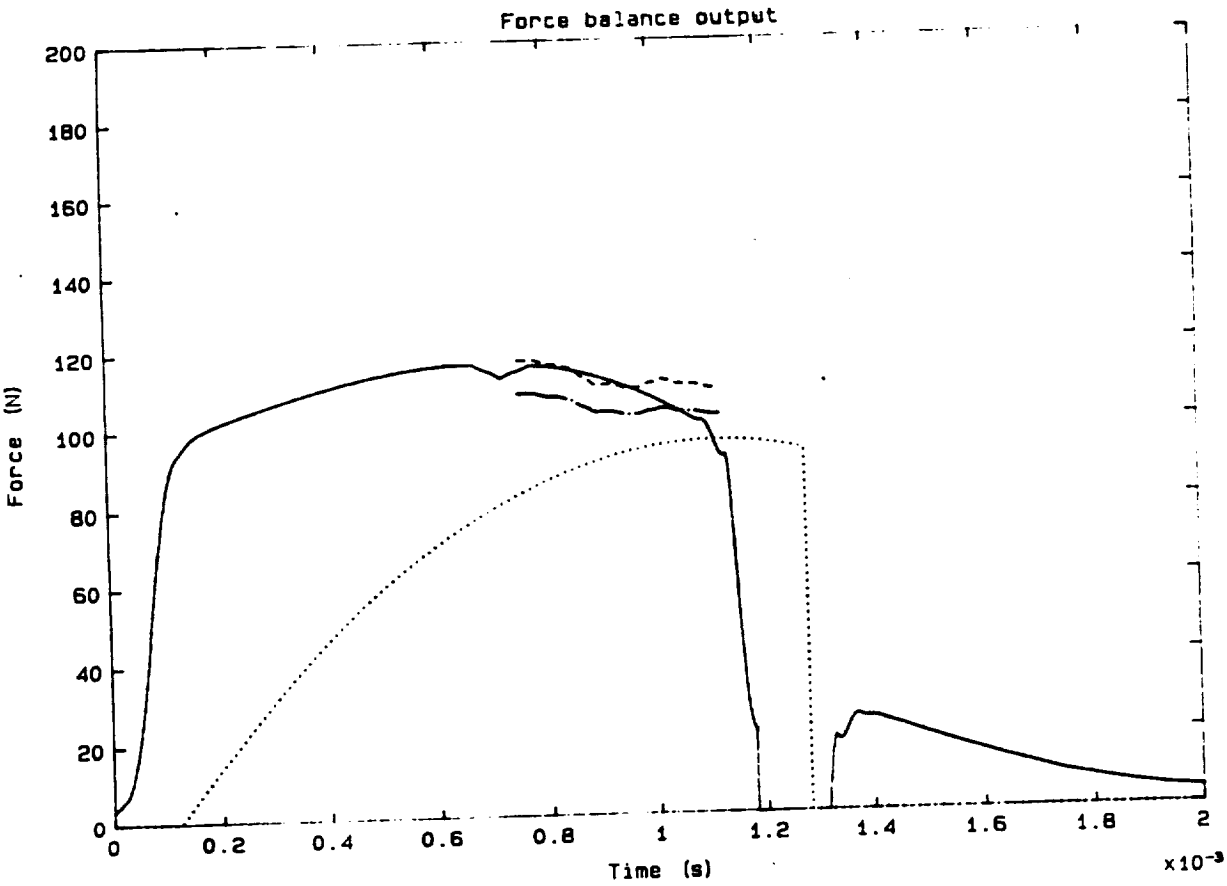

SHOT # 1189 - semi-conductor strain guages

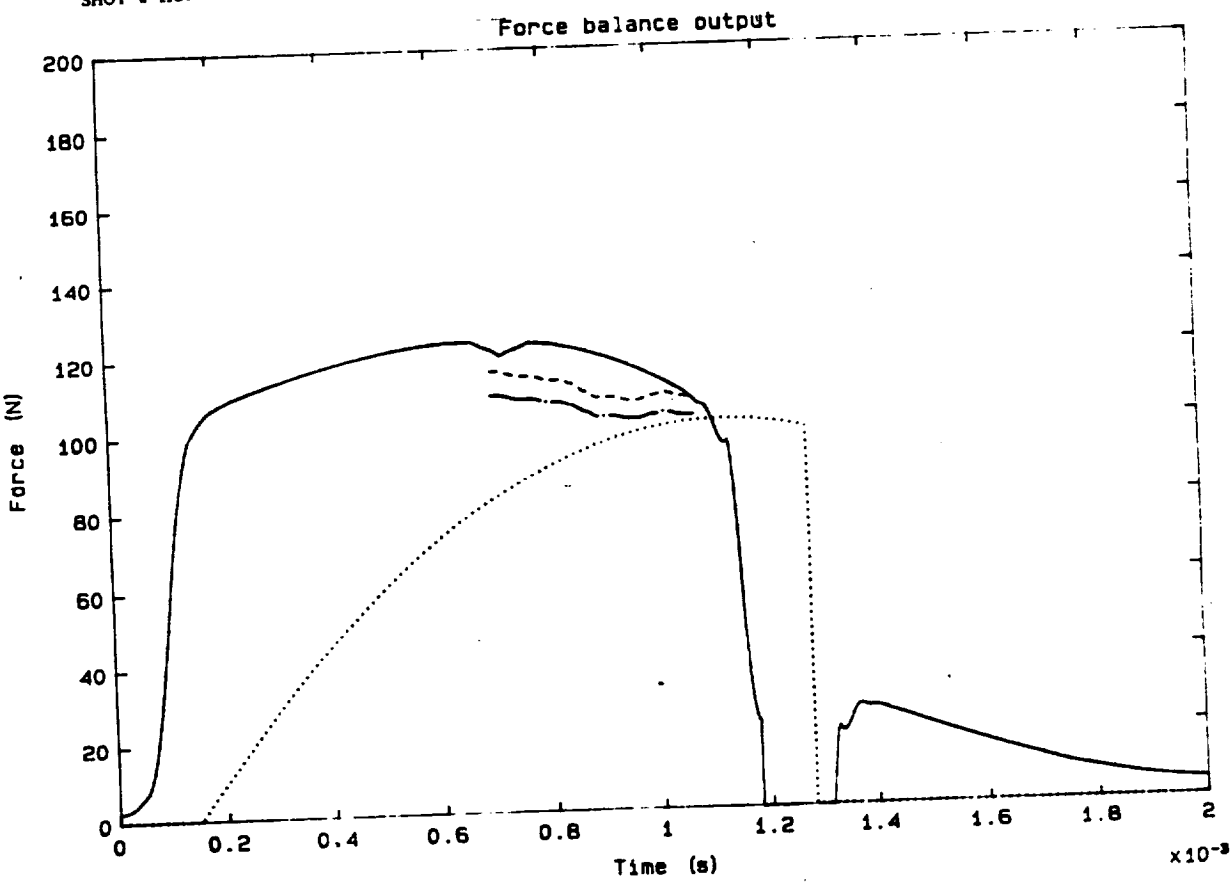

DEVELOPMENT OF A SKIN FRICTION GAUGE FOR USE IN AN IMPULSE FACILITY

Gabrielle Kelly

The skin friction gauge designed for use in T4, as described in the previous submission, was designed using piezoceramics. The ceramic PZT-7A Shear Plate was selected as the appropriate piezoceramic material due to its sensitivity in shear and theoretical zero cross axis sensitivity. A sensitivity to axial pressure was detected and in order to decouple the extranous pressure effect which distorts the true shear signal two identical sections of the ceramic were used. One was inverted with respect to the other in the axial plane. Thus the summation of the two separate signals cancels the pressure effect and doubles the shear stress signal. The design was tested in June 1989 in T4 using an existing flat plate model. Since the signal generated was predicted to be small it was amplified as close as possible to the site of signal detection in order to prevent contamination of the signal by noise. As such a cavity had to be built into the model to house a suitable charge amplifier.

In the first set of results we found the signals to be much larger than expected. This we summised was for two reasons. Firstly, despite the fact that heat transfer calculations had indicated the thermal cover thickness was sufficient to precludethe piezoceramic from "seeing" a temperature rise in the test time, thermal expansion of the cover material had not been taken into account. As such part of the signal generated was due to thermal expansion of the cap placing the piezoceramic under strain. This effect was in fact in the opposite direction on each of the ceramics so that summation of the signals canncelled this thermal effect to the first order. Thus the original design catered for this oversight. It was however preferable to reduce this effect since the magnitude of the real shear stress signal was swaped by the thermal signal and any real accuracy in determining shear

stress was diminished. The other extraneous effect was that resulting from the test gas coming into contact with the electrical configuration of the charge amplifier. Since in this particular model it was impossible to completely seal off the cavity in which the charge amplifier was situated the effect of the gas contacting the electrical connections was apparent. The signal was concluded to be an ionization effect even though little ionization was predicted at the test conditions used. In the presence of Argon the signal generated was as expected. In air it was swamped by the ionization factor. Reduction in temperature reduced the effect but it was impossible to remove it other than through the use of Argon.

The next series of tests run, were using a new flat plate model in which the cavity for the charge amplifier was able to be completely sealed. The results were vastly improved. The new model also was designed with a thicker thermal cover which was capped off with bakelite disc (a material which exhibits a zero coefficient of thermal expansion). This series of tests brought the signals down to a sensible and expected level. Unfortunately the signal did not emulate the behaviour of the stagnation pressure. After an original rise the signal seemed to have a decaying sinusoidal wave superimposed on it. This behaviour was exhibited by both ceramic transucers - identical in size and nature, but opposite in sign. This would seem to suggest that the effect was one experienced in the axial direction of the transducer and perhaps could be explained as the presence of stress waves through the thermal cover to the ceramic. Unfortunately due to the limited time available in T4 the tests were concluded in October 1989. Due to the fact that I wish to bring these tests to a conclusion as soon as possible I have opted to test the gauges in TQ. This facility is in less demand and can be operated by the user alone and has the added advantage of a short turn around time. This effectively means the gauge can

undergo more thorough testing and I can reach conclusions as to the last extraneous effect as soon as possible. I feel confident that this behaviour can be explained by either the presence of stress waves or a still unresolved thermal effect. The results of these tests will be finalised in the next two months.

TENTH AUSTRALASIAN FLUID MECHANICS
CONFERENCE - UNIVERSITY OF MELBOURNE
11-15 DECEMBER 1989

HYPERVELOCITY FLOW IN AXISYMMETRIC NOZZLES

P.A. JACOBS and R.J. STALKER

Department of Mechanical Engineering
The University of Queensland, St. Lucia, Qld. 4067
AUSTRALIA

ABSTRACT.

We describe a simple procedure for the design of axisymmetric supersonic nozzles for use in reflected-mode shock tunnels. This method has been used to design a moderate Mach number (M = 4) nozzle and a high Mach number (M = 10) nozzle. Both nozzles have been calibrated by measuring the pitot profiles near the nozzle exit planes and, although the M = 4 nozzle performs well, the M = 10 appears to have reached a Mach number - pressure limit in which the unsteady nozzle boundary layers significantly affect the test flow.

INTRODUCTION.

A new generation of aerospace planes is currently being developed. These vehicles will be powered by air-breathing engines and so spend a considerable fraction of their flight accelerating through the atmosphere. This means that high speed (v ~ 3-7km/s) aerodynamics will again become a focus for fluid dynamic researchers.

Experimental facilities capable of providing test flows at these speeds supply a pulse of test gas that lasts only a few milliseconds. To make the best use of the high enthalpy test gas, it is expanded to a high-speed uniform and parallel flow. For the shock tunnel facility T4 (Stalker & Morgan 1988), this is achieved by using an axisymmetric nozzle in which the gas is initially allowed to expand through a conical section and is then redirected by the contoured part of the nozzle wall to produce a uniform test flow at the nozzle exit plane.

Impulse facilities such as T4 typically operate at total enthalpies (H_s) of 10 - 30 MJ/kg with associated stagnation temperatures (T_s) of 5000 - 12000 K and stagnation pressures (P_s) of 40 MPa. At these conditions there is a strong coupling between the chemical reactions of the dissociated air and the axisymmetric gas flow. This coupling complicates the design calculations significantly. However axisymmetric nozzles for non-reflecting shock tunnels have been designed using the method of characteristics (MOC) with chemical reactions by Mudford *et al* (1980). In their design they note that the contour shapes computed for a chemically reacting flow were similar to that computed for a perfect gas with a suitably chosen ratio of specific heats, γ.

This leads us to approach the design process in a simple fashion and treat the total flow as two relatively simple flows patched together. We treat the early expansion of the test gas in the conical section as a quasi-one-dimensional flow with finite-rate chemical kinetics. At the exit of this cone we assume that the flow is a uniform source flow and that the chemical reactions are frozen. We then treat the flow in the contoured section as axisymmetric flow of a perfect gas where γ has been chosen to approximate a chemically reacting flow over the same expansion. The MOC calculation of the flow in the contoured section is then the "standard" perfect gas procedure described in Liepmann & Roshko (1957).

This approach has been used to design a nozzle with exit Mach number, M = 4 for use in supersonic combustion studies (see figure 1a). Its performance in terms of flow uniformity appears to be adequate. A high Mach number (M = 10) nozzle was also constructed (see figure 1b). It has a two-stage initial expansion to reduce the time required for the test flow to reach steady state. Unfortunately, for nozzle stagnation pressure P_s < 40 MPa, the boundary layers that develop on the nozzle wall significantly affect the uniformity of the flow.

MACH 4 NOZZLE.

We will consider the design of a specific nozzle with M = 4 and a throat diameter of 25.0mm, at nominal stagnation conditions P_s = 30.4MPa, H_s = 16.2MJ/kg (T_s = 8000K). The conceptual layout of the nozzle is shown in figure 2. For computational convenience, we set the origin of the axial coordinate, x, at the start of the conical expansion.

For the initial conical expansion, we choose a cone half-angle of 12° and we assume the flow to be a uniform source flow at the end of this section (x = 98mm). Zonars (1967) indicated that throats with a constant area section with length equal to the throat diameter produced "excellent high temperature source flow characteristics when measured in conical nozzles". Hence we do not analyse the transonic flow near the throat as done in a number of other studies (*e.g.* Sivells 1978).

The flow in the conical section is strongly influenced by the chemical reactions associated with the dissociation and recombination of the molecules in test gas. We treat this flow as a quasi-one-dimensional flow with finite rate chemical kinetics. Computations are performed with a FORTRAN program NENZF (Lordi *et al* 1964). The stagnation region (labelled 1 in figure 2) and the subsonic flow up to the throat is considered to be in chemical equilibrium but, once the program steps into the conical expansion, a nonequilibrium chemistry model is used.

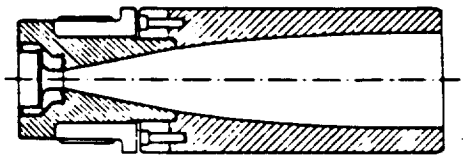

M = 4

100mm

Figure 1.

M = 4 and M = 10 axisymmetric nozzles constructed for the T4 shock tunnel facility.

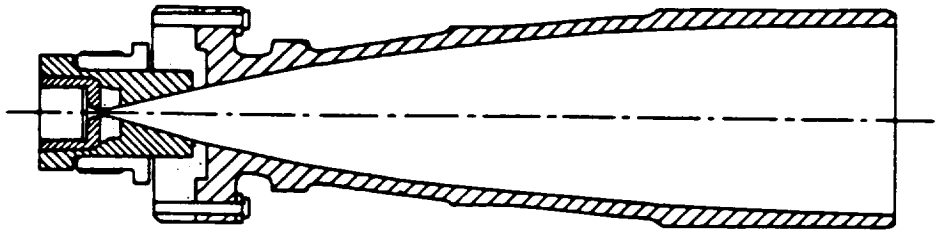

M = 10

We use the flow properties (M and γ) at the end of the conical section as the starting point for the MOC calculation of the flow in region 3 (source flow), region 4 (transition from source flow to parallel flow) and region 5 (parallel and uniform flow). The gas flow is considered to be chemically frozen and a value of M at the end of the conical expansion is calculated using an estimate of the speed of sound $a = (\gamma\ S\ \mathcal{R}_0\ 1000\ T)^{0.5}$, where S is the sum of the species concentrations (mole/gm-mixture) $\mathcal{R}_0 = 8.314$ J/gm-mole/K and T is the static temperature in K. Here a = 1380 m/s. The computation was performed with the aid of the program "MOC" documented in Jacobs (1988). The inlet boundary is specified as a uniform source flow with $M_A = v/a = 2.804$ and $\gamma = 1.334$. Only 12 points were used on the inlet boundary as the program retains all of the mesh data in the memory of the microcomputer. We believe this to be sufficient because Schurmeier (1959) indicates that a 10 point mesh produced a 0.1% error in exit height for a two- dimensional nozzle calculation. The Mach number on the axis at point C (in figure 2) is computed to be $M_c = 4.12$. We then step along the axis downstream of point C and compute the flow field in region 4 by proceeding upstream along characteristics such as CA.

Once the characteristic mesh is generated, a streamline can be interpolated through the mesh, starting at point A and finishing where it intersects the characteristic CD. The data points on the interpolated streamline are then used in a spline fitting routine to define the nozzle wall as a cubic spline with eight knots and specified end slopes. See table 1 for the wall coordinates. A boundary layer modification was added to give a total wall radius

$$r_{total} = r_{inviscid} + \frac{x}{511}\,\delta^*_{exit}$$

where δ^*_{exit} was estimated to be 1.4mm.

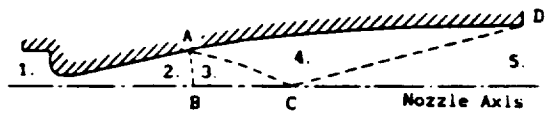

Figure 2. Conceptual view of a hypersonic nozzle.
1. Stagnation region.
2. Transition to source flow.
3. Source flow region.
4. Transition to parallel flow
5. Uniform flow parallel to nozzle axis.

Calibration of the Mach 4 Nozzle.

The performance of the nozzle was evaluated by measuring the pitot pressure, P_{pitot}, at a plane normal to the nozzle axis and located a distance z = 120mm downstream of the nozzle exit plane. Each pitot probe was fitted with a PCB-112 piezo-electric pressure transducer which measured the stagnation pressure behind a detached shock that formed over the upstream face of the probe. Several probes were mounted in a rake and a number of shots of the shock tunnel were required to build up each pitot profile.

Figure 3 shows the time history of some of the pressures. The "raw" traces for both P_s and P_{pitot} (figure 3A) show the impulsive start and subsequent decay associated with "under-tailored" operation of the shock-tube. In this mode, the shock that compresses the test gas reflects in such a way as to allow the compressed test gas to expand back up the shock-tube. This reduces P_s during the test flow time but delays contamination of the test gas (air) by the driver gas (helium). To eliminate the time variation from our pitot pressure measurements, we normalize P_{pitot} by P_s with a suitable time delay (here 0.2 msec) and filter (time constant = 0.05msec). The normalized traces for 4 pitot probes are shown in figure 3B. We then discard the first 0.5msec of the trace which contains the starting pulse and measure the mean value over the next 0.5msec. This mean value, together with an estimate of its variation over the test time is plotted as a single point on the pitot pressure profile.

Figure 4 shows pitot profiles for a nominal stagnation pressure P_s = 13Mpa and three enthalpies H_s = 16, 8.8 and 6.6MJ/kg. There is some fall-off at the edge of the core flow but this is due to the expansion fan from the trailing edge of the nozzle propagating into the test flow. The performance of the nozzle appears to be satisfactory but we cannot measure how parallel the flow is because the pitot probes are insensitive to small changes in flow angle.

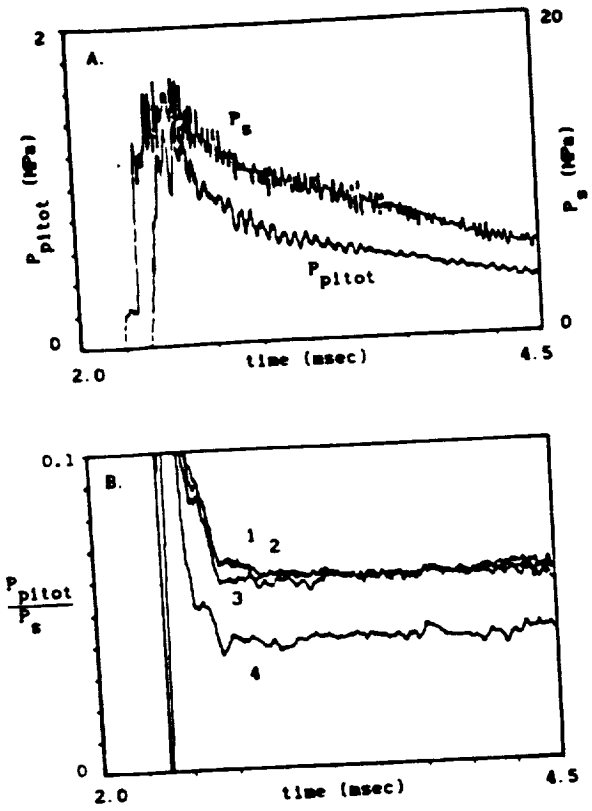

Figure 3. Pressure-time traces for the M = 4 nozzle. P_s = 13MPa, H_s = 16MJ/kg.
A. "Raw" stagnation and pitot pressure.
B. Normalized pitot pressure.

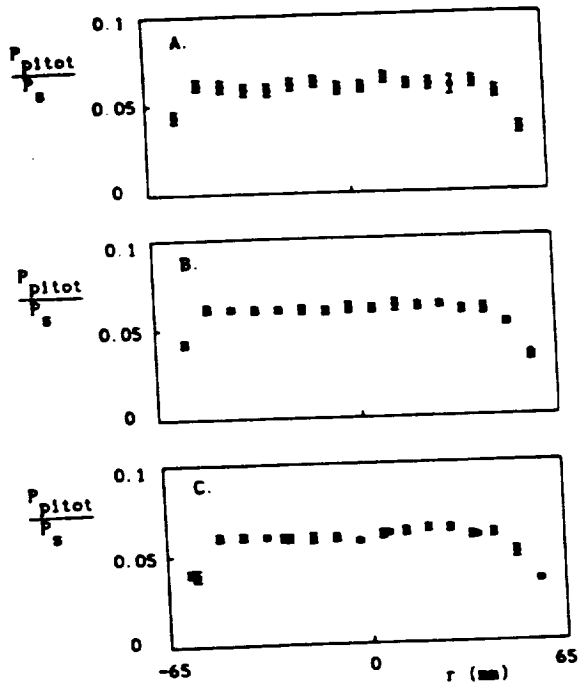

Figure 4. Pitot pressure profiles for the M = 4 nozzle. P_s = 13Mpa, H_s = 120mm.
A. H_s = 6.6MJ/kg
B. H_s = 8.8MJ/kg
C. H_s = 16MJ/kg

MACH 10 NOZZLE.

The starting process for the flow in a hypersonic nozzle involves the propagation of primary and secondary shock waves and an unsteady expansion through the nozzle. Smith (1966) has shown that the time, t_s, required for the flow to approach steady state is dominated (in general) by time taken to sweep the upstream head of the unsteady expansion out of the nozzle. For conical nozzles with fixed divergence angle, t_s increases rapidly with M. To reduce t_s (and hence reduce the amount of gas consumed in the starting process) for a nozzle with large M, we may increase the divergence angle of the initial conical section. However, if the angle is too large, the flow will separate.

We will now describe a nozzle with M = 10 and a two-stage initial expansion designed to avoid flow separation. Immediately after the throat (diameter d = 6mm), the gas is expanded through a cone with a 15° half-angle. From previous experience, this was the largest divergence that would give reasonably uniform flow. Starting at x = 2d, the half-angle is incremented a further 5° (in 1° steps) over the next 8d. The resulting conical section (20° half-angle) is then truncated further downstream (at x = 47.7mm) and a contoured section added to straighten the flow.

This contoured section was designed in such the same way as that for the M = 4 nozzle but at nominal conditions H_s = 35MJ/kg (T_s = 11000K) and P_s = 30MPa. NENZF was used to compute M = 3.69 and γ = 1.41 at the start of the contoured section. This relatively high value of γ is a result of the large fraction of monatomic species found at the end of the conical expansion. Coordinates for the complete contour are given in table 2. No boundary layer modification was added to these inviscid coordinates. To reduce the length of the fabricated nozzle without affecting the usable test core, we truncated the nozzle at the x-station where the characteristic CD intersects the estimated position of the edge of the boundary layer. Because of the large exit Mach number, the fabricated nozzle was much shorter (l = 1036mm) than the full inviscid contour (l = 1777mm).

Calibration of the Mach 10 Nozzle.

As for the M = 4 nozzle, the performance of the M = 10 nozzle was evaluated by measuring the pitot pressure downstream of the nozzle exit plane. Figure 5 shows pitot profiles for two flow conditions. Profile A (P_s = 20MPa, H_s = 30MJ/kg) indicates that the nozzle is not performing well and may even have a conical shock present in the flow. We performed some finite- difference computations with a parabolized Navier- Stokes program and obtained similar pitot profiles when a shock was present. Profile B (z = 369mm) shows a better profile, possibly because the shock has passed out of the test flow core at this axial position. The expansion propagating from the trailing edge of the nozzle has reduced the diameter of the test core at this axial position. We note also that the normalized pitot traces for this condition changed continuously through the test time. This indicates that the boundary layers on the nozzle wall did not reach steady

state.

Operating the nozzle at higher pressure (see profile C, P_s = 40MPa) significantly improves the flow uniformity but there is still a depression in the centre of the pitot profile. We suspect that this improvement in nozzle performance is a result of reducing the boundary layer that grows along the nozzle wall. For profiles A and C, we estimate the total boundary layer thickness at the exit plane to be δ_A = 82mm and δ_C = 58mm. These values scale as $Re^{-1/2}$ which indicates that the boundary layer is laminar. Assuming that displacement thickness $\delta^* = 0.33\,\delta$, the effective area ratio of the nozzle is reduced from the design value 2290 to 1450 and 1680 for profiles A and C respectively. Values of pitot pressure computed with MENZF for these effective area ratios are shown as dashed lines in figure 5.

In conclusion, it appears that our design approach is satisfactory for hypervelocity nozzles with moderate exit Mach number. However, nozzles with high values of exit Mach number need to be operated at sufficiently high pressure to ensure that their boundary layers do not disturb the core flow.

ACKNOWLEDGEMENTS.

We wish to thank Dr. Peter Killen and Ken Dudson for constructing the M = 10 nozzle, Denis Sussmilch for constructing the M = 4 nozzle and Craig Brescianini for performing finite-difference calculations of flow in the M = 10 nozzle. This work was supported by ARC and NASA (under grant NAGW-674).

REFERENCES.

Jacobs, P.A. 1988 "An interactive graphics program for computer assisted calculation of isentropic flows." Report 7/88, Department of Mechanical Engineering, University of Queensland.

Liepmann, H.W. & Roshko, A. 1957 *Elements of Gasdynamics*. John Wiley & Sons.

Lordi, J.A., Mates, R.E. & Moselle, J.R. 1966 "Computer program for the numerical solution of nonequilibrium expansions of reacting gas mixtures." NASA-CR-472.

Mudford, N.R., Stalker, R.J. & Shields, I. 1980 "Hypersonic nozzles for high enthalpy nonequilibrium flow." *Aeronautical Quarterly* May 1980, 113-131.

Schurmeier, H.M. 1959 "Design and operation of a continuous-flow hypersonic wind tunnel using a two- dimensional nozzle." AGARDograph 38.

Sivells, J.C. 1978 "A computer program for the aerodynamic design of axisymmetric and planar nozzles for supersonic and hypersonic wind tunnels." AEDC-TR-78-63.

Smith, C.E 1966 "The starting process in a hypersonic nozzle." *J. Fluid Mech.* 24, 625-640.

Stalker, R.J. & Morgan, R.G. 1988 "The University of Queensland free piston shock tunnel T4 - Initial operation and preliminary calibration."

Zonars, D. 1967 "Nonequilibrium regime of airflows in contoured nozzles: theory and experiment." *AIAA J.* 4(1), 57-63.

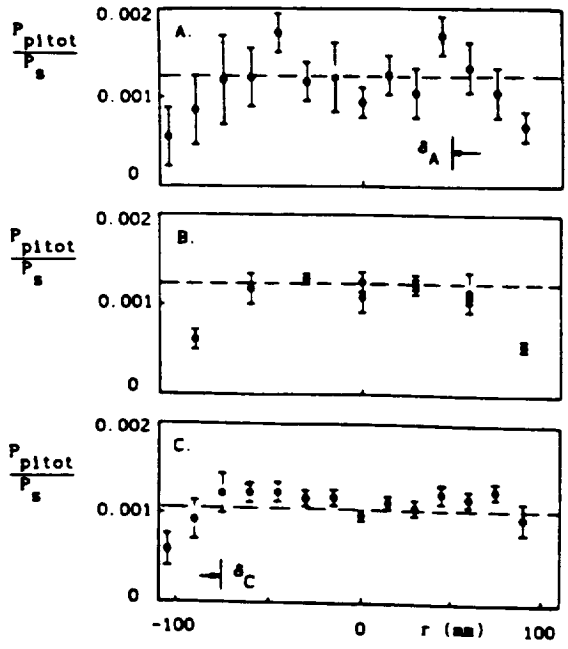

Figure 5. Pitot pressure profiles for the M = 10 nozzle. The dashed lines indicate the MENZF computed level with $\delta^*/\delta = 0.33$.
A. P_s = 20Mpa, H_s = 30MJ/kg, z = 139mm.
B. P_s = 20Mpa, H_s = 30MJ/kg, z = 369mm.
C. P_s = 40Mpa, H_s = 25MJ/kg, z = 139mm.

Table 1. Coordinates for the M = 4 inviscid contour. Points with x ≥ 98mm are knots on a cubic spline.

x (mm)	$r_{inviscid}$ (mm)	comment (slope)
0.0	12.5	start of 12° cone
98.43	33.43	start of contour (0.2126)
157.48	44.45	
216.54	52.79	
275.59	58.56	
334.65	62.30	
393.70	64.66	
452.76	65.88	
511.81	66.07	end of contour (-0.0048)

Table 2. Coordinates for the M = 10 inviscid contour. Points with x ≥ 47mm are knots on a cubic spline.

x (mm)	$r_{inviscid}$ (mm)	comment (slope)
0.0	3.00	start of 15° cone
12.0	6.24	end of 15° cone
15.0	7.09	
18.0	8.03	
21.0	9.00	
24.0	10.03	start of 20° cone
47.70	18.66	start of contour (0.3640)
294.78	74.51	
541.85	104.66	
788.93	121.57	
1036.00	132.76	
1283.08	139.13	
1530.16	142.44	
1777.23	143.55	end of contour

REAL GAS EFFECTS IN HYPERVELOCITY FLOWS OVER AN INCLINED CONE

by
R.M.Krek

1. INTRODUCTION

Pressure and heat transfer measurements obtained from experiments on a cone with a half angle $\theta = 15^\circ$ at angles of incidence $\beta = 0^\circ$ and $\beta = 30^\circ$, in a hypervelocity flow with a nominal Mach number of 5 are presented. Three stagnation enthalpies were used, H_o = 6, 28, and 36 MJ/kg. The pressure results agree reasonably well with Newtonian theory, Taylor-Maccoll theory and with detailed three-dimensional calculations when the flow is frozen. Pressure measurements at high enthalpy indicate unresolved effects of enthalpy on the leeward flow. Heat transfer results are also given and are compared with theoretical values for zero incidence. The data derived from the 30° incidence experiments, show the same trends as the pressure distribution around the cone.

The aim of this project is understand the basic dissociation phenomena which occur in three dimensional high enthalpy flows. A simplified model consisting of an inclined cone in a hypervelocity flow of pure Nitrogen is used. Experimental study of this flow at sufficiently high enthalpy should provide insight into the interaction between nonequilibrium dissociation chemistry and hypervelocity aerodynamics, and thus help to evaluate the influence of real gas effects on the pressure and the heat transfer distributions on the cone.

The expected structure of hypervelocity flow about an inclined cone is shown in figure 1. The conical bow shock is of greatest strength at the windward stagnation plane but weakens with increasing azimuthal angle ϕ. If the angle of incidence β, is sufficiently large, the flow in the plane normal

to the cone axis is supersonic. As the flow expands around the cone surface, the fluid may be expected to first accelerate, and then decelerate as it approaches the leeward plane of symmetry. The pressure recovery required at the symmetry plane requires a pair of cross-flow shocks. Owing to the strong entropy gradients along these shocks the vorticity of the shock-processed flow is greatly enhanced, with the resultant formation of a complex three-dimensional flow containing one or more pairs of streamwise vortices, and possible shock induced separation from the cone surface. This flow structure is essentially inviscid (see Marconi 1989) but will be modified by the presence of shock induced boundary layer separation. We note that for frozen flow at low enthalpy, (ie. constant γ), the approximately conical flow will contain no dominant length scale.

2. EXPERIMENTAL PROCEDURE

The experiments were carried out in The University of Queenslands T4 free piston shock tunnel which is capable of achieving the high temperatures and thus the enthalpy conditions which are experienced during reentry. A Nitrogen test gas was used to further isolate the basic dissociation chemical reactions which occur at these high temperatures. The expected freestream conditions in the test flow for the three enthalpy conditions are presented in Table 1 below.

H_o MJ/kg	T_∞ K	P_∞ kPa	ρ_∞ kg/m^3	u_∞ km/s	Mach N°	γ	α_∞
6.42	775	5.88	.0256	3.35	5.84	1.4	~ 0
28.0	2560	9.92	.0099	5.67	4.79	1.38	.140
36.0	3518	10.05	.0076	6.17	4.49	1.44	.268

Table 1 Freestream Conditions in Test Section

The cone used for the experiments had a half angle $\theta = 15^{\circ}$ and an axial length 180 mm. The instrumentation on the cone consisted originally of ten Entran pressure transducers and ten Pt-PtRh thermocouple heat transfer gauges. Both the pressure transducers and the thermocouples were mounted in rows of five gauges each, with the rows equispaced around the cone. The arrangement of the cone and it's instrumentation is shown in figure 1. Due to pressure transducer problems, we were only able to obtain five gauges that operated satisfactorily.

3. PRESSURE RESULTS

The results from the calibration experiments at $\alpha = 0^{\circ}$ are displayed in figure 2 which show plots of P_c/P_{pitot} versus cone position for the conditions with H_o= 6.42 MJ/kg and H_o= 27.98 MJ/kg. The experiments are compared with Taylor-Maccoll solutions, for which an appropriate value of γ is required. For the equilibrium case, it was found that the flow is vibrationally frozen, and that we can take $\gamma = 1.4$. For H_o=28 MJ/kg, the flow is relaxing vibrationally and we take $\gamma = 4+\alpha/3$, assuming ideal dissociating gas behaviour. Figure 2a shows that the measured P_c/P_{pitot} agrees quite well with the Taylor-Maccoll solution when H_o= 6 MJ/kg. The average of the experiments differs by 5% from the Taylor-Maccoll theory. For the non-equilibrium case, figure 2b, the average value of the pressure signals is 22% below that of the Taylor-Maccoll value. Apart from the discrepancy in figure 2b, it can be seen that the pressure on the cone surface during the experiment at zero incidence, for both enthalpies is approximately constant along a ray.

Now consider the results obtained from experiments for $\alpha = 30^{\circ}$. Figures 3-5 show plots of pressure in two forms, 1) P_c/P_{pitot} ,and 2) $\ln(P_c/P_{\infty})$

verses ϕ at each of the five measuring stations, for H_o= 6, 28 and 36 MJ/kg, respectively. The experiments are compared with the Newtonian estimate for pressure, which in the hypersonic limit and assuming perfect gas behaviour, is given by,

$$P_c/P_\infty = \gamma M_\infty^2(\sin\theta\cos\beta + \cos\theta\sin\beta\cos\phi)^2 + 1. \qquad (1)$$

Figure 3 also shows results obtained from detailed three-dimensional calculations performed by Macrossan *et al* (1989), and these compare favourably with experiments. For all enthalpy cases it can be seen that the Newtonian value of pressure for the first 60° of the windward surface is higher than the values derived from experiments (figures 3b-5b).

The main aim of this project is to investigate the effects of real gas chemistry on the leeward surface of the cone. From figures 3a-5a it can be seen that the data provides some evidence that cross-flow shocks are occurring on the leeward surface, as suggested in figure 1. The cross-flow shocks occur at about ϕ = 150°, but the resolution of the plots and the reliability of the pressure gauges make any conclusive quantitative assessment of the results difficult. It is proposed that further experiments on the leeward surface of the cone be conducted using more sensitive pressure gauges, and that a finer survey of the leeward surface be taken. This should allow accurate measurement of the azimuthal position of cross-flow shocks.

4. HEAT TRANSFER RESULTS

As said above heat transfer was measured via the use of Pt-PtRh thermocouples. Calibration of the thermocouples independent of the experiments proved impractical, thus the thermocouples were calibrated by scaling the gauge measurements for heat transfer to the cone surface at zero incidence, and in low enthalpy flow, to the predications of Eber (1952). From Eber's laminar boundary laminar analysis, the heat transfer at a

distance x from the apex along the cone surface may be expressed as

$$St_x = 0.575\, Re_x^{-1/2}\, Pr^{-2/3} \qquad (2)$$

where St_x, Re_x, and Pr are the Stanton number, Reynolds number, and Prandtl number respectively and are based on freestream conditions.

Knowing the theoretical values for the heat transfer we are able to calibrate the experimental data. Figure 6 shows the heat transfer data plotted in terms of St verses Re, for the three enthalpy conditions and are compared with their respective theoretical values. Figure 6a is the equilibrium case from which the calibration factors can be determined for each individual thermocouple. Figures 6b and 6c are the two nonequilibrium conditions, from which it can be seen that calibrated experimental data are higher than the theoretical values.

The data obtained from experiments performed at $\beta = 30^\circ$ are normalised with the zero incidence data for each enthalpy condition. Figures 7-9 show $St_\phi/St_{\alpha=0}$ verses ϕ, for H_o= 6, 28, and 36 MJ/kg respectively. These figures show a decrease in the heat transfer until there in a local minimum at about $\phi = 150^\circ$, with a rise in the heat transfer to $\phi = 180^\circ$, similar to the pressure distribution around the cone. This again suggest the existence of separation and counter-rotating vortices occurring on the leeward surface. As with the pressure data the resolution of heat transfer is not sufficient to establish any quantitative arguments of the leeward surface.

5. CONCLUSIONS

The pressure and heat transfer results presented compare reasonably with their respective theories. Both the pressure and heat transfer suggest the existence of crossflow shocks on the leeward surface, but more detailed experiments are required. The experiments that will be conducted will have

more sensitive pressure transducers and thinfilm heat transfer gauges to investigate a finer survey of the leeward surface of the cone. From these experiments we shall be able to pinpoint the crossflow shocks and determine the effects of varying enthalpy on the crossflow shocks. A further use for the thinfilm gauges is to compare actual experimental data with theory at zero incidence and to calibrate the windward thermocouples.

REFERENCES

Eber,G.R., 1952, *J. Aeronautical Sciences*, 19, 1-6

Krek, R.M., Hannemann, K., Pullin, D.I., 1989, Submitted to 10th AFMC

Macrossan, M.N., Pullin, D.I. & Richter, N.J., 1989, Submitted to 10th AFMC.

Marconi, F., 1989, *J. Comp. and Fluids*, 17, 151-163.

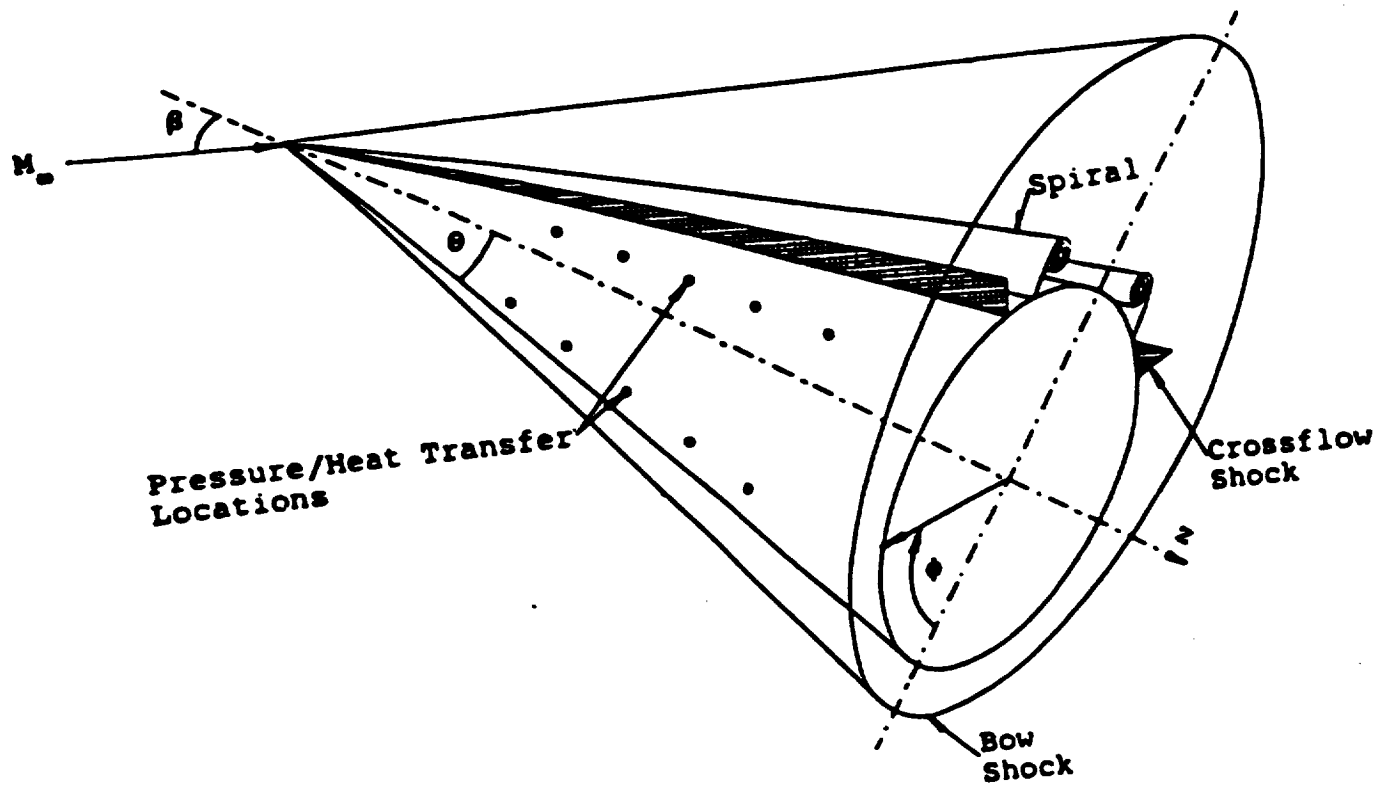

Figure 1: Flowfield for a cone at incidence in a hypervelocity flow. θ - cone half angle, β - angle of incidence, ϕ - azimuthal angle, z - axial distance.

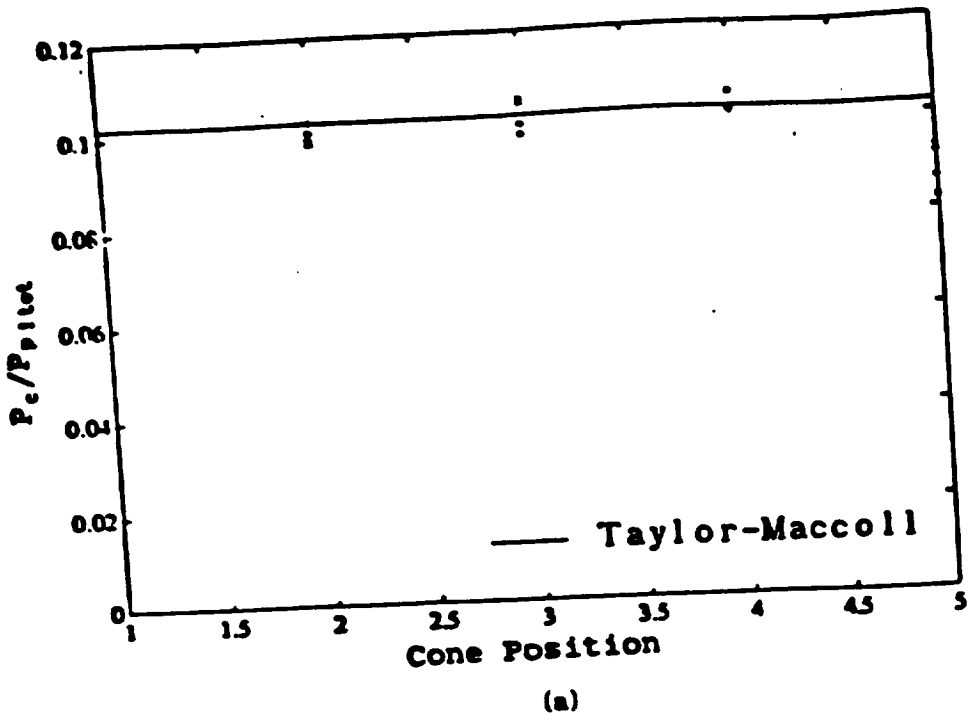

(a)

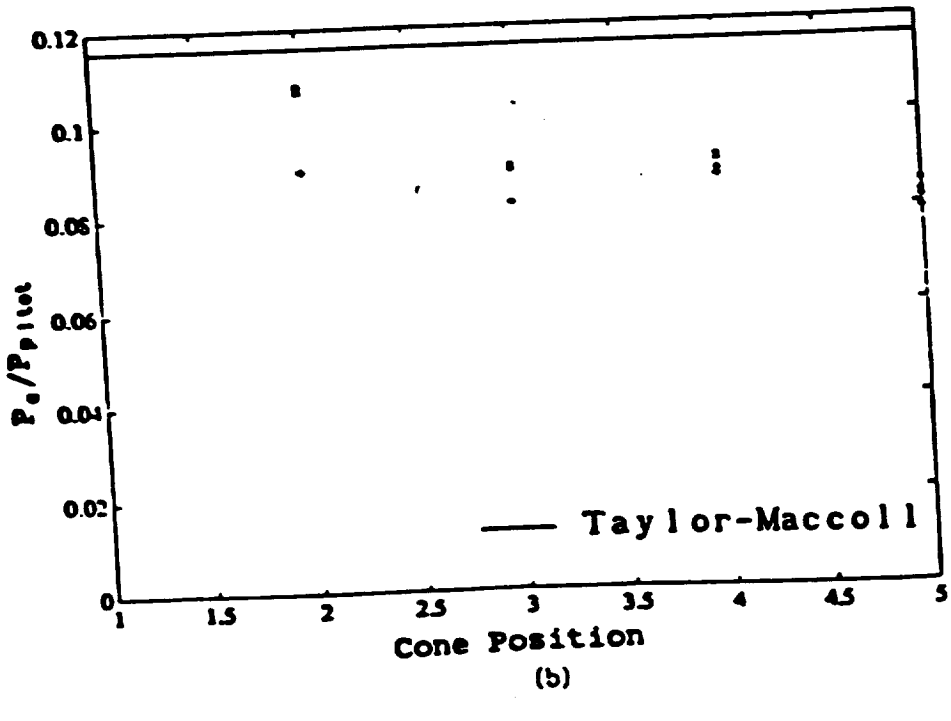

(b)

Figure 2: P_{cone}/P_{Pitot} verses cone position for $\beta = 0^{\circ}$.
(a) H_o = 6 MJ/kg, γ = 1.4, M = 5.84. + s500, * s501, x s502.
(b) H_o = 28 MJ/kg, γ = 1.38, M = 4.79. + s503, * s511, x s512.
——— Taylor-Maccoll Theory.

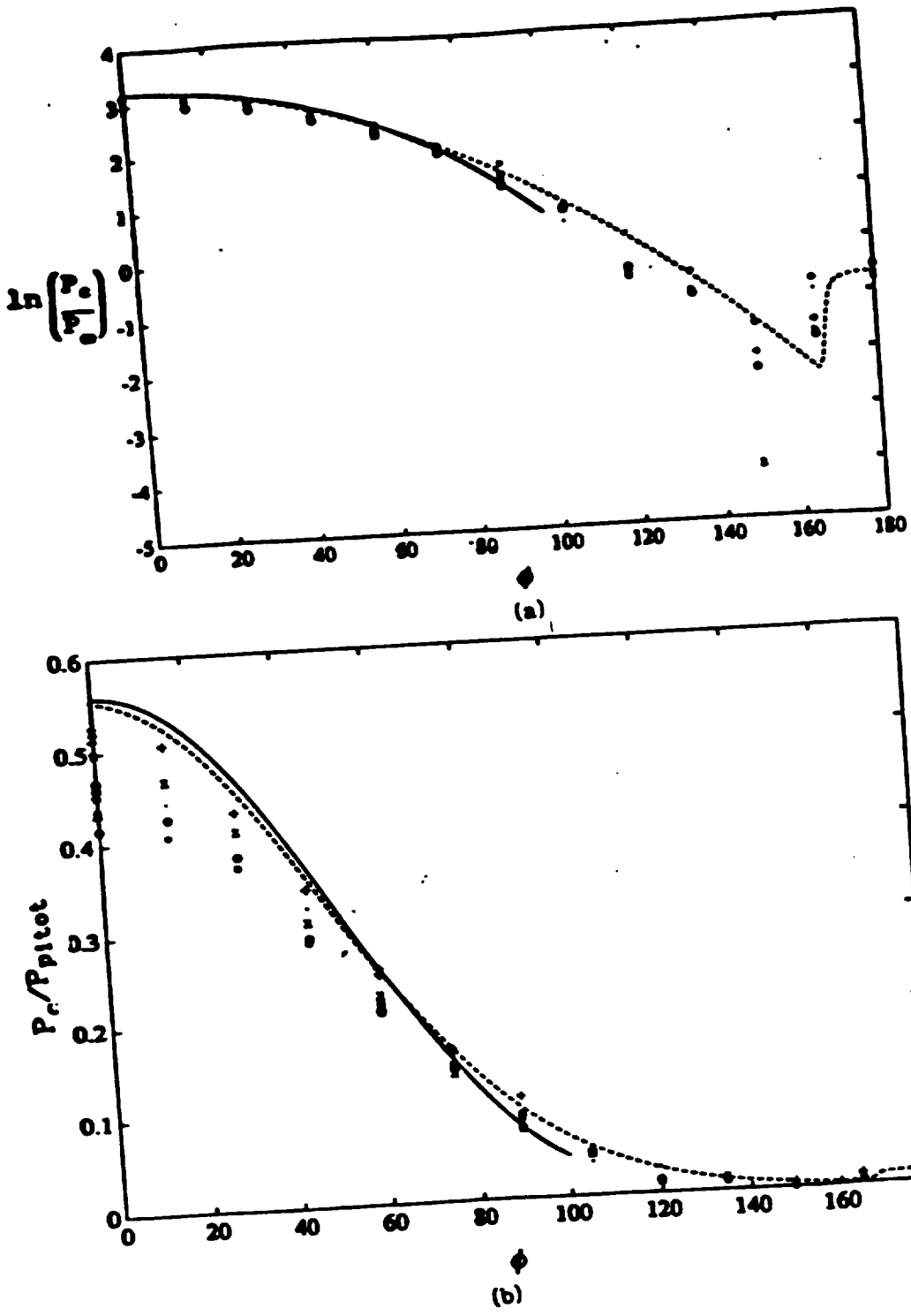

Figure 3: $\beta = 30°$, $H_o = 6$ MJ/kg

(a) $\ln(P_c/P_\infty)$ verses ϕ

(b) P_c/P_{Pitot} verses ϕ

. Position 1, + Position 2, x Position 3, * Position 4, • Position 5

_ _ _ _ Macrossan *et al* 1989, ———— Newtonian.

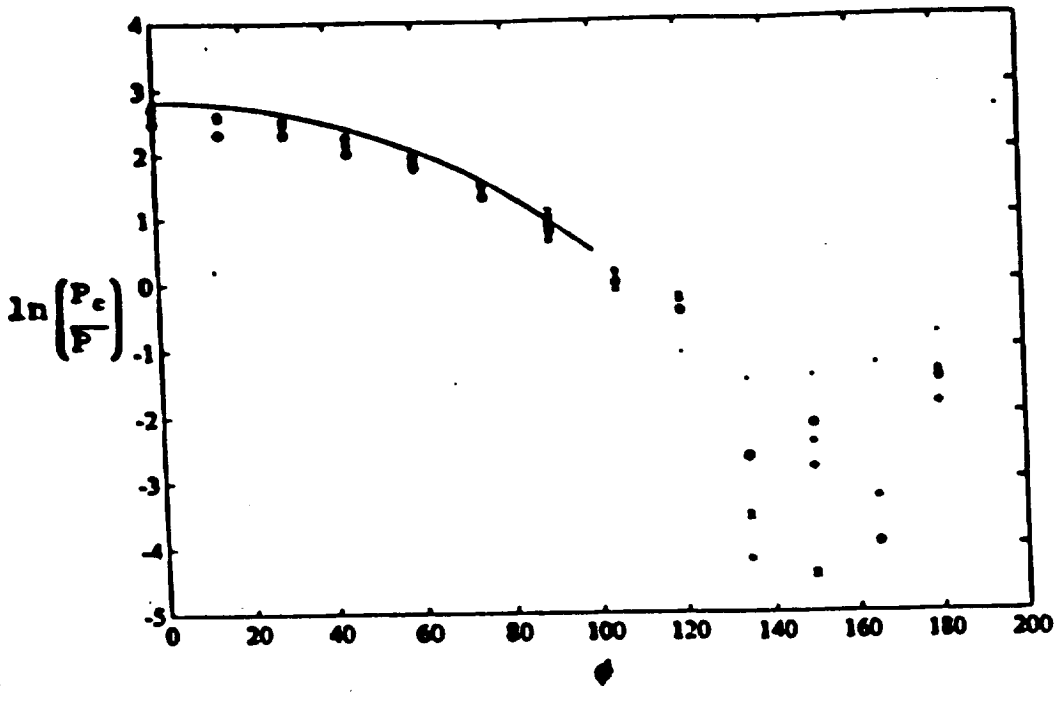

(a)

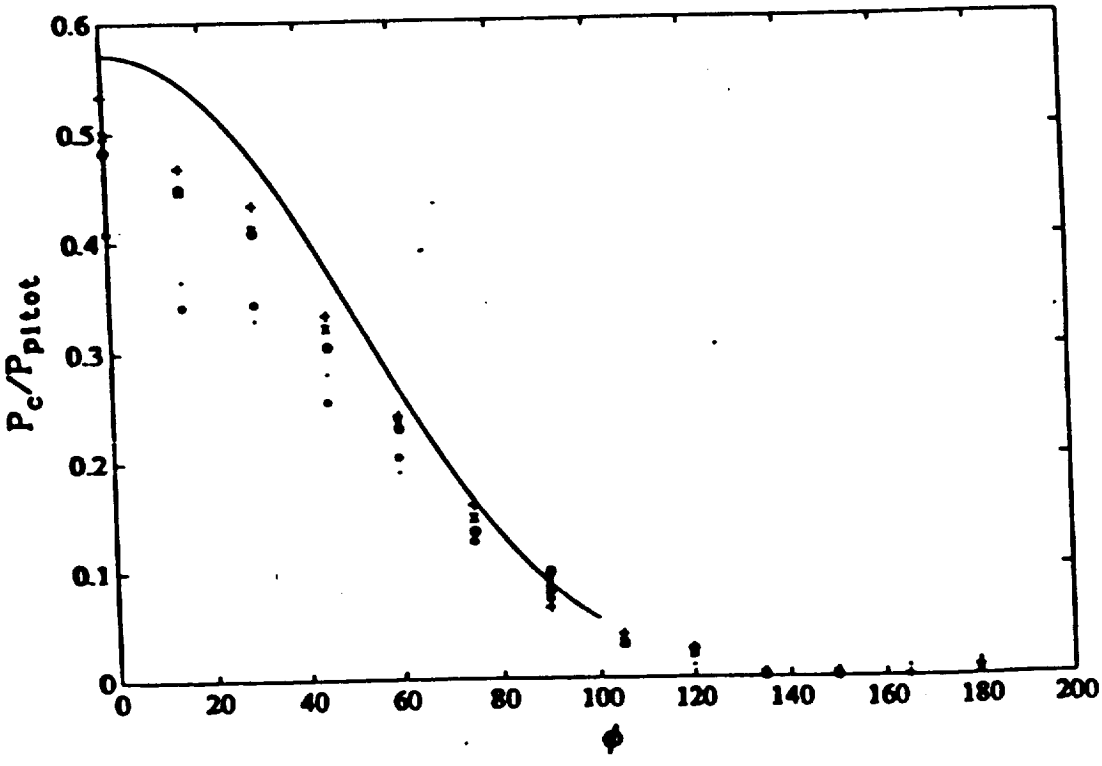

(b)

Figure 4: $\beta = 30^\circ$, $H_o = 28$ MJ/kg

(a) $\ln(P_c/P_\infty)$ verses ϕ

(b) P_c/P_{Pitot} verses ϕ

. Position 1, + Position 2, x Position 3, • Position 4, • Position 5

——— Newtonian.

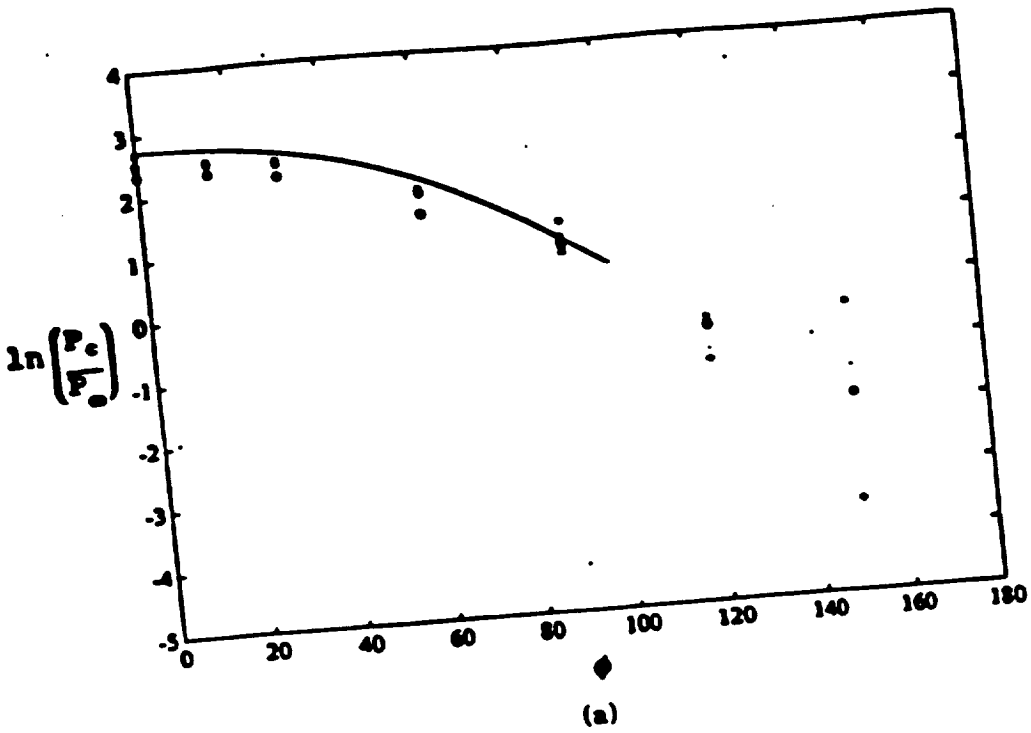

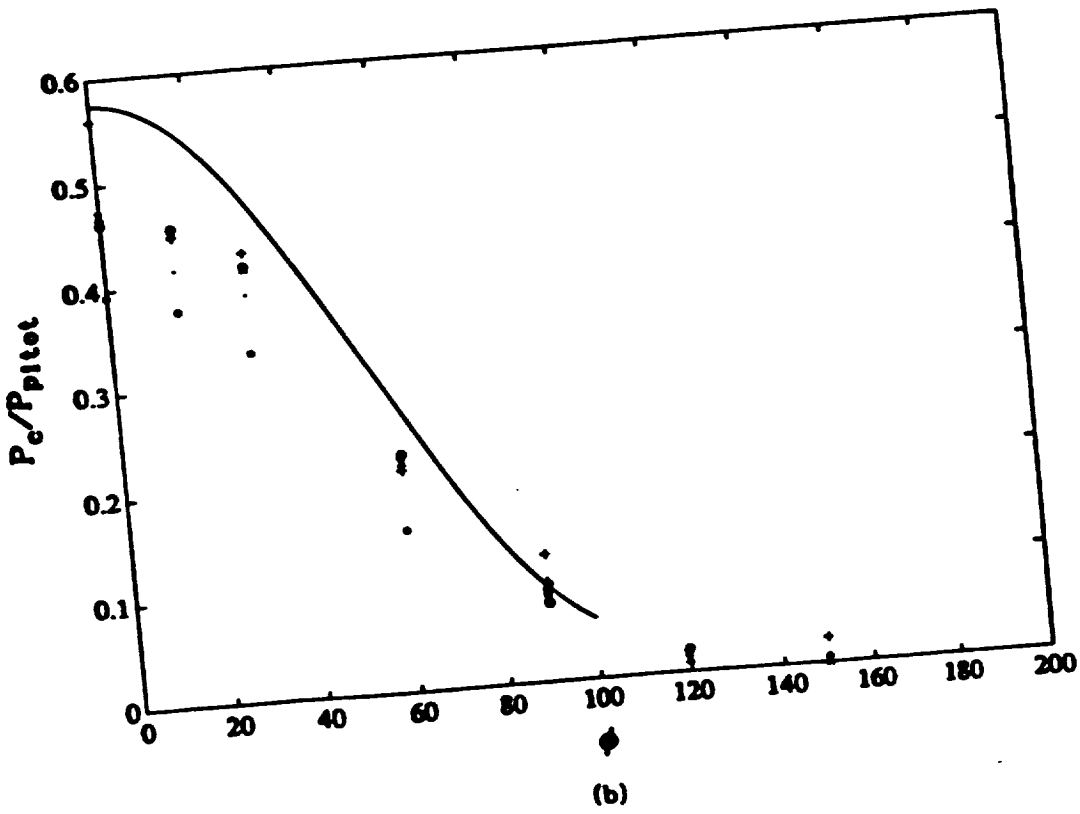

Figure 5: $\beta = 30°$, $H_o = 36$ MJ/kg

(a) $\ln(P_c/P_\infty)$ verses ϕ

(b) P_c/P_{Pitot} verses ϕ

. Position 1, + Position 2, x Position 3, * Position 4, • Position 5

———— Newtonian.

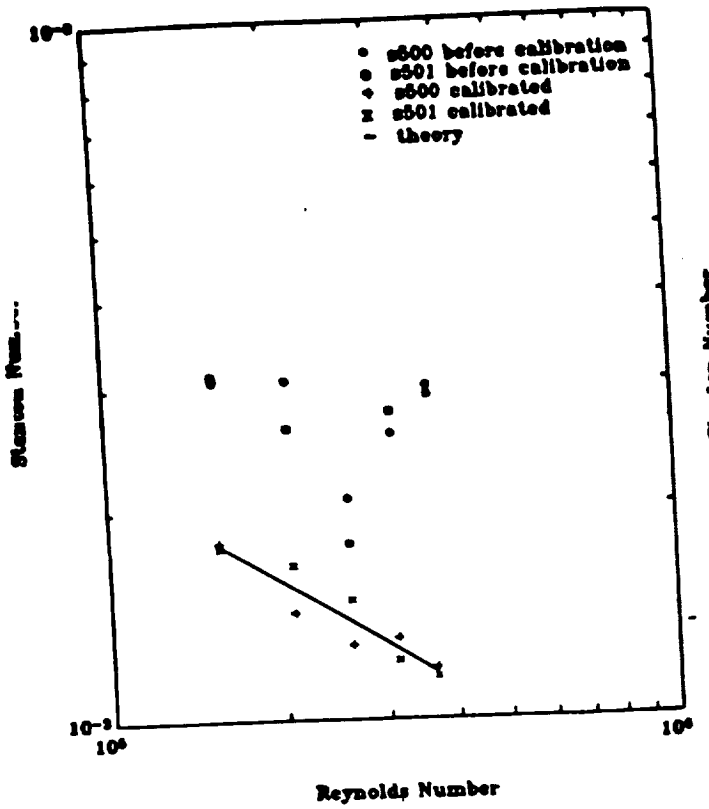

(a)

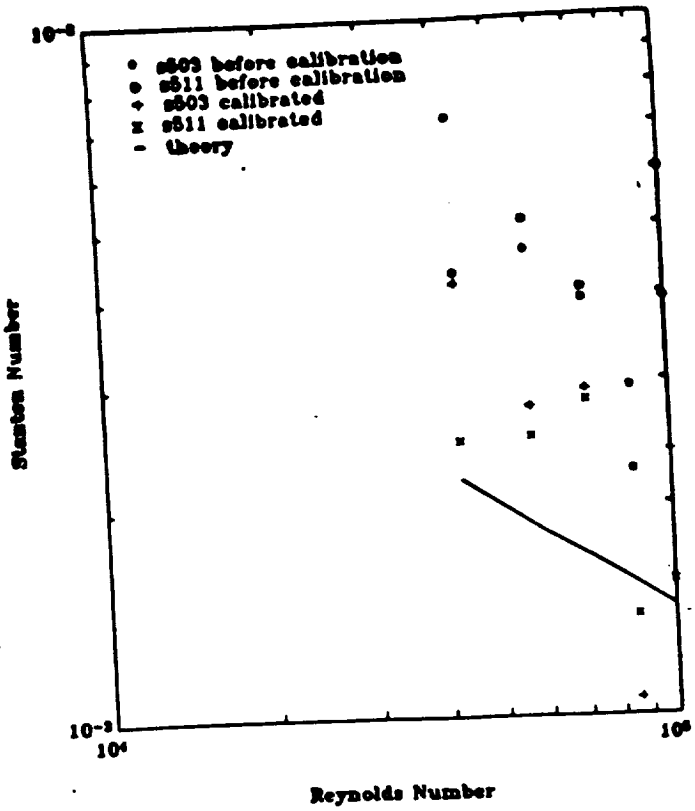

(b)

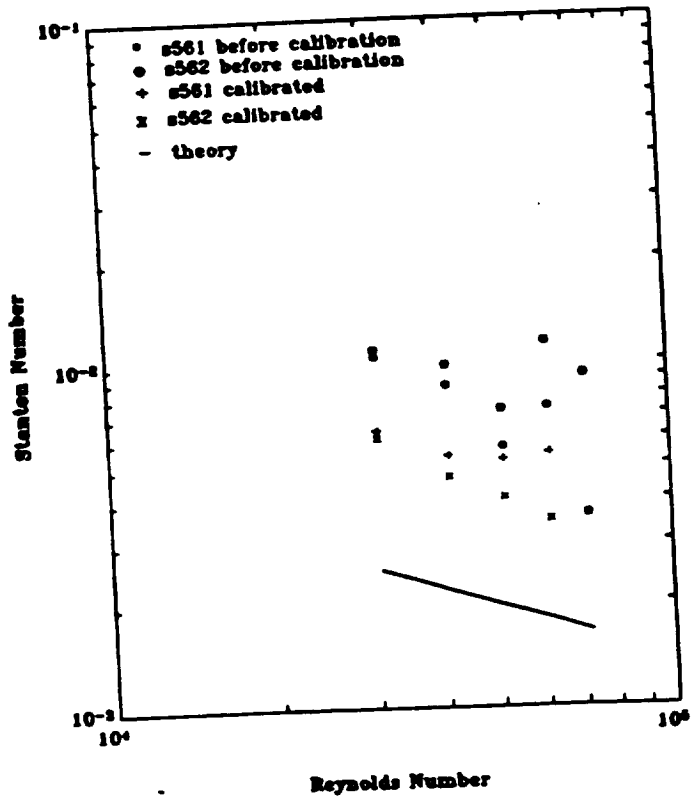

(c)

Figure 6: Stanton Number verses Reynolds Number for $\beta = 0^\circ$
(a) H_o = 6 MJ/kg, (b) H_o = 28 MJ/kg, (c) H_o = 36 MJ/kg.

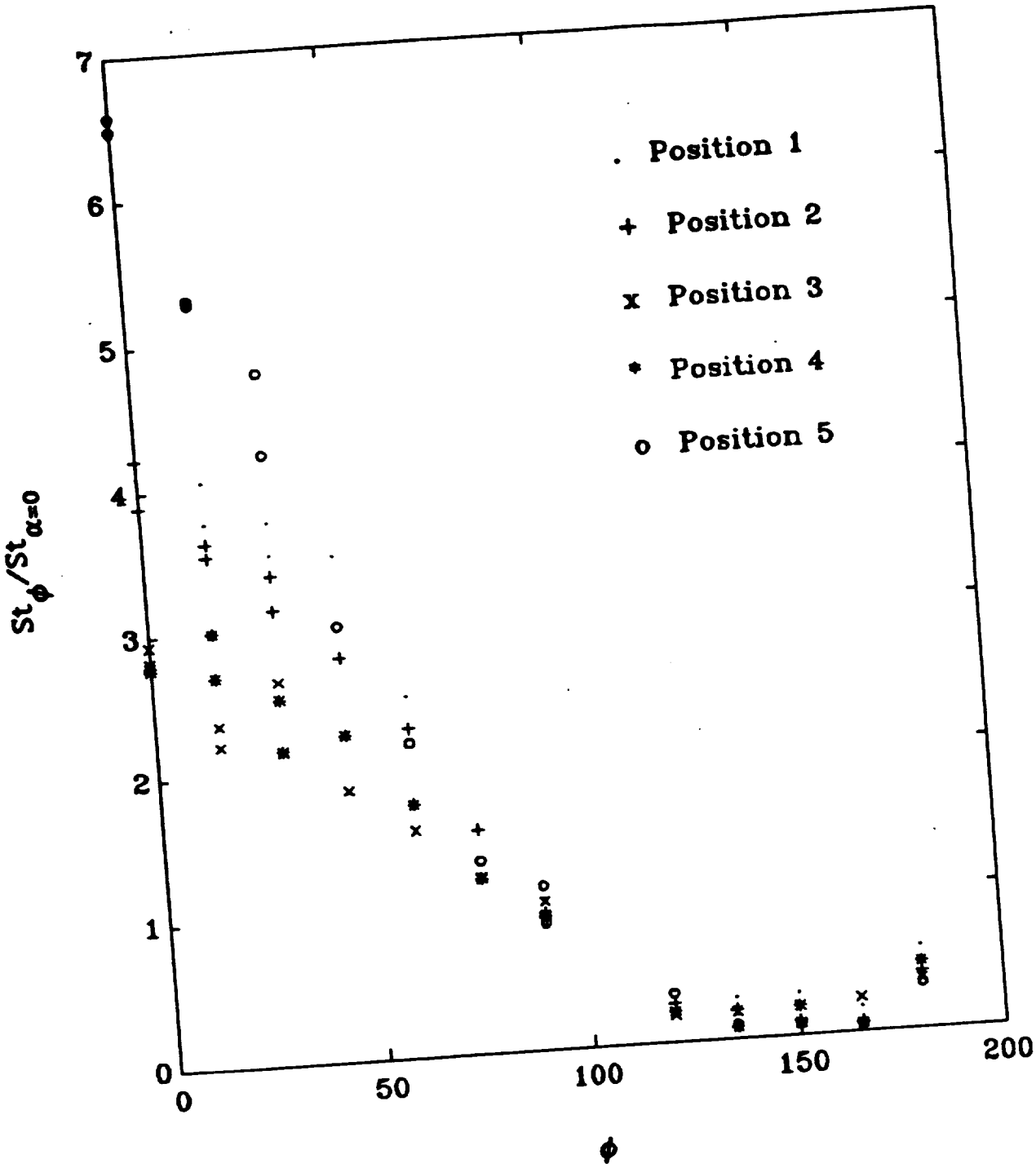

Figure 7: $St_\phi/St_{\alpha=0}$ verses ϕ for $\beta = 30°$, $H_o = 6$ MJ/kg.

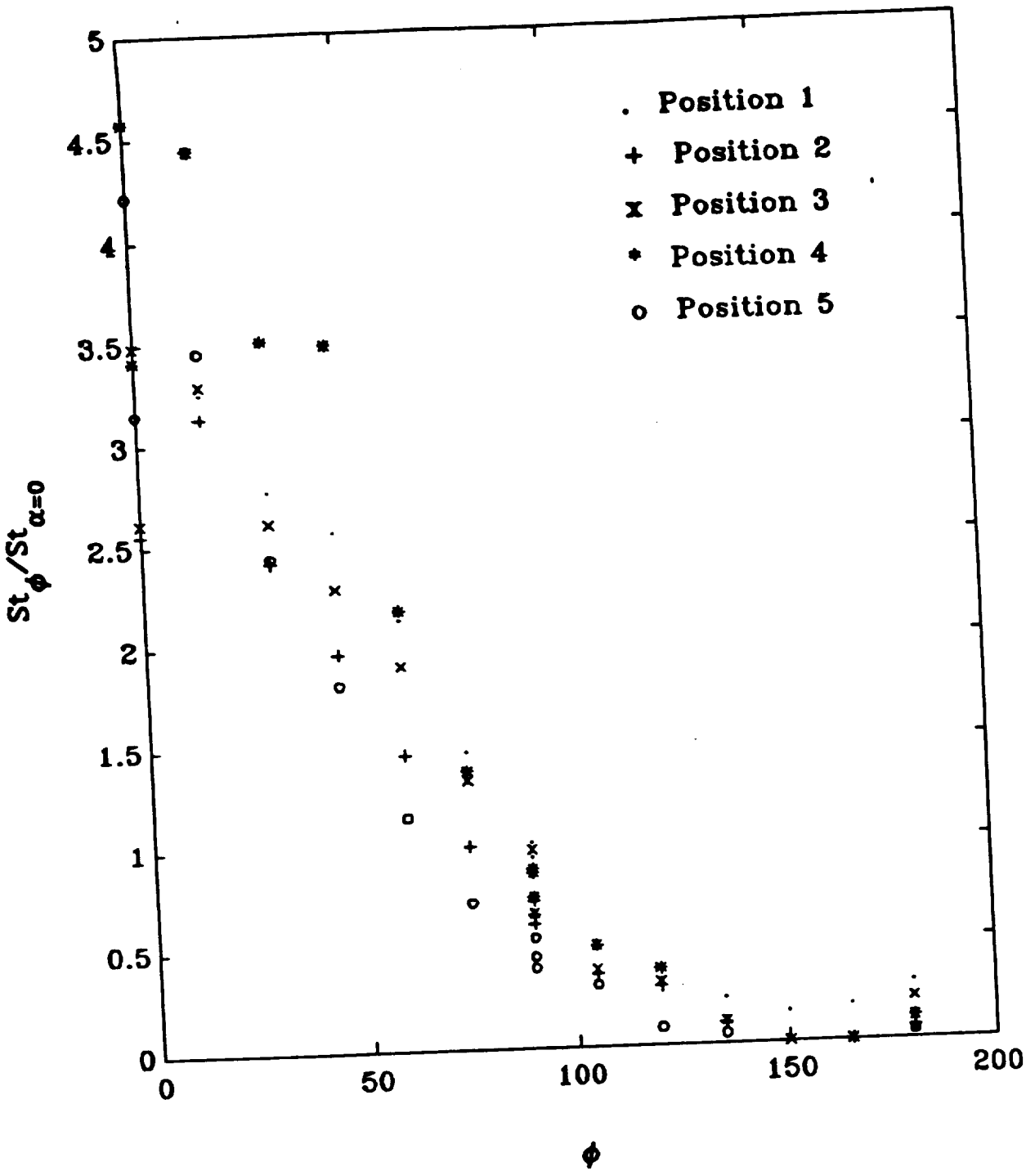

Figure 8: $St_\phi/St_{\alpha=0}$ verses ϕ for $\beta = 30°$, $H_o = 28$ MJ/kg.

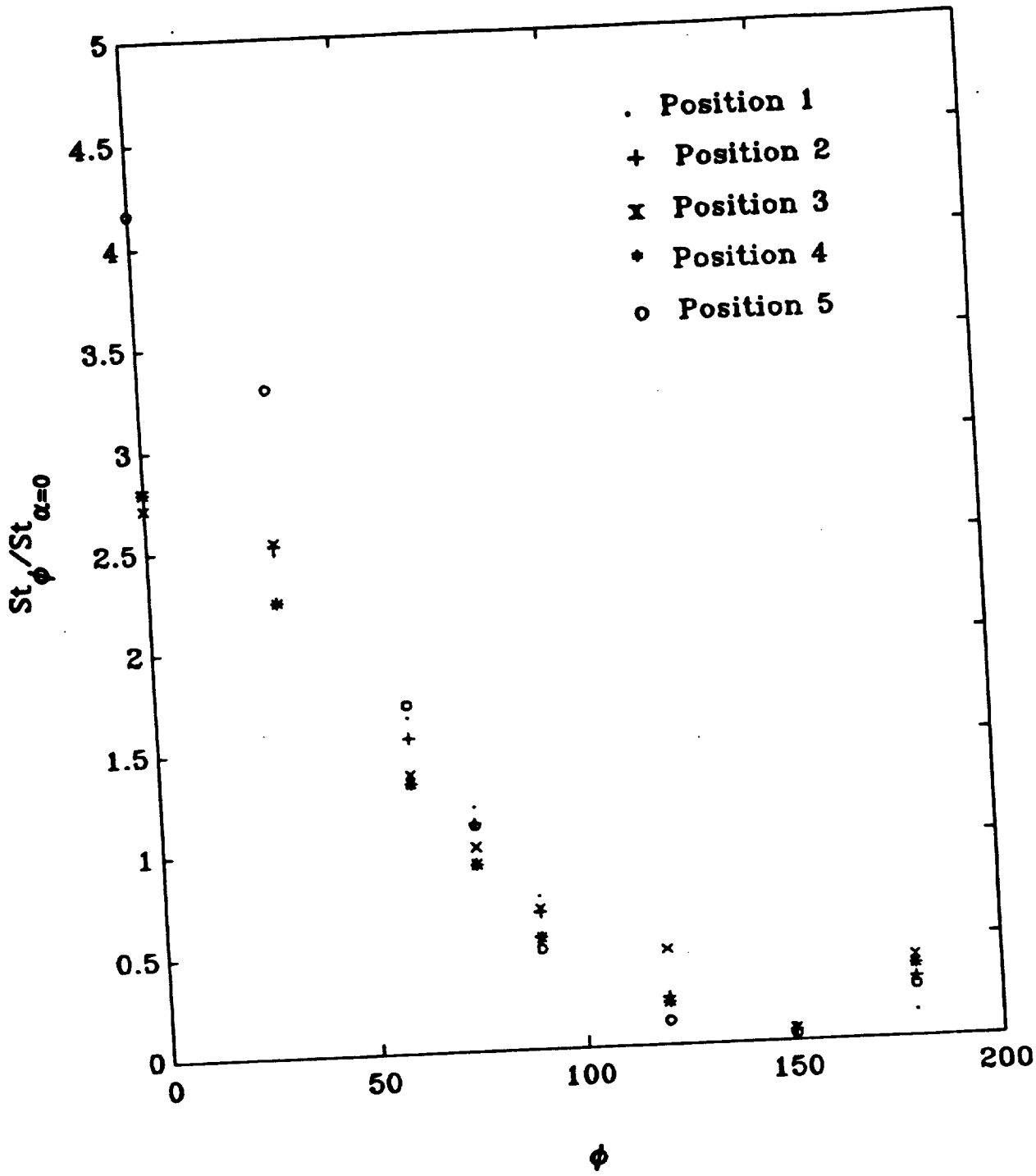

Figure 9: $St_\phi/St_{\alpha=0}$ verses ϕ for $\beta = 30°$, $H_o = 36$ MJ/kg.

SHOCK TUNNEL DEVELOPMENT (Supplementary Project)

R.J. Stalker and R.G. Morgan

Raising Operating Pressures

A major target of the 1989 program was to raise the operating pressure levels of The University of Queensland shock tunnel T4. Specifically, this meant raising the pressure after shock reflection at the downstream end of the shock tube - i.e. at the nozzle entrance. With a free piston shock tunnel, this can be done in two ways. Either, by operating at a high driver gas volumetric compression ratio, a high main diaphragm burst pressure. The Page-Stalker effect (i.e. the loss of pressure at shock reflection in the driver gas at the downstream end of the shock tube), then causes the pressure at the nozzle entrance (nozzle stagnation pressure) to be reduced. Or, by operating at a lower driver gas volumetric compression ratio, and a lower diaphragm burst pressure. The reduction in the Page-Stalker effect then can allow similar nozzle stagnation pressure levels to be reached.

In both cases, the pressure driving the piston remains the same, ensuring that the same energy is imparted to the driver gas during the compression process. The first method has the advantage that longer test times are obtained at a given stagnation enthalpy. The second method has the advantage that lower peak pressures are produced in the apparatus.

Tests were made to compare the operation of T4 in the two modes, and resulting nozzle stagnation pressure records are shown in Fig. 1. Record A was obtained with a main diaphragm burst pressure of 170 MPa, a driver volumetric compression ratio of 120 and a piston driver reservoir pressure of 8.3 MPa. Record B was obtained with a main diaphragm burst pressure of 86 MPa, a driver volumetric compression ratio of 60, and a piston driver reservoir pressure of 8.9 MPa.

It can be seen that the nozzle stagnation pressure for B is a little higher than for A, even though the main diaphragm burst pressure is only one half of that for A. Thus a given nozzle stagnation pressure is produced with much lower peak pressures in the apparatus.

The number of flow passes over an 0.5 m long model also is shown in the figure, together with the estimated time at which contamination by driver gas occurs. The stagnation enthalpy for A was 27 MJ/kg, whilst that for B was 13 MJ/kg (the test gas for A was nitrogen, and that for B was air, but this does not influence the operating characteristics under discussion) and it can be seen that approximately the same number of flow passes takes place before contamination in each case, in spite of the fact that increasing stagnation enthalpy with given driver conditions reduces the time for contamination. Thus, changing the driver conditions by raising the diaphragm burst pressure and the driver volumetric compression allows operation at high enthalpies without reducing the effective test time.

It might be noted that the higher diaphragm burst pressures are associated with considerable technical problems. For example, the high pressure stainless steel diaphragms which are used do not "petal" cleanly, and fragments of the order of 10 to 20 mm in diameter tend break away, to impact the downstream end of the shock tube, or to pass into the nozzle. The steel high pressure plate of the entrance to the shock tube tends to ablate, and the high stresses induced in the nozzle by high shock reflection pressures cause deformation of the surface contour. Although all of these are problems

can be solved by the application of time and technical effort, they are nevertheless a practical discouragement to high pressure operation.

Hypersonic Combustion

The purpose of raising the tunnel operating pressure levels was to make it possible to produce reasonably vigorous, hypersonic combustion of hydrogen fuel. With the pressures which were achieved, it was considered that it may be necessary to increase the combustion duct length in order to allow an adequate streamwise distance for the combustion to develop. Accordingly, the long duct designed for the scaling experiments (see "Pressure-Length Correlations in Supersonic Combustion") was used. The intake was modified to allow effective "direct connect" operation, rather than the expansion after the intake which is shown in Fig. 2 of the above report, and the same central injection strut was used.

Static pressure distributions along the duct are shown in Fig. 2. Tests were conducted not only with hydrogen, but also with ethane, as fuel. Although the wave structure resulting from the modified inlet somewhat confuses the display of results, the clear cut increase in static pressure, amounting to a factor of two , which is achieved when air replaces nitrogen as test gas is evidence that combustion is taking place. It is interesting to note that ethane produces combustion pressure increases which are only a little below those experienced with hydrogen.

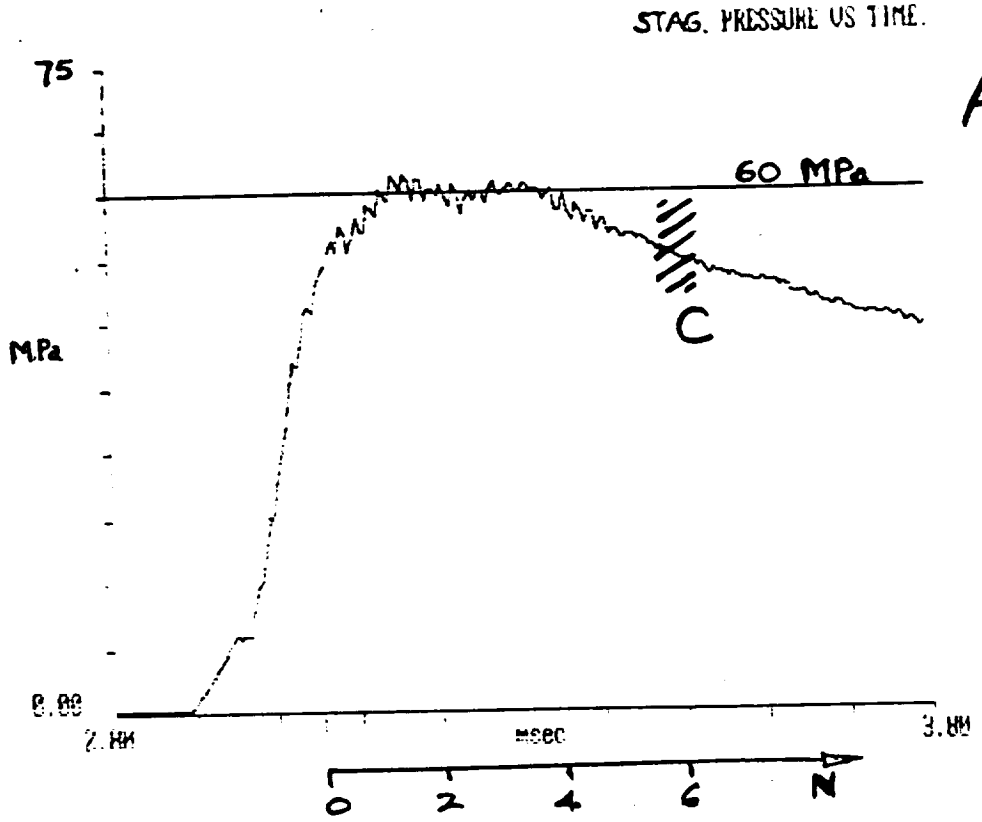

N = NO. OF FLOW PASSES (0.5 m. MODEL)
C = DRIVER GAS CONTAMINATION

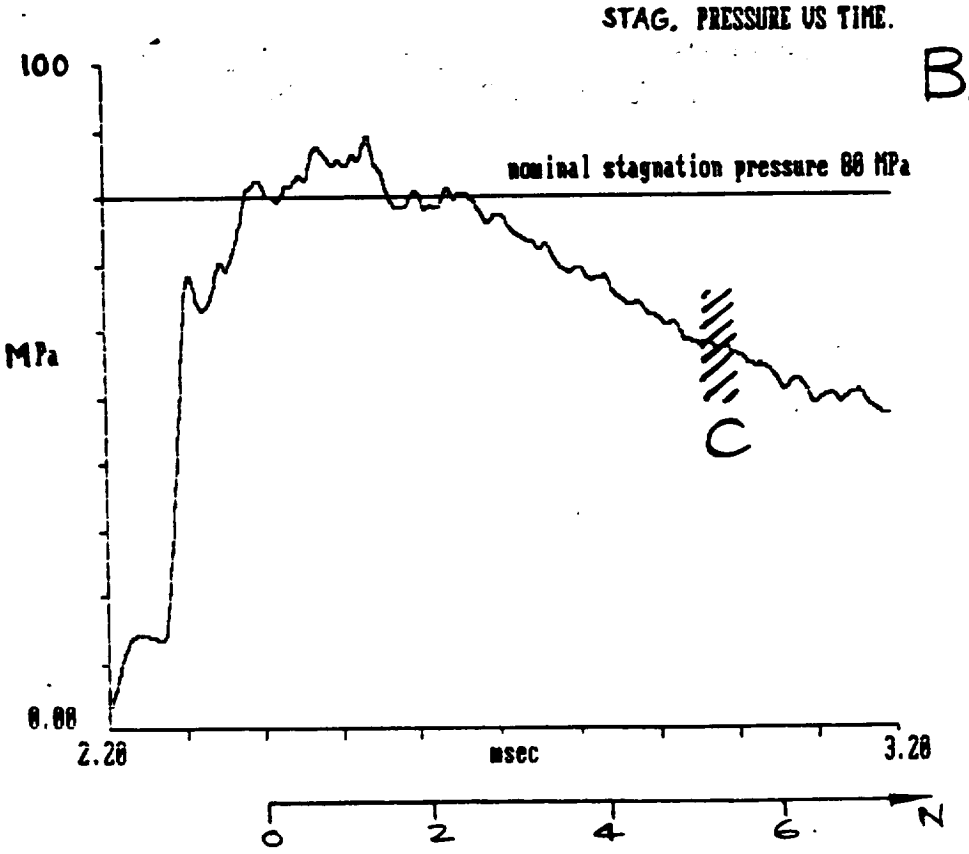

FIG. 1 DRIVER OPTIONS

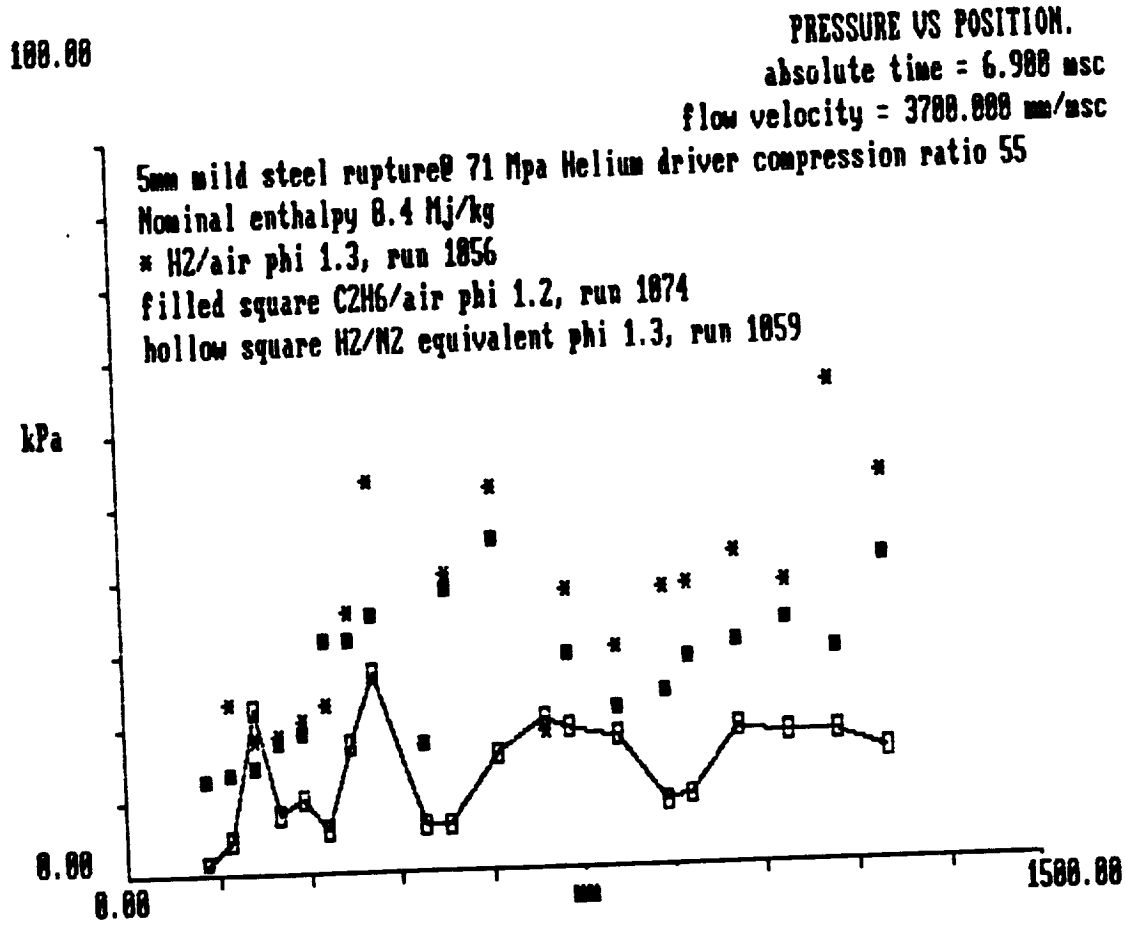

FIG. 2 HYPERSONIC COMBUSTION

(M = 5·5 , Stag. Press. = 67 ± 5 MPa.)

UNIVERSITY OF QUEENSLAND

Department of Mechanical Engineering

INVESTIGATION OF FLOW CHARACTERISTICS IN TQ EXPANSION TUBE

NASA Report 1990

Andrew Neely

In the early part of 1989 the work on the analytical predictions of test gas flow conditions for an ideal dissociating gas and an ionizing gas in an expansion tube was continued. The work continued to the point where the simulation was shown to work for low enthalpy flows but was still having problems with the high enthalpy flows.

The program is driven by the input of the initial fill pressures in the shock tube and the acceleration tube and the measured shock speeds in the shock and acceleration tubes. The calculation process is set out in flow chart form in FIGURES 1 & 2 . The governing equations for the flow processes were set out in last year's report.

Initial calculations with the program using the expected end velocity from 1 - D perfect gas calculations returned a negative value of α_{final} indicating that full recombination had occurred during the expansion process. Substitution of $\alpha = 0$ into the velocity expression confirms this. That is it confirms that ionisation will fall to approximately 0 before the expansion process is complete and the end conditions are reached. The point where this occurs is designated the point of transition.

It is necessary to find this transition point, but as the exact isentropic relation fails for a zero level of ionisation it is required to find the finite but very small level of ionisation which when reached during the expansion can nolonger contribute to the flow energy.

This transition level is found by varying α_{final} and observing its effect on the final Test Gas pressure P_T. This pressure can be found by relating the gas flow conditions through the unsteady expansion from the secondary diaphragm but also by relating conditions back across the secondary shock. This is possible because by physical constraints the pressures on either side of the acceleration gas/test gas interface must be equal. The test gas velocity is similarly constrained to the velocity of the acceleration gas behind the secondary shock.

The relations used to find P_4 and U_4 are

$$P_4 = P_3 \left(\frac{2\gamma M^2}{\gamma+1} - \frac{\gamma-1}{\gamma+1} \right)$$

$$U_4 = \frac{U_4}{A_3} A_3$$

where $$\frac{U_4}{A_3} = M_3 - M_4 \sqrt{\frac{T_4}{T_3}}$$

$$M_4 = \left(\left(1 + \frac{\gamma-1}{2 M_3^2} \right) / \left(\gamma M_3^2 - \frac{\gamma-1}{2} \right) \right) \frac{1}{2}$$

$$\frac{T_4}{T_3} = \left(\gamma M_3^2 - \frac{\gamma-1}{2} \right) \left(1 + \frac{\gamma-1}{2 M_3^2} \right) / \frac{(\gamma+1)^2}{4 M_3^2}$$

The expansion process is thus divided into two stages. A real gas model is used to relate from the beginning of the acceleration tube through the unsteady expansion to the transition point at which the level of ionisation has reached a final negligible level, then a simple perfect gas model is used to relate through to the end of the tube. Since the gas at this stage can be considered to be behaving in an ideal manner, using the shock speed and the quiescent acceleration gas pressure the conditions behind the secondary shock can be found using 1-D shock relations.

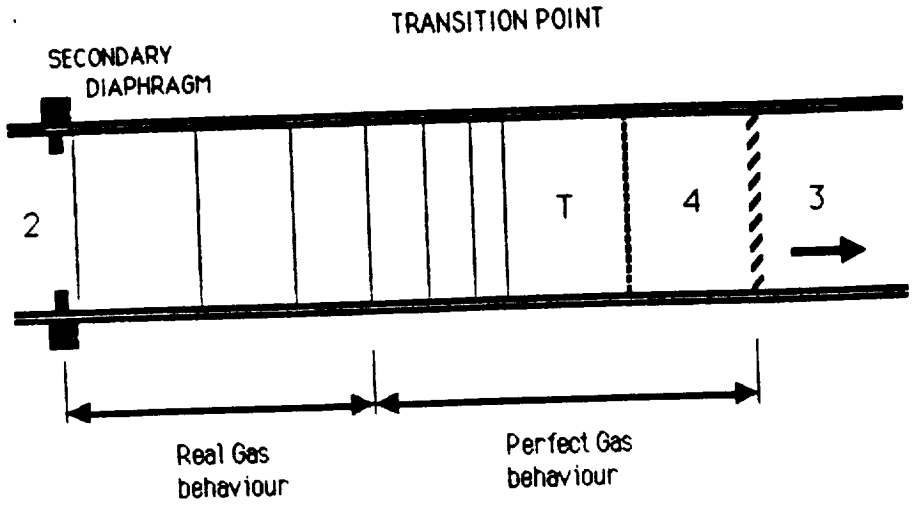

These relations give values of velocity and pressure in the region behind the secondary shock, i.e. U_4 and P_4. By physical constraint these are known to be equal to the velocity and pressure of the test gas that lies behind the secondary contact surface.

In the case of Dissociating gas the same technique that was used in the ionisation case is followed. This is because once again it is observed that when the level of dissociation is set to zero the resulting velocity does not correspond with the known test conditions, it is too low. The flow process is divided into real and ideal gas stages, with the change occurring at the transition point.

The equations are set up and the value of the final level of dissociation is adjusted until the test gas pressure P_T matches the acceleration gas pressure P_4 at the gas interface, giving the end flow conditions.

These two models allow the prediction of the flow conditions of the test gas at the end of the acceleration tube given the initial fill pressures and the observed shock velocities. The models assume that an equilibrium flow process is occuring.

A comparison of the measured and predicted flow conditions for a low enthalpy dissociation shot using Argon driver gas are as follow

AIRTESTGAS	MEASURED	PREDICTED
ACCELERATIONTUBE		
Shock Velocity (m/s)	4000	———
TEST FLOW		
Dissociation Fraction		0.00034
Static Pressure (Pa)	5158	5170
Pitot Pressure (kPa)	230	194
Density (kg/m^3)		0.0197
Temperature (K)		912

While the agreement has been good for low enthalpy test conditions , as yet the program has not been able to match static pressures for the high enthalpy shots The program is being modified to account for the likelyhood that total recombination does not occur for these conditions.

To assist in the calibration of the simulation programs an adapter section with a static pressure probe was added to the end of the acceleration tube. This transducer allowed the measurement of the static pressure for the duration of the flow process providing further evidence of the steady state of the test flow as shown by the flat traces. (FIGURE 3)

It was also proposed to use the laser interferometer originally set up by Dr T. Posillico at the beginning of 1989, to measure the density changes in the flow and thus determine the free stream density of the test gas.

The laser interferometer (FIGURE 5) passes two parallel beams from the same source through the test section. One beam passes through the test flow exiting the end of the acceleration tube while the other does not. The beams are optically recombined and made to interfere on a light detecting diode. The change in intensity of the combined beam can then be related to the change in density of the test flow.

The system works on an infinite fringe pattern where

Fringe shift $N = \beta \frac{L}{\lambda} \left(\frac{\rho_2 - \rho_1}{\rho_S} \right)$ (Liepman & Roshko)

where L = length of flight across the test section which in this case is the width of the jet of gas exiting the tube. approx 32 mm

λ = wavelength of the light source i.e. the He - Ne laser 632.8 nm

ρ_S = density of gas at standard temperature and pressure.

ρ_1 = initial density of acceleration gas

ρ_2 = density of gas behind the shock

The laser interferometer was shown to be able to detect the arrival of a shock and qualitatively show the density change in the flow (FIGURE 4). The problem came when it was attempted to quantify the density change observed. The diode light detector outputs a voltage proportional to the intensity of the interfering beams. For an infinite fringe pattern the intensity varies sinusoidally with fringe shift.

$$\text{i.e. Intensity} = a + b \sin (N + \theta)$$

Hence to calibrate the interferometer the starting point must be known and the maximum full scale change in intensity must be determined. The only way to determine these constants is to calibrate the system with a known density change. The electronics will only respond to a very high speed change of the order of time scale associated with flow in the tunnel.

The tunnel was fired in shock tube mode in a series of tests to provide known high speed density changes , but it still proved inadequate to determine the required constants. It was decided that calibration of the system is impractical in terms of time and effort at this time but if an accurate and simple method of calibration could be found then the laser interferometer would be a useful non-intrusive diagnostic tool.

SUMMARY OF SOLUTION METHOD

FIGURE 1 SHOCK TUBE SECTION

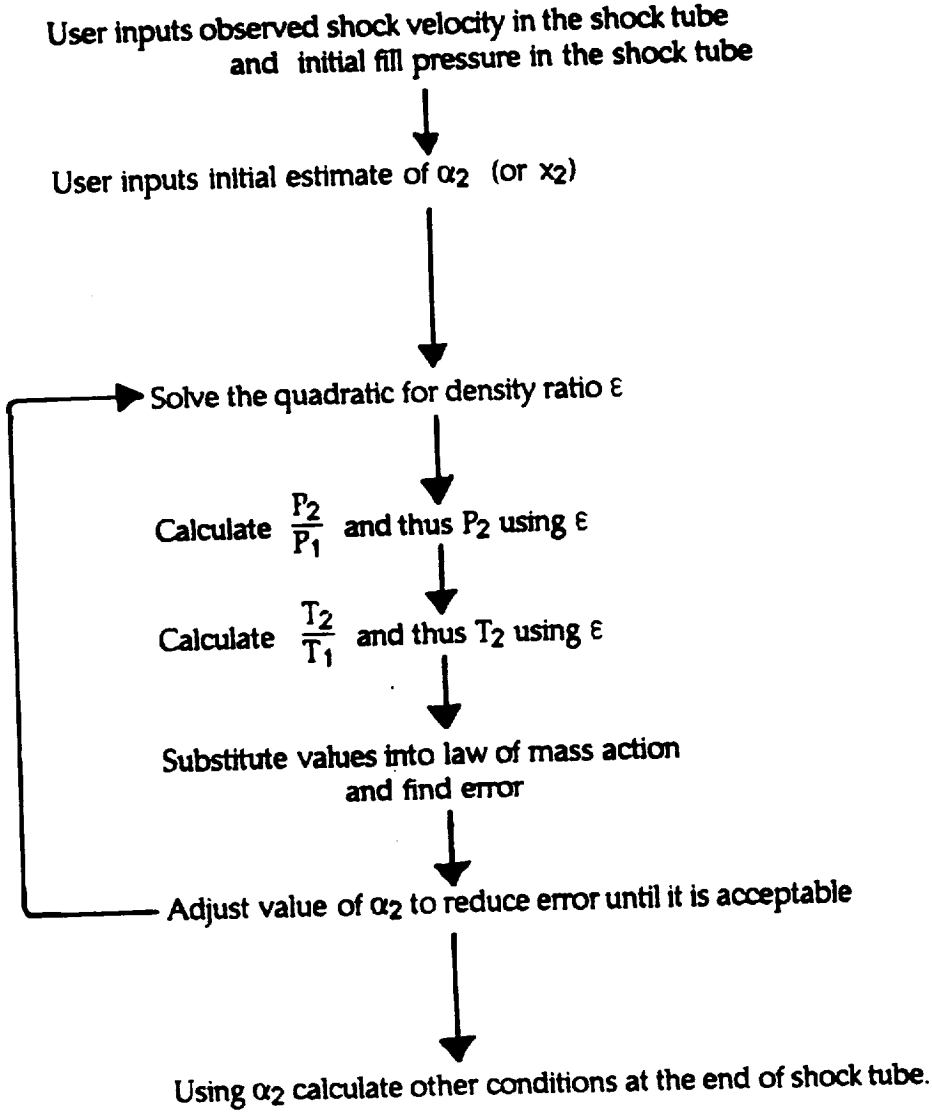

FIGURE 2 ACCELERATIONTUBESECTION

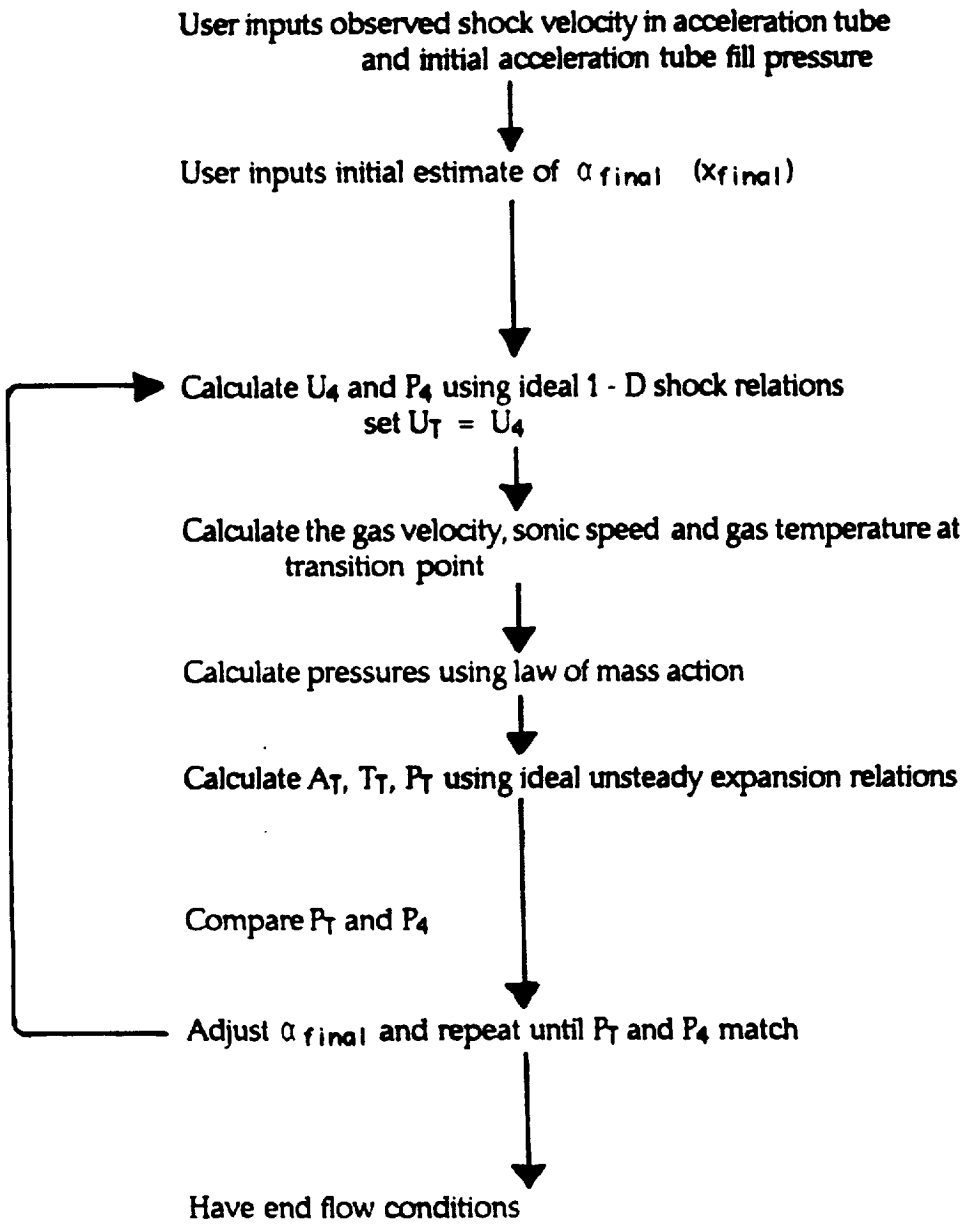

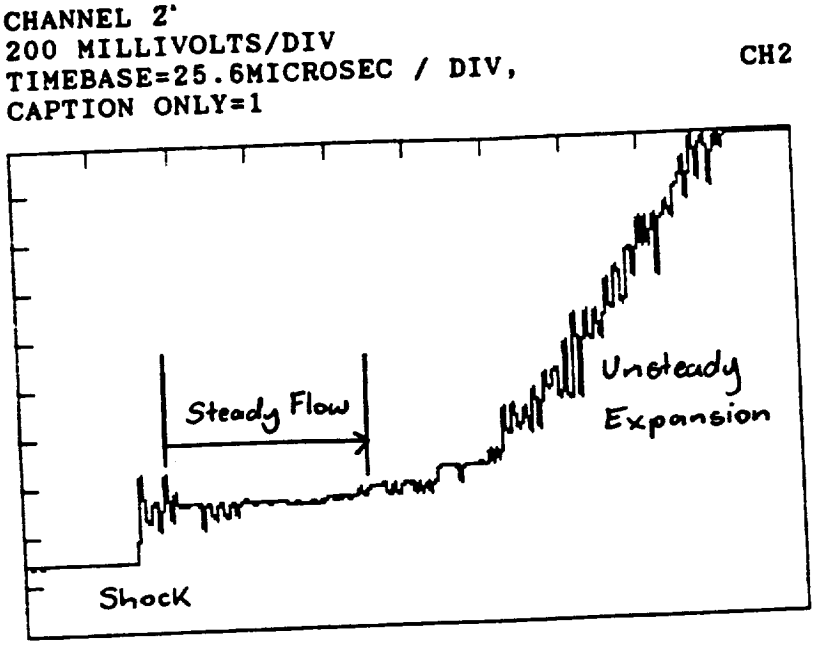

FIGURE 3: Static Pressure Trace of Flow At Exit of Acceleration Tube

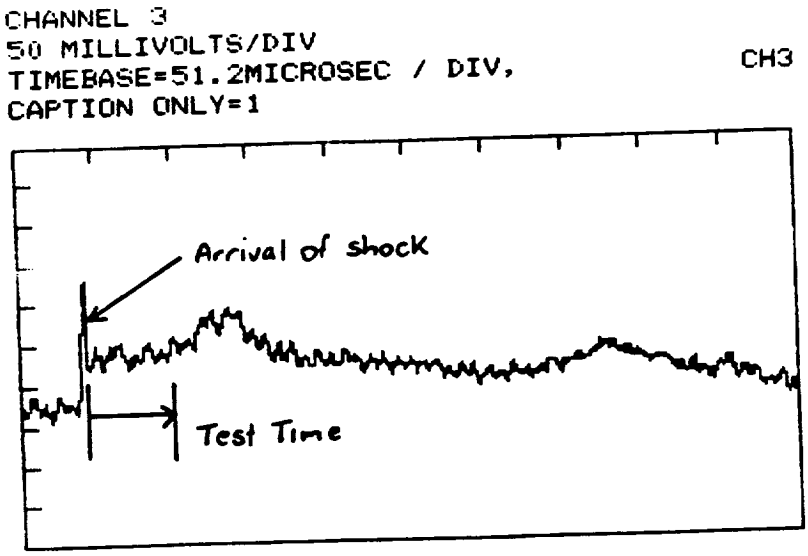

FIGURE 4: Laser Interferometer Trace

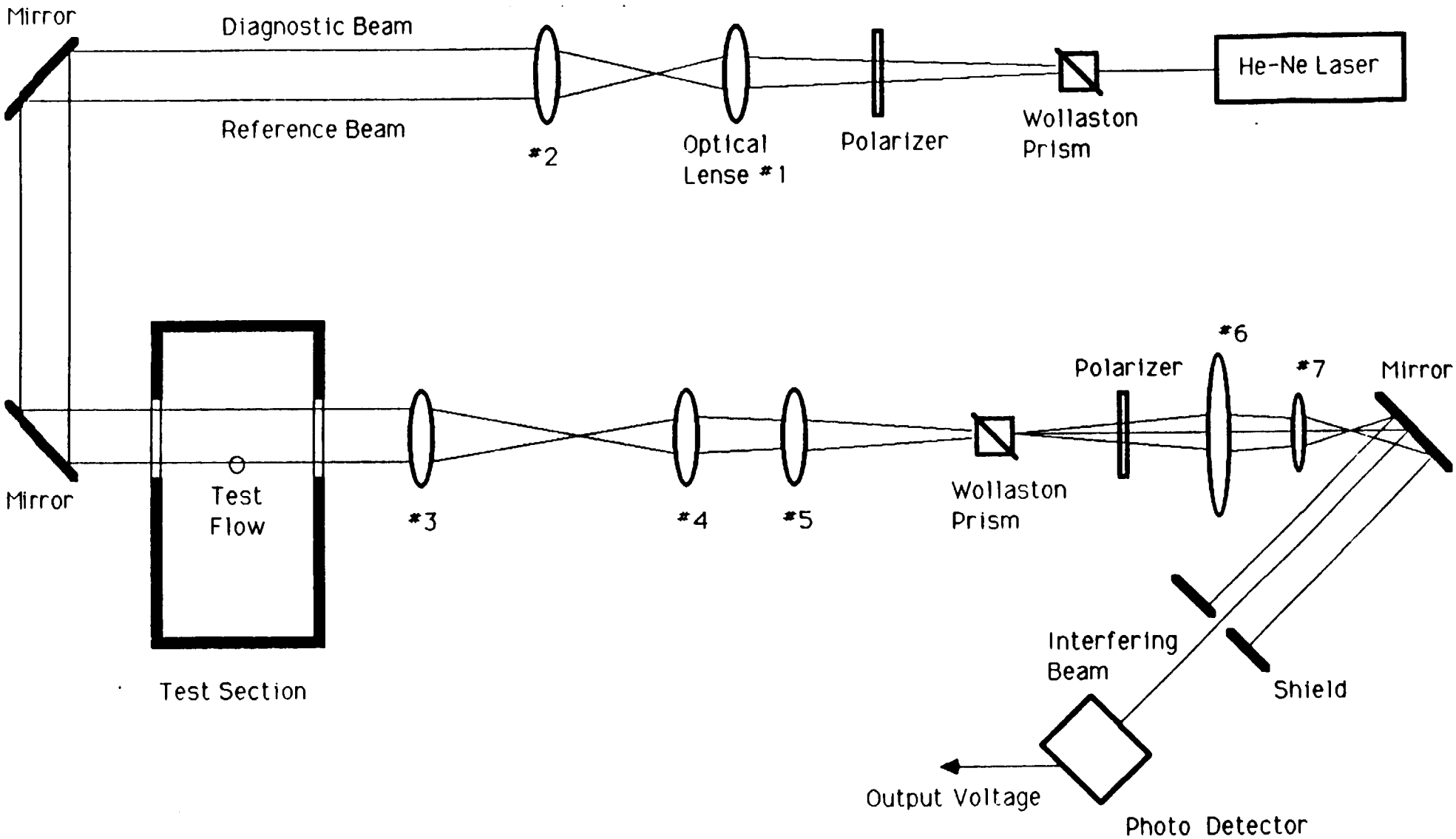

FIGURE 6 : Layout of Infinite Fringe Laser Interferometer

DISTURBANCES IN THE DRIVER GAS OF A SHOCK TUBE

A. Paull and R. J. Stalker

Mechanical Engineering Department
University of Queensland

1. Introduction

It has been observed (Stalker) that expansion tube test times are limited at low enthalpies by large regular disturbances which disrupt the centreline pitot pressure. Previously, these disturbances have been attributed to bubbles which are mixtures of driver and test gases and which are less dense than the test gas. However, laser interforometry experiments (Possilico) which measured test gas density at the expansion tube exit detected a much smaller density change than was expected for a large bubble. This indicates that either, the bubbles are elongated in the flow direction or, more fundamentally, the bubbles do not cause these disturbances. In this report it will be assumed that the latter is correct and an alternative theory which is based on longitudinal and lateral waves is developed which is expected to explain the structure of the pitot pressure disturbances.

It has been observed that similar disturbances exist in the test and driver gases following a shock in a shock tube. It is believed that a model for these disturbances could be used to determine test time limitations in the more complex flows of an expansion tube. There are advantages of analyzing shock tube flows rather than the flow from an expansion tube. The primary advantage is that shock tube flows are not accelerated by the unsteady expansion centred at the secondary diaphragm of an expansion tube. This reduces the complexity of the flow history and thus reduces the possibility of additional unknowns distorting the fundamental problem.

This report describes the disturbances which are observed in the driver gas of a shock tube.

2. Experimental Description

This report centres on a series of tests in which the exit wall pressure and centreline pitot pressure where measured in a shock tube (see figure 1). The shock tube was 5.435 m long and has an inside diameter of 38 mm. A free

piston driver was used to heat the driver gas.

Throughout the experiments the driver conditions remained the same. The filling pressure of the reservoir behind the piston was 3.4 MPa and the compression tube was filled with helium to 130 kPa. The helium driver gas was compressed to rupture a 1mm cold rolled mild steel diaphragm at nominally 34.5 Mpa.

Shock speeds were varied between 2.4 km/s and 6 km/s by altering the shock tube filling pressure between 320 mm $_{Hg.}^{\wedge}$ and 5 mm $_{Hg.}^{\wedge}$ respectively. The shock tube and dump tank were filled with undried air extruded from the atmosphere. Shock speeds were measured with ionization gauges stationed at five locations as shown in figure 1.

Wall pressure was measured 15 mm from the shock tube exit and the pitot probe leading edge was positioned centrally approximately 5mm from the shock tube exit. The pitot design is shown in figure 2. For all experiments each analog signal was sampled every microsecond.

3. Results and Observations

Figure 3 displays the pitot pressure as a function of time measured for different shock speeds. Figure 4 displays the corresponding wall pressure records and table 1 displays the shock speeds calculated from the time delay between excitation of neighbouring ionization gauges. A typical record from the ionization gauges is shown in figure 7. The predicted driver-test gas interface location is displayed in figures 3 and 4. This prediction was made using turbulent boundary layer entrainment theory (Mirel). The shock speeds where assumed to be that observed between the two ionization gauges closest to the diaphragm.

Verification of the repetitiveness of these results is given in figures 5 and 6 where the the shock tube filling pressures of 5, 10 and 20 mm were repeated. In these experiments a more sensitive wall pressure gauge was used. In can be seen that the results from these series of experiments are in reasonable agreement with each other.

Three features of the unsteady nature of each pair of wall and pitot traces should be observed.

(i) A sharp dip is sometimes observed in the pitot pressure in the vicinity of the interface.

(ii) At the higher shock speeds the pitot pressure mean does not follow the wall pressure mean.

(iii) The pitot pressure has well defined oscillations superimposed on its mean, but the oscillations in the wall pressure are not as pronounced.

The third feature is believed to be a fluid mechanical feature and is not the result of stress waves in the pitot probe. This was verified with an experiment in which the tapping to the pitot pressure transducer was blocked. Virtually no vibrational noise is detected from the pitot pressure transducer.

3.1. The interface

The predicted interface lies close to the dip or a point where the nature of the pitot pressure traces changes. It will be seen from the theoretical results discussed later that in addition to a mean pitot pressure change due to the difference between the driver and test gas densities, there will also be a change in the frequency and amplitude of the oscillations across the interface. This information has been used and the most likely interface positions are shown in figures 3-6. Ideally to the left and right of the interface the gases are air and helium respectively.

3.2. The mean trend

From figure 4 it can be seen for a shock tube filling pressure (P_s) of 5 mm that after the observed driver-test gas interface the wall pressure rises steadily. The gradient of this rise becomes less as P_s is increased until P_s = 80mm where there is no rise. If P_s is greater than 80 mm the wall pressure falls.

Not every aspect of this trend is seen in the pitot pressure record. For P_s= 5mm, the pitot pressure rises rapidly after the interface and then rises slowly (if at all) for the remainder of the trace. This trend is repeated for P_s= 10mm and 20mm with the rise in pitot pressure being less dramatic as the shock tube filling pressured is increased. An interesting result occurs at P_s= 40mm. At this filling pressure, after the interface, the pitot pressure falls as the wall pressure rises.

It can be seen that the long term overall trend is for the pitot pressure to have a lesser gradient than the wall pressure.

3.3. Oscillation features

Oscillations can not be seen in the wall pressure traces of figure 4 at the higher shock speeds. It is only when the disturbances are extreme at the lower shock speeds that oscillations appear in the wall pressure. This is partially due to the insensitivity of the gauge used. In figure 6 where the sensitivity of the wall pressure gauge was approximately twenty five greater than that used for figure 4 it can be seen that high frequency oscillations

do exist at the higher shock speeds, however, these oscillations are still small compared with those observed in the pitot pressure.
The oscillation frequency increases with shock speed and at the three highest shock speeds the high frequency oscillations are superimposed on a much lower frequency disturbance which has a period of approximately 250 μs.

4. Theoretical Results

In this section a model based on longitudinal and lateral acoustic waves is developed which is consistent with the oscillatory nature of the flow. In addition, it is shown that identification of the compression following the dip with an unsteady expansion travelling upstream can explain the different trends observed between the pitot and wall pressure records.

4.1. Acoustic waves

Acoustic disturbances are those in which the sound speed remains constant to first order. If the velocity and pressure are perturbed about a mean value then it can be shown (Whitham) that to first order there exists a potential ϕ for which

$$\underline{u}^{\bullet} = \nabla\phi \tag{4.1}$$

$$P = P_0 - \rho_0 \frac{\partial\phi}{\partial t} \tag{4.2}$$

$$\rho = \rho_0 - \rho_0 c^{-2} \frac{\partial\phi}{\partial t} \tag{4.3}$$

$$c^2 = P'(\rho_0) = \gamma \frac{P_0}{\rho_0} \tag{4.4}$$

where $\gamma, u^{\bullet}, P, \rho$ c and t are the specific heat ratio, velocity, pressure, density, sound speed and time respectively and subscripts "o" refer to the condition which is being perturbed. The spatial origin is stationary with respect to the mean flow so that the unperturbed velocity is zero. From conservation of mass and momentum it can be shown that ϕ obeys the wave equation

$$\frac{\partial^2\phi}{\partial t^2} = c^2 \nabla^2\phi \tag{4.5}$$

If a change of origin is made and is fixed with respect to the shock tube

then (4.1) is rewritten as

$$\underline{u} = \underline{u}_0 + \nabla\phi. \tag{4.6}$$

From (4.2), (4.4) and (4.6) and the Rayleigh Pitot pressure formula it can be shown to first order in the derivatives of ϕ that for supersonic flows the pitot pressure is

$$\mathcal{P} = \mathcal{P}_0\left(1 - \frac{1}{c^2}\frac{\partial\phi}{\partial t} + \left(\frac{2\gamma(2M_0^2-1)}{u_0(2\gamma M_0^2-\gamma+1)}\right)\frac{\partial\phi}{\partial z}\right) \tag{4.7}$$

where the positive z-direction is in the unperturbed flow direction ($u = \frac{\partial\phi}{\partial z}$). The term containing the derivative with respect to time is the contribution due to pressure fluctuations and the term containing the derivative with respect to z is the contribution to to velocity fluctuations.

4.2. Wave equation solutions

In this section solutions of the wave equation which have the properties observed in the experimental results are obtained. It will be assumed that the shock tube is cylindrical with an inside diameter of 2a. Let (z,r,θ) be cylindrical polar co-ordinates fixed in a frame of reference in which the unperturbed gas is at rest. At the shock tube wall it is assumed that there is slip but no penetration so that

$$\frac{\partial\phi}{\partial r}(z,a,\theta,t) = 0. \tag{4.8}$$

Solutions of the wave equation obtained by separation in the z,r,θ and t variables and which are single valued, periodic in time and finite at r=0 have the form

$$\phi = J_m(\lambda_n r)\, e^{i(\omega t \pm \beta_n Z \pm m\theta)} \tag{4.9}$$

where m and n are integers,

$$\beta_n = \left(\left(\frac{\omega}{c}\right)^2 - \lambda_n^2\right)^{\frac{1}{2}} \tag{4.10}$$

and J_m is an m th. order Bessel function of the first kind. If the boundary condition (4.8) is imposed on (4.9) then this requires that

$$J_m'(\lambda_n a) = 0. \qquad (4.11)$$

Hence, $\lambda_n a$ is the n th. root of (4.11).

Any mode or any combination of modes given by different values of m and n may exist, however the properties of most of these modes will not fit the properties observed in figures 3-6. For example, if m≠0 then the m th. order Bessel is zero at r=0, however, experimental results show that the centreline pitot pressure is not less, but considerably larger than the wall pressure. The only solutions of the form (4.9) with this property are the zero th order (m=0) Bessel function solutions. The zero th order Bessel function has its largest maxima at r=0 (figure 8) and oscillates to zero as r approaches infinity. If it is therefore assumed that the required solutions have m=0 then as $-J_1$ is equal to the derivative of J_0 it follows that $\lambda_n = Z_n/a$, where Z_n is the n th zero of J_1 which are available from tables (Abramowitz).

If n=0 then λ is zero (as Z_0 is zero) and solutions are strictly dependent on z and time. Solutions of this form will be referred to as longitudinal waves. In contrast to the zero th order mode all other solutions have a radial dependence and thus will be referred to as lateral waves. A first order lateral wave has n=1 and $\lambda_n = 3.83/a$. Pressure contours of this mode in the (z,r) space are plotted in figure 9. Higher order lateral waves may also occur, however, at this stage studies will be restricted to the first order lateral waves and the longitudinal waves on the grounds that more energy will be needed to excite higher order modes and therefore the lower order modes would be excited first.

4.3 Pitot pressures of longitudinal and lateral waves.

From (4.7) it can be seen that if a disturbance is travelling in the flow direction ($\phi=\phi(z-ct)$) the velocity fluctuations enhance the pressure fluctuations to give a larger percentage fluctuation in pitot pressure than would be seen in the wall pressure. If the disturbance travels upstream the effect on pitot pressure due to pressure fluctuations is decreased by the velocity fluctuations.

If the peak centreline pressure fluctuation is P_1 then from (4.2) and (4.9) along the centreline

$$\phi = -i \frac{P_1}{\rho_0 \omega} e^{i(\omega t \pm \beta_n Z)} \qquad (4.12)$$

Hence, the magnitude of the centreline pitot pressure fluctuation is

$$\mathcal{P}_0 \frac{P_1}{P_0} \left(\gamma \mp \frac{2(2M^2 - 1)}{M\left(2\gamma M^2 - \gamma + 1\right)} B_n \right) \tag{4.13}$$

where the Mach number $M = U_0/c$ and

$$B_n = \left(1 - \left(\frac{\lambda_n c}{\omega} \right)^2 \right)^{\frac{1}{2}} = \beta_n c/\omega. \tag{4.14}$$

If γ=1.667 then the coefficient

$$\frac{2(2M^2 - 1)}{M\left(2\gamma M^2 - \gamma + 1\right)} \tag{4.15}$$

is equal to one for M = 1.8. In the case of a longitudinal wave B_0 is equal to one, hence, since in the experiments described here the driver gas Mach number is less than three the contribution from longitudinal wave velocity fluctuations to the pitot pressure fluctuations is comparable to that from the static pressure variations. If a longitudinal wave is travelling in the flow direction then the terms bracketed in 4.13 will add and the pitot pressure fluctuation will be approximately double the static pressure fluctuation. If a longitudinal wave travels upstream then the bracketed terms will subtract, hence, it will be difficult to detect in the pitot pressure.

In the case of a lateral wave less precise statements can be made due to the variation of the dispersion term B_n with w/c. In general it can be said that if a longitudinal and lateral wave had the same amplitude then the pitot pressure fluctuation observed for a lateral wave travelling in the flow direction would be less than that of the longitudinal wave because B_n<1. Furthermore a lateral wave travelling upstream would produce a greater pitot pressure fluctuation than the longitudinal wave travelling upstream.

It can also be seen for constant Mach number that as the sound speed decreases a lateral wave will produce a greater fluctuation in the pitot pressure. This may be important in the application of acoustic wave theory to the flow in an expansion tube since a reduction in the sound speed across an expansion will tend to increase the relative importance of the lateral waves.

4.4. Doppler shifts

If the change of origin

$$x = ut + z \tag{4.16}$$

is made so that the origin of the (x,r,t) space is fixed with respect to the shock tube then the coefficient of the exponent in (4.9) with m=0 is

$$i\left(\left(\omega \mp u\beta_n\right)t \pm x\beta_n\right) \tag{4.17}$$

Hence, a Doppler shift occurs in the frequency due to the velocity of the gas. If a wave is travelling in the direction of the flow (the positive x-direction) then the frequency is increased to $\omega + u\beta_n$. However, if waves are travelling upstream then the frequency decreases to $\omega - u\beta_n$. It should be seen that if the velocity is sufficiently large so that $\omega - u\beta_n < 0$ then this wave would also represent a wave travelling in the positive x-direction. In the simple case of a longitudinal wave this would occur if u>c.

It should also be observed from (4.17) that the frequency shift is dependent upon sound speed. For a longitudinal wave the frequency shift is $\omega(1\pm u/c)$. Thus across an interface where the sound speed changes there would be a change in the period of the disturbance which is dependent upon the Mach number either side of the interface. A similar result is true for lateral waves, however, the frequency shift is dependent upon u, c, ω and a independently.

4.5. Reflection and transmition coefficients

If a wave travelling in the positive z-direction strikes an interface at which the sound speed and the specific heat ratio change then the reflection and transmition coefficients are obtained by requiring that the pressure and velocity be continuous across the interface. If an incoming longitudinal wave has unit amplitude then the transmitted and reflected waves have amplitudes of

$$\frac{2\gamma_1\beta_{n1}C_2^2}{\gamma_1\beta_{n2}C_2^2 + \gamma_2\beta_{n1}C_1^2} \tag{4.18}$$

and

$$\frac{\gamma_2\beta_{n1}C_1^2 - \gamma_1\beta_{n2}C_2^2}{\gamma_1\beta_{n2}C_2^2 + \gamma_2\beta_{n1}C_1^2} \tag{4.19}$$

respectively (n=0), where

$$\beta_{n1} = \left(\left(\frac{\omega}{c_1}\right)^2 - \lambda_n^2 \right)^{\frac{1}{2}} \qquad (4.20)$$

and subscripts 1 and 2 refer to the mediums which the incident and transmitted waves respectively traverse.

If the incident wave is a lateral wave then it is not possible to collectively satisfy continuity in the pressure, the longitudinal velocity component ($\partial\phi/\partial z$) and the lateral velocity component ($\partial\phi/\partial r$) across the interface. One of these restrictions has to be ignored. To be consistent with the wall boundary condition, slip at the interface will be tolerated. With this assumption the reflection and transmition coefficients will be the same as that for a longitudinal wave.

There is an additional point to consider for lateral wave transmition which does not arise with longitudinal waves. There is the possibility that the transmitted lateral wave can not be supported in the new medium. If region 1 supports a lateral wave then $\omega > C_1\lambda_n$, however if the sound speed in region 2 is sufficiently large so that $\omega < C_2\lambda_n$ then β_{n2} will be imaginary and thus the transmitted wave will decay exponentially.

4.6. Receding unsteady expansions

In this section the pitot pressure properties of a receding unsteady expansion are determined as a function of Mach number. From these properties it will be concluded (section 5) that the compression observed following the driver-test gas interface can be modeled as an unsteady expansion travelling upstream. The unsteady expansion is assumed to be a disturbance for which it is too large to ignore sound speed variations. Thus, the properties of one-dimensional isentropic inviscid flow are used.

Across an unsteady adiabatic expansion travelling upstream into an ideal inviscid isentropic gas the velocity and sound speed are related to the steady upstream condition (subscript o) by

$$u + \frac{2}{\gamma-1} c = u_0 + \frac{2}{\gamma-1} c_0 \qquad (4.21)$$

The wall pressure and sound speed are related by

$$P = P_0 \left(\frac{c}{c_0}\right)^{\frac{2\gamma}{\gamma-1}} . \qquad (4.22)$$

The Rayleigh pitot pressure formula written in terms of wall pressure and Mach number (M=u/c) is

$$\mathcal{P} = PM^2\left(\frac{\gamma+1}{2}\right)^{\frac{\gamma}{\gamma-1}}\left(\gamma - \frac{\gamma-1}{2}M^{-2}\right)^{\frac{-1}{\gamma-1}} \qquad (4.23)$$

From (4.21) the sound speed across an unsteady expansion may be written in terms of Mach number and thus from (4.22) and (4.23) the wall and thus the pitot pressure can also be written as functions of the Mach number.
By examining the derivative of the pitot pressure with respect to the Mach number it can be shown that

$$\frac{d\mathcal{P}}{dM} < 0 \quad ; \quad M > \frac{1+5^{\frac{1}{2}}}{2} \cong 1.62 \qquad (4.24)$$

and

$$\frac{d\mathcal{P}}{dM} > 0 \quad ; \quad 1 < M < \frac{1+5^{\frac{1}{2}}}{2} \qquad (4.25)$$

independent of specific heat ratio.
If an unsteady expansion is travelling upstream in a flow with Mach number greater than one then the wall pressure will rise and the Mach number will fall as the expansion is convected downstream past a fixed point on the tube and thus the expansion will appear as a compression. If the flow Mach number at the beginning of the compression is greater than 1.62 then since the Mach number is decreasing with time the pitot pressure will increase until the Mach number is 1.62. If the Mach number decreases further the wall pressure shall continue to increase but the pitot pressure wall fall.

5. Receding Unsteady Expansion Results

The following three observations show that the compression following the interface observed in the wall pressure measurements can be modeled as a receding unsteady expansion.

1. The expansion has a decreasing gradient as the flow Mach number upstream of the expansion decreases. This is consistent with an expansion travelling upstream. The expansion head travels upstream at a speed c_0 with respect to the flow and is convected downstream with a velocity u_0 and as the shock speed decreases u_0 decreases and c_0 increases thus the separation between the

expansion head and the interface will increase. If $u_0 = c_0$ then the expansion head is stationary with respect to the tube, so the observed compression would be very slight.

2. Table 2 lists the pitot pressure ($\mathcal{P}_0$) and wall pressure (P_0) which are measured at the expansion head at the four highest shock speeds. From these two quantities the flow Mach number (M_0) at the expansion head is determined using Rayleigh pitot pressure formula (4.23). The fifth column of Table 2 lists the wall pressure at the driver-test gas interface, which is assumed to be the trailing edge of the expansion. It is then assumed that the expansion is unsteady and the Mach number behind the interface (M_1) is determined using the relation

$$M_1 + \frac{2}{\gamma-1} = \left(M_0 + \frac{2}{\gamma-1} \right) \left(\frac{P_0}{P_1} \right)^{\frac{\gamma-1}{2\gamma}} \qquad (5.1)$$

which is obtained from the unsteady and adiabatic relationships (4.25) and (4.22) respectively.

Knowing M_1 and P_1 the pitot pressure behind the interface is determined with (4.23) and is tabulated in column 7. It can be seen that these values agree very well with those observed (column 4).

At lower shock speeds than those tabulated the agreement is not as good. However, the compression observed in the wall trace for P_s= 80mm has only a slight gradient which would indicate that the upstream Mach number is approaching one (and the Mach number is less for P_s>80mm), thus the Pitot probe may be outside the Mach cone in which case the above analysis is no longer valid. Theoretical ideal gas calculations indicate that the driver gas is at Mach 1 when the shock speed is approximately 3.3 km/s which is consistent with this deduction as this theoretical shock speed is only slightly less that that measured (see Table 1).

3. It was seen in the previous section that an unsteady expansion would produce a rise in both the pitot and wall pressures provided the Mach number is greater than 1.62 and the pitot pressure would fall as the wall pressure rose if the Mach number was less than 1.62 (and greater than one). It can be seen from figures 3 and 4 that this trend is observed, however, the turning point would appear to be approximately Mach 2 rather than Mach 1.62.

6. Spectral Distributions of Measured Disturbances

Fourier analysis have been used to study the frequency distributions of the pitot pressure disturbances in the driver gas. The frequency spectrums in

figure 10 where made using fast Fourier transform techniques over 256 points from data sampled at a rate of 1 MHz.

It can be seen that there is a definite band of frequencies different from zero at which the disturbance is dominate. The band width is a function of filling pressure. It can be seen that the Fourier decomposition of the repeat pitot pressures (figure 5) have similar forms. The decomposition has been taken over the time period in which the unsteady expansion was detected. It can be seen from 4.10 that for a given sound speed that the fundamental frequency of a lateral wave must be greater than $c\lambda_n$. All lateral waves with fundamental frequencies less than this will decay. It should be observed that there is not a non-zero lower bound on the fundamental frequency of a longitudinal wave since $\lambda_0=0$.

From Table 2 the Mach number immediately behind the interface (M_1) for P_s=5mm is 2.57. The shock speed measured (Table 1) was 5.82 km/s. Hence, for an ideal gas (γ=1.4) the gas speed would be 4.85 km/s. Therefore, the sound speed of the driver gas behind the interface would be 1.89 km/s. For a first order lateral wave (n=1) λ_1=201.6, hence, the fundamental frequency of a first order lateral wave must be greater than $380450/2\pi$=60550 Hz. From 4.17 because $\beta_n>0$ it then follows that in the laboratory frame of reference the frequency of a first order lateral wave travelling in the direction of the flow would also be greater than this frequency. Following the same arguments it can be shown that the frequency of a second order lateral wave travelling in the flow direction must be greater than 110980 Hz. It can be seen from the Fourier decompositions of figure 10 that a large number of the dominant frequency components are between the lowest observable frequencies of the first and second order lateral waves for P_s=5mm (Similar statements can be made for P_s=10mm and P_s=20mm). From this alone it can not be concluded that these disturbances are lateral waves because longitudinal waves can exist at any frequency.

However, the dominance of the lateral wave would be consistent with the reduced amplitudes observed in the wall pressure disturbances. The Bessel function $J_0(\lambda_1 a) \cong 0.4\ J_0(0)$, thus the static pressure along the wall is 0.4 that of the centreline static pressure. This enhances the increase in pitot pressure fluctuations which results from the contributing velocity component from a disturbance travelling in the flow direction (section 4).

Furthermore the dominance of lateral waves is also consistent with Possilico's interforometry results which did not detect a large variation in the integrated density across the test gas. In a lateral wave the density variation is both positive and negative across the test section and thus the

integrated density would be reduced. It can be shown that

$$\frac{\int_0^a J_0(\lambda r)dr}{\int_0^a dr} = \frac{1.08}{3.83} \cong \frac{1}{4} \qquad (6.1)$$

so that the fringe shift which would be observed in a lateral wave would be approximately one quarter of that for a longitudinal wave.
Hence, it can be concluded that many of the properties of the disturbances which could not be explained through the existence of longitudinal waves can be understood if the disturbances are lateral waves.

7. Hypulse Results

The G.A.S.L Hypulse facility has made one run (run no. 1) in which it was a shock tube. The test gas was air, the driver gas was helium, the filling pressures of the driver and shock tubes where 11 MPa and 8.5 mm respectively. The inside diameter of the Hypulse facility is 152.4 mm. The average shock speed was approximately 2.5 km/s. It can be seen from figure 11 that disturbances similar to those observed in the University of Queensland TQ facility are also observed in the Hypulse facility.
A further observation can be made from the Hypulse facility which could not be made in TQ. Due to the larger diameter of Hypulse seven pitot pressure measurements could be made concurrently across the flow. These are displayed in figure 11. It can be seen that the amplitude is the greatest at the centre which is consistent with lateral waves.

8. Conclusions

1. An compression is observed in the driver gas which starts immediately behind the driver-test gas interface. This compression can be modelled as an unsteady expansion travelling upstream.
2. First order lateral waves (n=1) would appear to be the dominate oscillitory disturbance which exist in the driver gas.

9. Bibliography

Abramowitz, M. and Stegun, A. Handbook of Mathematical Functions with Formulas, Graphs, and Mathematical Tables. National Bureau ofStandards. Applied Mathematics Series 55.

Possilico, T. personal communication.

Stalker, R.J. Paull, A. and Stringer, I. Experiments on an expansion tube with a free piston driver -Mech. Eng U.Q. report 13/88

Whitham, G.B. Linear and nonlinear waves. Wiley N.Y 1974.

TABLE 1.

SHOCK TUBE FILLING PRESSURE (mm)	320	160	80	40	20	10	5
SHOCK SPEED BETWEEN GAUGES (km/s)							
1 AND 2	-	-	4.65	5.06	5.44	5.72	6.19
2 AND 3	-	3.48	4.15	4.69	5.17	5.76	6.13
3 AND 4	2.39	3.10	3.60	4.19	4.82	5.50	5.97
4 AND 5	2.12	2.69	3.18	3.79	4.41	5.27	5.82

TABLE 2.

P_s mm	$\mathcal{P}_0$ kPa	P_0 kPa	M_0	$\mathcal{P}_{1meas}$ kPa	P_1 kPa	M_1	$\mathcal{P}_{1calc}$ kPa
5	3350	500	2.05	2950	300	2.57	3070
10	3150	550	1.89	2880	350	2.35	2980
20	3350	670	1.75	3690	460	2.13	3240
40	3880	830	1.69	4550	560	2.07	3800

FIGURE 2. PITOT PROBE DESIGN.

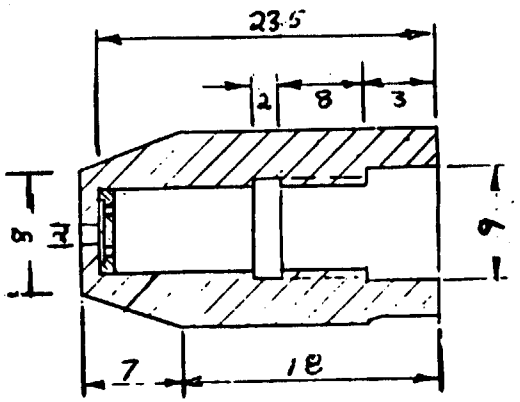

Scale 2:1

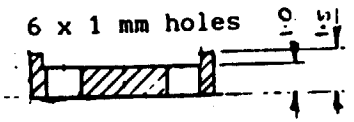

Scale 4:1

ALL MEASUREMENTS IN MILLIMETRES.

x ionization gauge

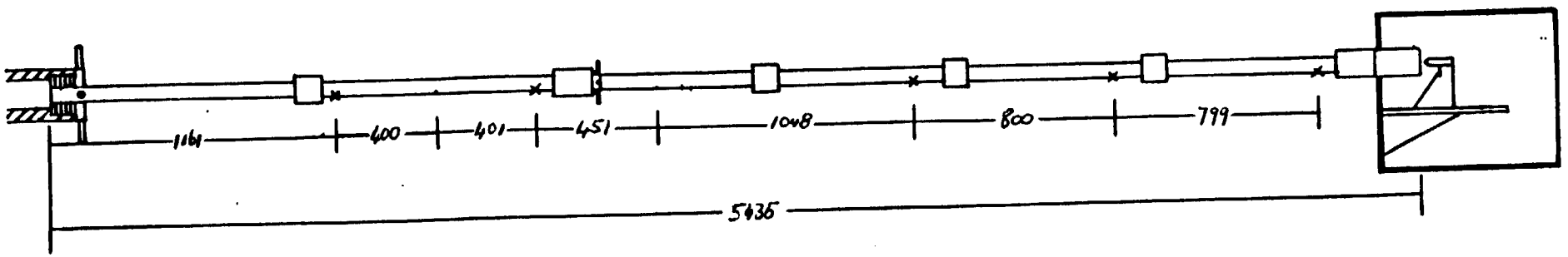

FIGURE 1. SHOCK TUBE AND TEST SECTION.

TI Theoretical interface based on average shock speeds
MI Most likely interface position

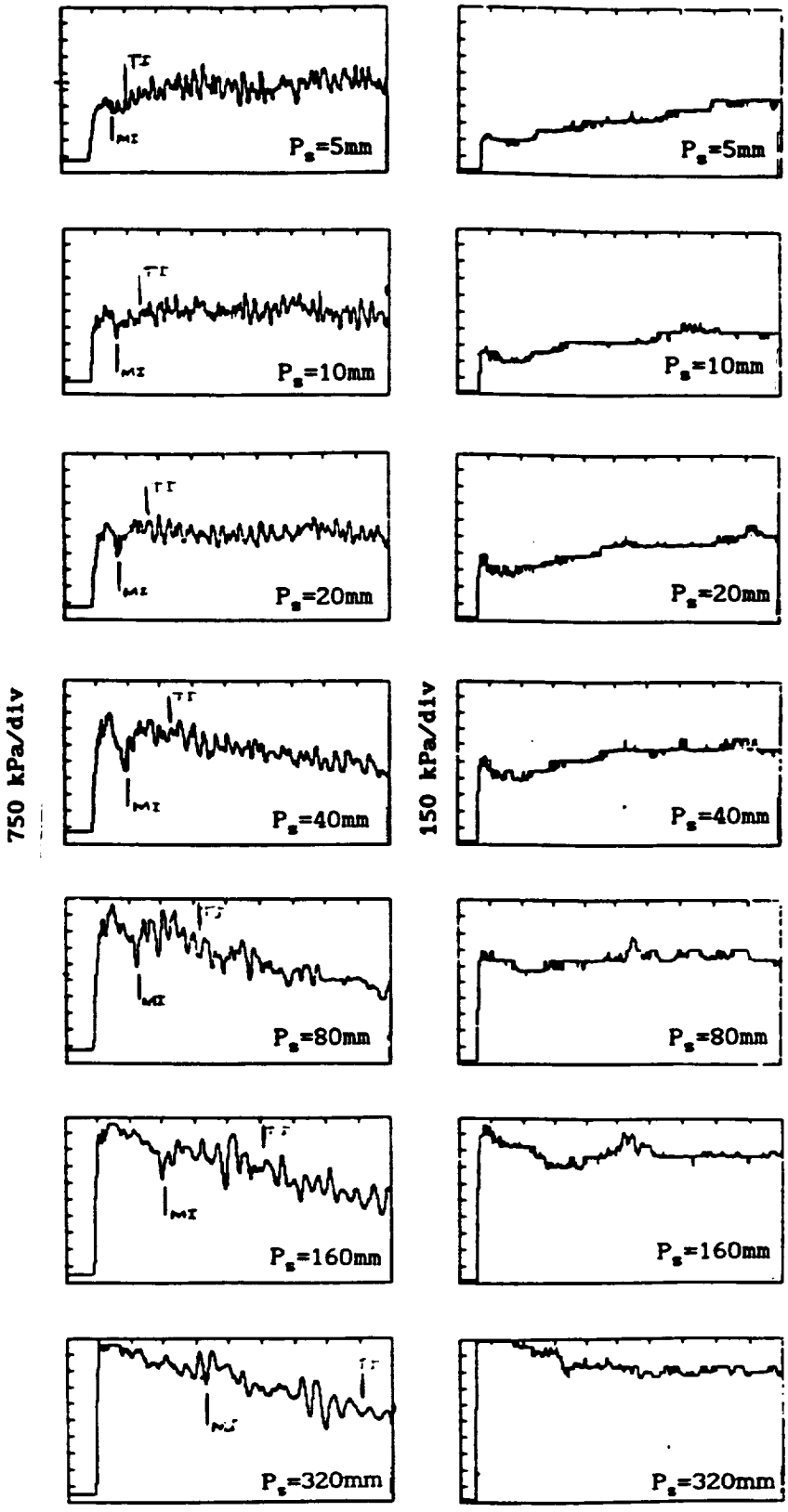

FIGURE 3.
PITOT PRESSURE AS A FUNCTION OF TIME FOR DIFFERENT SHOCK TUBE FILLING PRESSURES.

FIGURE 4.
WALL PRESSURE AS A FUNCTION OF TIME FOR DIFFERENT SHOCK TUBE FILLING PRESSURES.

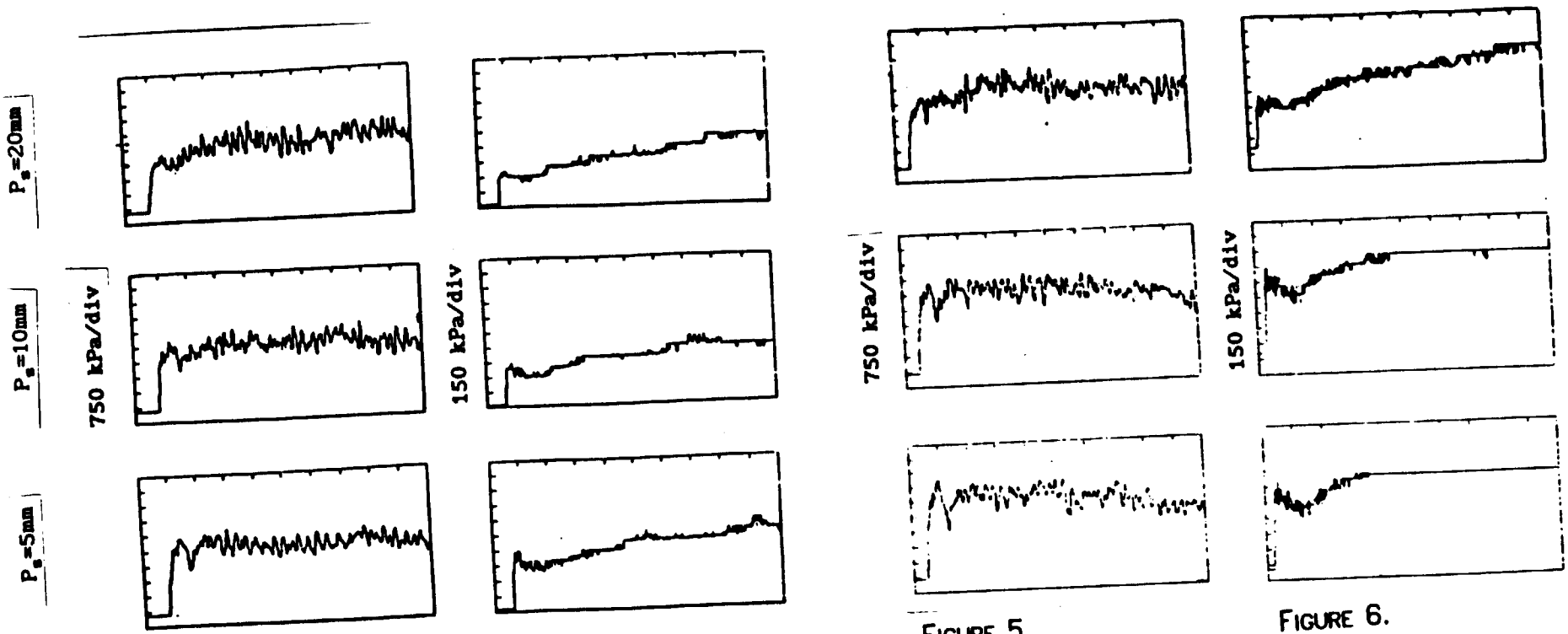

FIGURE 3
PITOT PRESSURE

FIGURE 4
WALL PRESSURE

FIGURE 5.
PITOT PRESSURE

FIGURE 6.
WALL PRESSURE

FIGURES 5 AND 6. COMPARISON OF PITOT AND WALL PRESSURES BETWEEN

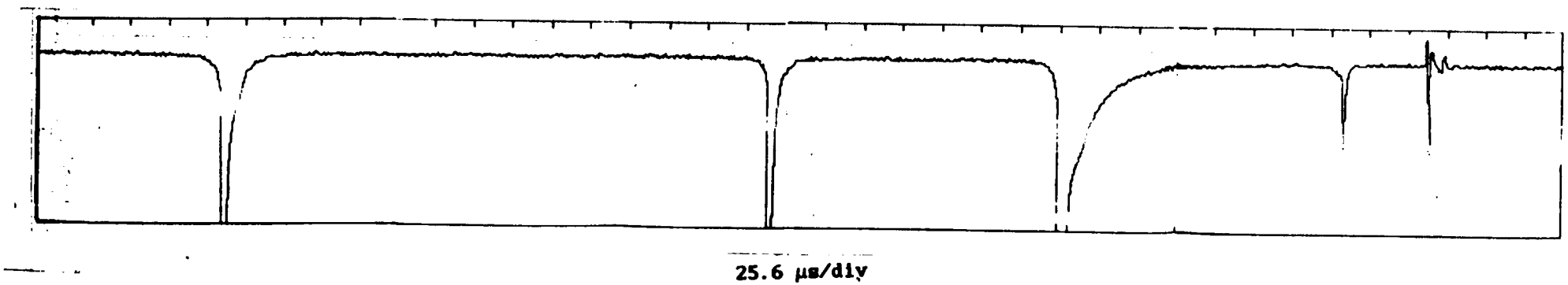

FIGURE 7. IONIZATION GAUGES RECORD.

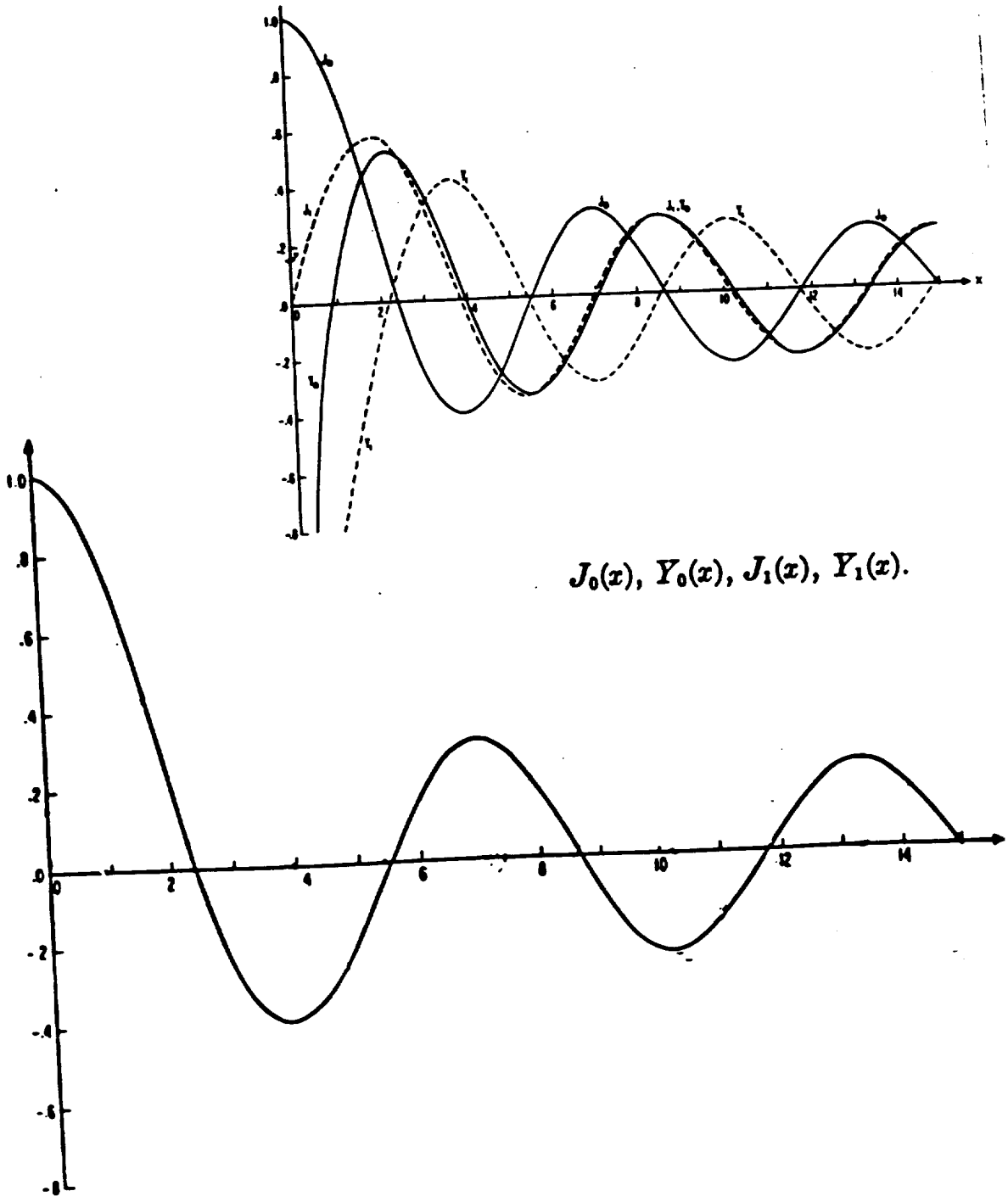

FIGURE 8. ZEROTH ORDER BESSEL FUNCTION.

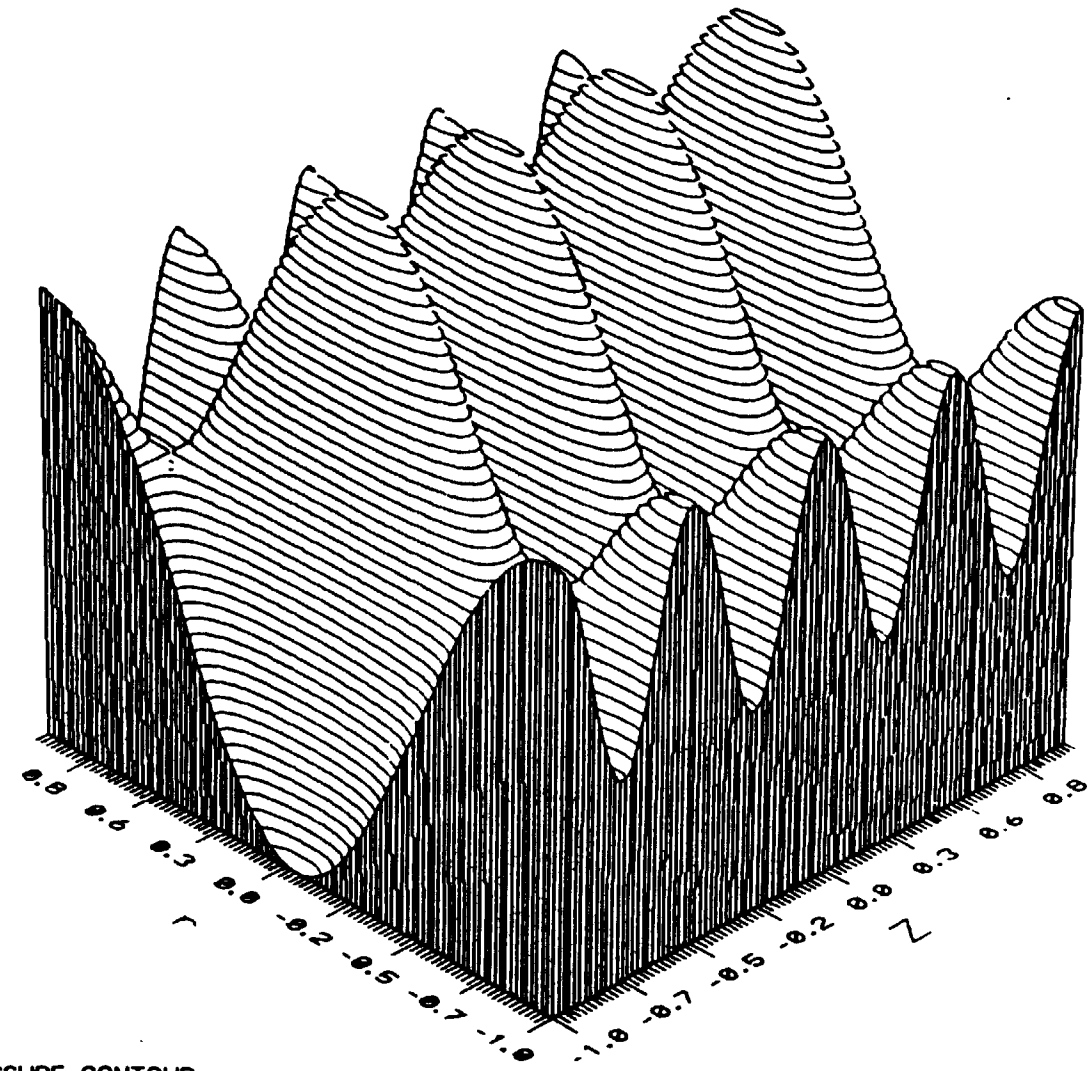

FIGURE 9. ISOMETERIC REPRESENTATION OF PRESSURE CONTOUR LINES FOR FIRST ORDER LATERAL WAVES.

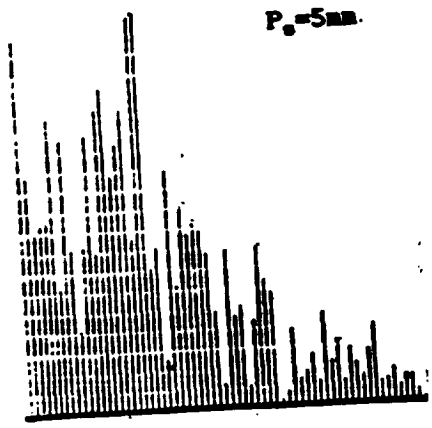

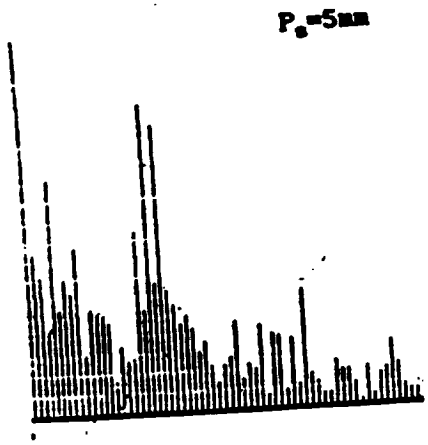

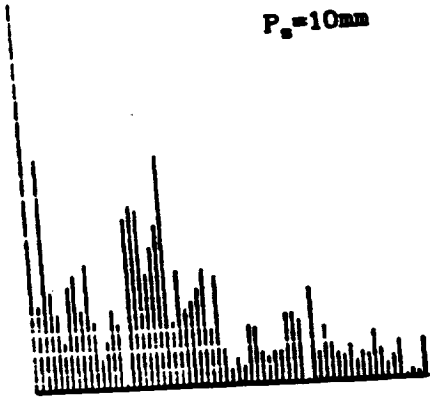

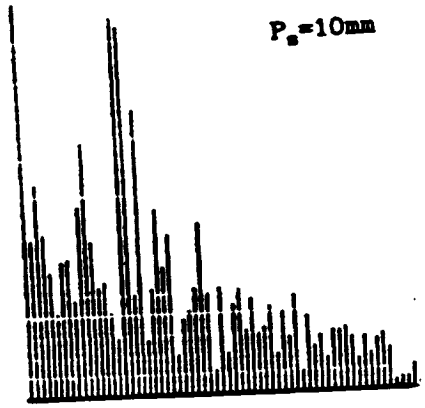

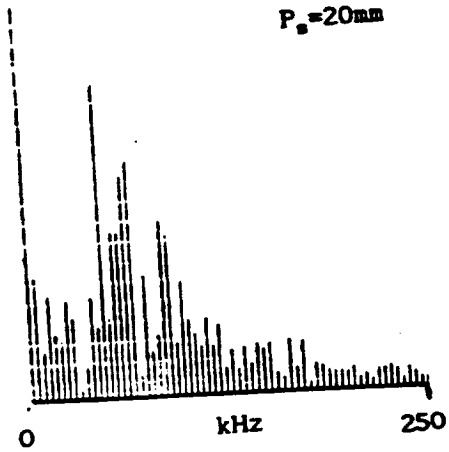

FIGURE 3

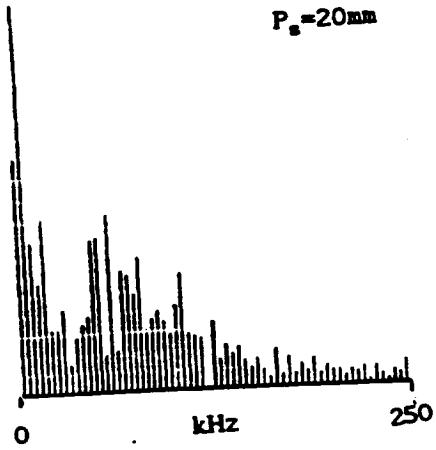

FIGURE 6

FIGURE 10. SPECTRAL DECOMPOSITIONS OF PITOT PRESSURE RECORDS IN FIGURES 3 AND 6 BETWEEN 200 AND 456 MICROSECONDS AFTER SHOCK ARRIVAL.

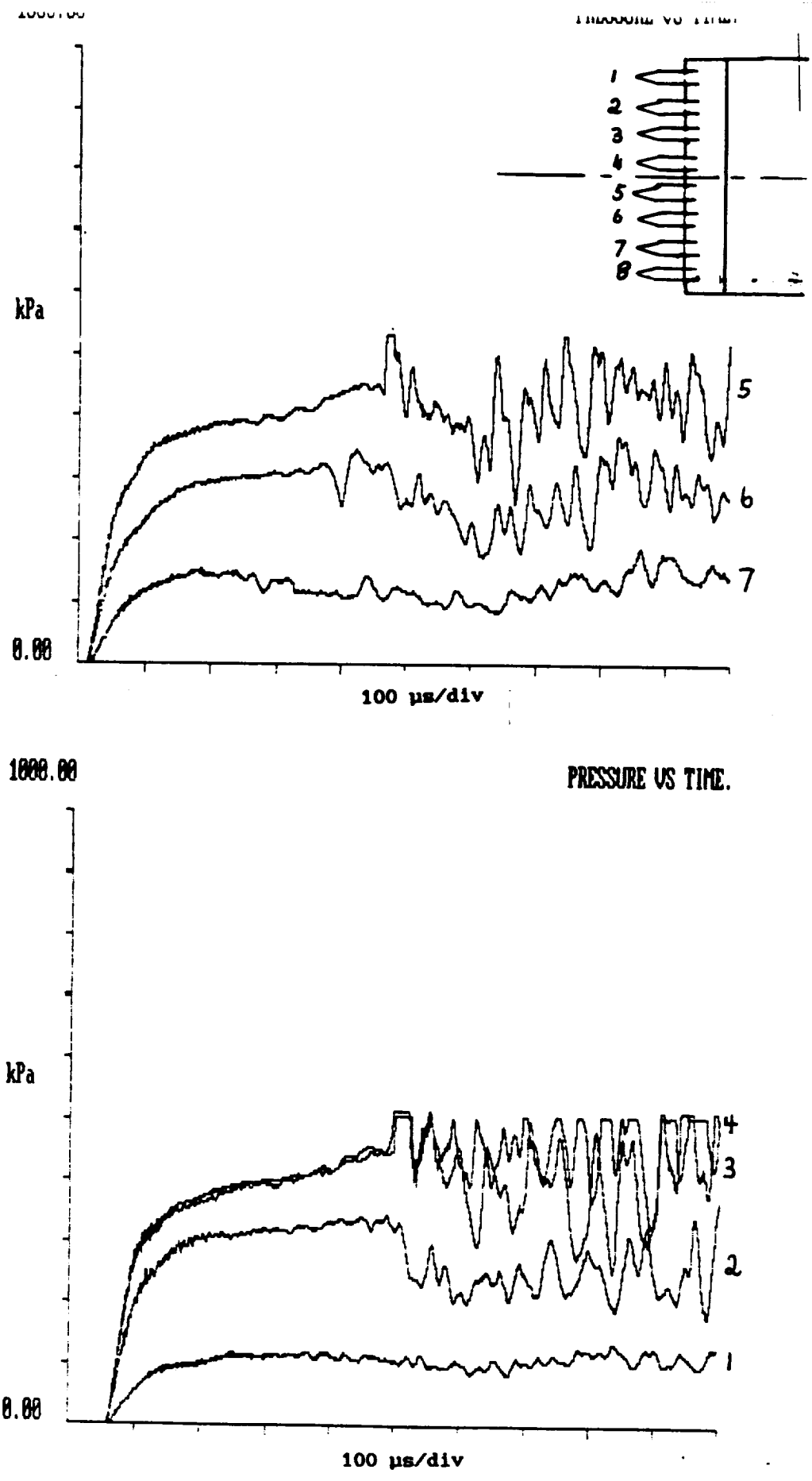

FIGURE 11. HYPULSE PITOT PRESSURE AS A FUNCTION OF TIME AT DIFFERENT RADIAL LOCATIONS.

NASA
National Aeronautics and Space Administration

Report Documentation Page

1. Report No.	2. Government Accession No.	3. Recipient's Catalog No.
NASA CR-182096		

4. Title and Subtitle
Shock Tunnel Studies of Scramjet Phenomena - Supplement 5

5. Report Date
October 1990

6. Performing Organization Code

7. Author(s)
R. Casey, R. J. Stalker, C. P. Brescianini, R. G. Morgan, P. A. Jacobs, M. Wendt, N. R. Ward, N. Akman, G. A. Allen, K. Skinner, S. L. Tuttle, J. M. Simmons, G. Kelly, R. M. Krek, A. Neely, A. Paull

8. Performing Organization Report No.

10. Work Unit No.
505-62-40-02

9. Performing Organization Name and Address
University of Queensland
Dept. of Mechanical Engineering
St. Lucia, Queensland
AUSTRALIA

11. Contract or Grant No.
NASW-674

13. Type of Report and Period Covered
Contractor Report, CY 1989

12. Sponsoring Agency Name and Address
National Aeronautics and Space Administration
Langley Research Center
Hampton, VA 23665-5225

14. Sponsoring Agency Code

15. Supplementary Notes
Langley Technical Monitor: Griffin Y. Anderson
Interim Report - Supplement 5

16. Abstract

As in previous reports, this consists of a series of reports on specific project areas, with a brief general introduction commenting on each report. The introduction is structured by project areas, with the title of the relevant report stated under the project area heading. The reports themselves follow in the order of the project area headings.

The commentary begins with a brief review of the program of work planned for 1989.

17. Key Words (Suggested by Author(s))	18. Distribution Statement
scramjet, shock tunnel, hypersonic mixing, combustion	Unclassified - Unlimited Subject Category 34

19. Security Classif. (of this report)	20. Security Classif. (of this page)	21. No. of pages	22. Price
Unclassified	Unclassified	200.	A09